technische universität
dortmund

MAX PLANCK INSTITUTE
OF MOLECULAR PHYSIOLOGY

Understanding mechanisms of membrane protein Prm1 for membrane fusion during cell-cell fusion of *Saccharomyces cerevisiae*

Dissertation

zur Erlangung des akademischen Grades eines Doktors der

Naturwissenschaft

(Dr. rer. nat.)

Vorgelegt an der Fakultät Chemie und Chemische Biologie der

Technischen Universität Dortmund

Angefertigt am Max-Planck-Institut für molekulare Physiologie in

Dortmund

Vorgelegt von

Anson Hao Tian Shek

2023

Referees

First referee

Prof. Dr. Stefan Raunser

Department of Structural Biochemistry, Max Planck Institute of Molecular Physiology, Dortmund

Faculty of Chemistry and Chemical Biology, Technical University Dortmund

Second referee

Priv.-Doz. Dr. Leif Dehmelt

Faculty of Chemistry and Chemical Biology, Technical University Dortmund

Date of submission: 05.04.2023

Formal Declaration

The work described in this thesis was carried out from November 2018 until February 2023 in the group of Dr. Matias Hernandez in the Department of Structural Biochemistry, led by Prof. Dr. Stefan Raunser at the Max Planck Institute of Molecular Physiology, Dortmund, Germany.

I hereby declare that I carried out the work independently and did not use any aid, other than the ones mentioned.

‘The new phenomenon of cell fusion, a laboratory trick on which much of today's science of molecular genetics relies for its data, is the simplest and most spectacular symbol of the tendency. In a way, it is the most unbiologic of all phenomena, violating the most fundamental myth of the last century, for it denies the importance of specificity, integrity, and separateness in living things. Any cell--man, animal, fish, fowl, or insect--given the chance and under the right conditions, brought into contact with any other cell, however foreign, will fuse with it. Cytoplasm will flow easily from one to the other, the nuclei will combine, and it will become, for a time anyway, a single cell with two complete, alien genomes, ready to dance, ready to multiply. It is a Chimera, a Griffon, a Sphinx, a Ganesha, a Peruvian god, a Ch'i-lin, an omen of good fortune, a wish for the world.’

Lewis Thomas, The Lives of a Cell: Notes of a Biology Watcher

Acknowledgements

I have immense gratitude to Dr. Matias Hernandez for providing me the opportunity to join his research group. Out of the many points for acknowledgement that came to me during the course of writing this section, a select few would persistently appear. I am grateful for your mentorship and directing me to becoming an independent scientist. I will always remember how you instilled in me to strive to see the 'big picture'. Thank you for putting up with my cynicism during the stumbling times of my doctorate journey.

I thank Prof. Dr. Stefan Raunser for his valuable advice and critical input towards the project. My thanks also go to the members of the Structural Biochemistry department for their assistance over the years, particularly with regards to protein purification and *in vitro* techniques.

I also thank Dr. Leif Dehmelt for taking the time to act as my second referee.

Many thanks to my fellow AG Hernandez members: Dr. Sheila Mainye, Angela Hagemeier, Lisa Kratzenberg and Diana Ludwig for their companionship and support in the lab. You made it a fun journey and I will cherish our memories together. Thanks to Dr. Farid Ghasemalizadeh for your advice pertaining artificial vesicles and for the funny chats. To Dr. Kitso Kewagamang, who together began our graduate studies at the same time, thank you for your camaraderie and support.

Thank you to Dr. Lucia Sironi and Christa Hornemann for their support, both personally and through the running of the IMPRS and providing a great student experience. Without the IMPRS I would not have had the chance to present my work and meet the many wonderful cell-cell fusion researchers at the 2022 GRC Cell-Cell Fusion meeting.

Thank you to my parents for their constant support whilst I was apart from them in a different country.

To Clarissa, thank you for your unrelenting love and encouragement. You have supported me through the highs and lows of my PhD journey, from the very start to the finish. It hardly needs saying that without you, this work would not exist.

Table of contents

List of figures

List of tables

Abbreviations

Abbreviation	Meaning
AA	Amino acid
DOPE	1,2-Dioleoyl-sn-glycero-3-phosphoethanolamine
BiFC	Bimolecular fluorescence complementation
C-GFP	C-terminal split GFP
CDS	Coding sequence
CHAPS	3-cholamidopropyl dimethylammonio 1-propanesulfonate
CMC	Critical micelle concentration
ConA	Concanavalin A
DDM	n-dodecyl β-D-maltopyranoside
dNTP	Deoxyribose nucleotide triphosphate
DTT	Dithiothreitol
EDTA	Ethylenediaminetetraacetic acid
eGFP	Enhanced green fluorescent protein
EGTA	Ethylene glycol-bis(β-aminoethyl ether)-N,N,N′,N′-tetraacetic acid
ER	Endoplasmic reticulum
FM4-64	(*N*-(3-Triethylammoniumpropyl)-4-(6-(4-(diethylamino)phenyl)hexatrienyl)pyridinium dibromide)
FSEC	Fluorescence-detection size-exclusion chromatography
GDN	Glyco-diosgenin
IPC	Inositolphosphorylceramide
LCB	Long-chain base
LDAO	Lauryldimethylamine-N-oxide
LiAc	Lithium acetate
LMNG-CHS	Lauryl maltose-neopentyl glycol-cholesteryl hemisuccinate
$M(IP)_2C$	Mannosyldiinositol phosphorylceramide

MIPC	Mannosylinositol phosphorylceramide
MW	Molecular weight
N-GFP	N-terminal split GFP
OD_{600}	Optical density at 600 nm
OG	n-octyl-β-D-glucopyranoside
ORF	Open reading frame
PAGE	Polyacrylamide gel electrophoresis
PBS	Phosphate-buffered saline
PCR	Polymerase chain reaction
PEG	Polyethylene glycol
PIC	Protease inhibitor cocktail
PMSF	Phenylmethyl sulfonylfluoride
Rhodamine-PE	1,2-Dioleoyl-sn-glycero-3-phosphoethanolamin-N-(lissamin-rhodamin B-sulfonyl)
RT	Room temperature
SC	Synthetic complete
SD	Synthetic defined
SDS	Sodium dodecyl sulphate
SEC	Size-exclusion chromatography
TCA	Trichloroacetic acid
TLC	Thin-layer chromatography
TMD	Transmembrane domain
UTR	Untranslated region
VLCFA	Very-long-chain fatty acid
YPD	Yeast extract peptone dextrose

Abstract

Cell-cell fusion is an essential phenomenon for life to exist. Despite decades of research, the model eukaryotic organism *Saccharomyces cerevisiae* possesses a significant gap in regards to the fusion requirements at the fusion of the two plasma membranes during sexual reproduction. Only a few candidates are known to act at this step, one of which is a multi-pass membrane protein, Prm1. Through an overexpression genomic screen to identify additional fusion regulators, I found that in Δ*prm1* mutants, the remaining capacity for membrane fusion is influenced by a sphingolipid mannosyltransferase, Sur1. Further examination in fact suggested that the levels of $M(IP)_2C$ sphingolipids at the membrane are critical for Δ*prm1* fusion. $M(IP)_2C$ levels enact a strong influence on the cell-fusion of Δ*prm1* mutants, particularly at the level of the plasma membranes. Absence of $M(IP)_2C$ allows nearly all Δ*prm1* mutants to fuse successfully, mimicking wild type efficacies. On the other hand, higher $M(IP)_2C$ levels act antagonistically towards fusion propensity.

In the second part, I explored the behaviour of Prm1 towards the goal of elucidating its mechanism of action. I found that a conserved ectoplasmic amphipathic domain in Prm1 is partially required for its fusion supporting activity. The remaining part of the protein acts redundantly to when plasma membranes are depleted in $M(IP)_2C$. I also initiated efforts to purify and reconstitute Prm1 into liposomes to investigate its function in isolation. Using flow cytometry, I found that when Prm1 was reconstituted into the membrane of liposomes, such proteoliposomes were docked to one another. The docked liposomes could become undocked upon proteolytic cleavage of Prm1. Altogether, the results support the existence of a capacity for Prm1 to interact with membranes by itself. In summary, this study unravels the fusion landscape in fungal systems. The dissection of Prm1 regions important for its activity here provides a newfound framework upon which to unravel its mechanism of action.

Zusammenfassung

Die Zell-Zell-Fusion ist ein wesentliches Phänomen für die Existenz von Leben. Trotz jahrzehntelanger Forschung existiert beim eukaryontischen Modellorganismus *Saccharomyces cerevisiae* eine erhebliche Wissenslücke hinsichtlich der Fusionsanforderungen bei der Verschmelzung der beiden Plasmamembranen während der sexuellen Fortpflanzung. Nur wenige Komponenten sind bekannt die diesen Prozess regulieren, wie das Multipass-Membranprotein Prm1. Mit Hilfe einer genomisch basierten Überexpressionsstudie zur Identifizierung zusätzlicher Fusionsregulatoren habe ich herausgefunden, dass in Δ*prm1* Mutanten die verbleibende Fähigkeit zur Membranfusion durch eine Sphingolipid-Mannosyltransferase, Sur1, beeinflusst wird. Weitere Untersuchungen ergaben, dass der Gehalt an $M(IP)_2C$ -Sphingolipiden in der Membran für die Δ*prm1* Fusion entscheidend ist. Der $M(IP)_2C$ -Gehalt hat einen starken Einfluss auf die Zellfusion der Δprm1-Mutanten, insbesondere auf der Ebene der Plasmamembranen. In Abwesenheit von $M(IP)_2C$ fusionieren fast alle Δprm1-Mutanten erfolgreich und erreichen nahezu die Fusionseffizienz des Wildtyps. Im Umkehrschluss wirken sich höhere $M(IP)_2C$ -Konzentrationen antagonistisch auf die Effizienz aus.

Im zweiten Teil untersuchte ich wie Prm1 sich verhält, mit dem Ziel dessen Wirkmechanismus aufzuklären. Ich fand heraus, dass eine konservierte ektoplasmatische amphipathische Domäne in Prm1 teilweise für die fusionsfördernde Aktivität erforderlich ist. Der verbleibende Teil des Proteins wiederum ist redundant, wenn die Plasmamembranen arm an $M(IP)_2C$ sind. Ich habe bereits erste Versuche unternommen, Prm1 aufzureinigen und in Liposomen zu rekonstituieren, um dessen Funktion isoliert zu betrachten. Mit Hilfe der Durchflusszytometrie konnte ich zeigen, dass wenn Prm1 sich in der Membran von Liposomen befindet, diese sogenannten Proteoliposomen aneinander andockten. Diese Verbindung konnte durch proteolytische Spaltung von Prm1 wieder gelöst werden. Insgesamt veranschaulichen die vorgelegten Ergebnisse, dass Prm1 selbst die Fähigkeit besitzt mit Membranen zu interagieren. Zusammenfassend lässt sich sagen, dass diese Studie dazu beiträgt den Fusionsprozess in Pilzsystemen aufzuklären. Die Aufgliederung der für die Aktivität von Prm1 wichtigen Regionen liefert eine neuartige Grundlage mit Hilfe der genaue Wirkmechanismus von Prm1 entschlüsselt werden kann.

Chapter 1. Introduction

Cell-Cell fusion is a process essential for eukaryotic life to exist, occurring namely during sexual reproduction and organ development. The molecular biophysical process underlying this phenomenon is membrane fusion. The reader will first be introduced to basic concepts underlying the membrane fusion reaction **(Section 1.1)**, followed by the description of protein-mediated membrane fusion namely mediated by fusogens **(Section 1.2)**. Some examples of diverse cell-cell fusion systems under current research will then be discussed **(Section 1.3)**. In the work described in this thesis, the fungal eukaryote *Saccharomyces cerevisiae* was utilised as the studied fusion system and thus I dedicate a section to familiarise fusion in this system **(Section 1.4)**.

1.1 Membrane fusion: stalk-pore hypothesis

The fusion between two distinct compartments comprising distinct phospholipid bilayers results in the formation of a single compartment, possessing a unified membrane. Membrane fusion can be thought of as a rearrangement of the planar packing of bilayers. For this, the stalk-pore model was proposed (Markin et al., 1984), which represents the lowest energy reaction and the most common pathway for membrane fusion **(Figure 1)**. The proximal leaflets of the two membranes first merge, forming a non-bilayer intermediate known as a hemifusion stalk (Chernomordik and Kozlov, 2008; Markin et al., 1984). In this intermediate, the lipids in the proximal leaflets are able to mix, however the inner distal leaflets remain uncontacted. Subsequent radial expansion of the stalk allows the distal leaflets to contact, forming a structural intermediate termed as a hemifusion diaphragm. Even in the hemifusion diaphragm state however, the lipids of the distal leaflets do not mix. The hemifusion diaphragm is then disrupted, forming a fusion pore. Subsequent expansion of the nascent pore allows mixing of the luminal contents.

Local point-like protrusions of the membrane are proposed as the most favourable initiators of hemifusion (Chernomordik and Kozlov, 2008). Early evidence for the hemifusion stalk came from studies on virus-cell fusion (Chernomordik et al., 1998; Kemble et al., 1994) along with molecular simulations of membrane fusion. Later studies in cell

fusion systems also observed the existence of the hemifusion stalk, suggesting that this intermediate could be a universal on-pathway intermediate during biological membrane fusion. Finally, it should be noted that other models of lipidic rearrangements have been proposed for the membrane fusion reaction. For instance, stalks could resolve directly to a fusion pore, without progression to a hemifusion stalk.

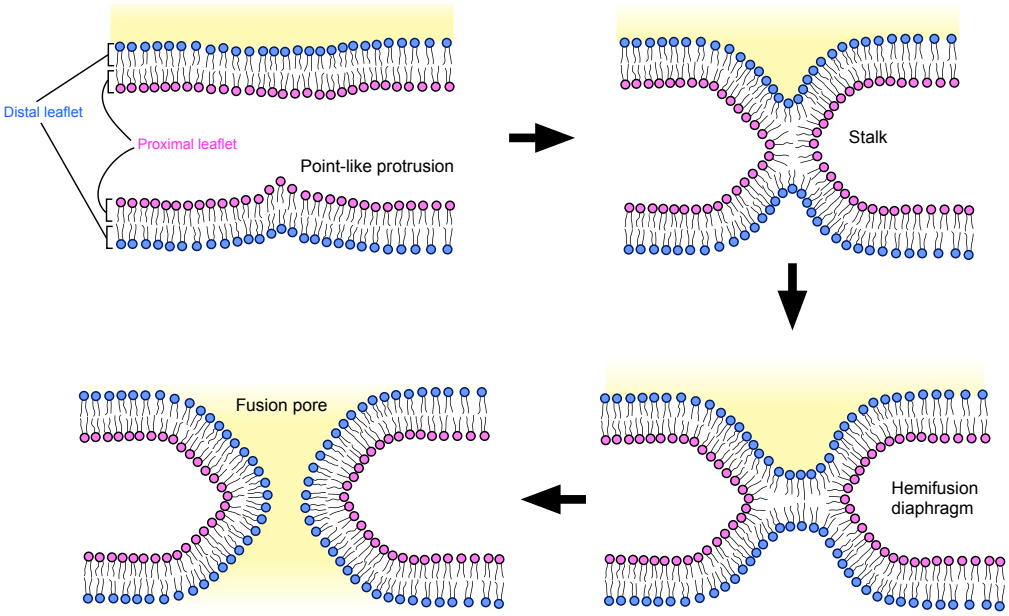

Figure 1. The stalk-pore model of membrane fusion. The outer proximal leaflets (magenta) of the two opposing membranes first merge, forming a stalk intermediate. The inner distal leaflets (blue) then merge, forming a hemifusion diaphragm. Disruption of the hemifused diaphragm induces formation of a fusion pore. The fusion pore allows the mixing of the two lumens (represented by traversal of yellow).

1.2 Fusogens directly mediate fusion of biological membranes

Fusion of biological membranes does not occur spontaneously (Chernomordik and Kozlov, 2008). As two membranes approach, significant interbilayer hydration forces present a large energy barrier (Rand, 1989). The water molecules between the two bilayers need to be ‘squeezed out’ for any membrane merger to proceed. In order to carry out the

membrane fusion process, biological systems utilise specialised proteins known as fusogens. Fusogens help to overcome the hydration forces and supply the energy required for the lipid rearrangements during membrane fusion. Two classes of fusogens have been extensively characterised, the first class being responsible for intracellular vesicle fusion, the soluble N-ethylmaleimide-sensitive-factor attachment receptor (SNARE) proteins and the second of which are the viral fusogens. Thorough characterisation of these fusogens disclosed major understanding of the principles used by fusogens to fuse membranes, and these principles have extended towards divergent cell-cell fusion systems. I therefore briefly present these two cases.

1.2.1 SNAREs

The fusion events required for the intracellular trafficking of vesicles are carried out by SNARE proteins. Typically, SNARE proteins possess an amino terminal cytosolic domain, followed by a transmembrane domain (TMD) and a short C-terminal luminal domain. The cytosolic domain contains the defining SNARE motif, comprising a series of repeats, known as heptad repeats. Within eukaryotic cells, fusion between two membrane bound compartments require SNARE proteins situated in the membrane of one compartment (*vesicular* v-SNARE) and cognate SNARE proteins (t-SNARE) in the *target* compartment membrane. Interaction between v-SNAREs and t-SNAREs form a tightly bundled SNARE complex. This complex is composed of four helices, with one helix each provided by v-SNARE and the t-SNARE, while another membrane associated t-SNARE provides two (SNAP-25 in the neuronal SNARE complex).

The interactions which stabilize the SNARE complex are primarily hydrophobic and can be observed as a series of layers (Sutton et al., 1998). One specific layer, termed the '0-layer', is hydrophilic, consisting three glutamine and one arginine side chains **(Figure 2A)**. This '0-layer' is invariably conserved amongst different SNARE complexes and upon this finding SNAREs were reclassified as either Q-SNAREs or R-SNAREs, based on whether they provided Q or R side chains (Fasshauer et al., 1998). In the SNARE complex, the bundles are arranged in parallel fashion. Assembly occurs first from the N-terminus towards the C-terminal TMD, in a zipper-like fashion. This zippering is thought to provide the energy required to pull and fuse opposing membranes **(Figure 2B)**. Importantly, zippering must

also be extended to both the linker region and the transmembrane domains to maintain the rigidity. Whether such extension occurred was initially unclear since early structures of the SNARE complex were achieved using only the soluble fragments of the SNARE motifs (Sutton et al., 1998); until the structure of the neuronal SNARE complex with complete TMDs elucidated by Stein and colleagues **(Figure 2B)** showed that helicity is indeed fully extended towards the TMDs. This observation provided strong support for the zippering model as the mechanism of action (Stein et al., 2009).

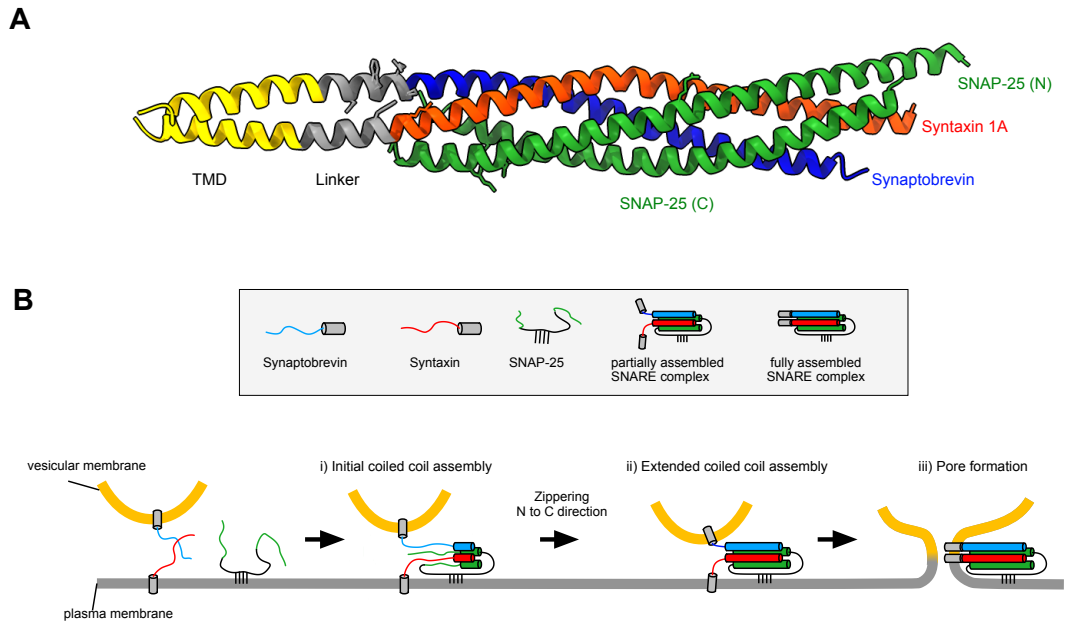

Figure 2. SNARE mediated fusion. A. The structure of the neuronal SNARE complex (PDB: 3HD7). Syntaxin (Sx1A) is denoted in red. Synaptobrevin (Syb2) is denoted in blue. SNAP-25 is denoted in green. Figure adapted from Stein et al., 2009. **B.** The zippering mechanism model of SNAREs during fusion. Here the neuronal SNAREs required for exocytosis are depicted as an example of zippering. In other SNAREs, makeups of the individual SNAREs can differ, however the central theme of coiled coil interactions are conserved. The SNARE motifs begin assembly at the N-terminus (depicted by coloured rectangles in the cytosolic domain) and proceeds in a zipper-like fashion towards the TMDs at the C-terminus. Progressive zippering and assembly of the SNARE complex is coupled to the fusion of the two membranes and pore formation.

1.2.2 Viral fusogens

Enveloped viruses contain genetic material within the nucleocapsid. Fusion between viral and cell-membranes facilitates nucleocapsid entry into the cytoplasm. The

fusogens utilised by enveloped viruses have been identified and characterised, probably because of the few proteins encoded in viral genomes and that their fusogens are essential for their pathogenicity. Fusion brought by these membrane proteins usually occur upon a trigger such as a low pH or by receptor binding. Receptor binding can be facilitated either by a subunit of the fusogen itself or cooperated by an associated receptor binding viral protein. Three classes of enveloped viral fusogens have been defined on the basis of their structural features. Class I viral fusogens in the post fusion conformation are predominantly found as α-helical hairpins. Class II viral fusogens possess β-sheets which refold to form trimeric hairpins. Class III fusogens show a mixture of class I and class II structural elements. A recently characterised class, class IV, comprises the fusion associated small transmembrane (FAST) fusogens. FAST fusogens belong to nonenveloped viruses and are interesting because of their small ectodomains.

1.2.2.1 Case study: Hemagglutinin

The first viral fusogen which was well characterised is Hemagglutinin (HA); a class I viral fusogen belonging to Influenza virus. The ectodomain is comprised of two subunits, referred as HA1 and HA2. HA2 contains a hydrophobic fusion peptide. In solved structures, HA is found as a trimer. Three atomic structures of HA have been solved, the uncleaved prefusion, the cleaved prefusion, and the postfusion trimer conformations (Podbilewicz, 2014). These structures are thought to represent metastable intermediates during HA-mediated fusion, with the postfusion state comprising the lowest free energy conformation. In the prefusion trimer, the fusion peptide is situated near the N-terminus of the eventual HA2 subunit. In the postfusion trimer, the hydrophobic fusion peptide and the TMDs are positioned at the same end of the hairpin structure, suggesting they are anchored to the same membrane (Podbilewicz, 2014).

Based on these structures, the fold-back model was conceived to propose how fusion is achieved in accordance with the movement of the fusion peptide between the prefusion and the postfusion conformation **(Figure 3)**. For this, HA is first proteolytically cleaved to generate HA1 and HA2. Upon cleavage, the C-terminal HA2 subunit is primed for fusion. Upon low pH, the fusion peptide is exposed from the interior trimer and becomes inserted into the target membrane by forming an extended intermediate **(Figure 3)**. This extended intermediate then folds back, forming a hairpin-like postfusion trimer, and this specific

transition is associated with hemifusion and pore formation. Whether the cleaved prefusion HA state truly refolds to form an extended intermediate had remained unclear for many years due to the absence of a solved structure of this intermediate, until a recent study by Benton et al. (2020). By studying HA particles using cryo-EM, they observed intermediate states of HA in conformations between the prefusion and postfusion states. One of these included an extended helical trimer conformation, which likely represents HA when bound to target membranes.

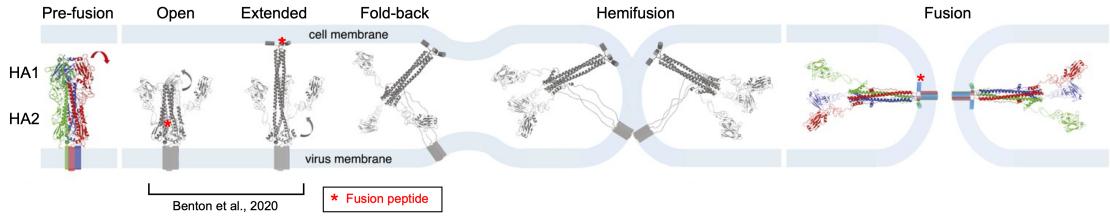

Figure 3. Hemagglutinin mediated fusion via a fold-back mechanism. Acidic pH induces change of HA2 to the open conformation and allows exposure of the hydrophobic fusion peptide (red asterisk). The fusion peptide then inserts into target membrane which is associated with the extended conformation. The folding back of the extended trimer to the post fusion conformation is correlated to hemifusion and pore formation. Solved prefusion HA and post fusion HA structures are coloured. Structural evidence for open and extended intermediates were identified by Benton et al. (2020). Figure adapted from Ivanovic et al. (2013).

From these two examples, general mechanistic principles on how fusogens mediate biological membrane fusion have been elucidated. Firstly, fusogens by themselves provide the work necessary to cover the energy costs required for fusing membranes (Akimov et al., 2020). This principle holds true for other fusogens which have been characterised to date. Studies on SNARE and viral fusion revealed that both fusogens utilise hemifusion as a lipidic intermediate (Chernomordik et al., 1998; Kemble et al., 1994; Xu et al., 2005). As we will see for other cell fusogens, hemifusion is also observed. For SNARE proteins, membrane fusion is driven by structural stability provided by the assembly of the coiled coil SNARE complex. Disruptions to the formation of the coiled coil through mutations which hamper the interactions between the layers of the coiled coil therefore adversely affect fusion. The stability required for SNAREs suggests that SNAREs act to bring membranes close and mechanically bend them to drive membrane merger.

For viral fusogens, their mechanism of action relies on the insertion of hydrophobic motifs to the opposing membrane of the fusogen. In addition, large conformational changes

in the protein are required to bring membranes into close contact and subsequent fusion. The interaction with target membranes is the reason for how they act unilaterally. In contrast, the SNAREs display a bilateral fusion requirement because at least one of the SNARE proteins which form the complex have to be present in each membrane.

1.3 Cell-cell fusion

In comparison to viral-cell fusion and intracellular fusion, the study of cell-cell fusion is more complicated. Often, cells have to undergo multiple stages before fusion of plasma membranes can take place. These include differentiation to achieve a fusion competent cell, cell-cell communication, migration and adhesion (Aguilar et al., 2013). Furthermore, for many years, the mechanisms of action of plasma membrane fusion in many cell fusion systems were enigmatic because in many cases the fusogen had remained unidentified. Recent advances into the understanding of how cells fuse plasma membranes have been propelled by the identification of their fusogens. The following section will describe some of the currently studied fusion systems and the key proteins required for their fusion. The aim is not to cover all fusion systems; rather a focus on the commonalities yet also unique differences between example systems will be provided.

1.3.1 Epithelial fusion in *Caenorhabditis elegans*

In *C. elegans*, the development of the tissue and organs and their lineages are well characterised (Podbilewicz and White, 1994). During *C. elegans* development, around one third of all somatic mononucleated cells fuse (Podbilewicz and White, 1994). A variety of epithelial fusions occur in this organism, such as the hypodermis, vulva, uterus and excretory glands. Fusion thus assists in sculpting the organs and tissue. Epithelial fusion is mediated by the fusogen epithelial fusion failure 1 (EFF-1) and a paralog anchor fusion failure 1 (AFF-1), which are both single-pass transmembrane proteins. Ectopic expression of EFF-1 and AFF-1 in *C. elegans* induces fusion between epithelial cells that do not normally fuse (Sapir et al., 2007; Shemer et al., 2004). Therefore, the expression of EFF-1 and AFF-1 during development is normally tightly regulated.

The sufficiency of EFF-1 and AFF-1 as fusogens was demonstrated when their expression was shown to induce fusion of non-fusing insect Sf9 cells (Podbilewicz et al., 2006). EFF-1 is required on the surfaces of both cells for fusion to occur, indicating a bilateral homotypic fusion mechanism (Podbilewicz et al., 2006). Additional evidence that the EFF-1 mechanism is bilateral arose when it was found that EFF-1 can substitute for fusogen-absent pseudotyped viruses and restore infectivity, but only provided EFF-1 is *also* present on the target cells (Avinoam et al., 2011). The study also showed that EFF-1 pseudotyped viruses could mediate fusion with target cells expressing AFF-1, indicating that EFF-1 could mediate fusion in a heterotypic manner with AFF-1, and that EFF-1 and AFF-1 likely share similar fusion mechanisms. The X-ray crystal structure of the EFF-1 ectodomain revealed a remarkable structural similarity towards the class II viral fusogens (Pérez-Vargas et al., 2014). However, despite the structural similarity of EFF-1 to unilateral acting viral fusogens, the bilateral fusion requirement of EFF-1 suggests a different mechanism of fusing membranes is employed, more akin to the zippering of SNAREs. The fact that the class II viral fusogen equivalent fusion loop of EFF-1 is negatively charged and likely does not directly interact with membranes supports this idea.

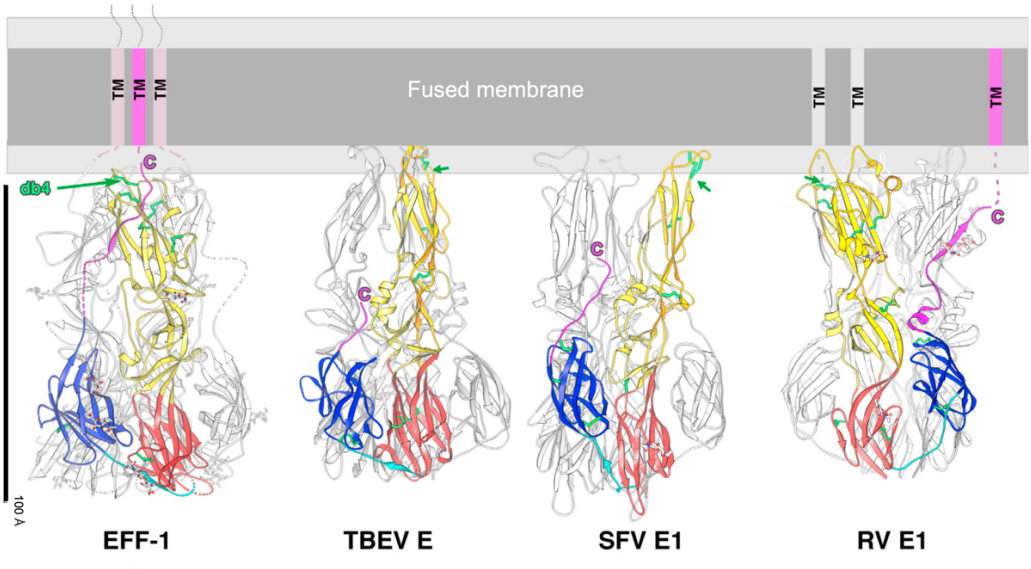

Figure 4. Structural similarity of EFF-1 to class II viral fusogens. EFF-1 displays an assembly of trimers comprising structural folds similar to that of class II viral fusogens. TBEV E (PDB: 1URZ), flavivirus; SFV E1 (PDB: 1RER), alphavirus; RVE1 (PDB: 4ADI), rubella virus. Green arrows indicate disulfide bonds. Adapted from Perez-Vargas et al. (2014).

1.3.2 Eukaryotic gamete fusion mediated by HAP2

Research from a number of independent groups, in a variety of different eukaryotic species, have found an ancient gamete cell fusogen known as Hapless 2 (HAP2). Initial discovery of HAP2 came from plants, where a male specific fertility factor was found to be required for fertilisation of *Lilium longiflorum* and *Arabidopsis thaliana* which was denoted GENERATIVE CELL SPECIFIC 1 (GCS1) (Mori et al., 2006). In the same year, a separate group made the same discovery in *A. thaliana* in which the gene encoding GCS1 was given the name *HAP2* (von Besser et al., 2006). Similarly to *GCS1*, *hap2* mutants are blocked in egg and central cell fertilisation. HAP2 orthologs were subsequently identified in protists such as *Plasmodium falciparum*, algae such as *Chlamydomonas reinhardtii* and invertebrate animals such as *Hydra* and honeybees (Clark, 2018; Mori et al., 2006; Steele and Dana, 2009; Wong and Johnson, 2010). With fungi and vertebrates as notable exceptions, HAP2 orthologs have now been found in many eukaryotic lineages and may have been present in the last eukaryotic common ancestor (LECA) (Clark, 2018). Recently, structural homologs of HAP2 were identified in archaea, opening the question to whether HAP2 in fact originated from prokaryotes (Moi et al., 2022). As an example of an organism which utilises HAP2 for cell fusion, the unicellular green alga Chlamydomonas will be provided.

1.3.2.1 HAP2-mediated fusion in *Chlamydomonas reinhardtii*

Asexually dividing *C. reinhardtii* haploids possess either two mating types, *plus* (+) or *minus* (-) which expresses upon nitrogen starvation. Mixture of *plus* and *minus* gametes leads to docking (also referred as adherence) and cell fusion to form diploid zygotes (Pinello and Clark, 2022). During mating, membrane protuberances known as mating structures form, which are brought into closer contact by cilia-mediated interactions **(Figure 5A)**. Once mating structures contact, further docking of the membranes occurs, which is mediated by a protein receptor pair, FUS1 and MAR1. Both are single-pass membrane proteins, and FUS1 is only expressed in *plus* gametes whilst MAR1 is only expressed in *minus* gametes. MAR1 and FUS1 interact *in vitro* (Pinello et al., 2021), and consistent with the FUS1-MAR1 pair interaction being the prevailing determinant for docking, absence of either FUS1 in the *plus* gamete or MAR1 in the *minus* gamete is sufficient to severely impair

docking (Misamore et al., 2003; Pinello et al., 2021). Thus, in *C. reinhardtii* docking of membranes is a critical prerequisite for HAP2-mediated plasma membrane fusion.

During mating, expression of HAP2 occurs only on *minus* gametes, indicating *C. reinhardtii* HAP2 acts unilaterally, akin to viral fusogens. Solved structures of the HAP2 ectodomain details a structure similar to that of class II viral fusogens and to that of *C. elegans* epithelial fusogen, EFF-1 (Fédry et al., 2017; Feng et al., 2018) **(Figure 5B)**. In addition, hydrophobic fusion loops could be identified which are required for fusion activity, analogous to the fusion peptides of viral fusogens (Feng et al., 2018; Zhang et al., 2021). In summary, even though HAP2 has the capacity to fuse membranes by itself, necessary strategies are required by cells in nature to bring plasma membranes into sufficient proximity.

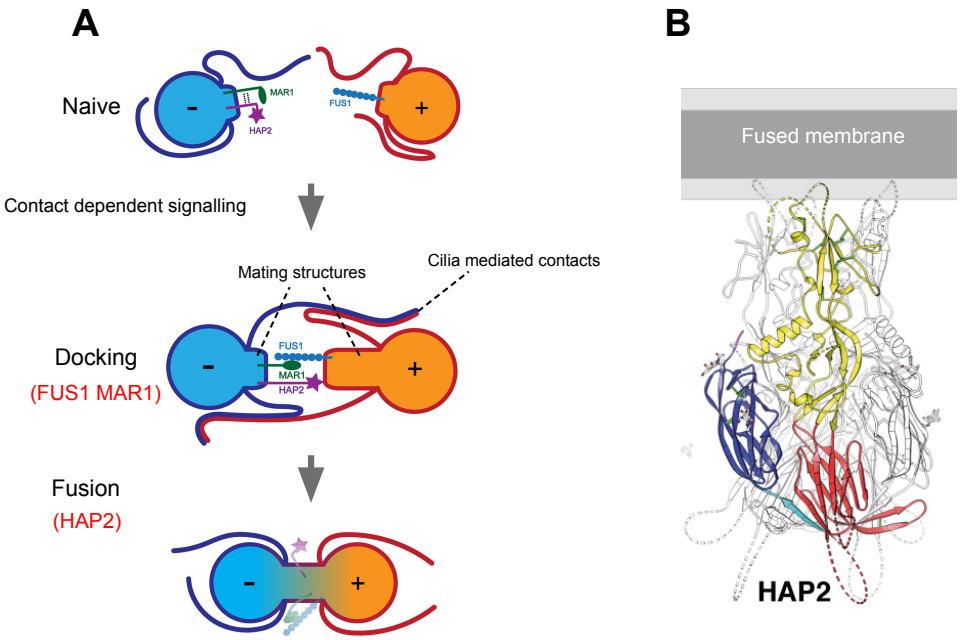

Figure 5. HAP2 mediated fusion in *C. reinhardtii* requires FUS1-MAR1 dependent docking. A. HAP2 mediated fusion of *C. reinhardtii* requires docking of membrane structures via heterotypic FUS1-MAR1 interactions. Figure adapted from Pinello and Clark (2022). **B.** HAP2 is structurally similar to EFF-1/AFF-1 and class II viral fusogens. *C. reinhardtii* HAP2 ectodomain in the post-fusion trimer conformation (PDB: 5MF1) is shown. Figure adapted from Fedry et al. (2017).

1.3.3 Vertebrate myoblast fusion is facilitated by Myomixer and Myomerger

Skeletal muscle are composed of multi-nucleated myotubes. Formation of myotubes relies on the cell-cell fusion of mononucleate myoblasts. Over the past decade, two small membrane proteins which orchestrate the membrane fusion step of myoblast fusion were identified through bioinformatic in silico searches. The first was Myomaker, a multipass membrane protein containing seven transmembrane domains (TMD) and subsequently Myomerger, a single pass transmembrane protein was discovered.

To test if Myomaker was sufficient for fusion, Millay and colleagues heterologously expressed Myomaker in fibroblasts, which are non-fusing (Millay et al., 2013). They found that Myomaker expressing fibroblasts did not fuse with each other; however, they did fuse with muscle cells, indicating additional muscle-specific factors which facilitated fusion (Millay et al., 2013). Three independent groups subsequently found another muscle regulated factor, Myomerger/Minion/Myomixer (Quinn et al., 2017; Shelton et al., 2017; Zhang et al., 2017). Co-expression of Myomaker and Myomerger in fibroblasts led to fusion, demonstrating Myomaker and Myomerger as the sufficient myogenesis fusogens. Further characterisation found that Myomaker is required to be present on the surface of both cells, whereas Myomerger is only required to be present on the surface of one of the cells. Unlike other fusogens, here distinct steps of the membrane fusion reaction are encoded on separate proteins, with Myomaker governing hemifusion, and Myomerger controlling pore formation (Leikina et al., 2018) **(Figure 6)**. Splitting the fusion mechanism may be adopted to exert more regulatory control and prevent unwanted fusions during muscle development.

The mechanistic details of how exactly Myomaker and Myomerger drive hemifusion and pore formation, respectively, is unclear. It is intriguing that these fusogens possess small ectodomains (Gamage et al., 2017; Millay et al., 2016), indicating that the fusion mechanism does not require large conformational rearrangements such as the viral fusogens, nor zippering like SNAREs. The intracellular C-terminus is the largest domain of Myomaker and contains cysteines which are palmitoylated and required for fusion activity (Gamage et al., 2017; Millay et al., 2016). It is speculated that the Myomaker might interact with the membrane in *cis* via this intracellular domain to achieve hemifusion competence. Further studies using *in vitro* systems will likely clarify if Myomaker can drive hemifusion

by itself or does so by interacting with other proteins present in myoblasts and fibroblasts. For Myomerger, pore formation was hypothesised to be facilitated by induction of membrane stress (Leikina et al., 2018). Evidence for this came from the observation that Myomerger-deficient myoblasts could be rescued to fuse by membrane stress inducing reagents such as octyl-β-glucoside and antimicrobial peptides that interacts with lipid bilayers. The C-terminal ectodomain of Myomerger contains two α-helices which are proposed to facilitate such membrane stress. The ability for fusion to be mediated by small ectodomain containing proteins is also found in class IV viral FAST fusogens. These single pass transmembrane proteins contain an extremely short ectodomain ranging from ~20-40 residues (Duncan, 2019).

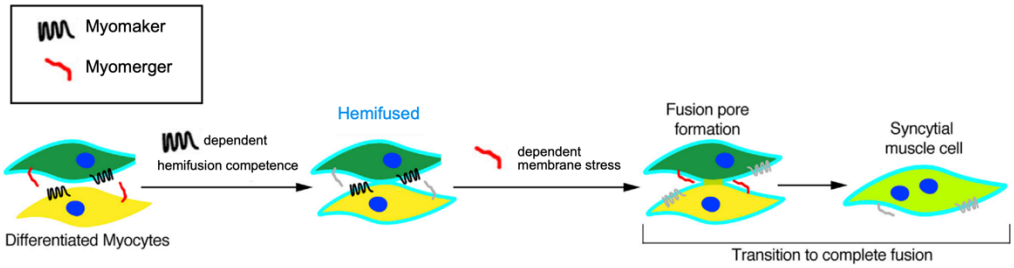

Figure 6. Myomaker and Myomerger independently govern hemifusion and pore formation. Myocytes require Myomaker to form hemifused connections. Subsequently, Myomaker acts to induce pore formation, completing cell fusion. Figure adapted from Leikina et al. (2018).

1.3.4 Vertebrate sperm-egg fusion

The fusion of sperm and egg during fertilisation is one of the most important events for mammals. Sperm has to penetrate the cumulus oophorus, as well as the zona pellucida, to reach the perivitelline space where the egg plasma membrane resides. Once the perivitelline space is reached, the sperm plasma membrane fuses with the oocyte plasma membrane. The exact fusogen responsible for sperm-egg fusion remains unclear, although a single-pass membrane protein, IZUMO1, which was first identified as a membrane docking protein, has recently been implicated to possess fusogenic activity (Brukman et al., 2023). Excluding IZUMO1, a number of other candidates have been found in recent years. These candidates are sperm acrosomal membrane proteins which are not required for binding and penetration of the zona pellucida, suggesting they act downstream at the

membrane fusion step. Furthermore, with the exception of IZUMO1's role for promoting docking, the mechanisms employed by these membrane proteins to facilitate membrane fusion remain largely elusive.

1.3.4.1 The IZUMO1-JUNO complex promotes docking of membranes

IZUMO1 was the first plasma membrane protein discovered to be involved in mammalian fertilisation. IZUMO1 is a sperm-specific single-pass membrane protein and binds to JUNO, an egg-specific GPI anchored glycoprotein receptor (Aydin et al., 2016; Bianchi et al., 2014). Atomic resolution structures of IZUMO1 and JUNO, in isolation and in complex have been solved **(Figure 7)**, which elucidated critical residues required for the IZUMO1-JUNO interaction (Aydin et al., 2016; Ohto et al., 2016). Initial studies found that neither IZUMO1 nor JUNO could induce syncytia formation when ectopically expressed in HEK293 cells, indicating they were not sufficient to induce membrane fusion. From this, the IZUMO1-JUNO interaction was implicated to facilitate docking of the sperm and egg membranes (Bianchi et al., 2014). This was the first such complex implicated in an essential docking step in vertebrate fertilisation.

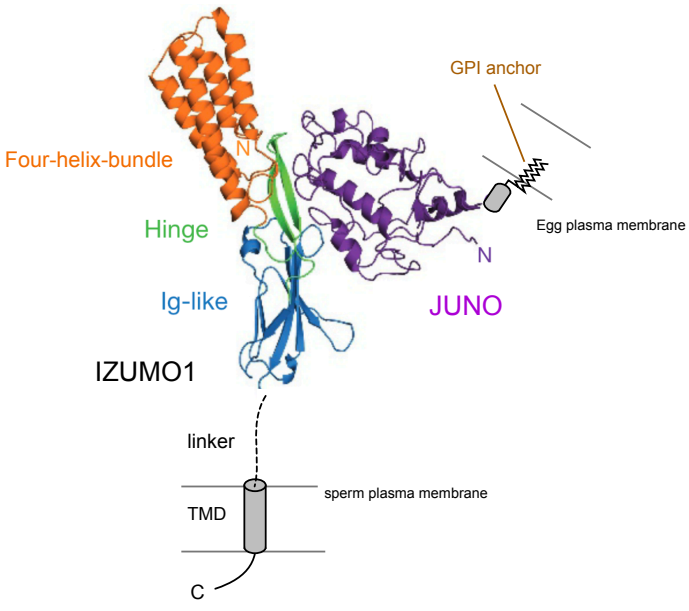

Figure 7. IZUMO1-JUNO complex required for docking of sperm and egg gametes. Human $IZUMO_{22-254}$ in complex with $JUNO_{20-228}$ shown in ribbon schematic (PDB: 5F4E). IZUMO1 comprises a four-helix-bundle, an anti-parallel β-strand hinge region and an immunoglobulin(Ig)-like domain. Figure adapted from Aydin et al. (2016).

1.3.4.2 IZUMO1 may fuse plasma membranes after IZUMO1-JUNO docking

Unexpectedly, a recent study from the Podbilewicz lab found IZUMO1 to possess fusogenic activity (Brukman et al., 2023). They found that expression of IZUMO1 could fuse normally non-fusogenic Baby Hamster Kidney (BHK) cells. IZUMO1-mediated fusion in the heterologous system was partially dependent on three exposed aromatic residues present on the four-helix-bundle domain. These residues are not thought to be required for binding to JUNO, as BHK cells expressing the four-helix bundle IZUMO1 mutant could still bind to eggs. Therefore, the fusogenic activity of IZUMO1 might be independent to its JUNO binding function. This is further supported by the fact that mutation of W148 in the IZUMO1 hinge region prevents JUNO binding but still allowed fusion of BHK cells. These findings lead to a model where during fertilisation, IZUMO1 first forms complexes with JUNO to facilitate membrane docking, and subsequently IZUMO1 mediates membrane fusion.

1.3.4.3 TMEM95

Transmembrane protein 95 (TMEM95) is a sperm specific single pass transmembrane protein. *Tmem95*-deficient sperm are able to penetrate the zona pellucida, but are unable to fuse with the egg membrane (Lamas-Toranzo et al., 2020; Noda et al., 2020). No interaction of TMEM95 with IZUMO1 nor JUNO was found (Lamas-Toranzo et al., 2020). HEK293T cells which expressed IZUMO1 and TMEM95 was unable to fuse with HEK293T cells which expressed JUNO, suggesting TMEM95 does not display fusogenic activity (Lamas-Toranzo et al., 2020). TMEM95 displays an α-helix and a β-hairpin similar to those found in IZUMO1. However, residues on the β-hairpin of TMEM95 differ to the equivalent ones found in IZUMO1. Recent elucidation of the TMEM95 1.5 Å-resolution X-ray crystal structure identified an evolutionarily conserved region containing a positively charged surface (Tang et al., 2022). The basic residues are necessary for TMEM95 activity. The ectodomain of TMEM95 is able to bind to hamster oocytes; additionally, monoclonal antibodies which bind to TMEM95 inhibit sperm-egg membrane fusion. These two observations suggest for an interaction between TMEM95 and an unidentified egg specific TMEM95 receptor which is needed for fusion (Tang et al., 2022).

1.3.4.4 SPACA6, FIMP and SOF1

Spaca6

SPACA6 is a transmembrane protein required for fusion. SPACA6 KO sperm are unable to fuse with oocyte membanes, in similar fashion to TMEM95. The structure of SPACA6 is similar to IZUMO1, containing a four-helix bundle and an Ig-like β-sandwich (Vance et al., 2022). SPACA6 and IZUMO1 interact in HEK293T cells and this interaction may be important *in vivo* (Noda et al., 2020). In support of this, the absence of IZUMO1 also leads to the absence of SPACA6 (Inoue et al., 2021).

FIMP

Fertilisation influencing membrane protein (FIMP) is another single-pass transmembrane protein specific to sperm (Fujihara et al., 2020). FIMP is broadly conserved in mammals including mice and humans. Zona pellucida penetration is possible in *Fimp* mutant sperm, however fusion is significantly impaired. It is unknown whether FIMP interacts with IZUMO1 or other sperm fusion proteins.

SOF1

SOF1 is a sperm specific transmembrane protein. *Sof1* mutant sperm show IZUMO1 expression, but cannot fertilise eggs (Noda et al., 2020). Similarly to TMEM95, *Sof1* sperm can penetrate the zona pellucida, accumulating in the perivitelline space. Expression of SOF1, TMEM95 and SPACA6 in IZUMO1 cells does not induce fusion. SOF1 is found as two molecular weight species and during the acrosome reaction one species disappears (Noda et al., 2020). The lower species may therefore be released during the acrosome reaction.

1.3.4.5 DCST1 and DCST2

DCST1 and DCST2 (DC-Stamp domain containing protein) are homologs of an osteoclast fusion related factor, dendritic cell specific transmembrane protein (DC-STAMP). DCST1 and DCST2 are both required for fertilisation in mice. *Dcst1/2*$^{-/-}$ male mice spermatozoa reach the zona pellucida but do not fertilise eggs (Inoue et al., 2021). The absence of either DCST1 or DCST2 in mice spermatozoa is enough to severely impair fertilisation. Similar results were reported in zebrafish, in which Dcst1 and Dcst2 single

knockout sperm fail to undergo fertilisation (Noda et al., 2022). DCST1 and DCST2 are multipass membrane proteins and possess orthologs involved in fertilisation in *C. elegans* (SPE-42 and SPE-49) and *D. melanogaster* (Sneaky), suggesting for a conserved functional role of these proteins.

1.3.4.6 CD9

CD9 is a tetraspanin which is expressed on the oocyte membrane. CD9 along with JUNO are presently the only female specific factors found for fusion. CD9-deficient eggs can bind to sperm; however, membrane fusion does not occur (Miyado et al., 2000). The exact role of CD9 in the plasma membrane fusion event is unclear, however one hypothesis is that it provides a scaffolding role in sperm-egg fusion, to bring other fusion related proteins into vicinity. In support of this, IZUMO1 was observed to be colocalised with CD9 (Chalbi et al., 2014). Additionally, CD9 has roles in forming curved membrane structures known as microvilli (Runge et al., 2007). Because of the high curvature of the microvilli, these regions have been speculated to act as optimal fusion sites.

1.3.4.7 Summary

For the majority of proteins identified in the fusion of sperm-egg fusion, it is unclear what roles they have in the plasma membrane fusion step. Since absence of IZUMO1 also results in absence of SPACA6, there may be strict requirements for correct organisation of the fusion proteins at the sperm-egg fusion site which are mediated by protein-protein interactions. This might explain why the absence of only one protein in most cases completely blocks plasma membrane fusion. It is also unclear why the fusogenic property of IZUMO1 was not identified in previous studies. In light of the new IZUMO1 finding, further attention is required to assess whether the other membrane proteins described possess fusogenic activity, especially TMEM95 and SPACA6, due to their similar structures.

1.4 Fungal cell-cell fusion

Studies on fungal cell fusion have elucidated mechanisms of pheromone signalling and cell communication during somatic cell fusions and sexual reproduction. However, the

molecular details of the events during plasma membrane fusion remain poorly understood. Furthermore, the identity of the fusogen(s) responsible for cell fusion in fungi presently remains unknown.

1.4.1 Mating of *S. cerevisiae*

Budding yeast *S. cerevisiae* is a unicellular organism. Haploid *S. cerevisiae* propagate vegetatively through a mitotic cell cycle. Additionally, *S. cerevisiae* contain a sexual phase in which yeast cells of different mating types can mate, forming a diploid organism **(Figure 8)**. Haploid *S. cerevisiae* possess a mating type of either **a** or α, which is determined by the presence of either the *MAT***a** or *MAT*α allele at the *MAT* locus, respectively (Bender and Sprague, 1989). Each mating type secretes their own distinct mating pheromones, termed **a**-factor and α-factor, respectively. Pheromones secreted by one mating type are sensed by the opposing mating type i.e. **a** cells respond to α-factor secreted by α cells, and α cells respond to **a**-factor secreted by **a** cells. Once cells of opposite mating type encounter each other, mating between **a** and α cells is initiated, resulting in cellular and nuclear fusion to generate an **a**/α diploid zygote.

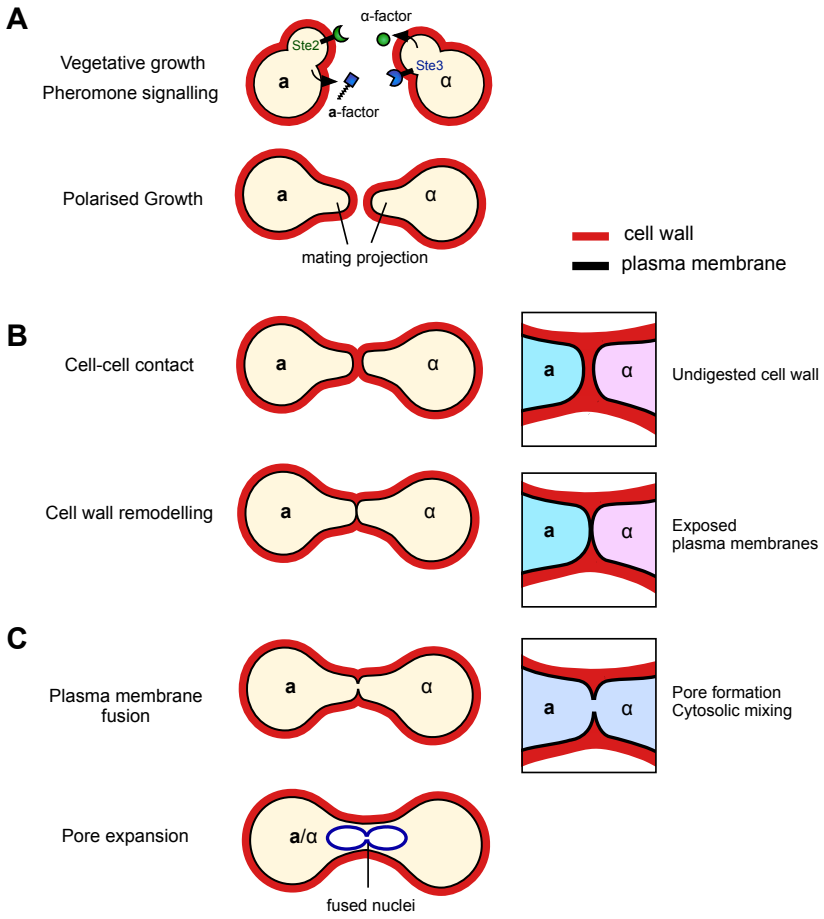

Figure 8. Yeast mating pathway overview. A. Initial detection of mating partners via pheromone signalling**.** Pheromone exchange between **a** and α cells induces vegetatively growing cells to undergo cell cycle arrest and form mating projections. α-factor secreted by α cells is detected by Ste2, the α-factor receptor. **a**-factor secreted by **a** cells is detected by Ste3, the **a**-factor receptor. **B.** Cell-cell contact leads to the assembly of a mating pair with fused cell walls. The cell wall at the cell-cell contact site is carefully digested, exposing the opposing plasma membranes between two partners. **C.** Plasma membrane fusion and pore expansion of the nascent zygote. Fusion of the two membranes allows the two cytosols to mix. Continued pore expansion is followed by fusion of the two nuclei (blue), forming a diploid zygote.

1.4.2 Pheromone reception and polarised growth

1.4.2.1 Pheromone reception

The reception of pheromones induces a variety of intracellular physiological changes which acts to prepare the haploid cell for mating. Three major outcomes are

achieved: **i)** cell cycle arrest in G1 phase, **ii)** upregulation of pheromone-regulated genes required for mating and **iii)** cell polarisation towards prospective mating partners **(Figure 9)**. The components, their interactions and temporal order in which they act are well understood. For brevity, only the components considered critical for the three outcomes will be described. Note that the intracellular signalling that ensues after pheromone detection are similar in both mating types, if not identical.

Pheromone signalling between **a** and α cells are governed by pheromone receptors; Ste2 (which binds α-factor) present only in **a** cells and Ste3 (which binds **a**-factor) present only in α cells (Bender and Sprague, 1986; Hagen et al., 1986; Jenness et al., 1983). Ste2 and Ste3 are G protein-coupled receptors (GPCRs) which reside on the plasma membrane. Binding of pheromones to the cognate receptors changes their conformation, allowing GDP within the Gα subunit to be exchanged for GTP **(Figure 9)**. Binding of GTP in turn changes the conformation of the α subunit, causing the β and γ subunits to dissociate (Ste4 and Ste18) (Bardwell, 2004). The now freed Gβγ is a critical effector of the subsequent response. Dissociated Gβγ is able to recruit Ste5, the scaffold protein for Mitogen activated protein kinase (MAPK) signalling. Free Gβγ also binds Cdc24, a guanine nucleotide exchange factor (GEF), which activates the GTPase Cdc42. Activated Cdc42 activates Ste20, a protein kinase also required for subsequent MAPK signalling. In addition, free Gβγ binds Far1, which induces cell cycle arrest at the G1 phase (Chang and Herskowitz, 1990).

MAPK signalling commences from Ste20-phosphorylation of Ste11, the top most member of the MAPK cascade (MAPKKK) (Bardwell, 2004). The phosphorylation of Ste11 activates Ste11 and consequently activates the MAPKK Ste7 by phosphorylation. In turn, activated Ste7 phosphorylates the MAPK Fus3. The Ste5 scaffold is a central component for the signalling cascade as it recruits each protein kinase of the MAPK cascade. Phosphorylated Fus3 activates Ste12, a positive transcriptional regulator for pheromone response genes. In the absence of pheromone, Ste12 is bound by two repressors, Dig1 and Dig2. Ste12 activation occurs by Fus3 mediated phosphorylation of the Dig1/Dig2/Ste12 complex, releasing Ste12 (Tedford et al., 1997).

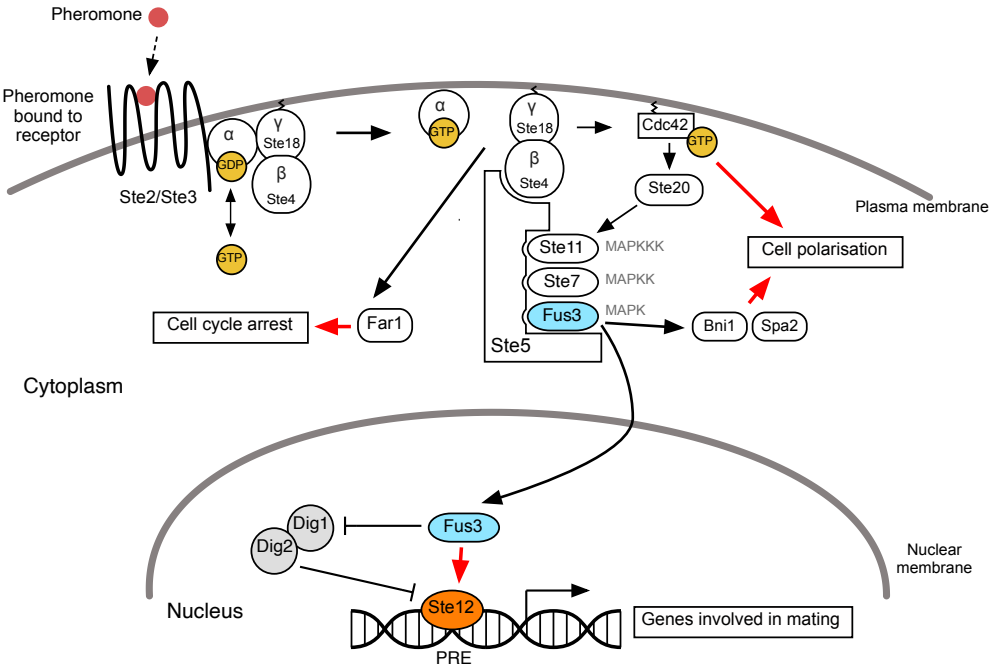

Figure 9. Pheromone signalling response. Pheromone binding to the pheromone receptor leads to the release of Gβγ subunits. This release triggers Far1-mediated cell cycle arrest and the activation of the MAPK cascade. Activated Fus3 leads to activation of Ste12, which activates transcription of genes involved in mating. Ste12 binds to pheromone response element (PRE) DNA motifs in the promoters of pheromone regulated genes. Active Fus3 also phosphorylates Bni1 and Spa2 which acts to polarise the cell.

1.4.2.2 Polarised growth

The final outcome of the pheromone response is to elicit polarisation in the direction of the pheromone gradient established by the mating partner. Polarised growth is achieved by the polarised secretion of vesicles, actin cytoskeleton remodelling and cell wall remodelling. Consequently, the cell forms mating projections, and the morphology of this elongated yeast cell is often referred to in the literature as a ‘shmoo’. Cell polarity is established primarily by the activation and compartmentation of Cdc42 via the MAPK pathway. Cdc42 acts to orient the actin cables to the site of growth, resulting in the assembly of a polarised actin cytoskeleton. Such polarisation is necessary to direct the transport of secretory vesicles. The assembly of actin cables is regulated by the formin Bni1, which itself is also activated by Fus3 (Matheos et al., 2004). Actin nucleation is also assisted by other polarity regulators such as Spa2 (also activated by Fus3 (Waszczak et al., 2019)) and Pea2,

which together with Bni1 comprise a macromolecular complex known as the polarisome (Bni1, Spa2, Pea2) (Sheu et al., 1998; Xie and Miao, 2021).

1.4.3 Cell-cell contact and cell wall degradation

Polarised gametes eventually form physical contacts with a closely located partner cell. Cell-cell adhesion is assisted through cell wall associated glycoproteins known as agglutinins, which are upregulated upon pheromone induction (Terrance and Lipke, 1987; Zhao et al., 2001). Upon cell-cell contact, the two cell walls at the point of contact are remodeled. This process comprises two major steps. Firstly, the formation of a continuous cell wall layer which acts to physically link the two cells together; at which stage is referred as a mating pair (also termed in the field as prezygotes). In the second step (likely acting concurrently with the first), the cell wall at the cell-cell contact site is selectively degraded by glucanases to expose the opposing underlying plasma membranes to each other, allowing for their fusion. The full set of glucanases responsible are unknown, although some putative glucanases have been implicated, such as Scw4 and Scw10 (Cappellaro et al., 1998). Likely a number of glucanases are involved, because no single glucanase sufficiently blocks degradation when genetically knocked out.

Cell wall removal is primarily governed by Fus1 and Fus2 (Gammie et al., 1998; Trueheart et al., 1987). Fus1 is a single-pass membrane protein which directs secretory vesicles to the mating tip projection. Δ*fus1* mutants fail to cluster vesicles at the cell-cell contact site (Gammie et al., 1998). In contrast, Fus2 is a cytoplasmic protein, and Δ*fus2* mutants display wt-like clustered vesicles at the cell-cell contact site, indicating Fus2 regulates an aspect of cell wall remodeling other than vesicle clustering. Fus2 interacts with Cdc42 and a BAR domain protein, Rvs161 (Brizzio et al., 1998; Nelson et al., 2004; Stein et al., 2016; Ydenberg et al., 2012). Due to the ability of BAR domains to sense membrane curvature, it is suggested Fus2/Rvs161 complexes may recognise changes in plasma membrane curvature during the transition from curved membranes at mating projections to flat membranes at cell-cell contact sites of mating pairs (Smith et al., 2017). Such recognition might aid clustering of Cdc42 and promote secretory vesicle release. Fus1 and Fus2 regulate two independent pathways for cell wall removal, because Δ*fus1*Δ*fus2* × Δ*fus1*Δ*fus2* mating pairs are completely blocked in fusion, exhibiting an undigested cell wall at the cell-cell contact site (Gammie et al., 1998; Trueheart et al., 1987).

1.4.4 Plasma membrane fusion

Once the intervening cell wall is degraded, the plasma membranes are exposed to one another. Fusion occurs quickly upon degradation, indicating a tight coupling between cell wall degradation and the membrane fusion reaction. Mating pairs which are undergoing cell wall remodelling require ongoing secretion of vesicles. Presumably, these vesicles contain the fusion machinery components required for plasma membrane fusion to occur (Grote, 2010).

1.4.5 Molecular players acting at plasma membrane fusion

1.4.5.1 Pheromone regulated membrane protein 1 (Prm1)

The main fungal protein known to regulate the membrane fusion step is Prm1, a 4-pass transmembrane protein containing two large ectoplasmic loops. Prm1 is only expressed upon pheromone exposure (Heiman and Walter, 2000), where it is localised to the mating projection surface and to the eventual cell-cell contact sites of the mating pair (Heiman and Walter, 2000; Olmo and Grote, 2010a).

Only ~50% of Δ*prm1* × Δ*prm1* crosses successfully fuse (Heiman and Walter, 2000). The fusion arrested mating pairs are dead-end states, showing a dissolved cell wall and either unfused plasma membranes or lysis. The unfused plasma membranes, separated by ~8 nm, protrude into the cytoplasm of one of the partners, phenotypically termed as a cytoplasmic bubble (Heiman and Walter, 2000) **(Figure 10)**. In addition to bubbles, cell lysis of Δ*prm1* mating pairs can occur after contact of the two opposing plasma membranes (Jin et al., 2004). Therefore, the lysis phenomenon is interpreted as an excessive or mis-regulated force of cell-membranes during fusion of the bilayers. Since a proportion of mating pairs are able to fuse in the absence of Prm1 and is therefore not strictly essential, Prm1 is thought not to be a fusogen *per se*, but rather a regulator which allows fusion to proceed safely upon fusion machinery engagement.

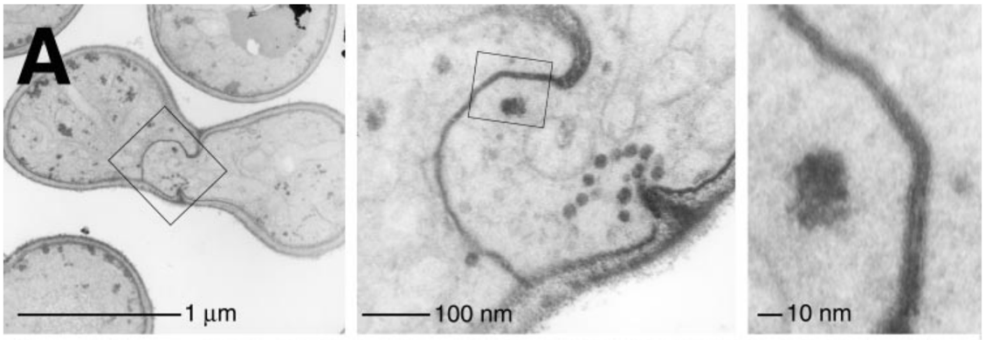

Figure 10. Cytoplasmic bubbles of Δ*prm1* mating pairs. Electron micrographs of Δ*prm1* mating pairs show that the intervening cell wall of the mating pair has been digested, however the two plasma membranes are unfused, separated by ~8 nm. Figure is from Heiman and Walter (2000).

Unlike wt mating pairs, fusion of Δ*prm1* mutants are sensitive to external Ca^{2+} levels. Depletion of Ca^{2+} results in higher frequencies of lysis. A similar increase in frequency of lysis is observed when Δ*prm1* pairs are additionally absent for Tcb3, a synaptotagmin homolog. Since synaptotagmins are Ca^{2+} dependent regulators of intracellular membrane fusion, it was suggested that Tcb3 can partially suppress fusion attempted-lysis in Δ*prm1* mutants by a Ca^{2+} dependent membrane repair pathway (Aguilar et al., 2007). Prm1 homologs are present in numerous fungi, and those organisms in which Prm1 was studied have confirmed its role in mating. In *Neurospora crassa*, Prm1 acts similarly to Prm1 in *S. cerevisiae*. *N. crassa* Δ*prm1* × Δ*prm1* matings display an approximate 50% fusion defect (Fleißner et al., 2009). In addition to fertilisation, *N. crassa* carry out somatic cell fusions between vegetatively growing germlings and hyphae to form syncytial networks. *PRM1* null mutants also display fusion arrest during these fusion events (Fleißner et al., 2009). The non-fused cells display unfused plasma membranes pushed into the cytoplasm of one of the cells akin to the cytoplasmic bubbles found in *S. cerevisiae* Δ*prm1* pairs. *N. crassa* Δ*prm1* mating pairs also display lysis, and this is influenced by external Ca^{2+} levels (Palma-Guerrero et al., 2014).

In the fission yeast *Schizosaccharomyces pombe*, deletion of Prm1 leads to a stronger fusion defect; less than 5% of pairs fuse. In contrast to budding yeast, *S. pombe* Δ*prm1* × Δ*prm1* mating pairs do not display cytoplasmic bubbles as the endpoint phenotype. Instead, the pairs are separated by cell wall material. This may be due to a more efficient cell wall deposition mechanism present in *S. pombe* in contrast to *S. cerevisiae*, which quickly repairs

openings in the cell wall of the mating junction. Consistent with the idea of a quickly repaired cell wall, Δ*prm1 S. pombe* mating pairs do not lyse. In *S. pombe,* Prm1 was also implicated to organise the membrane. During mating of wt cells, phosphatidylserine (PS) is excluded from cell-cell contact sites shortly before fusion takes place. Such exclusion of PS does not occur in Δ*prm1* mating pairs (Curto et al., 2014).

Prm1 was also confirmed to be required for mating in *Cryptococcus*. *C. neoformans* Δ*prm1* mutants are significantly fusion arrrested (Fu and Heitman, 2017). In *C. deneoformans*, Prm1 displays a unilateral arrest when deleted i.e. Δ*prm1* × wt pairs show a significant fusion arrest. This is unlike the cases described for the other mentioned fungal species, where Prm1 needs to be absent in both partners for fusion arrest to take place. Regardless of these differences, it is clear that Prm1 plays a central and conserved role for fusion in the fungal kingdom. Since no Prm1 homologs are found in other kingdoms, the fusion mechanism employed in fungi is likely to be distinct from the currently characterised fusion proteins.

1.4.5.2 Fig1

Fig1 is a 4-pass transmembrane protein which like Prm1, is pheromone regulated and localised to mating junctions (Aguilar et al., 2007; Erdman et al., 1998). In *S. pombe*, the mating-involved Dni1 and Dni2 proteins show sequence similarity to Fig1 and together these proteins form part of the fungal claudin family (Clemente-Ramos et al., 2009). The proteins contain a claudin like consensus motif within the first ectodomain, which was first described for mammalian claudins (Zhang et al., 2006). Deletion of Dni1 or Dni2 in *S. pombe* result in a cell fusion defect primarily at the stage of cell wall remodelling (Clemente-Ramos et al., 2009). Deletion of *FIG1* results in a mild fusion defect during mating, and such mating pairs display cytoplasmic bubbles or lysis (Aguilar et al., 2007). The deletion of both *PRM1* and *FIG1* results in a greater frequency of fusion arrested mating pairs than the single mutant counterparts, indicating Prm1 and Fig1 have independent functions (Aguilar et al., 2007). In these Δ*prm1*Δ*fig1* mating pairs, cytoplasmic bubbles are the predominant phenotype. During mating, Ca^{2+} influx pathways are activated and Fig1 is a regulator of such influx into the cell (Muller et al., 2003). High Ca^{2+} concentrations can suppress the Δ*fig1* cell fusion arrest. It is unclear whether the Ca^{2+} influx function of Fig1

is involved in cell fusion, because removal of external Ca^{2+} does not affect the fusion of wt mating pairs.

1.5 Membrane requirements for *S. cerevisiae* cell fusion

1.5.1 Ergosterol structural requirements for fusion

Unlike cholesterol in mammalian cells, ergosterol is the primary sterol present in *S. cerevisiae*. In ergosterol biosynthesis enzyme mutants, sterol intermediates instead of ergosterol become prevalent. A number of *erg* mutants are impaired for fusion, with some, such as Δ*erg3* and Δ*erg6* displaying a strong plasma membrane fusion arrest with cytoplasmic bubbles **(Figure 11)**. Electron micrographs of Δ*erg6* mating pairs show the presence of cytoplasmic bubbles similar to ones observed in Δ*prm1* mating pairs (Jin et al., 2008). Unlike Δ*prm1* mutants however, the plasma membrane fusion arrest phenotype is not a dead-end, as the Δ*erg6* cytoplasmic bubbles can resolve over time to allow a fusion pore to form. In addition, ergosterol and Prm1 have independent roles in promoting membrane fusion, because Δ*prm1*Δ*erg6* mating pairs are more strongly fusion arrested than their respective single null mutant pairs (Jin et al., 2008). In *N. crassa*, changes in sterol composition also impair fusion. Germling mutants of Δ*erg10a*/Δ*erg10b* (homologs of *S. cerevisiae ERG3*) show unfused plasma membranes during vegetative cell fusion (Weichert et al., 2020). The requirement of ergosterol to facilitate membrane fusion is therefore conserved across different fungal species.

In addition to regulating plasma membrane fusion, ergosterol has a role in mediating proper pheromone signalling. The MAPK scaffold Ste5 is less polarised in Δ*erg3* cells (Jin et al., 2008). *FUS1* transcription in response to pheromone is also weakened in Δ*erg3* and Δ*erg6* cells. Could the plasma membrane fusion defect of ergosterol mutants simply be explained by the upstream impairment of pheromone signalling? There is some evidence to suggest that this is not the case. Inactivating Ste5 activity through a temperature sensitive *ste5* mutant indeed inhibits fusion, however mating pairs are instead arrested at the level of cell wall remodelling. This suggests that ergosterol inhibits plasma membrane fusion by a mechanism independent to its role in pheromone signalling.

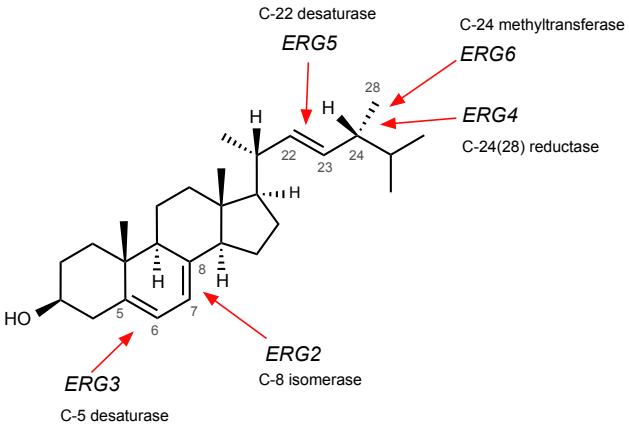

Figure 11. Ergosterol chemical structure and biosynthesis mutants which display fusion arrest phenotypes. *ERG* genes assessed for effects on yeast cell fusion were from Jin et al. (2008) and Aguilar et al. (2010). Out of the genes tested, deletion of *ERG3* and *ERG6* results in the strongest frequency of plasma membrane fusion arrest.

1.5.2 Sphingolipids and lipid rafts

Sphingolipid metabolic pathways are conserved between mammals, plants and fungi. The head groups of mammalian sphingolipids typically possess one or more sugar residues. Sphingomyelins, the predominant sphingolipid in mammals, are formed from attachment of a phosphatidylcholine head group to ceramide. In *S. cerevisiae*, complex sphingolipids instead contain inositol-based head groups **(Figure 12)**. Mass spectrometry based lipidomic studies generally found either inositol phosphorylceramide (IPC) or the terminal sphingolipid mannosyldiinositol phosphorylceramide ($M(IP)_2C$) to be the most abundant (Ejsing et al., 2009; Klose et al., 2012; Surma et al., 2011). Furthermore, complex sphingolipids also show preferred localisation to certain subcellular organellar membranes. IPC is enriched in the Golgi and vacuoles whereas the mannosylated sphingolipids are enriched in the plasma membrane (Hechtberger et al., 1994). Thus, regardless of whichever sphingolipid species is most abundant, it is generally accepted that mannosylated sphingolipids are enriched in the plasma membrane compared to other organelles (Hechtberger et al., 1994; Surma et al., 2011).

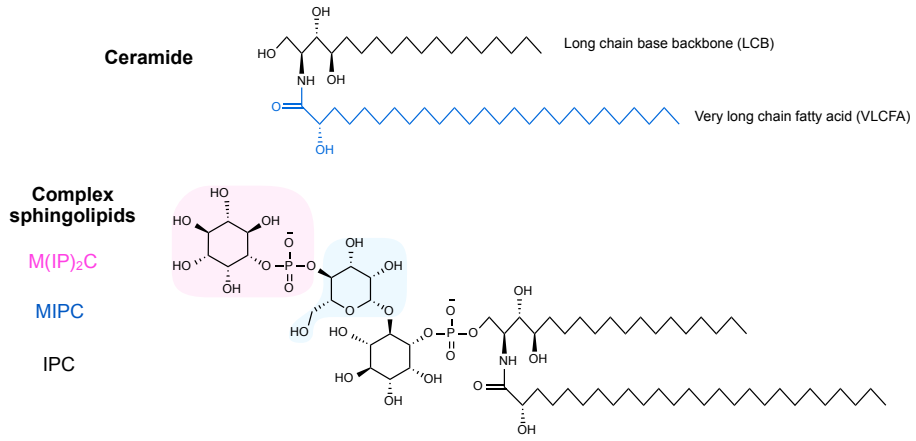

Figure 12. *S. cerevisiae* sphingolipid species. The sphingolipid species comprises ceramide, which consist of a long chain base (LCB) backbone (black) and a very long chain fatty acid moiety (VLCFA) (blue). Ceramides are formed by acylation of LCBs with VLCFA-Coenzyme A. Complex sphingolipids are formed by the attachment of head groups. The simplest is IPC, containing an inositol phosphate head group. Two further distinct head group attachments, mannose and inositol phosphate, form the terminal sphingolipid $M(IP)_2C$.

Eukaryotic cells contain membrane microdomains known as lipid rafts. According to the lipid raft model, lipid rafts are formed by interactions between ergosterol and sphingolipids, whereby the sphingolipids laterally associate, and the ergosterol molecules fill in the voids (Simons and Ikonen, 1997). Lipid rafts are hypothesised to be required for the sorting of membrane proteins and to act as a signalling hub. The existence of such domains in mammalian cells has been debated because in such cells the microdomains are small (approximately 5-200 nm), making them difficult to study. Studies utilizing emergent stimulated emission depletion (STED) fluorescence microscopy suggest that such microdomains do exist in mammalian cells (Eggeling et al., 2009).

Unlike mammalian cells, yeast possess membrane microdomains which are larger (micron-meter sized) and more stable, allowing their detection by fluorescence microscopy. Furthermore, the tip of the yeast mating projection is particularly enriched with ergosterol, and thus is likely to possess lipid rafts. The lipid rafts are therefore postulated to both segregate and retain mating related membrane proteins to the tip of the mating projection. For instance, Fus1 is normally tightly clustered at the tip of mating projections during the polarised growth of pheromone responding cells (Bagnat and Simons, 2002a). The clustering does not necessarily depend on polarised growth, because Fus1 that is ectopically expressed and already present on the plasma membrane of vegetative cells also cluster to

the early mating projection upon pheromone treatment (Bagnat and Simons, 2002a). This suggests in favour of a lipid raft dependent mechanism of segregation. Ergosterol and early sphingolipid biosynthesis mutants (at the level of ceramide synthesis) fail to retain Fus1 at the mating tip and instead localisation is more diffuse alongside the rest of the cell body. These mutants also mate less efficiently, and the failure to retain mating related proteins to the tip of the mating projection is likely a major contributing factor to this phenotype. Furthermore, studies using sphingolipid biosynthesis mutants suggested that mannosylated sphingolipids are not required for cell fusion. Cells do however, require ceramide synthesis for pheromone signalling, such as cell cycle arrest and MAPK dependent transcription of pheromone regulated genes (Villasmil et al., 2016). With the lipid raft model in mind, this may suggest that lipid rafts in yeast may be sufficiently formed with ceramide as the sphingolipid species.

1.6 Aims of this study

Given the incomplete penetrance of the fusion arrested phenotype of Δ*prm1* mutants, it is evident that there are additional unknown genes which are involved in the fusion step. Therefore, the first motivation in this study was to identify novel regulators which act on the cell-membrane fusion step. To take advantage of the genetic tractability of yeast, I set up a genome-wide screen based on genetic overexpression, using Δ*prm1* as a query sensitised background. The choice of Δ*prm1* was important; because Prm1 is not involved in the upstream process of mating, I hypothesised that any genes identified here would also act specifically on the plasma membrane fusion reaction.

The second motivation of the study was to elucidate the mechanism of action employed by Prm1 to promote plasma membrane fusion. From the existing literature, it is clear that Prm1 lies at the core of the plasma membrane fusion reaction across numerous fungi. Therefore, elucidating this aspect is necessary to ultimately understand fungal cell fusion. As a four-pass multipass membrane protein, Prm1 is unique when compared to other well understood membrane fusion proteins, which are usually single-pass membrane proteins. Furthermore, there are a number of other multipass membrane proteins involved in plasma membrane fusion in other systems (such as DCST1 and DCST2 in sperm-egg fusion) with scant information on how they function. Prm1 might enact similar roles to

these proteins and therefore the knowledge gained from such elucidation might offer new hypotheses for other distinct cell fusion proteins. To this end, mutational analysis was performed to characterise domains of interest on the large ectodomain of Prm1.

Through the mutational investigations into Prm1 *in vivo* during this study, a hypothesis arose that Prm1 might act by interacting with membranes in *trans*. As a complementary approach to study this putative molecular function of Prm1, I initiated attempts to study Prm1 *in vitro*, which better reports function in a minimalist system. For this, I carried out an approach to purify full-length Prm1 from native yeast cells and subsequently reconstituted Prm1 into synthetic vesicles. With the exception of pheromone receptors, to my knowledge this is the first instance of an attempt to study a purified component of the putative yeast cell membrane fusion machinery (Shi et al., 2007).

Chapter 2. Materials and Methods

2.1 Electronic devices and instruments

Table 1. Devices and instruments used in this study.

Device	Supplier	Use
12-manifold vacuum	Millipore	Yeast mating assays
96-well manifold vacuum	Enzo Life Sciences	96-well yeast mating assays
96-well pin replicator VP408FH	V & P Scientific	96-well yeast colony library maintenance
Avanti® J-26 XP centrifuge	Beckman Coulter	Harvest of 1 L cultures
BD Accuri™ C6 Plus flow cytometer	BD Biosciences	BiFC fusion experiments and proteoliposome measurements
Benchtop centrifuge 5424	Eppendorf	Centrifugation of 1.5 mL Eppendorf samples
Benchtop centrifuge 5810R	Eppendorf	Harvest of 2-50 mL cultures
Cell density meter CO8000	Biochrom	Measurement of OD600 in cuvettes
ChemiDoc MP imaging system	Bio-Rad	In-gel fluorescence and chemiluminescence
DynaPro® NanoStar II® DLS detector	Wyatt Technology	DLS measurements
FastGene blue LED transilluminator	Nippon Genetics Europe GmbH	Visualisation of DNA agarose gels and gel extraction
Laser scanning confocal microscope 800 (LSM800)	Zeiss	Confocal microscopy
Mechanical cell disruptor bead beater	Biospec	Yeast cell lysis by glass beads
MSM400 Dissector microscope	Singer Instruments	Tetrad dissection of yeast spores
Nanodrop spectrophotometer	Thermo Scientific	DNA and protein concentration measurement
New Brunswick™ Excella® E24 orbital shaker	Eppendorf	Incubation and shaking of yeast cultures
NGC chromatography system	Bio-Rad	FSEC
Optima™ L-70K ultracentrifuge	Beckman Coulter	Ultracentrifugation of membranes

Optima™ MAX-XP tabletop ultracentrifuge	Beckman Coulter	Ultracentrifugation of small volume samples

2.2 Cloning

2.2.1 Construction of plasmids

Table 2. Plasmids used in this study. Abbreviations: RF, restriction free. RD, restriction digest. GA, Gibson assembly. All plasmids were generated in this study unless otherwise indicated.

Plasmid	Description	Method of generation	Parental vector	Reference
pGP564	Empty 2µ *LEU2* vector			Jones et al., 2008
pGBKT7	Empty vector (contains $_{pr}$*ADH1* and $_{T}$*ADH1*)			Clontech
pYM44	C-terminal yeGFP vector			Euroscarf
pRS425	Empty 2*µ* *LEU2* vector			Christianson et al., 1992.
pRS426	Empty 2µ *URA3* vector			Christianson et al., 1992.
pRS316	Empty *CEN6 URA3* vector			Sikorski & Hieter., 1989
pAS01	Empty 2µ *URA3* vector containing $_{pr}$*ADH1*-mcs-$_{T}$*ADH1*	RF PCR	pRS426	
pAS23	Empty 2µ *LEU2* vector containing $_{pr}$*ADH1*-mcs-$_{T}$*ADH1*	RD PvuI	pRS425	
pAS41	$_{pr}$*PRM1*(700 bp)-*PRM1*-$_{T}$*PRM1 CEN6 URA3*	GA SacI BamHI	pGP564	
pAS75	Empty *CEN6 URA3* vector containing $_{pr}$*ADH1*-mcs-$_{T}$*ADH1*	RD PvuI	pRS316	
	Sur1 fusion experiments			
pAS81	YGPM8p07 fragment 1 (*LCL1*)	RD PstI SalI	pGP564	
pAS82	YGPM8p07 fragment 2 (*SUR1*)	RD PstI SalI	pGP564	
pAS83	YGPM8p07 fragment 3 (*PDR12*, *GRX5*)	RD PstI SalI	pGP564	
pAS89	$_{pr}$*SUR1-SUR1-*$_{T}$*ADH1* 2*µ* *URA3*	RD NheI SacI	pAS01	
pAS95	$_{pr}$*SUR1-SUR1(AxA)-*$_{T}$*ADH1* 2*µ* *LEU2*	GA NheI AatII	pAS23	
pAS91	$_{pr}$*CSH1-CSH1-*$_{T}$*CSH1* 2*µ* *LEU2*	RD BamHI SalI	pGP564	
pAS92	$_{pr}$*CSG2-CSG2-*$_{T}$*CSG2* 2*µ* *LEU2*	RD BamHI SalI	pGP564	

pAS93	$_{pr}$*AUR1-AUR1-*$_{T}$*AUR1* 2μ *LEU2*	RD SacI SalI	pGP564
pAS94	$_{pr}$*IPT1-IPT1-*$_{T}$IPT*1* 2μ *LEU2*	RD BamHI SalI	pGP564
pAS241	$_{pr}$*CSG2-CSG2-*$_{T}$*CSG2* 2μ *URA3*	RD NheI SacI	pAS01
	Sur1-mNG experiments		
pAS57	*-mNG-*$_{T}$*ADH1* 2μ *URA3*		pAS01
pAS64	*-mNG-*$_{T}$*ADH1 CEN6 URA3*		pAS75
pAS87	$_{pr}$*SUR1-SUR1-mNG-*$_{T}$*ADH1* 2μ *URA3*	RD NheI SalI	pAS57
pAS88	$_{pr}$*SUR1-SUR1-mNG-*$_{T}$*ADH1 CEN6 URA3*	RD NheI SalI	pAS64
pAS98	$_{pr}$*SUR1-SUR1*(*AxA*)*-mNG-*$_{T}$*ADH1* 2μ *URA3*	RD NheI SalI	pAS57
	***PRM1 in vivo* experiments**		
pAS113	$_{pr}$*PRM1*(700 bp)*-PRM1-*$_{T}$*ADH1 CEN6 URA3*	GA KpnI SacI	pAS100
pAS153	$_{pr}$*PRM1-PRM1 L106A-*$_{T}$*ADH1 CEN6 URA3*	GA KpnI SacI	pAS113
pAS154	$_{pr}$*PRM1-PRM1 F109A-*$_{T}$*ADH1 CEN6 URA3*	GA KpnI SacI	pAS113
pAS186	$_{pr}$*PRM1-PRM1 I111A-*$_{T}$*ADH1 CEN6 URA3*	GA KpnI SacI	pAS113
pAS155	$_{pr}$*PRM1-PRM1 L113A-*$_{T}$*ADH1 CEN6 URA3*	GA KpnI SacI	pAS113
pAS156	$_{pr}$*PRM1-PRM1 C120S-*$_{T}$*ADH1 CEN6 URA3*	GA KpnI SacI	pAS113
pAS192	$_{pr}$*PRM1-PRM1 L106D-*$_{T}$*ADH1 CEN6 URA3*	GA KpnI SacI	pAS113
pAS193	$_{pr}$*PRM1-PRM1 F109D-*$_{T}$*ADH1 CEN6 URA3*	GA KpnI SacI	pAS113
pAS194	$_{pr}$*PRM1-PRM1 I111D-*$_{T}$*ADH1 CEN6 URA3*	GA KpnI SacI	pAS113
pAS195	$_{pr}$*PRM1-PRM1 L113D-*$_{T}$*ADH1 CEN6 URA3*	GA KpnI SacI	pAS113
pAS114	$_{pr}$*PRM1-*Δ4K*-PRM1-*$_{T}$*ADH1 CEN6 URA3*	GA KpnI SacI	pAS113
pAS157	$_{pr}$*PRM1-PRM1 L140A I141A-*$_{T}$*ADH1 CEN6 URA3*	GA KpnI SacI	pAS113
pAS158	$_{pr}$*PRM1-PRM1 L143A V144A-*$_{T}$*ADH1 CEN6 URA3*	GA KpnI SacI	pAS113
pAS159	$_{pr}$*PRM1-PRM1 V151A-*$_{T}$*ADH1 CEN6 URA3*	GA KpnI SacI	pAS113
pAS161	$_{pr}$*PRM1-PRM1 I165A I166A-*$_{T}$*ADH1 CEN6 URA3*	GA KpnI SacI	pAS113
pAS162	$_{pr}$*PRM1-PRM1 F179A F180A-*$_{T}$*ADH1 CEN6 URA3*	GA KpnI SacI	pAS113
pAS200	$_{pr}$*PRM1-PRM1* Δ140-180-$_{T}$*ADH1 CEN6 URA3*	GA KpnI SacI	pAS113
pAS201	$_{pr}$*PRM1-PRM1* Δ140-200-$_{T}$*ADH1 CEN6 URA3*	GA KpnI SacI	pAS113
pAS216	$_{pr}$*PRM1-PRM1* Δ140-220-$_{T}$*ADH1 CEN6 URA3*	GA KpnI SacI	pAS113
pAS199	$_{pr}$*PRM1-PRM1* 8-alanine-$_{T}$*ADH1 CEN6 URA3*	GA KpnI SacI	pAS113
	***PRM1-mNG* experiments**		
pAS100	$_{pr}$*PRM1-PUN1-mNG CEN6 URA3*	RD SphI SalI	pRS316
pAS143	$_{pr}$*PRM1-PRM1-mNG-*$_{T}$*ADH1 CEN6 URA3*	RD SphI SalI	pAS100
pAS243	$_{pr}$*PRM1-PRM1 L106D-mNG-*$_{T}$*ADH1 CEN6 URA3*	RD SphI SalI	pAS100
pAS244	$_{pr}$*PRM1-PRM1 F109D-mNG-*$_{T}$*ADH1 CEN6 URA3*	RD SphI SalI	pAS100
pAS245	$_{pr}$*PRM1-PRM1 C120S-mNG-*$_{T}$*ADH1 CEN6 URA3*	RD SphI SalI	pAS100
pAS207	$_{pr}$*PRM1-PRM1* Δ140-180- *mNG-*$_{T}$*ADH1 CEN6 URA3*	RD SphI SalI	pAS100
pAS211	$_{pr}$*PRM1-PRM1* Δ140-200- *mNG-*$_{T}$*ADH1 CEN6 URA3*	RD SphI SalI	pAS100
pAS218	$_{pr}$*PRM1-PRM1* Δ140-220- *mNG-*$_{T}$*ADH1 CEN6 URA3*	RD SphI SalI	pAS100
pAS205	$_{pr}$*PRM1-PRM1* 8-alanine- *mNG-*$_{T}$*ADH1 CEN6 URA3*	RD SphI SalI	pAS100
	***PRM1-V5* experiments**		
pAS144	$_{pr}$*PRM1-PUN1-V5 CEN6 URA3*	RD SphI SalI	pAS75
pAS150	$_{pr}$*PRM1-PRM1-V5-*$_{T}$*ADH1 CEN6 URA3*	RD SphI SalI	pAS144

pAS206	$_{pr}$*PRM1-PRM1* Δ140-180-*V5-$_{T}$ADH1 CEN6 URA3*	RD SphI SalI	pAS144
pAS210	$_{pr}$*PRM1-PRM1* Δ140-200-*V5-$_{T}$ADH1 CEN6 URA3*	RD SphI SalI	pAS144
pAS219	$_{pr}$*PRM1-PRM1* Δ140-220-*V5-$_{T}$ADH1 CEN6 URA3*	RD SphI SalI	pAS144
pAS204	$_{pr}$*PRM1-PRM1* 8-alanine-*V5-$_{T}$ADH1 CEN6 URA3*	RD SphI SalI	pAS144
pAS212	$_{pr}$*PRM1-PRM1 L106D-V5-$_{T}$ADH1 CEN6 URA3*	RD SphI SalI	pAS144
pAS213	$_{pr}$*PRM1-PRM1 F109D-V5-$_{T}$ADH1 CEN6 URA3*	RD SphI SalI	pAS144
pAS214	$_{pr}$*PRM1-PRM1 I111D-V5-$_{T}$ADH1 CEN6 URA3*	RD SphI SalI	pAS144
pAS215	$_{pr}$*PRM1-PRM1 L113D-V5-$_{T}$ADH1 CEN6 URA3*	RD SphI SalI	pAS144
pAS181	$_{pr}$*PRM1-PRM1 C120S-V5-$_{T}$ADH1 CEN6 URA3*	RD SphI SalI	pAS144
	Prm1 purification		
pAS151	$_{pr}$*GAL1-VSVG-mCherry 2μ URA3*		pAS01
pAS163	$_{pr}$*PRM1-PRM1-eGFP-StrepII URA3 CEN*	RD SalI SacI	pAS143
pAS198	$_{pr}$*GAL1-PRM1-eGFP-StrepII 2μ URA3*	RD XhoI SacI	pAS151
pAS223	$_{pr}$*GAL1-PRM1-HRV3C-eGFP-StrepII 2μ URA3*	RD SalI SacI	pAS198
pAS226	$_{pr}$*TEF1-PRM1-HRV3C-eGFP-StrepII 2μ URA3*	GA KpnI NheI	pAS01
pAS231	$_{pr}$*GAL1-PRM1-HRV3C-yeGFP-StrepII 2μ URA3*	RD SalI NotI	pAS223
pAS235	rDNA Up Down *NatNT2*	RD SalI AscI RD SacI SpeI	pFA6-natNT2
pAS236	$_{pr}$*GAL1-PRM1-HRV3C-yeGFP-StrepII* integration *NatNT2*	RD XbaI SacI	pAS235

2.2.1.1 Restriction digest

Restriction digests were performed with restriction enzymes from NEB. Incubation was done at 37 °C for at least 2 h. After incubation, digested DNA was ran via gel-electrophoresis, gel extracted using a Qiagen Gel Extraction Kit, and eluted in 20 μL of elution buffer (Qiagen).

Table 3. Typical restriction digest reaction. 20 μL reaction volumes were used.

Reagent	Volume (μL)	DNA amount (ng)
Plasmid DNA or	X	400-500
PCR amplicon DNA	Y	50-1000
Cutsmart buffer (NEB) (10X)	1	
Restriction enzyme 1 (NEB)	1	
Restriction Enzyme 2 (NEB)	1	
ddH_2O	Make up to 20 μL reaction volume	

2.2.1.2 DNA Ligation

DNA digested with restriction enzymes were ligated with T4 DNA Ligase (NEB) at RT for 30 min – 1 h **(Table 4)**. 1 μL of a 10 μL ligation reaction was then transformed into 80 μL chemically competent XL-10 Gold *E. coli* cells.

Table 4. Example ligation reaction. 3:1 molar insert:vector ratio was used. Example DNA sizes are shown, with calculated DNA amount required for 3:1 ratio. Volumes of insert fragment and cut vector will depend on DNA concentration and amount of DNA.

Reagent	Volume (µL)	DNA amount (ng)	DNA size (bp)
Insert fragment	X	12	1000
Cut vector	Y	20	5000
DNA Ligase buffer (10X)	1		
DNA Ligase	1		
ddH_2O	Make up to 10 µL reaction volume		

2.2.1.3 High copy *URA3* plasmid pAS01

A variant of the high copy pRS426 (Christianson et al., 1992) plasmid containing the *ADH1* promoter and *ADH1* terminator sequences flanking the multiple cloning site was generated. pGBKT7, which contains the *ADH1* promoter, was used to amplify the *ADH1* promoter by polymerase chain reaction (PCR) using primers AS001 and AS002. Phusion high fidelity (HF) polymerase (NEB) was used for typical 50 µL PCR reactions **(Table 5 and Table 6)**. The ends of the amplicon contain sequence homology to regions of pRS426 so that the promoter sequence can be inserted into the region directly upstream of the multiple cloning site. A subsequent PCR using both the amplicon (van den Ent and Löwe, 2006) and pRS426 was carried out, referred to as restriction free (RF) PCR. Here the amplicon effectively acts as the primer pair since the 3' ends contain short homology regions. This PCR generated a plasmid construct containing the *ADH1* promoter upstream (pRS426-*ADH1*$_{pr}$). Using pGBKT7, primers AS003 and AS004 were used in a PCR to amplify

the *ADH1* terminator. Using RF PCR, the *ADH1* terminator amplicon was inserted into pRS426-*ADH1*$_{pr}$ directly downstream the multiple cloning site. This final construct was denoted pAS01 **(Figure 13)**. To generate yeast gene overexpression plasmids, yeast coding sequences were PCR amplified from prepared genomic DNA (Blount et al., 2016). Primers were designed so that the resultant amplicon contained short homologous regions flanking KpnI-SacI cut pAS01 for cloning by restriction digest cloning **(Table 3 and Table 4)** or by Gibson assembly **(Table 7)**. Because inconsistent results were achieved with the RF PCR method, subsequent cloning procedures instead relied on restriction digest or Gibson assembly cloning.

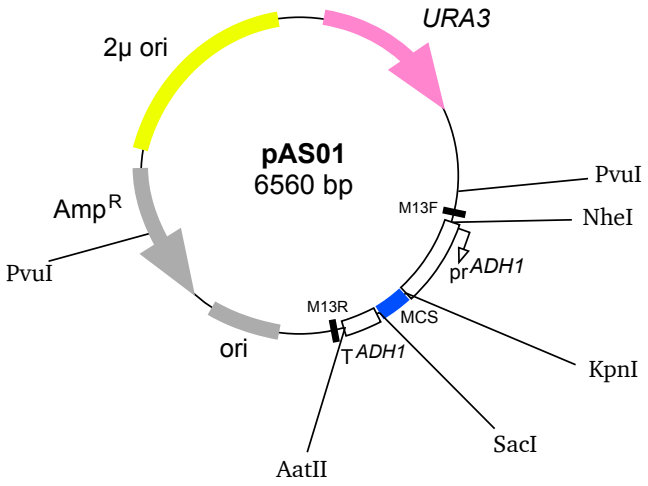

Figure 13. High copy empty plasmid pAS01 map. An origin of replication sequence (ori, grey) is present for plasmid propagation in *E. coli*. The ampicillin resistance cassette (Amp^R, grey) facilitates *E. coli* selection. The 2µ origin of replication (2µ ori, yellow) maintains the plasmid at high copy number in yeast. The *URA3* cassette (pink) allows plasmid selection in *ura3* auxotrophic yeast. Flanking unique restriction sites of the multiple cloning site (MCS) is shown. $_{pr}$*ADH1, S. cerevisiae ADH1* promoter. $_{T}$*ADH1*, *S. cerevisiae ADH1* terminator. M13F and M13R are commonly used sequencing sites. Subsequent cloning procedures typically used the KpnI and SacI sites to insert ORFs via restriction digest or Gibson assembly.

Table 5. Typical PCR reaction using Phusion polymerase. [1]genomic DNA was prepared by Chelex method (Blount et al., 2016).

Reagent	Volume (µL)	DNA amount (ng)	Comments
Plasmid DNA template or	1	10-20	

Genomic DNA[1]	4
Forward primer (5 μM)	5
Reverse primer (5 μM)	5
Phusion HF buffer (5X)	10
dNTPs (12.5 mM)	0.8
Phusion HF polymerase	0.3
ddH_2O	Make up to 50 μL reaction volume

Table 6. Phusion PCR thermocycling conditions.

Step	Temperature (°C)	Time	Cycles
1. Initial denaturation	98	30 s	
2. Denaturation	98	15 s	
3. Annealing	55	30 s	
4. Extension	72	30 s/kbps	
5. Final extension	72	5 min	
Cycles (Step 2-4)			20-25

Table 7. Example Gibson assembly reaction. 3:1 molar insert:vector ratio was used. Typically, 25 ng of cut vector was used. Example DNA sizes and the corresponding amount of PCR fragment needed for a 3:1 molar insert:vector ratio is provided. Reactions were then incubated at 50 °C for 35 minutes.

Reagent	Volume (μL)	DNA amount (ng)	DNA size (bp)
PCR fragment	X	15	1000
Cut vector	Z	25	5000
Gibson assembly mix (2X)	5		
ddH_2O	Make up to 10		

2.2.1.4 Low copy plasmids

Low copy *CEN* variants of high copy *URA3* pAS01 plasmids were generated using pRS316 (Sikorski and Hieter, 1989) which contains *CEN6* and *URA3* (gifted by Prof. Dr.

Heinz Neumann). For this, pAS01 was digested with PvuI (NEB) and the mcs and *ADH1* regulatory sequence containing fragment was extracted after gel electophoresis. The mcs fragment was then ligated to the *CEN6* containing fragment of PvuI digested pRS316 to generate pAS75 **(Figure 14)**.

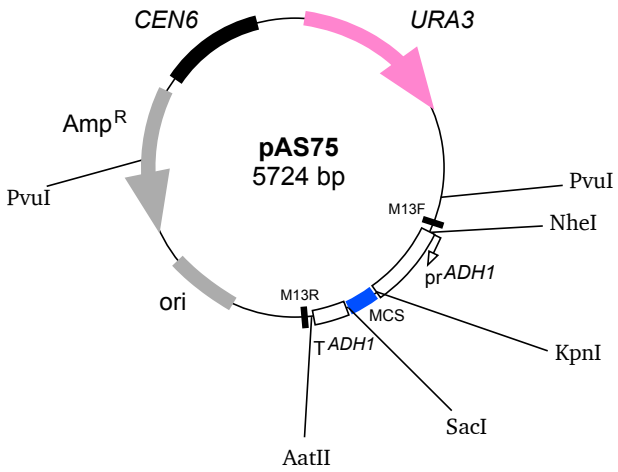

Figure 14. Low copy CEN empty plasmid pAS75 map. *CEN6* maintains the plasmid at 1-2 copies in yeast. 2μ ori, 2μ origin of replication. *URA3*, auxotrophic *URA3* marker for yeast selection. Amp^R, ampicillin resistance cassette. MCS, multiple cloning site. $_{pr}$*ADH1, S. cerevisiae ADH1* promoter. $_{T}$*ADH1*, *S. cerevisiae ADH1* terminator. M13F and M13 are commonly used sequencing sites.

2.2.1.5 High copy endogenous promoter plasmids

The majority of overexpression constructs under the endogenous promoter were assembled in pGP564 **(Figure 15)** (Jones et al., 2008); kindly gifted from Dr. Gerben Vader. This plasmid was used as the backbone vector for construction of the yeast genomic tiling collection (Jones et al., 2008). Notable features of pGP564 are shown below. The 2μ origin of replication sequence facilitates high copy propagation of the plasmid once introduced into the yeast cell. Furthermore, pGP564 also possesses a *LEU2* marker allowing for auxotrophic yeast selection and a kanamycin resistance marker (kan^R) for *E. coli* selection.

Individual yeast genes were cloned into pGP564 by conventional restriction digest or Gibson assembly. Primers were designed so that the coding sequence, flanked by ~700 bp of the immediate 5' UTR region and ~100 bp of the 3' UTR was amplified by PCR. For restriction digest of PCR fragments, primer ends were designed to contain the restriction

site sequence flanked additionally by 3-4 random nucleotides for efficient restriction enzyme cutting. If Gibson assembly was used, primer ends incorporated overlap of ~20 bp sequence homology to the sequences flanking the pGP564 BamHI-SacI site.

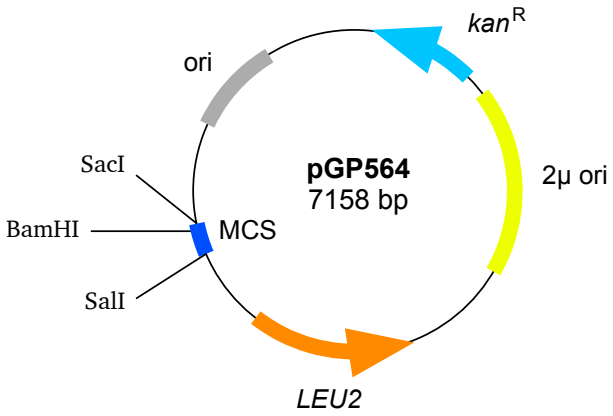

Figure 15. Plasmid map of pGP564. ori, origin of replication is present for *E. coli* plasmid propogation. *kan*^{R}, kanamycin resistance cassette. 2µ ori, 2µ origin of replication. The *LEU2* cassette (orange) is used for plasmid selection in *leu2* auxotrophic yeast. SacI and SalI are the flanking restriction sites of the mcs. For typical cloning procedures, the SacI and BamHI sites were utilised to introduce yeast ORFs via restriction digest or Gibson assembly.

2.2.1.6 Prm1-eGFP-StrepII high copy plasmid

A high copy 2μ plasmid encoding for $_{pr}$*GAL1*-Prm1-eGFP-StrepII was generated for initial purification trials. More specifically, the StrepII tag utilised is actually the Twin-Strep-tag, which is comprised of two *Strep*-tag®II moieties connected by a short 12 aa linker (AWSHPQFEKGGGSGGGSGGSAWSHPQF) (Schmidt et al., 2013), which in this study will simply be referred as StrepII. Firstly, eGFP-StrepII was cloned into a $_{pr}$*PRM1-PRM1* 2μ *URA3* plasmid. For this, eGFP-StrepII was amplified from plasmid 2107 (Raunser lab, MPI Dortmund) using primers AS519 and AS520. The PCR product was cloned via SacI/SalI restriction digest cloning into pAS143, generating pAS163. Then, *PRM1-eGFP-StrepII* was then amplified using primers AS521 and AS520 and cloned into pAS151 (which contains $_{pr}$*GAL1*) by XhoI/SacI (NEB) cloning, generating pAS198.

A variant of pAS198 containing HRV3C cleavage site before eGFP was generated. This was generated by PCR of eGFP with primers AS608 and AS520. AS608 contains the

sequence for HRV3C cleavage site. The PCR product was inserted into pAS198 with SalI/SacI (NEB) restriction cloning generating pAS223.

2.2.1.7 rDNA integration Prm1-yeGFP-StrepII plasmid

pFA6-natNT2 (Euroscarf) was used as the parental vector since it contains the NatNT2 marker (NrsR gene and *ADH1* terminator). The 35S rDNA Up homology arm was amplified by PCR with primers AS629 and AS631, using plasmid YGPM14n23 (Yeast genomic tiling collection, Dharmacon) as the template. The PCR product was subsequently cloned into pFA6-natNT2 by restriction digest using AscI (NEB) and SalI-HF (NEB) and the subsequent plasmid named pnatNT2-Up. The 35S rDNA Down homology arm was amplified by PCR using AS637 and AS638 using plasmid YGPM14n23 as the template. The PCR product was cloned by restriction digest into pnatNT2-Up using XbaI (NEB) and SpeI-HF (NEB) to generate pnatNT2-UpDown (pAS235). A plasmid containing $_{pr}$*GAL1*-Prm1-yeGFP-StrepII was generated. For this, yeGFP was amplified from pYM44 using primers AS624 and AS628 and cloned into pAS223 via NotI-HF/SalI-HF (NEB) cloning to generate pAS231. $_{pr}$*GAL1*-Prm1-HRV3C-yeGFP-StrepII present in pAS231 was PCR amplified using primers AS640 and AS642. The PCR product was inserted into pAS235 through restriction digest cloning using XbaI and SacI-HF (NEB) to generate pAS236 **(Figure 16)**.

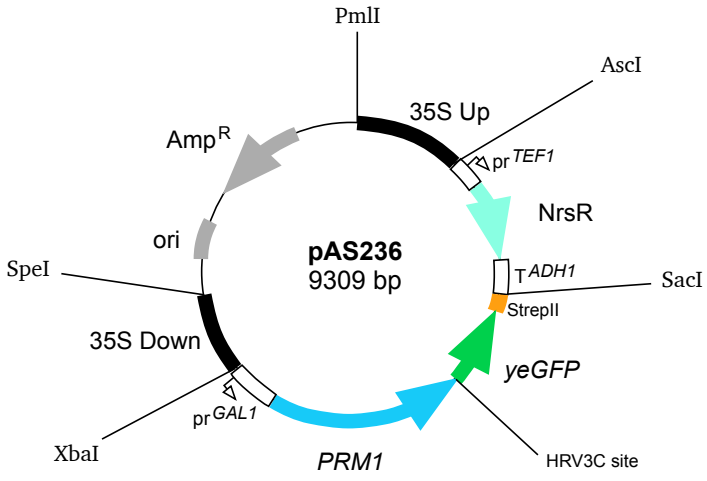

Figure 16. Prm1-yeGFP-StrepII integration plasmid pAS236 map. Origin of replication sequence (ori, grey) is present for plasmid propagation in *E. coli*. The ampicillin resistance cassette (Amp^R, grey) facilitates *E. coli* and plasmid selection. NrsR confers resistance to ClonNAT. yeGFP is yeast enhanced GFP. 35S Up and 35S Down refer to the flanking 35S rDNA homology arms. $_{pr}$*GAL1*, *S.*

cerevisiae GAL1 promoter. $_{pr}$*TEF1*, *S. cerevisiae TEF1* promoter. $_{T}$*ADH1*, *S. cerevisiae ADH1* terminator. StrepII signifies Twin-Strep-tag.

2.2.2 Subcloning of yeast tiling collection plasmids

Each tiling collection plasmid contains an insert of a yeast genomic region which average between 10-15kbps. For subcloning of genes in the hit plasmids identified in the genomic screen, conventional restriction digest-based cloning of PCR amplicons into the pGP564 empty vector was used **(Table 3 and Table 4)**.

2.2.3 Site directed mutagenesis

Site directed mutations to *PRM1* and *SUR1* were introduced using Gibson assembly **(Figure 17)**. Typically, two PCR fragments were used for each reaction. The 3' end of fragment 1 contains ~20 bp homology to 5' end of fragment 2. The desired mutation was usually incorporated into this region of homology during primer design. The two linear PCR fragments were then combined with a double digested linearised vector in a Gibson assembly reaction. A typical reaction is shown **(Table 8)**. Gibson assembly master mix was purchased from New England Biolabs (NEB). Gibson assembly reactions were incubated at 50 °C for 45 min and then 1 µL of the reaction was transformed into chemically competent XL-10 gold *E. coli*.

For *PRM1* mutagenesis, the F1 primer was typically AS432 and the R2 primer was AS433. These primer ends provide homology to KpnI/SacI digested pAS113. The R1 and F2 primers contained the mutation of interest. The two PCR fragments together encompass the *PRM1* promoter and the Prm1 variant coding sequence. For mutagenesis of *SUR1* DxD motif, the first PCR fragment was generated using F1 primer AS120 and R1 primer AS414. The second PCR fragment was generated using F2 primer AS413 and AS019. Both PCR reactions used pAS89 ($_{pr}$*SUR1-SUR1-*$_{T}$*ADH1*) as a template. The two PCR fragments were then recombined into NheI/AatII digested pAS23 via Gibson assembly.

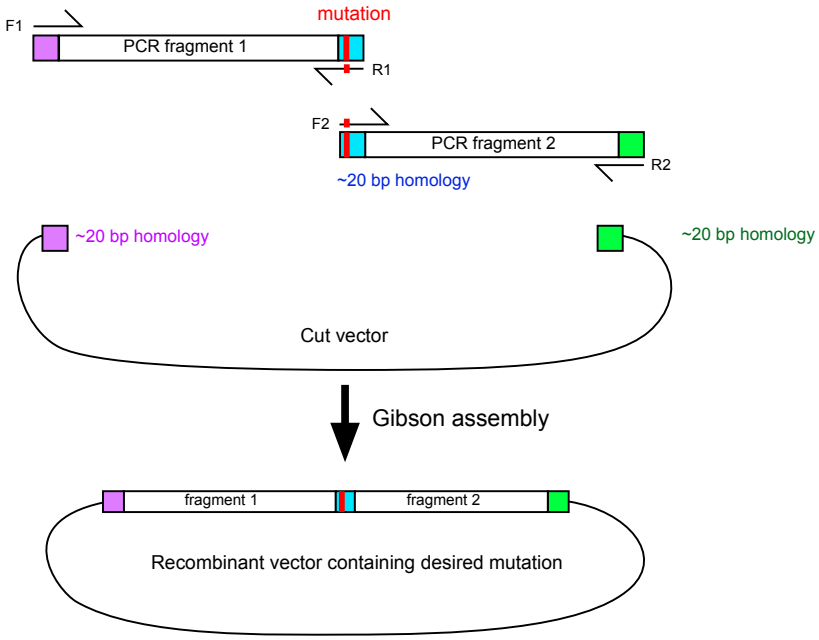

Figure 17. SDM via Gibson assembly. Two PCR fragments are generated which together comprise the insert. Fragment 1 is generated using primers F1 and R1. Fragment 2 is generated using primers F2 and R2. The DNA ends have regions of homology for assembly during Gibson reaction. In this example, the desired mutation (red) was designed within the homology end of fragment 1 and fragment 2 (blue). Each region of homology comprises approximately 20 bp.

Table 8. Example Gibson assembly reaction setup for SDM. Volumes of PCR fragment 1, fragment 2, and cut vector will depend on the DNA concentration, the amount of DNA added and the chosen ratio of insert:vector. A 2:1 molar insert ratio of insert:vector was observed to consistently lead to successful transformant colonies. An example of two PCR fragment sizes and the required DNA amount needed for a 2:1 molar insert ratio is provided.

Reagent	Volume (µL)	DNA amount (ng)	DNA size (bp)
PCR fragment 1	X	10	1000
PCR fragment 2	Y	10	1000
Cut vector	Z	25	5000
Gibson assembly mix (2X)	5		
ddH_2O	Make up to 10		

2.2.4 DNA sequencing

To confirm DNA sequences, samples were sent to Microsynth Seqlab, Germany. Between 40 - 100 ng/µL of plasmid DNA was sent for each sequencing reaction. Generally, sequencing primers AS132 and AS133 were used for sequencing reactions, which anneal 5' to M13 sequence M13 and M13R sequences, respectively. If these sequencing reactions were not sufficiently long enough to confirm the entire construct, additionally custom designed primers were used.

2.2.5 List of primers

Table 9. Primers used in this study.

Primer	Sequence (5'-3')	Description
AS001	GTAAAACGACGGCCAGTGCTAGCATCCTTTTGTTGTTTCCGGGTG	F RF primer $_{pr}$*ADH1*
AS002	GGCCCGGTACCCAATTCAGTTGATTGTATGCTTGGTATAGC	R RF primer $_{pr}$*ADH1*
AS003	CGGTGGAGCTCCAGCTTGGGCGAATTTCTTATGATTTATG	F RF primer $_{T}$*ADH1*
AS004	CAGGAAACAGCTATGACGGGACGTCCCGGTAGAGGTGTGGTC	R RF primer $_{T}$*ADH1*
	$_{pr}$***PRM1-PRM1* (*LEU2*)**	
AS109	TCACTAAAGGGAACAAAAGCTGGAGCTCGTAGCGCAATGGCTTGATACC	F GA $_{pr}$*PRM1-PRM1*
AS110	CGAATTCCTGCAGCCCGGGGGATCCCCGCGAATTTCAAATTCAACGC	R GA $_{pr}$*PRM1-PRM1*
	YGPM8p07 subcloning	
AS312	GTCCTGCAGGATCATATCACAGCAGTGCTTATC	F YGPM8p07 1
AS313	GCCGTCGACCGTGAGTGCAACAGCGGAAAATC	R YGPM8p07 1
AS314	GCCCTGCAGACTTCCTTGGCCAAGCCTTTC	F YGPM8p07 2
AS315	GCCGTCGACGCGCCTGAAAGTCTAAACTAAAC	R YGPM8p07 2
AS316	GTCCTGCAGGTTTCGGTTTCGGCTTTCAATTG	F YGPM8p07 3
AS317	GCCGTCGACGATCTGAGCTTATTGGAAAAACG	R YGPM8p07 3
	Sphingolipid genes	
AS396	AGTGGATCCGCATTATAATCTATTTCGCTATTATATTACAAATGCTAC	F *CSH1*
AS397	ATAGTCGACCCTTGCCATAGTCGATCGTTTCTTATTAACC	R *CSH1*
AS398	ATAGGATCCGATAGGCGGAGGTATGCCTC	F *CSG2* (pAS92)
AS399	AGTGTCGACGAGGCATGGTACTCCTTCTTATTC	R *CSG2* (pAS92)
AS410	GCTGGAGCTCGAAGAAGTACGGACAGACAT	F *AUR1*
AS411	CGAGGTCGACGTATAGCGCACAGGTTTTGAC	R *AUR1*
AS405	AGTGGATCCTTTTCTGGGAAAAAAGGAAATCTGTGTG	F *IPT1*
AS406	AGTGTCGACCGTGCTACTTGAGGAGGCC	R *IPT1*

AS120	GTAAAACGACGGCCAGT	M13 F
AS414	CAGCTAAAGCGATGTATACACCACCATAATGGGAC	R Sur1-AxA GA 1
AS413	GTGGTGTATACATCGCTTTAGCTGACGGCTGCGAAAGGAAAC	F Sur1-AxA GA 2
AS019	CACAGGAAACAGCTATGAC	M13 R
AS654	GCCAGTGCTAGCGAGTATACTTTTCTACGCCTCC	F *CSG2* (pAS241)
AS422	GCTGGAGCTCCTAATGGTGGTATTTACCTTCCC	R *CSG2* (pAS241)
	Prm1 mutants	
AS432	CGAATTTGTGAACGTTGATGATggtaccATGAGCGGTTTTAAATGCTATTTG	F Prm1 GA
AS433	CATAAGAAATTCGCCCAAGCTGGAGCTCTCAGTCAAAGGTGGCTTTGCG	R Prm1 GA
AS524	CAGGTCAATGGCAAAGTTTACAGCCCCCTCGCTCGCATATAC	R L106A GA 1
AS523	GCTGTAAACTTTGCCATTGACCTG	F L106A GA 2
AS528	CCCAAATACAGGTCAATGGCAGCGTTTACCAGCCCCTCGC	R F109A GA 1
AS527	GCTGCCATTGACCTGTATTTGGG	F F109A GA 2
AS534	TAAGTGCCCAAATACAGGTCAGCGGCAAAGTTTACCAGCCCCT	R I111A GA 1
AS533	GCTGACCTGTATTTGGGCACTTA	F I111A GA 2
AS530	AGCGTCAATGGCAAAGTTTAC	R L113A GA 1
AS587	GGTAAACTTTGCCATTGACGCT	F L113A GA 2
AS532	GAGGCATAAGTGCCCAAATAC	R C120S GA 1
AS531	GTATTTGGGCACTTATGCCTCTTTGATTGTTAGTGCCGTTG	F C120S GA 2
AS578	AATGGCAAAGTTTACATCCCCCTCGCTCGCATATAC	R L106D GA 1
AS577	GGGATGTAAACTTTGCCATTGACCTG	F L106D GA 2
AS580	CCCAAATACAGGTCAATGGCGTCGTTTACCAGCCCCTCGCTCGC	R F109D GA 1
AS579	GCCATTGACCTGTATTTGGG	F F109D GA 2
AS582	TAAGTGCCCAAATACAGGTCatcGGCAAAGTTTACCAGCCCCTC	R I111D GA 1
AS581	TATTTGGGCACTTATGCCTG	F I111D GA 2 (also F L113 GA 2)
AS583	CAGGCATAAGTGCCCAAATAGTCGTCAATGGCAAAGTTTACCAGC	R L113D GA 1
AS542	TCATTGACTAAGCTGGCAGCTTTTTCTGTAATGTTAGTAGCAACGTC	R L140A I141A GA 1
AS541	GCTGCCAGCTTAGTCAATGATACAGTTTCAAG	F L140A I141A GA 2
AS544	GAAACTGTATCATTGGCAGCGCTAATCAGTTTTTCTGTAATGTTAG	R L143A V144A GA 1
AS543	GCTGCCAATGATACAGTTTCAAGTGTGGC	F L143A V144A GA 2
AS546	CGTATCCAATTCATTAGCAGCACTTGAAACTGTATCATTGACTAAG	R V151A GA 1
AS545	GCTGCTAATGAATTGGATACGGGC	F V151A GA 2
AS550	CTTGATCACTTTATTGGCAGCTTTGGAGATGTCATTCAAGCCCGTATC	R I165A I166A GA 1
AS549	GCTGCCAATAAAGTGATCAAGGCCGCATC	F I165A I166A GA 2
AS552	CATCACCTGTGGCAGCATTCTCTACTTTGGATGCGG	R F179A F180A GA 1
AS551	GAATGCTGCCACAGGTGATGACGATGACAGTAAC	F F179A F180A GA 2
AS461	AATTCTCTACCGCGGATGCGGCCGCGATCACCGCATTGATTATCGCGGAGATGTC	R Δ4K GA 1

AS442	CCGCATCCGCGGTAGAGAATTTTTTCACAGGTGATG	F Δ4K GA 2
AS591	CATCACCTGTTTTTTCTGTAATGTTAGTAGCAACGTC	R Δ140-180 GA 1
AS590	CATTACAGAAAAAACAGGTGATGACGATGACAGTAAC	F Δ140-180 GA 2
AS593	GCGCAGATTTTTCTGTAATGTTAGTAGCAACGTCC	R Δ140-200 GA 1
AS592	CTAACATTACAGAAAAATCTGCGCTTCACAATTTATAC	F Δ140-200 GA 2
AS604	GTAATGTTAGTAGCAACGTCCACGGTACCATC	R Δ140-220 GA 1
AS603	GTGGACGTTGCTACTAACATTACAGAAAAAGCAAAGACGCCGGACTTTG	F Δ140-220 GA 2
AS589	AGCTTCATTAGCCACACTTGAGGCTGTATCATTAGCTAAGCTAATCAGTTTTTCTG TAATGTTAG	R 8-alanine GA 1
AS588	CAAGTGTGGCTAATGAAGCTGATACGGGCGCCAATGACGCTTCCAAAATAGCCAA TAAAGTGATCAAGGCCGCATCC	F 8-alanine GA 2
	V5 Plasmids	
AS151	AGTGCTAGCGTAGCGCAATGGCTTGATACC	F $_{pr}$*PRM1* (700 bp) NheI
AS468	AGCGGAGCCAGCGGATCCTGTCGACCCGTCAAAGGTGGCTTTGCG	R Prm1 SalI
	Sequencing primers	
AS132	TAAGTTGGGTAACGCCAGGG	F sequencing primer
AS133	GAGCGGATAACAATTTCACACAGG	R sequencing primer
AS565	TGACGAATGTGACCAACATAAG	F $_{pr}$*PRM1* sequencing
AS031	CAATGATACAGTTTCAAGTGTGGC	F Prm1 sequencing 1
AS566	GCCTTTGCGGAATGAGAGAC	F Prm1 sequencing 2
AS032	GGGTTATATAGCAGTGTTCCATTG	R Prm1 sequencing 1
AS131	GGTATCTCCGATTATATTGCTGG	R Prm1 sequencing 2
	Prm1-eGFP plasmids	
AS519	TGACGGGTCGACAGGATCCGCTGGCTCCGCTGCTGGTTCTGGCGAATTCACGCGT AGCAAGGGCGAGGAGCTG	F eGFP-StrepII F
AS520	CAAGCTGGAGCTCTTAATTACTAGTCTTCTCAAACTGAGGATGTGACCACGCCGAA CCTCCCGATCCACCTCCGGAACCTCCAC	R eGFP-StrepII
AS521	CTATACTTTAACGTCAAGGAGACTCGAGGGTACCATGAGCGGTTTTAAATGCTATT TG	F Prm1 XhoI
AS608	GACGGGTCGACATTAGAAGTTTTGTTTCAAGGTCCAGGATCCGCTGGCTCCGCTG CTGGTTC	F HRV3C cleavage site
	Integration plasmid	
AS629	TGCAGGTCGACCACGTGCCGGAACCTCTAATCATTCG	F 35S rDNA Up PmlI
AS631	GAGGCAAGCTAAACAGATCTGGCGCGCCGCAAGTACGGTCGTTTTAGG	R 35S rDNA Up AscI
AS637	TTCGCGAGCTCGAATTCATCGATGAATCTAGAATTATACCTCAAGCACGCAG	F 35S rDNA Down XbaI
AS638	AGGCCACTAGTAACGAACGAGACCTTAACCT	R 35S rDNA Down SpeI
AS640	ATAATTCTAGAGAATTCCGGATTAGAAGCCGCCGAG	F GAL1 XbaI
AS642	AGCTGGAGCTCTTAATTGCTAGTCTTCTCAAACTG	R StrepII SacI

AS624	GACGGGTCGACATTAGAAGTTTTGTTTCAAGGTCCAGGTGGTTCTAAAGGTGAAG AATTATTCACTG	F HRV3C-yeGFP
AS628	GCCATGCGGCCGCTTTTGTACAATTCATCCATACCATG	R yeGFP

2.3 *Escherichia coli* procedures

2.3.1 *E. coli* strains

Table 10. *E. coli* strains used in this study.

Strain	Use	Genotype	Reference
XL10-Gold	For cloning procedures	Tet^{r}Δ(*mcrA*)*183* Δ(*mcrCB-hsdSMR-mrr*)*173* *endA1 supE44 thi-1 recA1 gyrA96 relA1 lac* Hte [F′ *proAB lacI*^{q}ZΔ*M15* Tn*10* (Tet^r) Amy Cam^r]	Stratagene
DH10B	Harbours the yeast tiling plasmid collection	F – *mcrA*Δ (*mrr-hsd*RMS-*mcr*BC) *endA1 recA1* φ*80dlacZ*Δ*M15* Δ*lacX74 araD139* Δ*(ara, leu)*7697 galU galK rpsL (*StrR*) nupG λ-	Jones et al., 2008

2.3.2 Growth and maintenance

For routine growth, *E. coli* was cultured in LB liquid media **(Table 11)** or LB plates at 37 °C. For plasmid minipreps, *E. coli* was grown in 2TY liquid media **(Table 12)**. Solutions were sterilised by autoclaving at 121 °C for 20 min. For agar plates, 2% agar (Bacto™) was added to solutions before sterilisation via autoclaving. If antibiotic was added, ampicillin and kanamycin was added to final concentrations of 100 μg/mL and 50 μg/mL, respectively.

Table 11. LB Recipe.

LB	Gram for 1 L	Supplier
Tryptone	10	Bacto™
Yeast Extract	5	Bacto™
NaCl	10	

ddH_2O	Make to 1L

Table 12. 2TY Recipe.

2TY	Gram for 1 L	Supplier
Tryptone	16	Bacto™
Yeast Extract	10	Bacto™
NaCl	5	
ddH_2O	Make to 1L	

2.3.3 Chemically competent *E. coli* preparation

Chemically competent *E. coli* cells were prepared by an adapted protocol from Inoue (Inoue et al., 1990). A preculture was set up by inoculating 1 µL of competent cells into 5 mL LB media and grown overnight at 37 °C. The next day the OD_{600} of the culture was measured. Two flasks containing 100 mL LB were each inoculated with the preculture at final OD_{600} of 0.025 and 0.05, respectively. Cells were grown at 19 °C, 100 rpm for approximately 30 h until the OD_{600} = 0.5 - 0.6. Cells were placed on ice for 10 min, before centrifugation at 1,700 × *g* for 10 min at 4 °C. The supernatant was discarded, before resuspension of each pellet in 1 mL (per 50 mL culture) ice cold TB buffer (10 mM HEPES pH 6.7, 15 mM $CaCl_2$, 55 mM $MnCl_2$, 250mM KCl). 15 mL of TB Buffer was then added to each 1 mL cell mixture, mixed and left on ice for 10 min. Cells were centrifuged again and the supernatant was discarded. The cells were then resuspended in 4 mL of 7% DMSO dissolved in TB buffer. Cells were placed on ice for 10 min and then 80 µL aliquots were pipetted into pre-chilled 1.5 mL microcentrifuge tubes. Aliquoted cell suspensions were then shock frozen in liquid nitrogen and stored at -80 °C until use.

2.3.4 Transformation of plasmids

1 µL of plasmid was added to 80 µL of freshly thawed competent XL-10 Gold *E. coli*. The 1.5 mL microcentrifuge tube containing the plasmid-cell mixture was then mixed by gentle flicking and left on ice for 10 min. Cells were then heat shocked at 42 °C for 75 s and

subsequently placed on ice for 5 min. 900 μL of LB media was added and the mixture was incubated at 37 °C for 1 h. The entire cell suspension was centrifuged at 13,000 × *g* and 900 μL of supernatant was removed. The remaining mixture was resuspended and plated on LB media plates containing the appropriate antibiotic. Plates were incubated overnight at 37 °C to allow for colonies to form.

2.3.5 Plasmid miniprep

Plasmid DNA was prepared from plasmid harbouring *E. coli* using a QIAprep Spin Miniprep Kit (Qiagen). Typically, a single *E. coli* colony was inoculated into 5 mL of 2TY containing 100 μg/mL ampicillin or 50 μg/mL kanamycin. The culture was grown for 14-16 h overnight at 37 °C whilst shaking at 220 rpm. 4 mL of the culture was harvested via centrifugation at 15,000 × *g* in a microcentrifuge and plasmid DNA was subsequently extracted according to the manufacturer instructions. DNA was eluted in 50 μL elution buffer (Qiagen) and the concentration was measured via absorbance at 260 nm using a NanoDrop 1000 (Thermo Scientific).

2.3.6 96-well plasmid miniprep from *E. coli*

96-well *E. coli* culture minipreps were performed by the Dortmund Protein Facility (DPF). For minipreps *E. coli* maintained as 96-well glycerol stocks were thawed and pin replicated into 96-deep well plates. Each well of the 96-deep well plate contained 1.1 mL TB media and 50 μg/mL kanamycin. Plates were sealed with porous sealing tape and shaken overnight at 37 °C and 220 rpm. Plates were then processed by the DPF with a Hamilton Starplus liquid handing system and 96-well prep kit solutions (Macherey-Nagel), yielding approximately 1-2 μg plasmid DNA per well.

2.3.7 Pin replication sterilisation

Cells were pin replicated using a 96-floating pin replicator (V & P Scientific). The pin replicator was sterilised by incubating for 30 s in ddH_2O twice, followed by 30 s in sodium hypochlorite and 30 s in ddH_2O. This was followed by a 10 s incubation in 70%

ethanol and a 5 s incubation in 100% isopropanol, before passing the replicator through a flame.

2.4 Yeast procedures

2.4.1 Yeast liquid media

YPD was used for general cultivation of yeast (Table 13). YPGal was used for sporulation and galactose induction (Table 14). To select for yeast transformants containing plasmids, synthetic dextrose (SD) plates were generally used, unless indicated otherwise (Table 15). Media solutions were sterilised by autoclaving at 121 °C for 20 min. To generate agar plates, 2% agar (Bacto™, Ref 214010) was added to solutions before autoclaving.

Table 13. YPD recipes.

YPD	Gram for 1 L	Supplier
Yeast Extract	10	Bacto™
Bacto Peptone	20	Bacto™
Glucose	20	Formedium

Table 14. YPGal recipe.

YPG	Gram for 1 L	Supplier
Yeast Extract	10	Bacto™ (Ref 212730)
Peptone	20	Bacto™ (Ref 211677)
Galactose	20	Formedium

Table 15. SD recipe. For the amino acid supplements, 0.1546 g/L of an amino acid premix containing the appropriate amino acid dropout e.g. -leucine could also be used instead (Kaiser SC-Leu, Formedium).

SD	Gram for 1 L	Supplier

Glucose	20	Formedium
Yeast Nitrogen Base	1.9	Formedium
Ammonium Sulphate	5	Biochemica
Amino Acid Supplement		
Uracil	0.02	Formedium
Methionine	0.02	Formedium
Histidine	0.02	Formedium
Lysine	0.03	Formedium
Leucine	0.03	Formedium
Alanine	0.076	Formedium
Arginine	0.076	Formedium
Asparagine	0.076	Formedium
Aspartate	0.076	Formedium
Cysteine	0.076	Formedium
Glutamine	0.076	Formedium
Glutamate	0.076	Formedium
Glycine	0.076	Formedium
Isoleucine	0.076	Formedium
Phenylalanine	0.076	Formedium
Proline	0.076	Formedium
Serine	0.076	Formedium
Threonine	0.076	Formedium
Tryptophan	0.076	Formedium
Tyrosine	0.076	Formedium
Valine	0.076	Formedium

2.4.2 Yeast plate media

For plate media for general cultivation, the same recipe as the liquid media was prepared, with the addition of 20 g agar (Bacto™) per L. If antibiotic selection was required, antibiotics were added after the autoclaved media was sufficiently cooled before pouring. Antibiotics were added so that final concentrations were: G418 (Sigma) (400 μg/mL), Hygromycin B (Formedium) (300 μg/mL), ClonNAT (Jena Bioscience) (100 μg/mL). For small plates, approximately 25 mL of autoclaved, warm media was poured into each plate and allowed to solidify. For Omnitray (Thermo Scientific) plates used for cultivation of

colonies in 96-well format, 50 mL of autoclaved, warm media was poured per plate and allowed to cool.

2.4.2.1 Plates for mating

YPD plates used for standard mating assays used the same YPD recipe for cultivation of strains (Table 16).

Table 16. YPD standard fusion plates recipe.

YPD (standard fusion)	Gram for 1 L	Supplier
Yeast Extract	10	Bacto™ , 212730
Peptone	20	Bacto™ , 211677
Glucose	20	Formedium
Agar	20	Bacto™

For initial screening of the tiling collection, fusion assays were conducted on low Ca^{2+} YPD Omnitray (Thermo Scientific) plates (Table 17). The low Ca^{2+} present was due to the batch of YPD Broth formulation supplied by Formedium. Screening of the latter plates used standard fusion YPD plates prepared from Bacto™ yeast extract and peptone (Table 16).

Table 17. YPD low Ca^{2+} plates recipe.

YPD (low calcium)	Gram for 1 L	Supplier
YPD Broth	50	Formedium
Agar	20	Sigma, A7002-1KG

2.4.3 Yeast strains

The majority of *S. cerevisiae* strains used in this study were derived from S288C (Mortimer and Johnston, 1986). A table of yeast strains used in this study is listed below (Table 18). All strains were generated in this study unless otherwise indicated.

Table 18. Yeast strains used in this study.

Strain code	Description	Genotype	Reference
BY4741	wt S288C derivative	*MAT***a** *his3Δ1 leu2Δ0 ura3Δ0 met15Δ0*	Brachmann et al., 1998
PSAY981	N-GFP-NATMX4 *MAT*α	*eGFP(aa1-158)-TRP1-NatMX4 his3Δ1 leu2Δ0 lys2Δ0 ura3Δ0*	Gift from Pablo Aguilar
AH005-A	Δ*fus1* Δ*fus2 N-GFP MAT*α	Δ*fus1::hphNT1* Δ*fus2::kanMX6 eGFP(aa1-158)-TRP1-NatMX4*	Angela Hagemeier
AS04	C-GFP-NATMX4 *MAT***a**	*eGFP(aa159-240)-NatMX4 his3Δ1 leu2Δ0 met15Δ0 ura3Δ0*	
AS05	C-GFP-NATMX4 *MAT*α	*eGFP(aa159-240)-NatMX4 his3Δ1 leu2Δ0 met15Δ0 ura3Δ0*	
Δ*prm1* PSAY981	Δ*prm1* N-GFP *MAT*α	Δ*prm1::hphNT1 eGFP(aa1-158)-TRP1-NatMX4*	Mara Marques
AS13	Δ*prm1* C-GFP *MAT***a**	Δ*prm1::hphNT1 eGFP(aa159-240)-NatMX4*	
AS102	Δ*prm1*Δ*sur1* N-GFP *MAT*α	Δ*prm1::hphNT1* Δ*sur1::kanMX6, eGFP(aa1-158)-TRP1-NatMX4*	
AS103	Δ*prm1*Δ*sur1* C-GFP *MAT***a**	Δ*prm1::hphNT1* Δ*sur1::kanMX6 eGFP(aa159-240)-NatMX4*	
AS104	Δ*prm1*Δ*csh1* N-GFP *MAT***a**	Δ*prm1::hphNT1* Δ*csh1::kanMX6 eGFP(aa1-158)-TRP1-NatMX4*	
AS105	Δ*prm1*Δ*csh1* C-GFP *MAT*α	Δ*prm1::hphNT1*, Δ*csh1::kanMX6, eGFP(aa159-240)-NatMX4*	
AS106	Δ*prm1*Δ*csg2* N-GFP *MAT*α	Δ*prm1::hphNT1* Δ*csg2::kanMX6 eGFP(aa1-158)-TRP1-NatMX4*	
AS107	Δ*prm1*Δ*csg2* C-GFP *MAT***a**	Δ*prm1::hphNT1* Δ*csg2::kanMX6, eGFP(aa159-240)-NatMX4*	
AS108	Δ*prm1*Δ*ipt1* N-GFP *MAT*α	Δ*prm1::hphNT1* Δ*ipt1::kanMX6 eGFP(aa1-158)-TRP1-NatMX4*	
AS109	Δ*prm1*Δ*ipt1* C-GFP *MAT***a**	Δ*prm1::hphNT1* Δ*ipt1::kanMX6 eGFP(aa159-240)-NatMX4*	
AS133	Δ*prm1*Δscs7 N-GFP *MAT*α	Δ*prm1::hphNT1* Δ*scs7::kanMX6 eGFP(aa1-158)-TRP1-NatMX4*	
AS134	Δ*prm1*Δscs7 C-GFP *MAT***a**	Δ*prm1::hphNT1* Δ*scs7::kanMX6 eGFP(aa159-240)-NatMX4*	
AS135	Δ*prm1*Δ*sur2* N-GFP *MAT***a**	Δ*prm1::hphNT1* Δ*sur2::kanMX6 eGFP(aa1-158)-TRP1-NatMX4*	
AS136	Δ*prm1*Δ*sur2* N-GFP *MAT*α	Δ*prm1::hphNT1* Δ*sur2::kanMX6 eGFP(aa159-240)-NatMX4*	
AS110	Δ*sur1* N-GFP *MAT*α	Δ*sur1::kanMX6 eGFP(aa1-158)-TRP1-NatMX4*	

AS111	Δ*sur1* C-GFP *MAT***a**	Δ*sur1::kanMX6 eGFP(aa159-240)-NatMX4*	
AS112	Δ*csh1* N-GFP *MAT*α	Δ*csh1::kanMX6 eGFP(aa1-158)-TRP1-NatMX4*	
AS113	Δ*csh1* C-GFP *MAT***a**	Δ*csh1::kanMX6 eGFP(aa159-240)-NatMX4*	
AS114	Δ*csg2* N-GFP *MAT*α	Δ*csg2::kanMX6 eGFP(aa1-158)-TRP1-NatMX4*	
AS115	Δ*csg2* C-GFP *MAT***a**	Δ*csg2::kanMX6 eGFP(aa159-240)-NatMX4*	
AS116	Δ*ipt1* N-GFP *MAT*α	Δ*ipt1::kanMX6 eGFP(aa1-158)-TRP1-NatMX4*	
AS117	Δ*ipt1* C-GFP *MAT***a**	Δ*ipt1::kanMX6 eGFP(aa159-240)-NatMX4*	
AS118	Δ*sur1*Δ*csh1* N-GFP *MAT*α	Δ*sur1::kanMX6* Δ*csh1::kanMX6 eGFP(aa1-158)-TRP1-NatMX4*	
AS121	Δ*sur1*Δ*csh1* C-GFP *MAT***a**	Δ*sur1::kanMX6* Δ*csh1::kanMX6*	
AS123	Δ*prm1*Δ*sur1*Δ*csh1* N-GFP *MAT***a**	Δ*prm1::hphNT1* Δ*sur1::kanMX6* Δ*csh1::kanMX6 eGFP(aa1-158)-TRP1-NatMX4*	
AS124	Δ*prm1*Δ*sur1*Δ*csh1* C-GFP *MAT*α	Δ*prm1::hphNT1* Δ*sur1::kanMX6* Δ*csh1::kanMX6 eGFP(aa159-240)-NatMX4*	
AS125	Δ*scs7* N-GFP *MAT*α	Δ*scs7::kanMX6 eGFP(aa1-158)-TRP1-NatMX4*	
AS126	Δ*scs7* C-GFP *MAT***a**	Δ*scs7::kanMX6 eGFP(aa159-240)-NatMX4*	
AS127	Δ*sur2* N-GFP *MAT***a**	Δ*sur2::kanMX6 eGFP(aa1-158)-TRP1-NatMX4*	
AS128	Δ*sur2* C-GFP *MAT*α	Δ*sur2::kanMX6 eGFP(aa159-240)-NatMX4*	
	Δ*pep4::kanMX6 MAT***a**	Δ*pep4::kanMX6*	YKO collection
AS145	Δ*pep4::kanMX6* Δ*prm1::hphNT1 MAT***a**	Δ*pep4::kanMX6* Δ*prm1::hphNT1*	
AS152	$_{pr}$*GAL1-PRM1-HRV3C-yeGFP-StrepII* (short GS linker) *MAT***a**	$_{pr}$*GAL1-PRM1-HRV3C-yeGFP-StrepII* Δ*pep4::kanMX6*	

2.4.4 Yeast gDNA extraction

gDNA extracts were prepared for PCR. gDNA was extracted according to the Chelex method (Blount et al., 2016). A small clump of cells were scraped off an agar plate using a sterile pipette tip and resuspended in 100 µL 5 % Chelex 100 (Sigma). 0.5 mm glass beads (Sigma) measured by 1 small metal spatula was added. Samples were then vortexed at high speed for 5 min and then incubated at 95 °C for 10 min. Samples were then centrifuged at 15,800 × *g* in a microcentrifuge for 1 min. The supernatant which contains the gDNA could then be used for subsequent PCR.

2.4.5 Competent yeast cell preparation

Competent yeast cells for transformation were prepared using the lithium acetate method (Knop et al., 1999). Briefly, yeast were inoculated from a saturated preculture into 50 mL YPD media and grown overnight at 25 °C until an OD_{600}= 0.6–1.0. Cells were harvested by centrifugation at 1,700 × *g* for 4 min. Cells were washed once with 0.4 volumes sterile water at room temperature (RT) and resuspended with 0.4 volumes SORB solution (100 mM LiOAc, 10 mM Tris–HCl pH 8, 1 mM EDTA/NaOH pH 8, 1 M Sorbitol). Cells were left on ice for 15 min before centrifugation and resuspension in 360 μL SORB (per 50 mL of initial cells). 0.4 mL 8mg/mL ssDNA (Carl Roth) (prepared prior by heating at 95 °C for 5 min and kept on ice) was added. 50 μL was aliquoted into 1.5 mL eppendorfs. These competent cells could be used immediately for transformation or alternatively stored at -80 °C until use.

2.4.6 Yeast transformation

100 μL PEG solution (PEG MW 3350 (50% w/v) (Sigma), 100 mM LiOAc, 10 mM Tris-HCl pH 8, 1 mM EDTA/NaOH pH 8) was added to 50 μL competent cells, mixed by flicking tubes and left at RT for 30 min. Then, $1/9^{th}$ volume DMSO was added and cells were heat shocked at 42 °C for 20 min in a thermomixer (Eppendorf). Cells were then pelleted at 1,700 × *g* for 4 min. For plasmid transformation, cells were resuspended in 75 μL ddH_2O and immediately plated on SD plates. For PCR mediated knockout, cells were resuspended in 2 mL YPD and grown at 30 °C for 4 - 5 h to allow for expression of the antibiotic resistance marker. Cells were then harvested and resuspended in 80 μL water and then the entire suspension was plated on YPD + antibiotic plates. Plates were incubated at 30 °C for 2 days until colonies formed.

2.4.7 Generation of strains by PCR mediated knockout

PCR mediated knockout was used as the method of choice for the majority of yeast strain generations. Antibiotic resistance markers of either the *kanMX6* (resistance to G418), *hphNT1* (resistance to hygromycin B) or *natNT2* (resistance to ClonNAT) cassettes were amplified by PCR. The 5’ ends of the primers for PCR contain 40 bp homology to the

chromosomal locus of interest. This allows for integration into the chromosome via homologous recombination. PCR was conducted using DreamTaq polymerase (Thermo Scientific™) and then gel extracted using a gel extraction kit (Qiagen). 500 ng-1 µg of PCR product was added per 50 µL lithium acetate competent cells, transformed by PEG/heat shock **(2.4.6)** and plated on YPD + corresponding antibiotic plates.

2.4.7.1 Colony PCR verification

Transformant colonies were restreaked once on YPD selection plates to exclude spurious transformants, and surviving colonies were confirmed for correct gene knockout by colony PCR. For this, two PCR reactions were used. The first PCR uses a set of primers anneals inside the ORF to assess the presence of the wild type gene (wt check). The second PCR uses a forward primer annealing to 5' UTR, and a reverse primer annealing to the selection marker, thereby assessing whether the gene was replaced with the selection marker (KO check). Colonies which displayed absence of a band for the wt check PCR and a positive band for the KO check PCR were determined as correct transformants. Primers for amplifying the resistance marker, wt check and KO check for a given yeast gene were designed using the Primers4Yeast tool (Yofe and Schuldiner, 2014). Yeast genomic DNA was extracted by the Chelex method (Blount et al., 2016) (**Section 2.4.4)**. To test a number of colonies at once, a master mix for each PCR reaction was carried out **(Table 19)**. Corresponding colony PCR thermocycling conditions using DreamTaq™ DNA polymerase (Thermo Scientific) are listed in **Table 20**.

Table 19. Master mix for colony PCR. Once prepared, 21 µL of the master mix is added to 4 µL of genomic DNA.

Reagent	Volume (µL) (For 12 reactions)
Forward primer (5 µM)	30
Reverse primer (5 µM)	30
Phusion HF buffer (5X)	30
dNTPs (12.5 mM)	4.8
DreamTaq polymerase	3.5
ddH_2O	153.7
Total	252

Table 20. Colony PCR thermocycling conditions.

Step	Temperature (°C)	Time	Cycles
1. Initial denaturation	95	5 min	
2. Denaturation	95	30 s	
3. Annealing	55	30 s	
4. Extension	72	2 min	
5. Final extension	72	5 min	
Cycles (Step 2-4)			28

2.4.8 Generation of strains by tetrad dissection

Haploid cells were mated by mixing and streaking on a YPD plate. Diploids were then selected for by replica plating on selective plates (if possible). Diploids were scraped using a sterile pipette tip and inoculated into 5 mL of YPGal and grown overnight at 30 °C and shaking at 220 rpm. Cells were then pelleted at 1,700 × *g* for 4 min. The supernatant was poured away and the cell pellet was resuspended in the remaining volume (~100 µL). The cell suspension was plated out on K-acetate plates **(Table 21)** for 5 days at 20 °C to induce tetrad formation.

Table 21. K-acetate sporulation plate recipe. Uracil, leucine, histidine, methionine are added to complement the auxotrophic requirements of the BY derived strains.

K-acetate plates	Gram for 1 L	Supplier
K-acetate	50	TCI
Yeast extract	20	Bacto™
Glucose	0.5	Formedium
Uracil, leucine, histidine, methionine	0.005 each	Formedium
Zinc sulfate	0.025	Alfa Aesar

A pellet-size of cells were scraped off K-acetate plates using a sterile pipette tip and transferred to a 2 mL microcentrifuge tube containing 300 µL of 0.33 mg/mL zymolyase 100T (US Biological Corporation) dissolved in water. The cells were resuspended forming a cloudy suspension and incubated for 20 min at RT. Cells were then streaked using a sterile inoculation loop onto one end of a YPD plate in parallel vertical streaks and placed onto the MSM 400 tetrad dissector (Singer instruments). On average 8 tetrads were dissected per allele desired. Plates were then incubated at 30 °C for 1-2 days, after which visible colonies were observed. Colonies were then restreaked onto YPD plates containing antibiotic for appropriate selection of marker. Colonies which grew were then confirmed for the desired genotype using colony PCR.

2.4.9 Generation of an integrated Prm1-eGFP-StrepII strain

Since a multicopy integration was desired, an integration approach towards yeast endogenous rDNA sites was chosen. Linearised DNA will integrate at rDNA sites if the DNA ends contain homology arms to rDNA sequences. An integration plasmid (pAS236) encoding for Prm1-yeGFP-StrepII under the *GAL1* promoter was constructed. For this, 4 μg of pAS236 was linearised by restriction digest with 0.9 μL PmlI (NEB) and 0.9 μL SpeI-HF (NEB) in a 20 μL reaction for 3 h at 37 °C. The liberated natNT2-Prm1-yeGFP-StrepII fragment, which contains flanking 35S rDNA homology arms was extracted after DNA gel electrophoresis and eluted in 20 μL elution buffer (Qiagen). Approximately 1300 ng of linearised DNA was attained (measured by NanoDrop™ spectrophotometer).

The entire DNA solution was transformed into 50 μL competent Δ*pep4::kanMX6* cells which had been prepared under hydroxyurea stress (HU), which increases the copy number of integrated genes at rDNA sequences (Zheng et al., 2022). Treating the cells with HU reduces the native rDNA copy number (Salim et al., 2017), which is subsequently restored by rDNA amplification once HU stress is released. Heterologous genes which have integrated into rDNA sequences can therefore increase their copy number alongside the rDNA repeats during the rDNA amplification process (Zheng et al., 2022). For this, the cells were grown in YPD containing 150 mM HU (Alfa Aesar) for 8 days at 30 °C with shaking at 220 rpm (Zheng et al., 2022). A 1:10,000 dilution of the culture into fresh YPD containing 150 mM HU was carried out every 2-3 days to ensure continual cell divisions. 20 mL of cells at OD_{600}=0.8 were then made competent by the lithium acetate method (**Section 2.4.5)**

with the exception that SORB buffer also contained 150 mM HU. After heat shock, cells were pelleted at 1,700 × *g* for 4 min and resuspended in 2 mL YPD. The culture was incubated for 4 h to allow for the *natNT2* marker to be expressed. Cells were then pelleted again and the supernatant was decanted. Cells were resuspended in the residual supernatant and the entire suspension was plated on YPD plates containing G418 (400 μg/mL), ClonNAT (500 μg/mL) and 60 mM HU. Plates were incubated at 30 °C until colonies formed. Individual colonies were then restreaked on YPD plates with ClonNAT (100 μg/mL).

2.4.10 96-well transformation of Yeast Tiling Collection

2.4.10.1 Preparation of competent yeast cells

Competent yeast cells were prepared using the lithium acetate method (Knop et al., 1999) as described in **2.4.5** only in larger scale. Yeast were inoculated from a saturated preculture into 250 mL YPD media (enough for 100 transformations) and grown overnight at 25 °C until an OD_{600} of 0.8–1.0 was reached. The same procedure **(2.4.5)** was then followed, except the volumes after final resuspension were 4.5 mL SORB and 0.5 mL 8mg/mL ssDNA. 50 µL was aliquoted into the wells of a 96-well microtiter plate (Sarstedt) using a multichannel pipette. Competent cells were either used immediately for transformation or stored at -80 °C until use.

2.4.10.2 96-well transformation

Yeast were transformed via the lithium acetate method in 96 well format adapted from Gietz & Schiestl (Gietz and Schiestl, 2007; Knop et al., 1999). Δ*prm1* strains each harbouring one of the split GFP fragments were transformed with the yeast genomic tiling collection, which was purchased from Horizon Discovery (Cat #YSC4613). The tiling collection is arrayed as plasmid-harbouring *E. coli* glycerol stocks in 96-well format. Plasmid DNA was prepared in 96-well format to generate 17 plasmid microtiter plates by the Dortmund Protein Facility using a robotic system (Hamilton Star Plus, Hamilton).

For yeast transformations, 50–100 ng of plasmid was transferred to 50 μL competent yeast cells in each well of a 96-well microtiter plate and mixed by pipetting. For each microtiter plate, three wells were reserved for the following controls, **i)** a 2μ *LEU2* plasmid containing the wild type *PRM1* allele, **ii)** pGP564, the tiling collection empty vector and **iii)** addition of ddH_2O instead of plasmid. 100 μL of 50% PEG solution (50% w/v PEG 3350 (Sigma), 100mM LiOAc, 10mM Tris–HCl pH 8, 1mM EDTA/NaOH pH 8) was then added to each well. Microplates were then placed in a forced air incubator at 42 °C for 50 min. Cells were pelleted by centrifugation at 1700 × *g* for 4 min, washed once with sterile water, and resuspended in 50 μL SD-Leu. 50 μL suspensions were transferred to a 96-well microplate containing SD-Leu agar. Plates were incubated at 30 °C for 3-4 days until colonies formed. Transformants were then pin replicated onto SD-Leu OmniTray plates. Accounting for the controls, 18 plates of 96-well transformations were required to generate a transformant library encompassing the entire tiling collection for one strain background.

2.4.11 Cell-cell fusion BiFC assay

Yeast cell-cell fusion assays utilising Bi-fluorescence complementation (BiFC) of split-GFP was used in this study, which was developed by Aguilar and coworkers (Salzman et al., 2015). The assay involves labelling the **a** and α haploids with different cell wall binding fluorophore conjugates. After mating, the resultant population which includes non-paired haploids and mating pairs are injected into a flow cytometer. This enables rapid discrimination of the mating pairs (which are detected as two-coloured entities). The percentage of mating pairs which have successfully fused their cell-membranes (termed here as fusion efficiency) can be determined by cytosolic BiFC of two split-GFP fragments which are provided by each haploid.

2.4.11.1 Small scale BiFC assay

From a saturated preculture, 5 mL of yeast culture was grown overnight to an OD_{600}= 0.2-0.8. Cells were pelleted, washed once with ddH_2O and then resuspended in 2 mL D-phosphate-buffered saline (PBS). *MAT*α cells were then stained with 2.5 μg/mL Concanavalin A-Alexa647 (ConA-647) (Invitrogen) and *MAT***a** cells were stained with 12.5 μg/mL Concanavalin A-Tetramethylrhodamine (ConA-Tet) (Invitrogen) in the dark for 30

min. Cells were then washed once with 5 mL ddH_2O and resuspended in 5 mL sterile water. Then, 2×10^6 of stained *MAT***a** and *MAT*α cells were mixed together in 5 mL YPD media and then deposited onto 0.45 μm nitrocellulose filters (Millipore) using a 12-position vacuum manifold (Merck).

Cell-filters were then placed onto YPD plates and incubated for 3 h at 30 °C to ensure the mating process went to completeness. Mating reactions were then stopped with 1 mL TAF buffer (20mM Tris, pH 8, 20mM NaN_3, 20mM NaF), vortexed briefly to ensure removal of cells from the filters and subsequently placed on ice. Mating reactions was usually immediately measured in a BD Accuri C6 Plus flow cytometer (BD Biosciences); samples could also be stored overnight at 4 °C for measurement next morning.

2.4.11.2 96-well microplate BiFC assay

The yeast tiling collection *MAT*α *N-GFP-NatMX4* and *MAT***a** *C-GFP-NatMX4* transformants were inoculated using a stainless-steel pin floating pin replicator (V & G Scientific) from SD-Leu OmniTray plates into a 96-well microplate (Sarstedt) containing 180 μL SD-Leu media per well. Microplates were incubated at 30 °C overnight for cells to grow until saturation. Cells were then pin replicated from this saturated microplate into a new 96-well microplate containing 180 μL SD-Leu and incubated overnight at 25 °C until mid-log phase (OD_{600}= 0.02-0.2) on a microplate reader (BMG Labtech), equivalent to OD_{600}= 0.2-0.8 measured in cuvette.

Cells were transferred using a multichannel pipette to 96-well filter plates (Millipore) and vacuumed to remove the media. Cells were washed once with 100 μL ddH_2O, vacuumed and resuspended in 180 μL PBS. *MAT*α and *MAT***a** cells were then stained with 0.1 mg/mL ConA-647 and 0.5 mg/mL ConA-Tet, respectively, for 45 min in the dark. Cells were then washed twice with 100 μL YPD media and resuspended in 90 μL YPD. *MAT*α cells were then transferred to the microplate containing the *MAT***a** cells, mixed and then vacuumed onto the filter. The filter guard was removed and the filter plate was placed onto YPD agar (prepared in a large glass petri dish) for 4 h at 30°C to allow sufficient mating to occur. To stop the mating reaction, the plate was removed from the agar and cells were resuspended in 180 μL TAF buffer. Cells were resuspended via multichannel pipetting directly before data acquisition to ensure a homogenous cell suspension.

2.4.11.3 Flow cytometry analysis

The BD Accuri C6 Plus flow cytometer (BD Biosciences) is equipped with a 488 nm laser for excitation of GFP and ConA-Tet, and a 640 nm laser for excitation of Concanavalin A-Alexa647 (ConA-647). Band pass filters used for detection were 510/15 nm for GFP, 585/40 nm for ConA-Tet and 675/25 nm for ConA-647.

Measurements and gating were performed on the BD Accuri C6 Plus Software. An initial gating strategy comprised of a linear side scatter (SSC) versus linear forward scatter (FSC) plot to exclude cell debris from analysis (gate 1) **(Figure 18A)**. The gated population was then displayed in a logarithmic density plot of ConA-647 fluorescence versus ConA-Tet fluorescence **(Figure 18B)**. This allowed for discrimination between four subpopulations in the mating mixture: unstained cells (bottom left), ConA-647 stained *MAT*α cells (bottom right), ConA-Tet stained *MAT***a** cells (top left) and double stained ConA-647 and ConA-Tet mating pairs (top right) **(Figure 18B)**. In these mating pairs, the two gametes have sufficiently attached to one another i.e. the cell walls were adhered, such that they remain attached after vortexing and sonication (Salzman et al., 2015). After gating the ConA-647+ and ConA-Tet+ mating pairs (gate 2), GFP+ mating pairs could then be discriminated from GFP- mating pairs by plotting log (GFP) fluorescence on the x-axis and SSC on the y-axis. **(Figure 18C).** Fusion efficiency can then be calculated as the percentage of fused (GFP+) mating pairs (marked by the region labelled fused) out of the total number of mating pairs. In the example, 39.5% of mating pairs were fused.

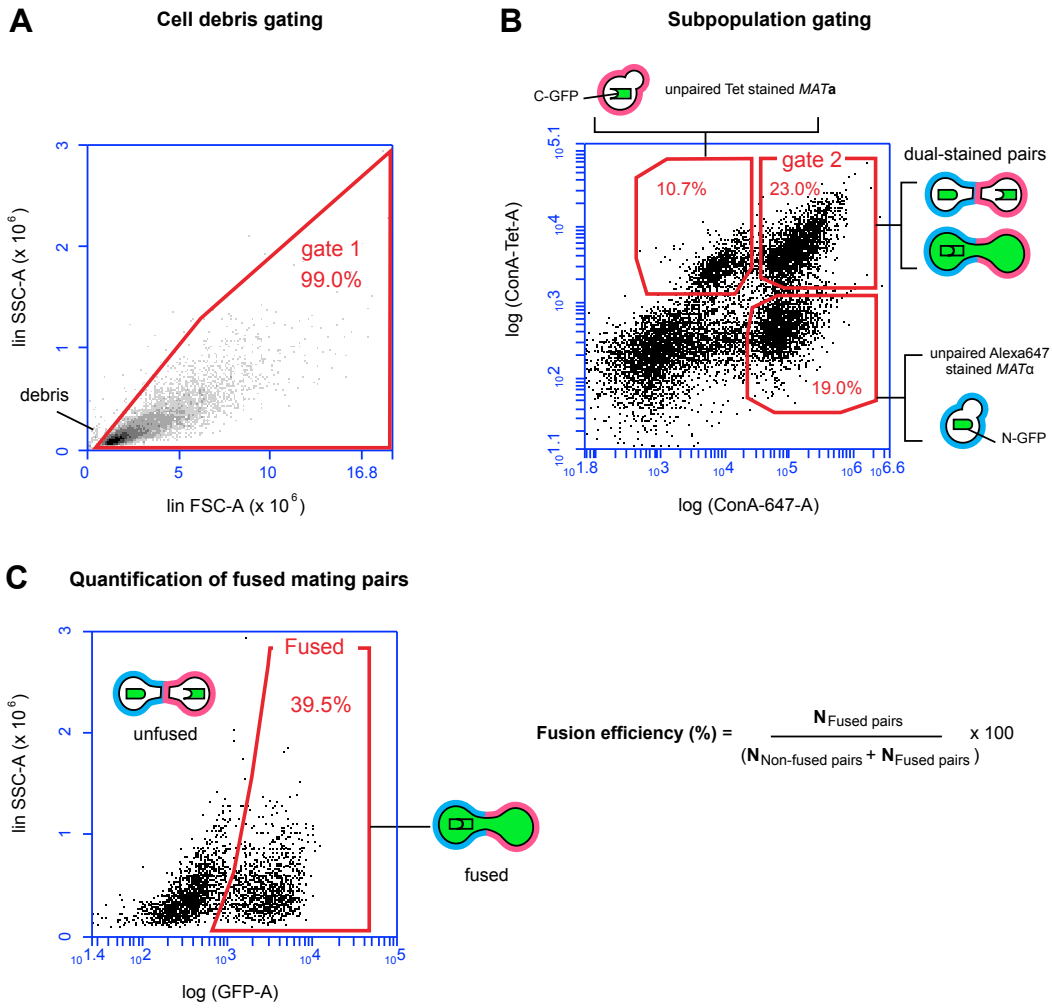

Figure 18. Gating strategy to determine fusion efficiency of mating pairs. A. Initial cellular debris gating. Usually 10,000 gated events (gate 1) were recorded for each mating reaction. **B.** Subpopulating gating of dual-stained mating pairs. ConA-647 versus ConA-Tet cytogram plotted in logarithmic scale allows identification of the mating reaction subpopulations. **C.** Gating to identify fused population of mating pairs. Cytogram displaying only double-stained entities (events in gate 2) is plotted as log (GFP) versus SSC. Two populations representing non-fused (GFP-) and fused (GFP+) mating pairs can be distinguished. Example cytogram denotes 39.5% of pairs are fused. Fusion efficiency is calculated as the number $(N)_{\text{fused pairs}}$ / ($N_{\text{fused pairs}}$ + $N_{\text{nonfused pairs}}$).

2.5 Protein procedures

2.5.1 SDS-PAGE

SDS-PAGE was conducted on 10% or 8% tris(hydroxymethyl)aminomethane (TRIS)-glycine SDS-PAGE gels (Table 22 and Table 23) or pre-cast Mini-PROTEAN TGX Stain-Free gels (Bio-Rad) using a Mini PROTEAN® Tetra Cell system (BioRad) in SDS running buffer (25 mM Tris, 192 mM Glycine, 0.1% (w/v) SDS). Gels were electrophoresed at 100 V until samples reached the stacking line, after which voltage was increased to 140 V. Electrophoresis was stopped once the dye front reached the bottom (approximately 90 min). Gels were subsequently used for Western blotting or in-gel fluorescence.

Table 22. Separating gel recipe. Volumes listed are enough for 2 gels.

Separating gel	Volume for 10% gel	Volume for 8% gel
Water	3.5 mL	4.1 mL
30% Acrylamide	3 mL	2.4 mL
1.5 M Tris-HCl pH 8.8	2.2 mL	2.2 mL
10% SDS	90 µL	90 µL
10% APS	90 µL	90 µL
TEMED	4 µL	6 µL

Table 23. Stacking gel recipe. Volumes listed are enough for 2 gels.

5% Stacking gel	Volume
Water	3.6 mL
30% Acrylamide	0.9 mL
1 M Tris-HCl pH 6.8	0.7 mL
10% SDS	53.3 µL
10% APS	53.3 µL
TEMED	5.3 µL

2.5.2 In-gel fluorescence

In-gel fluorescence was used to detect the presence of eGFP tagged proteins after SDS-PAGE. The method utilises the finding that fluorescence of GFP is maintained in SDS (Saeed and Ashraf, 2009), provided samples are not heated (Alkaabi et al., 2005). To excite eGFP, blue epi illumination was used along with a 510/28 nm filter set in a ChemiDoc MP Imaging System (Bio-Rad).

2.5.3 Prm1-eGFP-StrepII induction by galactose

2.5.3.1 Small scale induction

Prm1-eGFP-StrepII expression from high copy plasmids was induced by washing cells and resuspension in galactose containing media. For small volumes, approximately 10 – 20 mL cultures were used. Cells were incubated at 30 °C shaking at 220 rpm in 0.1% Glucose containing SD media. Once cells reached an OD_{600} = 0.6–0.8, cells were pelleted by a 1,700 × *g* spin for 4 min. Cells were washed once with sterile ddH_2O before resuspension in 2% galactose SD media. For induced expression of genomically integrated $_{pr}$*GAL1-PRM1-HRV3C-yeGFP-StrepII*, the same procedure was followed except cells were grown in YPD. After pelleting and washing with water, cells were resuspended in 2% YPGal.

2.5.3.2 Large scale induction (1 L)

Large scale inductions were performed with strain AS152, which is protease deficient (Δ*pep4*) and contains $_{pr}$*GAL1-PRM1-HRV3C-yeGFP-StrepII* integrated at rDNA sites. Cells from a 100 mL saturated preculture grown in YPD were inoculated into 1 L of YPD in a 5 L flask to initial OD_{600} of 0.1-0.2. Cultures were then placed in a Multitron shaker incubator (Infors HT) and incubated at 30 °C at 190 rpm until OD_{600} = 0.7-1 was reached. Cells were pelleted via 1,500 × *g* for 10 min in autoclave-sterilised 1 L Beckman Coulter polypropylene bottles using a JLA-8.1000 rotor (Beckman Coulter). The supernatant was decanted and cells were washed once with sterile ddH_2O and resuspended in freshly prepared 2% YPGal. 1 L cultures in 2% YPGal were cultured at 30 °C at 220 rpm. After 14

h, the cells reached an OD_{600}= 4-5. Prm1-eGFP-StrepII expression was confirmed by confocal microscopy.

2.5.4 Protein purification

AS152, which contains integrated $_{pr}$*GAL1-PRM1-HRV3C-yeGFP-StrepII* was used for purification. For 3-5 L expressions, cultures were harvested after 16 h incubation in YPGal by a 1,500 × *g* spin for 15 min at 4 °C using a JLA-8.1000 rotor (Beckman Coulter). 40 g of cells were then resuspended in 150 mL lysis buffer (50 mM Tris-HCl pH 7.5, 150 mM NaCl, 5 mM EDTA, 1× protease inhibitor cocktail (Sigma, P9599) and 1 mM PMSF). Cell lysis was performed using a Cell disruptor TS 0.75 (Constant systems) at 2,700 bar for 3 cycles. The cell debris was cleared via a 1,500 × *g* spin for 15 min at 4 °C in a tabletop swinging bucket centrifuge (Eppendorf). The supernatant was then ultracentrifuged at 200,000 × *g* for 1 h at 4 °C in a Beckman Coulter Optima L-70K ultracentrifuge using a Ti-45 rotor.

The membrane pellet was resuspended in cold 80 mL lysis buffer containing 2% (w/v) OG and kept on ice. The suspension was then repeatedly passed through a 50 mL dounce homogeniser until homogenous. The mixture was left at 4 °C for 1 h under rocking (40-50 rpm) for efficient solubilisation of Prm1. A second ultracentrifugation step at 200,000 × *g* for 1 h was performed and the resulting supernatant was diluted 1:1 with lysis buffer without detergent (final concentration 1% (w/v) OG). 10 mL Strep-Tactin® Sepharose® resin (IBA-lifesciences) was added to a PD10 column and equilibrated with 25 mL 1% (w/v) OG lysis buffer. The resin was then mixed with the lysate in a schott bottle and incubated overnight at 4 °C on a roller at 40 rpm for 12 h. The resin was then collected in a PD10 column and subsequently washed with 40 mL 1% OG lysis buffer in 8 mL series. Prm1-eGFP-StrepII was eluted by addition of 10 mL 1% OG lysis buffer containing 7 mM desthiobiotin. 1 mL fractions were collected. Fractions were then evaluated by SDS-PAGE and in-gel fluorescence of eGFP. Protein concentration was determined via absorbance at 280 nm using a Nanodrop 1000 (Thermo Scientific).

2.5.5 Prm1 reconstitution into liposomes

2.5.5.1 Lipid mix preparation

A yeast lipid stock solution (50 mg/mL) was prepared by adding 1 mL chloroform/methanol (2:1 v/v) to one vial of yeast polar lipid extract (50 mg in powder form) (Avanti). The solution was transferred to a glass vial which was flushed with argon gas beforehand. The stock solution was stored at -20 °C until use. To prepare an Atto655-DOPE/yeast polar extract/2% OG mix, 200 μL of the stock solution was mixed with 20 μL of 1 mg/mL Atto655-1,2-Dioleoyl-sn-glycero-3-phosphoethanolamine (abbreviated Atto655-DOPE) (Atto-TEC), a fluorescent lipid analogue, and subsequently dried using a vacufuge (Eppendorf). The dried lipid mix was then resuspended in 2 mL of 40 mM PIPES pH 7.0, 150mM KCl, 2% (w/v) OG and placed on an end-on-end rotator at 4 °C until lipids were fully solubilised. The final concentration of yeast polar extract in the lipid mix was therefore 5 mg/mL.

2.5.5.2 OG removal by dialysis

Prm1/1% OG was mixed with lipid mix in 1:1 volume ratio. Typically, 150–200 μL of 10 μM Prm1/1% OG solution was added per reconstitution. To remove OG, the Prm1 lipid mix solution was injected into a 0.5 mL Slide-A-Lyzer 2000 molecular weight cut-off (MWCO) dialysis cassette (Thermo Scientific). The dialysis cassette was placed into a beaker containing 1 L 40 mM PIPES pH 7.0, 150mM KCl and allowed to dialyse overnight at 4 °C under gentle stirring. For reconstitution of reduced Prm1, 10 mM DTT was added to the Prm1/1% OG mixture to reduce disulfide bonds. The dialysis buffer also contained 10 mM DTT.

2.5.6 eGFP cleavage

60 μg of Precission protease was added to 600 μL of Prm1-eGFP (0.9 mg/mL) and then incubated at 4 °C for 20 h. Assessment of Precission mediated eGFP release from Prm1 was determined by SDS-PAGE and in-gel fluorescence. For stain-free imaging, the gel was excited under UV illumination for 2-5 min.

2.5.7 Cell lysis for Western blot

3 x 10^7 cells were collected by centrifugation, washed once with 1 mL TAF buffer and resuspended in 150 μL lysis buffer (50 mM Tris-pH 8.0, 150 mM NaCl, 5 mM EDTA) containing Protease inhibitor cocktail (PIC) (Sigma). Additionally, 5 μL of 0.1 M phenylmethanesulfonyl fluoride (PMSF) (Serva) was added. Cells were lysed with 150 μL of 0.5 mm glass beads (Sigma) for a total of 4 min with 1 min pause intervals on ice per min of vortexing. Then, 50 μL of 4X SDS sample buffer (200 mM Tris-HCl pH 6.8, 100 mM DTT, 8% SDS, 40% glycerol, 0.4% Bromophenol blue) was added. Samples were heated at 65 °C for 5 min with shaking at 300 rpm using a thermoblock (Eppendorf). 10 μL was loaded onto an 8% SDS-PAGE gel.

2.5.8 Western blot

After SDS-PAGE, proteins were transferred to nitrocellulose membranes using wet transfer in Towbin buffer (25mM Tris, 192mM glycine, 0.04% SDS, 20% MeOH (pH 8.3)). Transfer was performed in a Mini-Trans Blot apparatus (Bio-Rad) together with a magnetic stirrer at constant current (90 mA) for 16 h at 4 °C. Membranes were washed with TBST (0.1% (v/v) Tween 20, 20mM Tris, 150mM KCl, pH 7.5) Membranes were then blocked with blocking solution (TBS containing 5% milk) for 1 h at RT. To detect V5 tagged proteins, 2.5 μL mouse anti-V5 monoclonal antibody (Invitrogen) was added to membranes. For actin detection, 3 μL mouse anti-actin monoclonal antibody (Novus Biosciences) was added to membranes. Primary antibody incubations were incubated at RT, rocking for 1 h. Membranes were then washed with 5% milk blocking solution for 10 min whilst rocking and then repeated two more times. For secondary antibody addition, goat anti-mouse IgG2a polyclonal HRP antibody (Abcam) was used to detect mouse anti-V5 antibody. Goat anti-mouse IgM polyclonal HRP antibody (Abcam) was used to detect anti-actin antibody. Membranes were washed again with 5% milk blocking solution in the same manner as before. Western blots were developed by chemiluminescence (GE Healthcare) and detected using a ChemiDoc MP Imaging System (Bio-Rad).

2.5.9 Detergent screen

A saturated preculture of of *Δprm1::hphNT1 Δpep4::kanMX6* cells carrying pAS198 was inoculated into 40 mL of 0.1% glucose SD-URA so that the initial OD_{600} was ~0.1. Cells were then grown whilst shaking (220 rpm) at 30 °C to OD_{600}= 0.6. Cells were then harvested by centrifugation at 1,700 × *g* and washed once with water and pelleted again. Then, Prm1-eGFP-StrepII expression was induced by resuspension in 2% galactose SD-URA. Cells were then cultured for 20 h, shaking at 30 °C and 220 rpm.

Cells were pelleted by centrifugation at 4 °C and resuspended in 3.5 mL lysis buffer (50 mM Tris-HCl pH 7.5, 150 mM NaCl, 5 mM EDTA, 10% glycerol, 1 mM PMSF and 1× PIC (P9599, Sigma)). Cells were lysed using glass beads and vortexing. The lysate was transferred to a new 15 mL falcon tube, whilst avoiding uptake of glass beads, which yielded approximately 3 mL of cell lysate. For each detergent tested **(Table 24)**, 60 μL detergent was added to 240 μL cell lysate and rotated at 4 °C for 2.5 h on an end-on-end rotator. Samples were then ultracentrifuged at 100,000 × *g* for 1 h at 4 °C using a TLA-55 rotor and Optima™ MAX-XP ultracentrifuge (Beckman Coulter). The supernatant which contains the detergent-solubilised membrane proteins was used for subsequent analysis.

Table 24. Detergents used in the Prm1 screen. [1] CMC values were retrieved from Anatrace website. [2] CMC shown is for LMNG.

Detergent	CMC mM (% w/v) [1]	Stock concentration % w/v	Final concentration % w/v
DDM	0.17 (0.0087)	10	2
GDN	0.018 (0.0021)	10	2
LMNG-CHS	0.01 (0.001) [2]	5 (LMNG), 0.5 (CHS)	1
Digitonin	0.25-0.5 (0.02-0.03)	5	1
CHAPS	8–10 (0.5–0.6)	10	2
Triton X-100	0.24 (0.0155)	10	2
OG	18-20 (0.53)	10	2
CYMAL-6	0.56 (0.028)	10	2
LDAO	1-2 (0.023)	10	2
Fos-Choline-13	0.75 (0.027)	10	2

For FSEC, an NGC Discover™ 10 chromatography system (Bio-Rad) was used. The system is equipped with an autosampler C-96 (Bio-Rad) and is coupled to a fluorescence detector RF-20A (Shimadzu). A Superose 6 increase 10/300 GL (GE Healthcare) column was used for the screen. The column was equilibrated with 2 runs of 25 mL lysis buffer containing 0.05% DDM under a flow rate of 0.3 mL/min. eGFP was excited by excitation at 475 nm and emission at 510 nm. A Gel filtration standard (BioRad, 1511901) was ran after the samples to calibrate the column.

2.6 TLC analysis

2.6.1 Lipid extraction

Lipids were extracted from cells of 5 total OD_{600} units. Late logarithmically growing cells (OD_{600}= 0.7-0.9) were pelleted, washed twice with sterile ddH_2O and resuspended in 375 µL ethanol/water (4:1 v/v) (Hanson and Lester, 1980). Cells were incubated at 100 °C for 15 min and then spun at 15,000 × *g* for 2 min in a microcentrifuge. The supernatant was transferred to a new tube and the extraction process was repeated with the original cell pellet. The supernatant was pooled and then dried in a vacufuge (Eppendorf). To deacylate phospholipids, 130 μL monomethylamine was added and samples were incubated at 53 °C for 1 h, before drying again in a vacufuge. Samples were kept at -20 °C until use.

2.6.2 TLC

Lipids were resuspended in 30 µL chloroform/methanol/water (5:4:1 v/v) and heated briefly (1 min) at 50 °C to ensure lipid solubilisation. The entire suspension was loaded onto a glass-backed silica 60 TLC plate (VWR) and developed using chloroform/methanol/4.2 M ammonia (9:7:1.5 v/v). The plate was then allowed to dry under a fume hood. To detect sphingolipids, the plate was stained with 10% copper sulfate in 8% phosphoric acid solution (Koga et al., 2022), allowed to dry and then heated at 180 °C for approximately 10-15 min until sphingolipid bands were observed.

2.7 Confocal microscopy

Confocal images were acquired through a Zeiss LSM 800 microscope. Either a Zeiss Plan-Apochromat 40 water immersion objective or a Zeiss Plan-Apochromat 63× oil immersion objective was used. Images were processed using the image processing package Fiji.

2.7.1 FM4-64 staining

Mating pairs were stained with 160 μM FM4-64 (Thermo) to label plasma membranes. In live cells labelled with FM4-64, FM4-64 is endocytosed into vacuoles. However, when labelled in cold conditions or metabolic arresting conditions such as NaN_3 and NaF, endocytosis is arrested and FM4-64 is retained in the plasma membrane. To label plasma membranes cells were therefore arrested with TAF buffer on ice prior to staining.

2.7.2 Mating pair phenotype classification

To determine frequency of mating pair phenotypes, mating reactions were set up on nitrocellulose filters (Millipore) and mated for 3 h at 30 °C. Cells were pelleted by 1,700 × *g* spin for 4 min and then stained with FM4-64 on ice. Confocal images were acquired in single planes in nine tiles. FM4-64 and GFP channels were acquired sequentially. The FM4-64 channel was acquired in airyscan mode. Both FM4-64 and GFP were excited at 488 nm. Counting was performed manually using Fiji.

2.7.3 Localisation of mNG tagged proteins

Prm1-mNG mutants and Sur1-mNG were determined for localisation in cells. mNG was excited by a 488nm laser. For imaging, 5 mL of logarithmically growing cells were pelleted at 1700 × *g*, washed once with ddH_2O and resuspended in 20 μL TAF buffer. 1.8 μL was spotted onto a microscope slide for imaging.

2.8 Liposome assays

2.8.1 Large liposome (400 nm) preparation

Large multilamellar liposomes approximately 400 nm in diameter were prepared. 25 mg of yeast polar lipid extract (Avanti) was dissolved in 2:1 chloroform/methanol (v/v). 50 μg of 1,2-Dioleoyl-sn-glycero-3-phosphoethanolamin-N-(lissamin-rhodamin B-sulfonyl) (abbreviated as Rhodamine-PE) (Avanti) in chloroform solution was added to the lipid mixture and the mixture was then dried in a vacufuge (Eppendorf). Then the dried lipid mix was hydrated in 40 mM PIPES pH 7.0, 150 mM KCl, which induces formation of multilamellar liposomes. The suspension was transferred to a pear-shaped flask and sonicated three times (30 s continuous pulses at setting 2 with 50% duty cycles) with 1 min ice intervals using a Branson Microtip Sonifier 450. 1 mL of the liposome mixture was extruded 25 times through a 400 nm polycarbonate membrane filter (Whatman) using a Mini-Extruder (Avanti).

2.8.2 Flow cytometry to detect liposomes

Liposomes were detected using a BD Accuri C6 Plus flow cytometer. Atto655-DOPE was excited by a 640 nm diode laser and the signal was detected by 675/25 nm BP filter. Rhodamine-PE was excited by a 488 nm solid-state laser and fluorescence detection by a 585/40 nm BP filter. Liposome mixtures were diluted 1:10 with dialysis buffer to a final volume of 180 μL and then measured on slow fluidic rate (14 μL/min).

2.8.2.1 Binding assay to large Rhodamine-PE liposomes

200 μL of Prm1-eGFP-StrepII proteoliposomes or empty liposomes which contained Atto655-DOPE were mixed with 200 μL of Rhodamine-PE labelled large liposomes and incubated at 30 °C and 300 rpm on a thermoblock (Eppendorf) for 1 h and then subsequently measured by flow cytometry.

2.8.3 Proteinase K treatment to Prm1 proteoliposomes

2 mg/mL Proteinase K (≥30 units/mg) (Sigma, SAE0009) was prepared in dialysis buffer. Proteinase K was added to liposome mixtures so that the final concentration was ~0.33 mg/mL**.** Samples were incubated at 25 °C and aliquots were measured by flow cytometry or SDS-PAGE at 2 h intervals.

For SDS-PAGE analysis, 2 mM PMSF (final concentration 2 mM) was added to 60 μL of the liposome mixtures to inhibit proteinase K activity. 22.5 μL aliquots were taken and added to 7.5 μL 4X SDS sample buffer without reducing agent. Samples were not heated to preserve eGFP fluorescence. 15 μL was loaded into Mini-PROTEAN TGX Stain-Free precast gels (Bio-Rad) for subsequent SDS-PAGE.

2.8.4 DLS measurements

DLS was used to assess the proteoliposome sizes. DLS was conducted on a DynaPro Nanostar II detector (Wyatt Technology). 10 μL of liposome mixtures were added to microcuvettes (Wyatt Technology). 3-5 measurements were conducted for each sample at 25 °C.

2.9 AlphaFold2 prediction

Prm1 homodimer models were predicted using the AlphaFold2 multimer pipeline. The *S. cerevisiae* Prm1 sequence was used for predictions. AlphaFold2 multimer version 2.2.0 was ran on a Raven High-performance computing system provided by the Max Planck Computing and Data Facility (MPCDF), Garching (Evans et al., 2022).

Chapter 3. Results

3.1 Identification of Sur1 as a regulator of Δ*prm1* fusion

3.1.1 An overexpression genomic screen uncovers 28 plasmids which enhance Δ*prm1* fusion arrest

Screening is a powerful tool to reveal novel regulators underpinning biological processes. Towards uncovering genes involved in fusion, I screened the yeast genome for overexpression factors which further perturbed fusion in a fusion sensitised mutant. For this, the yeast tiling collection (Jones et al., 2008), a minimal set of high copy plasmids which physically and functionally cover >95% of the *S. cerevisiae* genome was used. Each genomic fragment comprises ~10 kbp, encompassing multiple genes. Since the plasmid library is provided as an array, the effects of each genomic fragment could be systematically probed. This feature is advantageous to the usage of pooled libraries, which can suffer from biases due to insufficient coverage of the genome. The Δ*prm1* mutant was chosen as the query background because Prm1 is known to be specifically involved in the step of plasma membrane fusion and therefore it was likely that the majority of hit genes identified would also regulate this step.

To detect fusion between an **a**-α mating pair during the mating process (here defined as the occurrence of mixing of cytoplasms between the two cells), Bi-molecular fluorescence complementation (BiFC) was used as the basis of the fusion assay. In BiFC, the assay relies on complementation of two non-fluorescent fragments into a reconstituted fluorescent molecule. In the case of split GFP, the N-terminal fragment typically comprises residues 1-158, whilst the C-terminal fragment comprises residue 159 to the C-terminus.

To measure only fusion of mating pairs, Aguilar et al. combined the BiFC assay with labelling of the haploids using cell wall dyes prior to mixing of the two cell types (Salzman et al., 2015). When the assay is coupled to flow cytometry, one can record a large number of cells (typically 10,000) in a given mating reaction and quantify fusion of the **a**-α mating

pairs in the span of a few seconds (Figure 19). Therefore, the assay is much faster and less laborious to perform than the traditional microscopy-based counting methods used to measure fusion (Grote, 2010, 2008). Since the fusion readout is restricted to only **a**-α mating pairs which have already formed tight and stable contacts, the readout better reflects the efficiency at which cells carry out the latter stages of fusion.

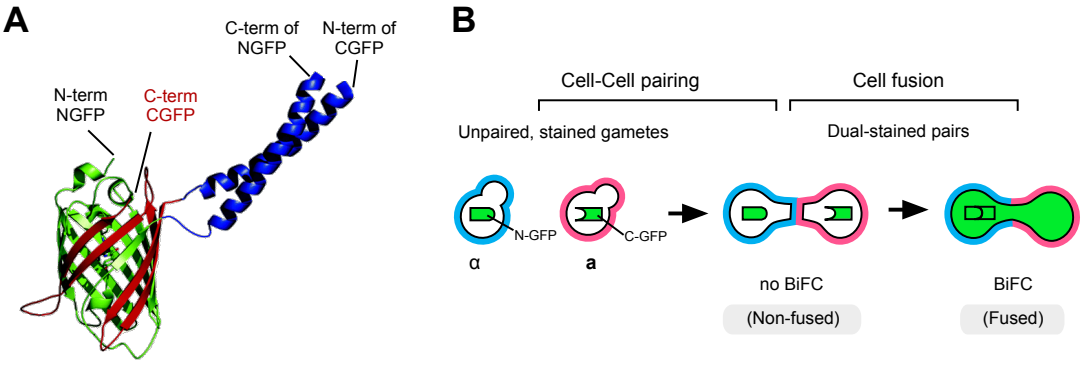

Figure 19. BiFC in conjunction with differential cell-wall staining to assay cell fusion in yeast mating pairs. A. BiFC using GFP. Structure of GFP with the N-terminal fragment coloured green and C-terminal fragment in red. GFP can be split at a surface-exposed loop between the 7th and 8th β-strands. The non-fluorescent fragments can assemble to reconstitute a fluorescent complex if brought into sufficient proximity; for instance, linking the fragments to additional leucine zippering domains (blue) (Magliery et al., 2005). Figure adapted from Magliery et al., 2005. **B.** Each mating type expresses only one of the split GFP fragments which is complementary to the GFP fragment expressed in the other mating type. Since reconstituted GFP only assembles upon mixture of the two cytoplasms, BiFC can be used to measure fusion dependent content-mixing.

The workflow of the screen is outlined in Figure 20. The tiling plasmid library, comprised of 1,588 plasmids, was introduced into Δ*prm1 MAT*α and *MAT***a** mutants. The *MAT*α strain contains a genomically integrated sequence encoding for cytosolic split N-GFP, whereas the *MAT***a** strain contains the corresponding split C-GFP encoding gene.

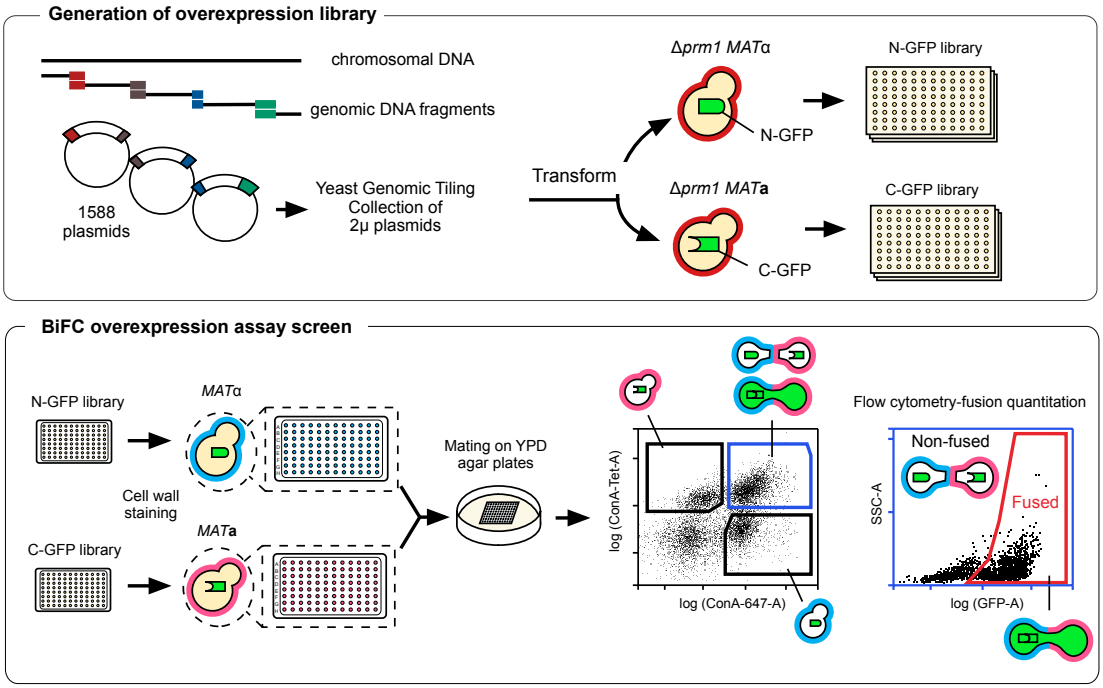

Figure 20. Overexpression cell fusion screen workflow. A high-throughput cell fusion screen was conducted using the Δ*prm1* genetic background to identify genetic cell fusion regulators. The plasmid library was transformed in 96-well format into Δ*prm1 MAT*α N-GFP and Δ*prm1 MAT***a** C-GFP cells to generate a Δ*prm1* N-GFP library and a Δ*prm1* C-GFP library. Each colony position comprises a *prm1* mutant containing a distinct tiling plasmid. Fusion efficiencies of Δ*prm1* × Δ*prm1* cells carrying the same plasmid are determined with the BiFC assay. Fusion efficiency is calculated as the number $(N)_{\text{fused mating pairs}}$ / ($N_{\text{fused pairs}}$ + $N_{\text{non-fused pairs}}$).

The screen was conducted in 96-well plate format. With the exception of the *PRM1* encoding plasmid, no dosage suppressors of the Δ*prm1* fusion arrest were identified. In contrast, plasmids which inhibited the remaining fusion pathway were identified. Primary screening identified 102 hit plasmids which conferred lower fusion efficiencies compared to empty vector control Δ*prm1* mating pairs (data not shown). A second screening round was performed to validate the hits and as a result, 28 genomic fragment bearing plasmids were confirmed to enhance the fusion arrest between Δ*prm1* × Δ*prm1* haploids. A plasmid was classed as an enhancer of Δ*prm1* fusion arrest if the fusion efficiency of mating pairs carrying that plasmid was <75% the fusion efficiency of Δ*prm1* empty vector mating pairs. The plasmids, including the genes encoded on the plasmids, are listed in Table 25.

Table 25. Secondary screening of putative Δ*prm1* fusion defect enhancers. [1]Ranking is sorted from highest fusion arrest to least. [2]Fusion efficiency of Δ*prm1* plasmid reactions were normalised to the fusion efficiency of Δ*prm1* empty vector controls to facilitate ranking. Tiling plasmids, genes encoded and their annotations are as provided in Jones et al. (2008). '[GENE]' indicates the ORF is intact but may be missing flanking sequences for correct regulation. '[GENE]*' indicates the 3' end of the gene is missing. '[GENE]&' indicates 5' end of the gene is missing. YGPM20k17 was excluded from subsequent analysis because the plasmid encodes the *MAT* locus which determine mating type. Thus, the Δ*prm1* fusion arrest enhancement conferred by YGPM20k17 was attributed to perturbance of cell type specification of *MAT*α cells.

Rank[1]	Fusion efficiency (%)[2]	Cell Pairing (%)	Plasmid	Genes										
1	28.88	52.29	YGPM27p16	[YJL007C]	[tM(CAU)J2]	CTK2	tL(UAA)J	CYR1	SYS1	[COX16]*				
2	36.12	42.75	YGPM14i08	[MRPL49]&	[BCK1]	KHA1	TOK1	[HPR5]*						
3	37.01	44.16	YGPM7p08	[SPA2]&	YLL020C	KNS1	YLL019W-A	COX19	[DPS1]&					
4	38.55	54.58	YGPM31e04	[SEC53]*	YOD1	YFL042C	YFL041W-A	FET5	YFL040W	ACT1	YPT1	[TUB2]*		
5	40.00	9.19	YGPM20k17	[RRP43]*	RBK1	PHO87	BUD5	YCR038W-A	MATA2	MATA1	YCR041W	[TAF2]&		
6	42.24	55.84	YGPM8p07	[GRX5]	PDR12	SUR1	LCL1	[LGE1]&						
7	44.82	43.75	YGPM20a02	[UTP10]*	PRM10	YJL107C	IME2	SET4						
8	44.86	48.54	YGPM13f19	[NUP85]	POL32	tM(CAU)J3	VPS55	SSC1	TAH11	tS(AGA)J	ANB1			
9	53.74	69.68	YGPM29d09	[YJR142W]&	PMT4	MGM101	RPS4A	YJR146W	HMS2	BAT2	[YJR149W]			
10	54.28	53.17	YGPM30n02	[KRE5]&	TEA1	YOR338W	UBC11	RPA43	[RPA190]*					
11	54.49	59.75	YGPM27k08	[YOL032W]&	SIL1	GAS5	YOL029C	YAP7	MDM38	MIM1	tS(GCU)O	LAG2	YOL024W	[IFM1]*
12	61.94	66.10	YGPM31d19	[SET2]*	ERG20	QCR8	HAL5	TPK1	[YJL163C]					
13	65.91	71.49	YGPM2h11	[YBR109W-A]&	[ALG1]	YSA1	SUS1	CYC8	YBR113W	RAD16	[LYS2]&			
14	66.25	72.47	YGPM28c19	[ABP1]&	FIG2	YCR090C	KIN82	[MSH3]&						
15	66.58	61.67	YGPM4n16	[PRE8]*	RPM2	YML090W	YML089C	UFO1	YML087C	ALO1	TUB1	YML084W	YML083C	[YML082W]*
16	67.24	49.12	YGPM18l24	[IRA1]*	BMT2	YBR141W-A	MAK5	[SUP45]						
17	67.83	49.45	YGPM4h24	[KRR1]*	FYV5	[YCL058W-A]	YCL057C-A	PRD1	PEX34	KAR4	SPB1	[PBN1]		
18	68.41	64.11	YGPM6d14	[RPB4]&	YUR1	TIF2	GLG2	YJL136W-A	RPS21B	YJL135W	[LCB3]*			
19	68.78	62.70	YGPM14a05	[EAP1]&	TOR2	YKL202W	[MNN4]&							
20	70.31	68.42	YGPM17p01	[UTP23]	DNL4	TSR3	SGT2	tR(ACG)O	SLG1	YOR008C-A				
21	70.72	53.69	YGPM8l10	[YGR039W]	KSS1	BUD9	MTE1	NQM1	RME1	YGR045C	[TAM41]*			
22	70.80	50.52	YGPM32d08	[SSB1]	YDL228C	HO	GCS1	SHS1	[WHI4]&					
23	71.14	61.17	YGPM33l21	[MRS3]	YJL132W	YJL131C	[URA2]&							
24	71.39	79.69	YGPM25h19	[ACH1]	tI(AAU)B	tG(GCC)B	RRN6	FMT1	[YBL012C]	[SCT1]*				
25	71.45	36.24	YGPM22n03	[ECM17]*	IML1	HOM6	[HIR3]&	YJR140W-A						
26	73.54	50.45	YGPM20m03	[TFC7]&	YOR111W	YOR112W	AZF1	YOR114W	TRS33	[RPO31]&				
27	73.67	50.83	YGPM2p16	[MRPL25]*	PEX8	PAC10	YGR079W	TWF1	SLX9	TOM20	GCD2	MRP13	[RPL11B]	
28	74.61	58.36	YGPM28n03	[AGP1]*	YCL023C	KCC4	YCL022C	tE(UUC)C	YCL021W-A	YCL019W	YCL020W			

3.1.1.1 Quantification of cell-cell pairing efficiency to isolate genes which strongly impair pheromone signalling

In addition to quantifying fusion efficiency between haploids which have formed a mating pair, the differential staining of the *MAT***a** and *MAT*α cells by cell wall dyes also allow for an independent quantification of cell pairing efficiency in the same mating reaction **(Figure 21A)**. This is calculated as the ratio of single stained haploids (specifically, whichever of the *MAT***a** or *MAT*α haploids were limiting in a given reaction) with respect to the double stained mating pairs. This metric provides an indication of how able cells could signal and establish tight irreversible contacts with a partner to form a mating pair. For example, mutations that disrupt pheromone signalling such as Δ*erg6* mutants (Jin et al., 2008) form **a**-α pairs less efficiently than wt cells **(Figure 21B)**. As expected, Δ*prm1* mutants pair as efficiently as wt cells because Prm1 is not involved in the upstream signalling process.

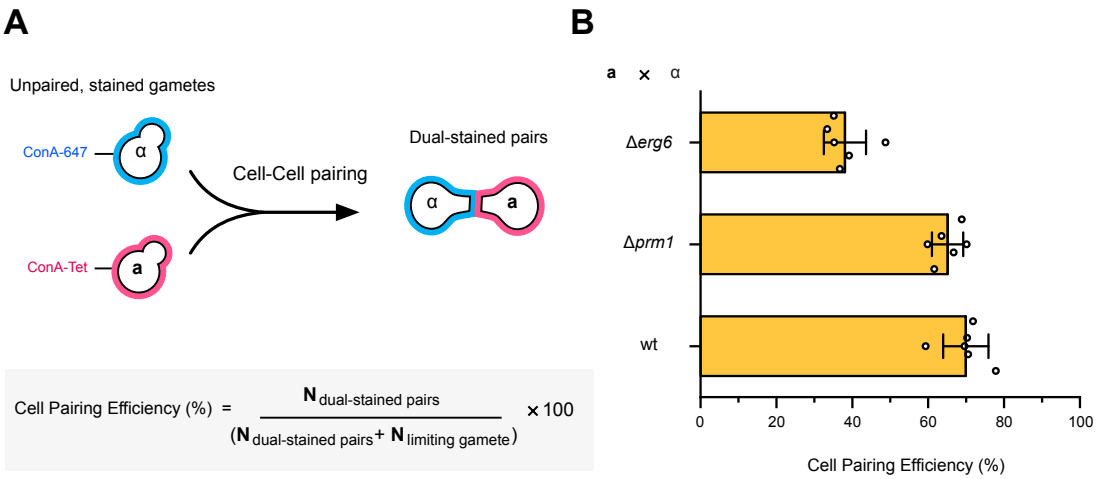

Figure 21. Cell pairing efficiency quantification can distinguish mutants with impaired pheromone signalling. A. Cell walls of *MAT*α cells are stained with ConA-647 and mated to ConA-Tet stained *MAT***a** cells. In a given mating reaction, cell pairing is quantified as the number $(N)_{\text{dual stained mating pairs}}$ / $(N_{\text{dual-stained pairs}} + N_{\text{limiting gamete}}) \times 100$. The limiting gamete is defined as the population of unpaired **a** or α gamete which was lower in frequency during flow cytometry acquisition. **B.** Mutants impaired in pheromone signalling such as Δ*erg6* correspondingly display reduced cell pairing efficiency in comparison to wt cells. Mating assays were conducted using the 12-manifold BiFC assay. Cell pairing datapoints are from a total of 2 independent experiments which each contained 3 biological replicates. Error bars signify SD.

20 out of 28 of Δ*prm1* mating pairs carrying tiling plasmids displayed a cell pairing efficiency between 50–80% **(Table 25)**, which was comparable to cell pairing efficiencies of wt strains **(Figure 21B)**. During the secondary screening process, the mean cell pairing efficiency of the Δ*prm1* empty vector control was 59.9% ±8.74 (SD) (n=13). Notably, Δ*prm1* cells containing plasmid YGPM20k17, were severely deficient at forming mating pairs (~10% cell pairing efficiency). Since Δ*prm1* cells are phenotypically normal for pheromone signalling, the low cell pairing of Δ*prm1* carrying YGPM20k17 was likely caused by gene(s) on the plasmid.

The genomic fragment of YGPM20k17 encompasses the mating type locus, specifically the *MAT***a** locus (since the plasmid library was prepared from a *MAT***a** strain). The mating type locus is a critical determinant of mating type behaviour. *MAT*α cells do not contain an actively expressed *MAT***a** locus, and ectopic expression of the *MAT***a** locus in a *MAT*α haploid results in a diploid behaving cell (Haber, 2012). Because diploids are non-mating, the *MAT*α haploids carrying YGPM20k17 likely no longer produce pheromone nor respond to pheromone. This would explain why cells carrying this plasmid YGPM20k17 formed mating pairs infrequently and in addition displayed an enhanced fusion arrest (40% fusion efficiency relative to empty vector). Therefore, this plasmid was not analysed further and excluded from subsequent investigations.

3.1.1.2 Identification of *SUR1* as a strong Δ*prm1* fusion defect enhancer

The other strongly fusion arresting plasmids possessed no obvious genes which could explain the enhanced Δ*prm1* fusion arrest. Excluding plasmid YGPM20k17, the nine strongest Δ*prm1* fusion arresting plasmids were then re-transformed into Δ*prm1 MAT*α N-GFP and *MAT***a** C-GFP cells and fusion efficiency was re-measured in triplicate to determine if the fusion arrest was reproducible **(Figure 22A)**. One plasmid, YGPM21b06, strongly enhanced the fusion arrest of Δ*prm1* mating pairs. After subcloning experiments, the gene in plasmid YGPM21b06 responsible for enhancing Δ*prm1* fusion arrest was found to be *SUR1* **(Figure 22B)**.

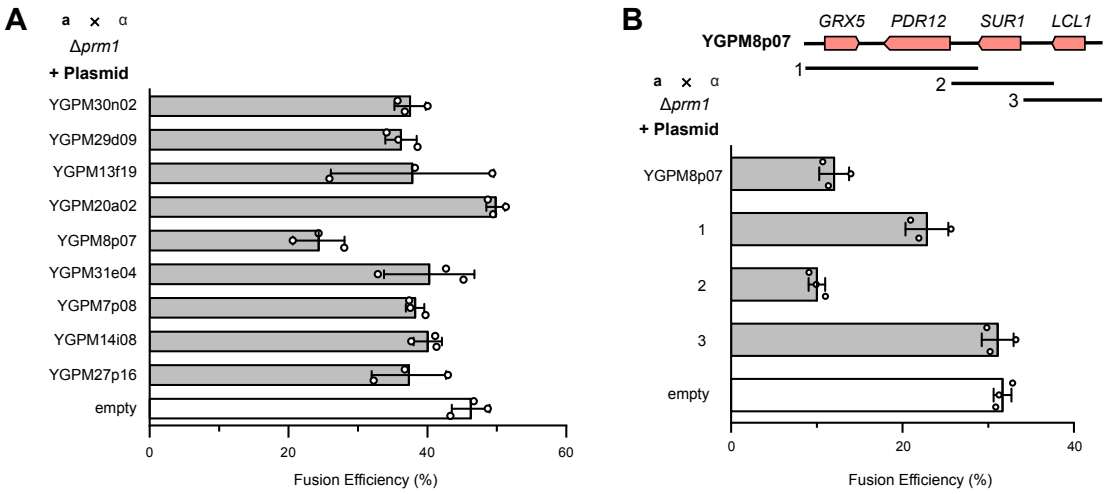

Figure 22. Identification of *SUR1* as a *prm1* fusion defect enhancer. A. Re-measurement of top 9 plasmids identified after secondary screening. **B.** *SUR1* is responsible for the strong fusion arrest effect of YGPM8p07. Genes in the genomic insert of YGPM8p07 were subcloned into plasmids. Fragment 2 containing *SUR1* recapitulated the enhanced fusion arrest of YGPM8p07. Error bars represent SD of 3 biological replicates.

3.1.2 Overexpression of the MIPC Synthase encoding *SUR1* leads to further Δ*prm1* plasma membrane fusion arrest

The gene responsible for the Δ*prm1* fusion defect enhancement in plasmid YGPM8p07 was found to be *SUR1* **(Figure 22)**. *SUR1* (also known as *CSG1*) encodes a sphingolipid mannosyltransferase responsible for the addition of mannose to inositol phosphorylceramide (IPC), forming mannosylinositol phosphorylceramide (MIPC) (Beeler et al., 1997). To ascertain the stage of mating that was arrested by *SUR1* overexpression, Δ*prm1* mating pairs overexpressing *SUR1* were stained with FM4-64, a lipophilic dye to label plasma membranes. The classes of phenotypes observed was then quantified **(Figure 23A)**. Four classes were used; i) fused, indicated by cytosolic complemented split-GFP, ii) flat interfaces, which suggest the presence of a cell wall, iii) cytoplasmic bubbles, indicative of plasma membrane fusion failure and iv) lysis, indicated by prominent FM4-64 signal in the cytosol and a collapsed mating pair observed under transmitted light.

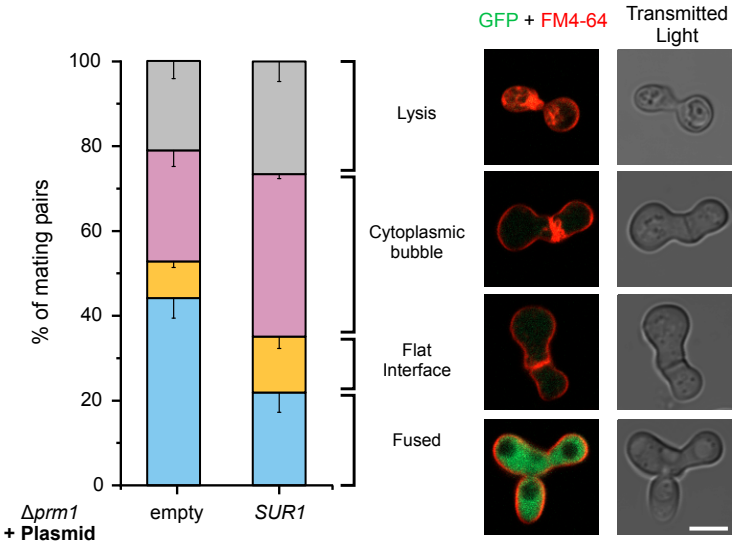

Figure 23. *SUR1* overexpression enhances plasma membrane fusion failure phenotype of Δ*prm1* mating pairs. Δ*prm1* mating pairs which overexpressed *SUR1* were assessed for phenotypes after staining. >150 mating pairs were counted. Error bars denote SD from 3 independent experiments. Scale bar denotes 5 µm.

The cytoplasmic bubble phenotype was more frequent in *SUR1* overexpressing Δ*prm1* mating pairs compared to control Δ*prm1* mating pairs, suggesting enhanced failure of plasma membrane fusion. *SUR1* overexpression did not impair cell wall degradation because the percentage of Δ*prm1* mating pairs with flat interfaces, was comparable to control Δ*prm1* mating pairs.

Next, I tested if Sur1 overexpression could inhibit fusion of wild type gametes **(Figure 24A)**. In contrast to the case in Δ*prm1* mating pairs, fusion of wild type mating pairs was unaffected by *SUR1* overexpression. Therefore, the presence of Prm1 precludes the fusion arresting effect of *SUR1* overexpression. Furthermore, mating pair formation was not affected by *SUR1* overexpression, suggesting the upstream preparatory steps of mating were not perturbed by *SUR1* overexpression **(Figure 24B)**. Taken together, Sur1 overexpression disrupts specifically the plasma membrane fusion step in Δ*prm1* mating pairs, resulting in enhanced penetrance of cytoplasmic bubbles.

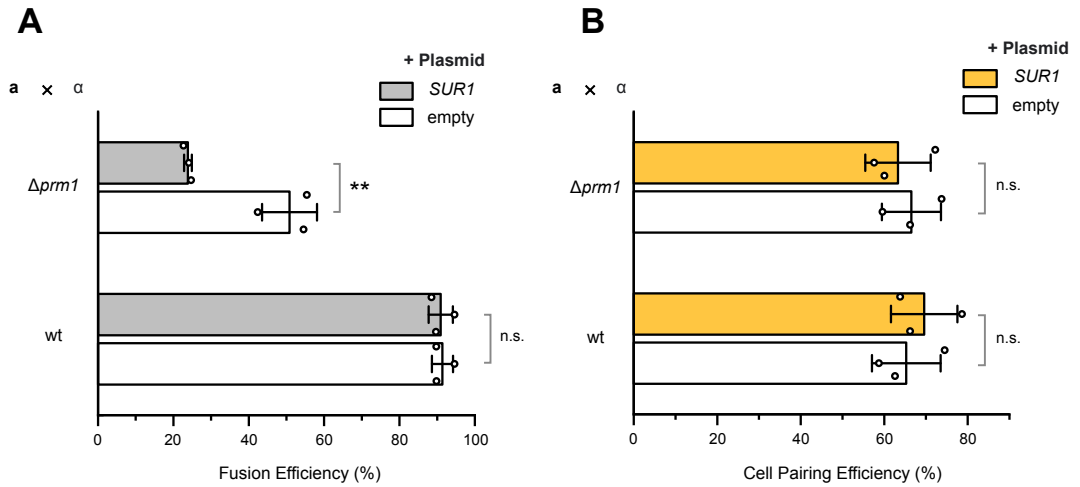

Figure 24. *SUR1* overexpression effect is specific to the Δ*prm1* mutation. A. *SUR1* was overexpressed in wt mating pairs or Δ*prm1* mating pairs. Fusion efficiency was determined by the BiFC assay. **B.** Cell pairing efficiency of wt or Δ*prm1* mating pairs overexpressing *SUR1.* Pairing quantification is the ratio of mating pairs to the total of mating pairs and limiting gamete. No pairing defect was observed. Error bars denote SD of 3 independent experiments each containing 3 biological replicates.

3.1.3 Overexpression of other sphingolipid genes do not strongly arrest Δ*prm1* fusion

The novel finding that a sphingolipid gene could further disrupt fusion of Δ*prm1* mating pairs prompted a further investigation into the sphingolipid pathway **(Figure 25A)**. As mentioned, Sur1 catalyses mannose addition to IPC, forming MIPC, which alongside $M(IP)_2C$, comprises the three complex sphingolipid species present in budding yeast. *S. cerevisiae* also possesses a paralog of Sur1, Csh1. Both Sur1 and Csh1 can directly associate with another membrane protein, Csg2, which regulates their activity. The absence of Csg2 hinders the activity of both Sur1 and Csh1, and in the case of Csh1, its activity is completely absent in the Δ*csg2* mutant (Uemura et al., 2003).

Since Csh1 has redundant functions to Sur1, I determined if *CSH1* overexpression inhibited Δ*prm1* fusion. Additionally, I investigated whether overexpression of other sphingolipid biosynthesis enzymes could also hamper Δ*prm1* × Δ*prm1* fusion. Therefore, the fusion efficiencies of Δ*prm1* mating pairs overexpressing *AUR1*, encoding the IPC synthase Aur1 and *IPT1*, which encodes the $M(IP)_2C$ synthase Ipt1 were determined

(Figure 25A). Out of the genes tested, only overexpression of *SUR1* conferred a strong fusion arrest in Δ*prm1* mating pairs, indicating particular susceptibility of the MIPC Synthase towards Δ*prm1* fusion. Overexpression of the sphingolipid genes did not affect the ability for cells to form mating pairs, as cell pairing efficiency was similar to Δ*prm1* empty vector mutants (Figure 25B).

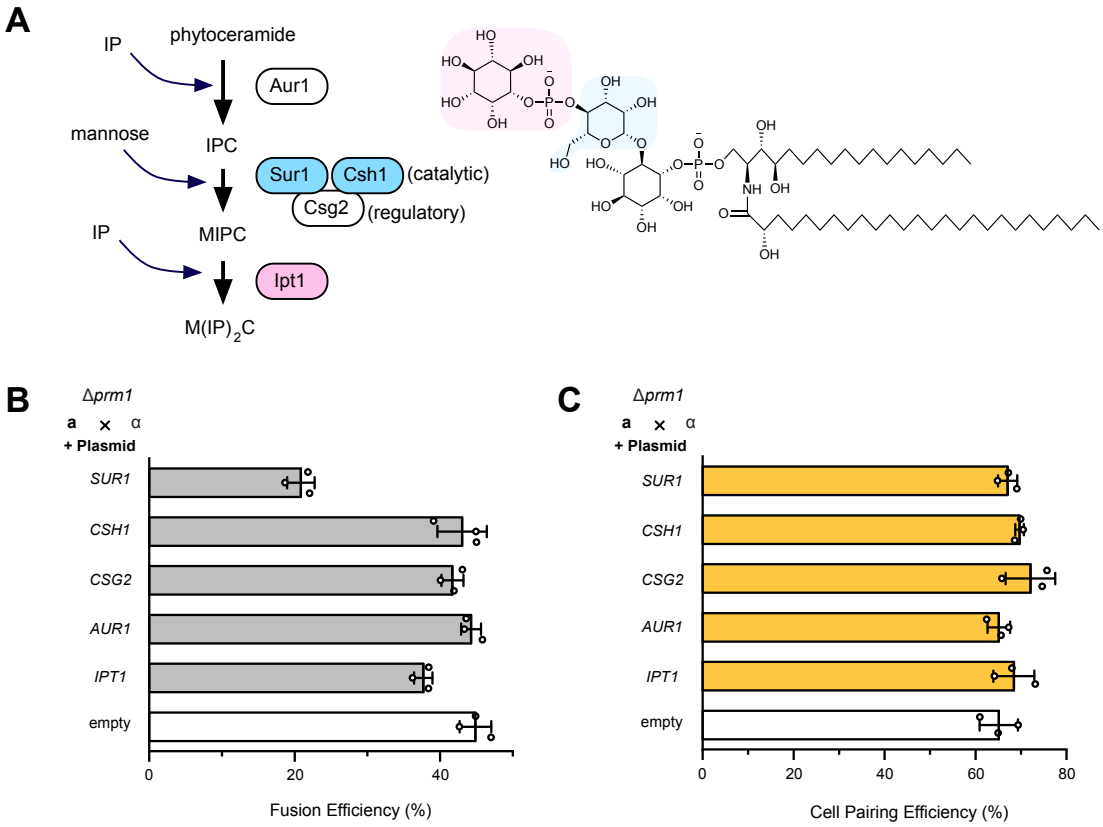

Figure 25. Overexpression of the sphingolipid mannosyltransferase *SUR1* specifically inhibits fusion of Δ*prm1* mating pairs. **A.** Late stage sphingolipid biosynthesis pathway. Chemical structure of $M(IP)_2C$ is shown to the right. **B.** Overexpression of sphingolipid genes on Δ*prm1* fusion. Genes encoding for the enzymes involved in the terminal steps of the sphingolipid biosynthesis pathway were overexpressed from high copy 2μ plasmids in Δ*prm1* mating pairs. Fusion efficiency was then determined by the BiFC assay. **C.** Cell pairing efficiency of Δ*prm1* mating pairs overexpressing sphingolipid genes. Error bars denote SD of 3 biological replicates.

3.1.4 Localisation of overexpressed Sur1-mNG is consistent with Golgi residence

The bulk synthesis of the complex sphingolipids IPC, MIPC, and $M(IP)_2C$ occurs in the Golgi apparatus (Levine et al., 2000). The mannose-GDP substrate used by Sur1 and Csh1 to convert IPC to MIPC, is transported from the cytoplasm into the Golgi lumen by a Golgi resident transporter, Vrg4 (Dean et al., 1997). Consistent with the Golgi lumen as the site of mannosylation, Sur1 and Csh1 are also localised in the Golgi membrane (Lisman et al., 2004; Uemura et al., 2007).

I investigated the localisation of Sur1 under both native-like expression and overexpression regimes **(Figure 26A)**. For this, a low copy (1-2 copy) CEN plasmid or a high copy 2μ plasmid encoding for Sur1-mNeonGreen (mNG) was introduced into wt *MAT***a** cells. In mitotic cells, Sur1-mNG was present in intracellular punctate compartments indicative of Golgi localisation. The additional vacuolar localisation of Sur1-mNG suggested a proportion of Sur1 was transported to the vacuole for degradation, which was previously reported (Uemura et al., 2007). Sur1-mNG which was overexpressed also showed punctate and vacuolar localisation. In some cells, the punctate structures containing Sur1-mNG were more numerous and also located at the cell periphery (white arrowheads). It is likely that in these cells saturation of the Golgi vesicles had occurred, causing Sur1-mNG to leak to other cellular compartments, such as endosomes, cortical ER or the plasma membrane. The high mNG signal in these cells indicated large amounts of Sur1-mNG was produced, further supporting the idea these compartments were saturated.

The results indicated that overexpressed Sur1 remained predominantly in the Golgi in mitotic conditions. To investigate if localisation of Sur1 remained consistent during mating, *MAT***a** haploids were treated with synthetic pheromone. Pheromone exposure stimulates the cell to form mating projections and thus mimics the early preparatory steps of mating. In haploids treated with pheromone; overexpressed Sur1-mNG persisted as punctate and vacuolar **(Figure 26B, upper)**. Furthermore, no Sur1-mNG was observed at the mating projection tips of pheromone treated cells. This was the case even in the cells which produced the highest amounts of Sur1 and leaked to peripheral compartments **(Figure 26B, lower)**. Therefore, the Δ*prm1* fusion arrest phenotype brought by Sur1 overproduction cannot be explained by ectopically localised Sur1 to mating projections or

eventual cell-cell contacts. Instead, the enhanced Δ*prm1* fusion arrest more likely arises from the elevated functional Sur1 levels in the Golgi, the predominant location of the enzyme.

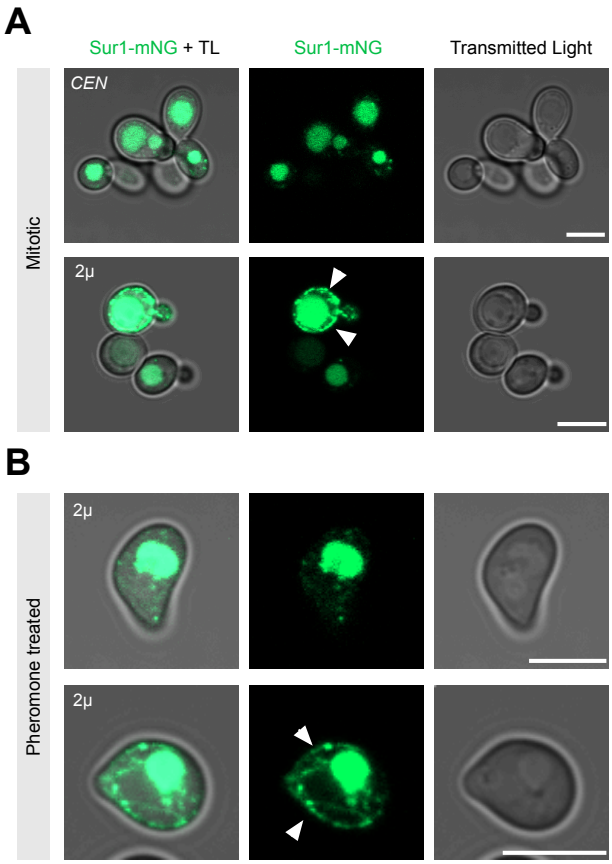

Figure 26. Localisation of Sur1-mNG in intracellular compartments in mitotic and pheromone treated cells. A. Sur1-mNG is present in the Golgi and the vacuole in mitotic cells. Sur1-mNG was expressed under the *SUR1* promoter from *CEN* or 2μ plasmids in logarithmic phase growing BY4741 *MAT***a** cells and imaged via confocal microscopy. **B.** Punctate localisation of overexpressed Sur1-mNG in pheromone treated cells indicates Golgi localisation is retained. Cells in logarithmic phase (OD_{600} = 0.5) were treated with 8 μM α-factor for 90 min at 30 °C, 220 rpm. In (A) and (B) panels, white arrowheads highlight Sur1-mNG present in peripheral compartments of the cell which was only observed when Sur1-mNG was overexpressed from 2μ plasmids. Scale bars denote 5 μm.

3.1.5 Sur1-mediated fusion arrest depends on the DxD motif

The Golgi localisation of overexpressed Sur1 indicated that Sur1-mediated fusion arrest of Δ*prm1* mutants could be associated to the mannosylation function of Sur1. Therefore, the mannosylation activity of Sur1 was investigated in further detail. Many

glycosyltransferases contain a DxD motif within the active site which are required for nucleotide-sugar transferase activity. The DxD motif is conserved amongst diverse families of glycosyltransferases, suggesting that the motif is critical for their enzymatic activity (Wiggins and Munro, 1998). Indeed, for yeast glycosyltransferases where mutation of the aspartates comprising their DxD motif have been tested, the mannosylation activity of each mutant protein was abolished (Kitajima et al., 2006; Striebeck et al., 2013; Wiggins and Munro, 1998). The aspartates of the DxD motif are involved in binding to the pyrophosphate moiety of the GDP-sugar substrate, through coordination of metal ion cofactors (Striebeck et al., 2013).

In Sur1 and Csh1, a DxD motif is present in their predicted Golgi luminal mannosyltransferase domain **(Figure 27A)**, which is also found in yeast mannosyltransferases Och1 and Hoc1. Although Och1 and Hoc1 do not mannosylate sphingolipids, they display a significant stretch of sequence homology to Sur1 and Csh1, which together constitute the Och1 gene family (Beeler et al., 1997; Moo et al., 2006; Wiggins and Munro, 1998). I investigated whether the enzymatic activity of Sur1 was required for the enhanced Δ*prm1* fusion arrest. D138 and D140 which comprise the Sur1 DxD motif were both mutated to alanine (AxA). Overexpression of the Sur1-AxA mutant was unable to further arrest fusion of Δ*prm1* mating pairs **(Figure 27B)**. The overexpressed mNG variant (Sur1-AxA-mNG) displayed intracellular localisation which was similar to wild-type Sur1-mNG **(Figure 27C)**, indicating that mutation of the DxD motif did not

adversely affect the stability of Sur1. The results indicate that the Sur1-mediated fusion arrest is dependent on its mannosylation activity.

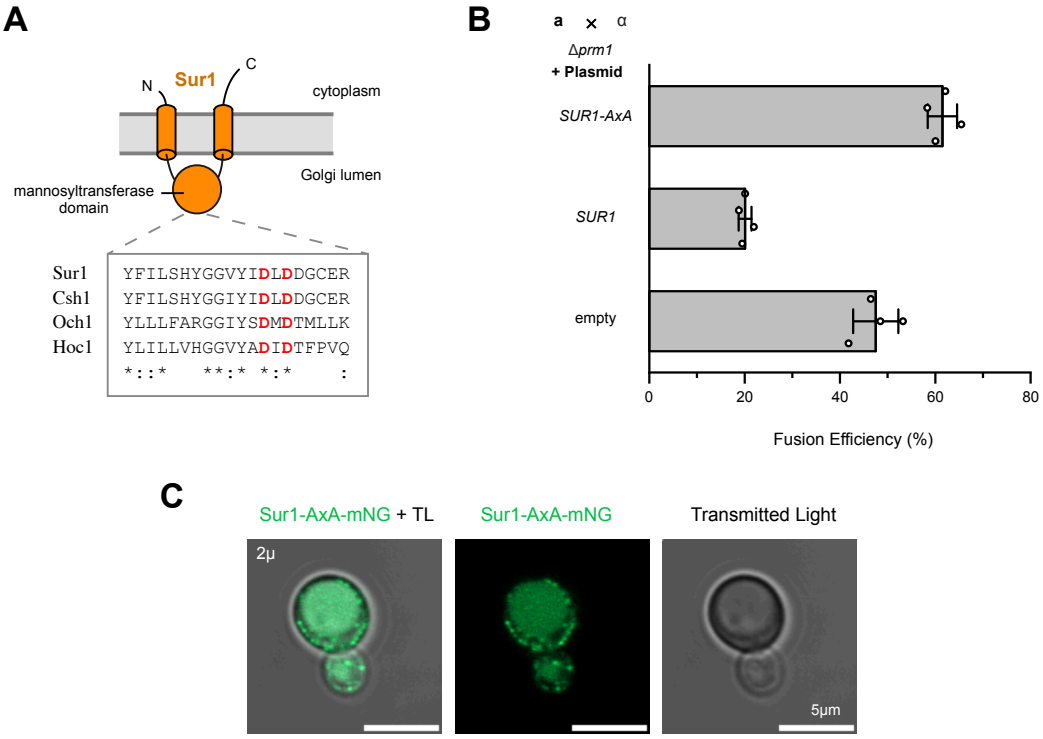

Figure 27. The DxD motif is required for Sur1-mediated fusion arrest of Δ*prm1* gametes. A. Conservation of the DxD motif in the Och1 gene family (Sur1, Csh1, Och1 and Hoc1). Multiple sequence alignment (MSA) of the region containing the DxD motif is shown. Sur1 and Csh1 are *S. cerevisiae* sphingolipid mannosyltransferases. Och1 and Hoc1 are *S. cerevisiae* mannosyltransferases which can be identified in BLAST searches of Sur1. MSA was generated by Clustal Omega (Sievers et al., 2011). **B.** Substitution of Sur1 DxD motif to AxA eliminates the fusion arrest effect conferred by Sur1 overexpression in Δ*prm1* × Δ*prm1* mating pairs. A variant of *SUR1* containing the AxA mutant was cloned in an equivalent 2μ plasmid to the wild type *SUR1* 2μ plasmid. Fusion efficiencies of Δ*prm1* × Δ*prm1* crosses overexpressing either *SUR1*, *SUR1-AxA* or contained empty vector was determined by the BiFC assay. Error bars denote SD of three biological replicates. **C.** Mutation of the DxD motif does not affect the expression of Sur1. Sur1-AxA-mNG was expressed from a 2μ plasmid and showed intracellular punctate localisation in mitotic cells.

3.1.6 Absence of M(IP)$_2$C suppresses Δ*prm1* fusion arrest

Evidently, the increased levels of mannosylation active Sur1 hampers the fusion between Δ*prm1* mating pairs. What then, would the consequence on cell fusion be if the endogenous sphingolipid mannosylation activity was removed?

The fusion efficiencies of bilateral (*MAT*α null mutants crossed to the *MAT***a** cells possessing the same null mutation) crosses were measured by the BiFC assay. *SUR1* deletion in a wild type background had no effect on the levels of fusion **(Figure 28A)** which was consistent with a previous study (Villasmil et al., 2016). Genetic knockout of the other terminal sphingolipid biosynthesis enzymes (Δ*ipt1*, Δ*csg2* and Δ*csh1*) in the sphingolipid biosynthesis pathway also showed no effect on fusion. The effect of IPC loss could not be tested because *AUR1* is essential (Hashida-Okado et al., 1996). No cell pairing defect was observed with the sphingolipid mutants **(Figure 28B).** These results suggest that the two mannosylated sphingolipid species MIPC and $M(IP)_2C$ are dispensable for *S. cerevisiae* cell fusion.

Since *SUR1* overexpression-mediated fusion arrest was Δ*prm1* specific, I subsequently investigated the effect of *SUR1* knockout in a Δ*prm1* null background. Given the functional redundancy of Sur1 and Csh1, it was expected that deletion of both genes would be required to exhibit a phenotype. Surprisingly, deletion of *SUR1* in Δ*prm1* alone was able to suppress the Δ*prm1* fusion defect and restore fusion close to wild type levels **(Figure 28C).** The behavior of Δ*prm1*Δ*csh1* × Δ*prm1*Δ*csh1* matings was in line with initial expectations; absence of Sur1 paralog Csh1 did not suppress the Δ*prm1* fusion defect, likely because Sur1 was still present in the Δ*prm1*Δ*csh1* mutant. The absence of the Sur1 and Csh1 regulatory subunit Csg2, was also able to suppress the Δ*prm1* fusion defect **(Figure 28C)**. The stabilities of Sur1 and Csh1 are weakened in the absence of Csg2, and as a consequence MIPC and $M(IP)_2C$ are almost completely absent in Δ*csg2* mutants (Uemura et al., 2003).

Finally, suppression of Δ*prm1* fusion arrest also occurred when Ipt1 was absent **(Figure 28C)**. In other words, eliminating biosynthesis of the terminal sphingolipid product $M(IP)_2C$ suppresses the Δ*prm1* fusion defect. In the context of this result, although the levels of both $M(IP)_2C$ and MIPC are reduced in Δ*sur1* mutants, we can conclude that suppression of Δ*prm1* fusion arrest brought by Δ*sur1* is caused by the specific reduction of $M(IP)_2C$ levels and not MIPC. The deletion of sphingolipid genes in Δ*prm1* mutants did not affect cell pairing when compared to Δ*prm1* **(Figure 28D).** The cell pairing data suggest that no major changes in the ability for cells to pair occurred by the sphingolipid alterations, reaffirming that sphingolipids are directly involved late in the membrane fusion process.

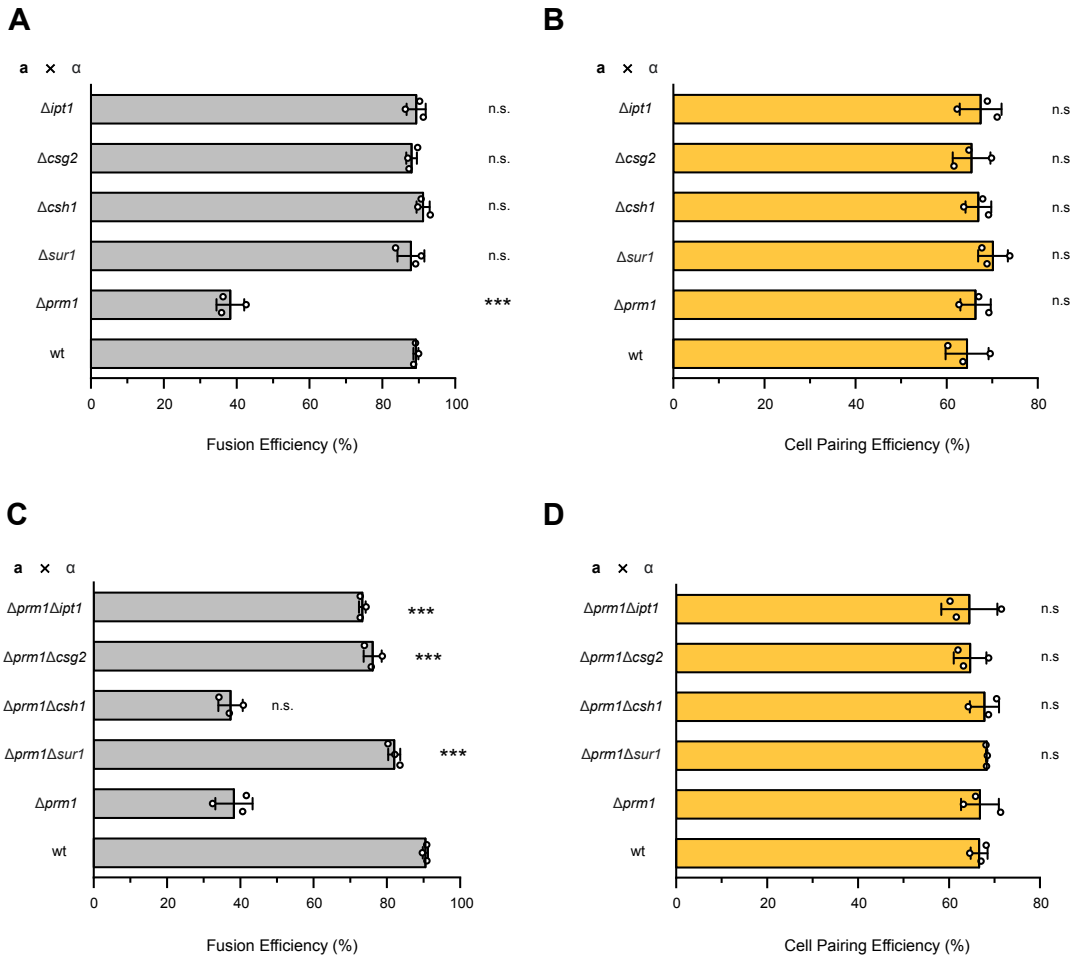

Figure 28. Suppression of Δ*prm1* fusion defects by sphingolipid headgroup mutants. A. Single gene deletions of complex sphingolipid biosynthesis enzymes are dispensable for efficient cell fusion. **B.** Cell pairing efficiency of the sphingolipid mutants were similar to wt cells. **C.** In the Δ*prm1* background, deletion of sphingolipid enzyme encoding genes suppresses the Δ*prm1* fusion defect, with the exception of *SUR1* paralog *CSH1*. **D.** Cell pairing efficiency of Δ*prm1* sphingolipid double mutants. P-values are two tailed unpaired Student's t-test between each mutant to wt in (A) and (B) and between each mutant to *prm1* in (C) and (D). *** indicates p<0.001. ** indicates p<0.01 and and p>0.05 was considered not significant (n.s.).

Since small amounts of MIPC and M(IP)$_2$C are present in Δ*sur1* cells (Uemura et al., 2003), a Δ*sur1*Δ*csh1* deletion mutant was generated to determine the effect of complete absence of MIPC and M(IP)$_2$C towards fusion. No fusion defect was observed between Δ*sur1*Δ*csh1* mutants **(Figure 29)**. Therefore, wt cells do not require MIPC nor M(IP)$_2$C for cell fusion. In the Δ*prm1*Δ*sur1*Δ*csh1* crosses, fusion efficiencies were comparable to Δ*prm1*Δ*sur1* crosses. In other words, depletion of MIPC and M(IP)$_2$C to low levels by Δ*sur1*

was sufficient to suppress the Δ*prm1* fusion arrest. Further elimination of the residual MIPC and M(IP)$_2$C in Δ*prm1*Δ*sur1* cells by additionally deleting *CSH1* does not suppress Δ*prm1* fusion arrest any further.

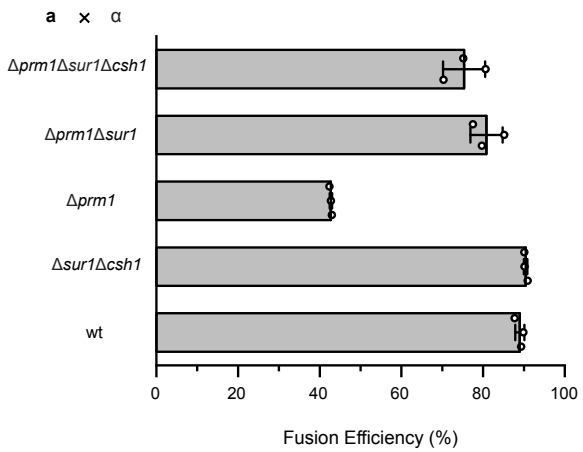

Figure 29. Additional absence of Sur1 paralog Csh1 does not further suppress fusion arrest of Δ*prm1*Δ*sur1* matings. Fusion efficiency was determined by the BiFC assay. Error bars denote SD of 3 biological replicates.

3.1.7 Sur1-mediated inhibition of Δ*prm1* fusion depends on Ipt1

As mentioned previously, suppression of Δ*prm1* fusion arrest conferred by Δ*sur1* is likely from the specific reduction of M(IP)$_2$C levels. Extension of this notion would suggest that in the other extreme, the enhanced Δ*prm1* fusion arrest conferred by Sur1 overexpression is primarily due to the increase of M(IP)$_2$C levels, even though both MIPC and M(IP)$_2$C are increased. To investigate this hypothesis and clarify which sphingolipid was responsible for the fusion arrest, I determined whether *SUR1* overexpression could further arrest fusion of Δ*prm1*Δ*ipt1* gametes, where M(IP)$_2$C is absent. In contrast to the case in Δ*prm1* mating pairs, *SUR1* overexpression in Δ*prm1*Δ*ipt1* mating pairs no longer induced a strong fusion arrest, indicating a strict dependency on M(IP)$_2$C production for the fusion arrest **(Figure 30)**.

If increased M(IP)$_2$C levels were indeed responsible for the fusion arrest, then Ipt1 overproduction should also arrest fusion of Δ*prm1* mating pairs. Indeed, this was the case; Ipt1 overproduction enhanced the fusion arrest of Δ*prm1* mating pairs **(Figure 30)**. To raise the levels of M(IP)$_2$C, the cell requires the precursor MIPC. As expected, no enhanced

Δ*prm1* fusion arrest was observed when *IPT1* was overexpressed in Δ*prm1*Δ*sur1* mating pairs.

In conclusion, these experiments demonstrate that both Sur1 overproduction and Ipt1 overproduction further inhibit the plasma membrane fusion of Δ*prm1* gametes, most likely due to increased $M(IP)_2C$ synthesis. Because Sur1 overproduction led to a greater fusion arrest than Ipt1, it further suggests that of the two enzymes, Sur1 overproduction leads to greater amounts of $M(IP)_2C$ synthesis.

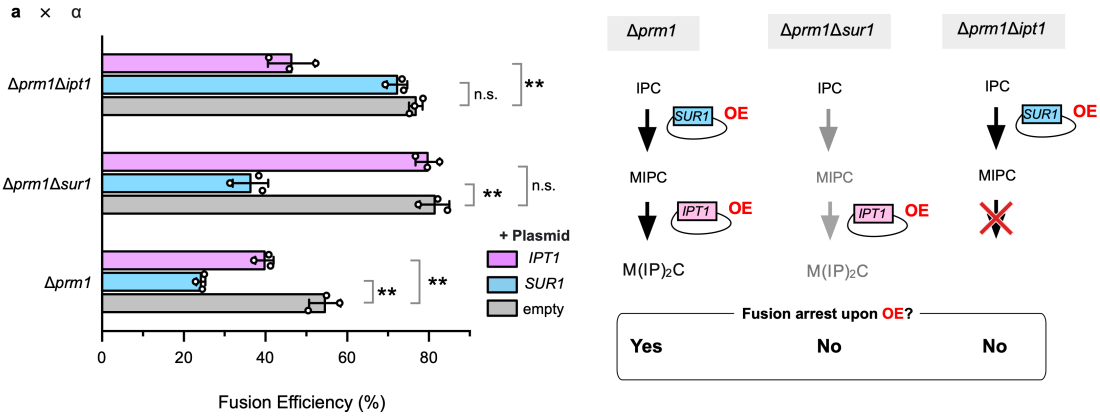

Figure 30. *SUR1* mediated fusion arrest of Δ*prm1* mating pairs requires *IPT1*. Cells contained 2μ plasmids overexpressing either Sur1 (blue) or overexpressing Ipt1 (magenta). Sur1 overexpression-mediated fusion arrest of Δ*prm1* cells was dependent upon Ipt1. Likewise, Ipt1-overexpression mediated fusion arrest of Δ*prm1* cells was dependent upon Sur1. Fusion efficiencies were determined by the BiFC assay. The scheme on the right illustrates the critical results found. Fusion arrest from Sur1 and Ipt1 overexpression (OE, red) depends on the availability of the cells to synthesize $M(IP)_2C$. The sphingolipid pathways depict the possible sphingolipid species that can be synthesized in the respective knockout mutants. Note that in Δ*prm1*Δ*sur1* cells, Csh1 is still present and so low amounts of MIPC and $M(IP)_2C$ are still produced (depicted as grey). Error bars denote SD from three independent experiments. P-values are two tailed unpaired Student's t-test. *** indicates $p<0.001$. ** indicates $p<0.01$ and and $p>0.05$ was considered not significant (n.s.).

3.1.8 Sur1 overproduction increases $M(IP)_2C$ levels

To confirm if $M(IP)_2C$ was increased upon *SUR1* overexpression, sphingolipids from cell-derived lipid extracts were analysed by thin layer chromatography **(Figure 31)**. To simplify the identification of sphingolipids, the lipid extract was treated with methylamine

to deacylate phospholipids prior to spotting the extract on the TLC plate (Clarke and Dawson, 1981; Morimoto and Tani, 2015). Under strong polar solvent systems, the deacylated phospholipids co-migrate with the solvent front and are thereby separated from the remaining sphingolipids, which migrate more slowly.

$M(IP)_2C$ was then identified by two pieces of evidence. Firstly, the band was absent in lipid extracts derived from Δ*sur1*Δ*csh1* mutants and Δ*ipt1* mutants. Secondly, the migration of the sphingolipid was slower (closer to the origin) than the other sphingolipids on the TLC plate, which was expected since $M(IP)_2C$ was more polar than IPC and MIPC (due to the additional inositol phosphate moiety). Bands corresponding to the precursor sphingolipids IPC and MIPC were assigned using the same line of criteria. As expected, in the Δ*ipt1* mutant, MIPC accumulated, whereas in Δ*sur1*Δ*csh1* mutants, accumulation of IPC occurred. In lipid extracts derived from cells which overexpressed Sur1, higher amounts of $M(IP)_2C$ was detected relative to the empty vector control. This was supported by quantitation of the $M(IP)_2C$ bands using densitometry **(Figure 31B)**. In conclusion, the TLC results support the idea that increased levels of $M(IP)_2C$ lead to the enhanced fusion arrest of Δ*prm1* mating pairs.

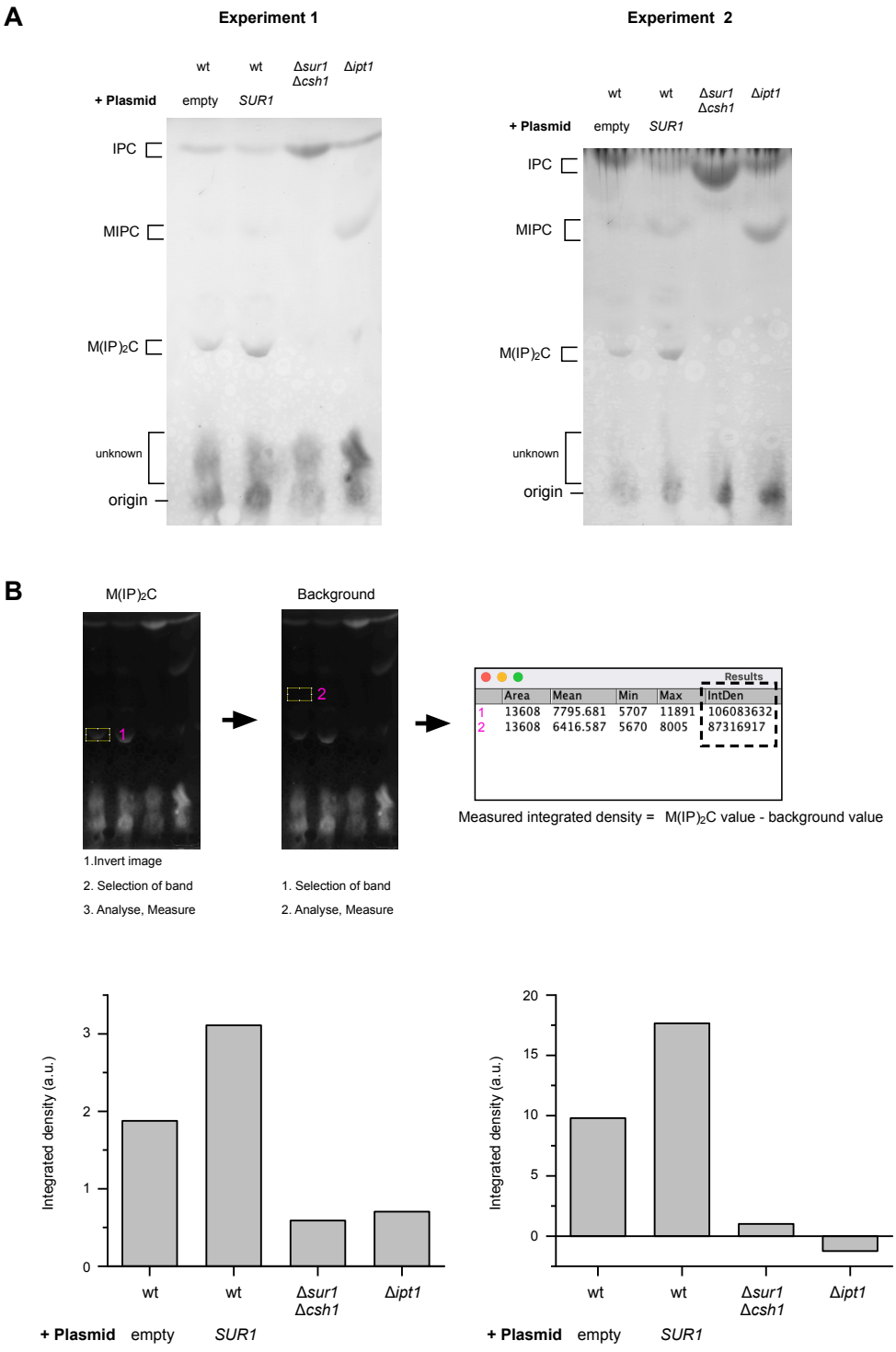

Figure 31. Increased levels of M(IP)$_2$C upon *SUR1* overexpression. A. Two representative TLC plates are shown. wt *MAT***a** cells carried either high copy empty plasmids or high copy *SUR1* plasmids under the *SUR1* promoter. Lipid extracts were treated with methylamine at 53 °C for 1 h to deacylate phospholipids. TLC was performed using chloroform/methanol/ammonia (9:7:2; v/v/v) as the solvent system. The plate was then stained using copper sulfate/phosphoric acid spray and

heating at 180 °C. Sphingolipids were assigned based on their reported migration patterns in the literature and the sphingolipid knockout mutants (Koga et al., 2022). The smears close to the origin are unknown and likely represent impurities. Such smears are also reported in the literature (Morimoto and Tani, 2015). **B.** Quantitation of $M(IP)_2C$ levels in each TLC plate. Upper, workflow to quantify $M(IP)_2C$ using integrated density. The image of the TLC plate was inverted, and a rectangle encompassing the band was created (1). Then, the integrated density of the band was calculated. This process was repeated to calculate the background density (2). The background was defined per lane in a region without any sphingolipid bands. The measured integrated density was the difference between the $M(IP)_2C$ and the background value.

3.1.9 Csh1 requires Csg2 co-overproduction to arrest Δ*prm1* fusion

Given the finding that Sur1 overexpression can further arrest fusion of Δ*prm1* mating pairs, the failure of its paralog Csh1 to further arrest Δ*prm1* fusion when overproduced was unexpected **(Figure 25)**. Assuming the mannosyltransferases have similar turnover, the different fusion outcomes may reflect inherent differences between the two paralogs. Previous studies reported that Csh1 requires to be complexed with Csg2 to successfully exit the ER and traverse to the Golgi (Uemura et al., 2007). The failure of Csh1 to form complexes with Csg2 also leads to Csh1 degradation through ER-associated degradation (ERAD). In contrast, Sur1 is able to exit the ER to the Golgi without Csg2 (Uemura et al., 2007). The different requirements of Sur1 and Csh1 for Csg2 would sufficiently explain the absence of an enhanced Δ*prm1* fusion arrest when *CSH1* was overexpressed. The overproduced Csh1 was probably retained at the ER or degraded, due to limited amounts of Csg2.

Thus, increasing the levels of both Csg2 and Csh1 should elevate the amounts of stable and active Csh1 at the Golgi and result in enhanced fusion arrest. Indeed, Δ*prm1* mating pairs which co-overexpressed *CSG2* and *CSH1* displayed an enhanced fusion arrest **(Figure 32)**. However, the extent of fusion arrest that was attained with *CSG2 CSH1* co-expression was mild and not as large as the ~2-fold enhanced fusion arrest conferred by *SUR1* overexpression alone **(Figure 15)**. Nevertheless, the demonstration that both Sur1 and Csh1 overproduction can further arrest Δ*prm1* fusion strengthened the idea that enhanced fusion arrest was associated to sphingolipid mannosylation activity. The stronger fusion arrest from *SUR1* may suggest that of the two paralogs, Sur1 is inherently more active and therefore the primary enzyme for MIPC synthesis. This is supported by the fact that the Δ*sur1* mutation is sufficient to suppress Δ*prm1* fusion arrest **(Figure 28)**.

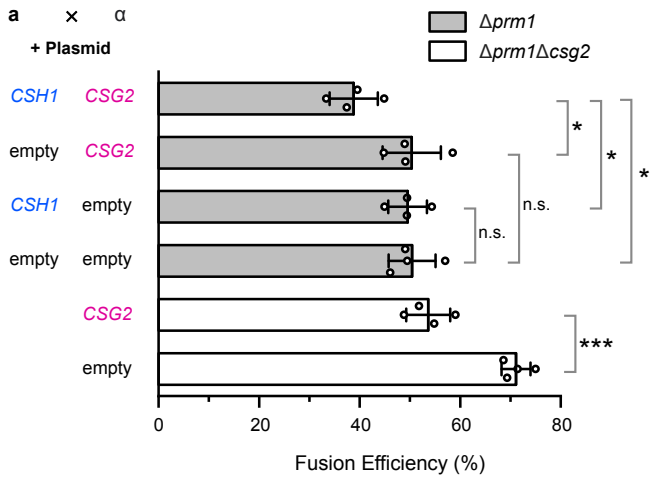

Figure 32. *CSG2 CSH1* co-overexpression arrests Δ*prm1* fusion. *CSG2* was expressed from a 2μ *URA3* plasmid and *CSH1* was expressed from a 2μ *LEU2* plasmid under native promoters. Fusion efficiency was determined by the BiFC assay. Error bars denote SD from 4 independent experiments each containing three biological replicates. P-values are two tailed unpaired Student's t-test; *** indicates p<0.001, * indicates p<0.05. p>0.05 was considered not significant (n.s.).

3.1.10 Hydroxylation status of sphingolipids does not account for suppression of Δ*prm1* fusion arrest

Sphingolipids possess an additional structural feature; namely different patterns of hydroxylation present on hydrocarbon tails. In *S. cerevisiae* and other eukaryotes, sphingolipids can be further modified by hydroxylation on either the long chain base (LCB) acyl chain or the very long fatty acid (VLCFA) acyl chain **(Figure 33A)**. Out of the three possible hydroxyl group modifications, the hydroxylases responsible for two of the hydroxyl modifications and the carbon position by which they do have been well characterised. Sur2 is responsible for the hydroxylation of carbon-4 of LCB (Haak et al., 1997). Scs7 adds a hydroxyl group to carbon-2 of the VLCFA (Haak et al., 1997). Sur1 and Csh1 show different substrate preferences, specifically pertaining to the hydroxylation status of IPC (Uemura et al., 2003), with Csh1 possessing lower specificity for IPC-B and IPC-C than Sur1. Due to this difference in substrate affinity, Δ*sur1* cells contain comparatively lower levels of $M(IP)_2C$-B and $M(IP)_2C$-C than Δ*csh1*.

I investigated if the absence of the aforementioned hydroxylated subspecies of $M(IP)_2C$ could suppress Δ*prm1* fusion arrest in a manner similar to Δ*prm1*Δ*sur1* and

Δ*prm1*Δ*ipt1* mating pairs. For this, I determined the fusion efficiencies of Δ*prm1* mutants containing additional deletions of *SCS7* or *SUR2* **(Figure 33B)**. Knockout of either *SCS7* or *SUR2* eliminates M(IP)$_2$C-C synthesis, whilst loss of *SUR2* eliminates M(IP)$_2$C-B synthesis. Neither Δ*scs7* nor Δ*sur2* mutations in a Δ*prm1* mutant suppressed the Δ*prm1* fusion arrest. In fact, Δ*prm1*Δ*sur2* mating pairs displayed an enhanced fusion arrest in comparison to Δ*prm1* × Δ*prm1* pairs, indicating that the LCB C-4 hydroxyl group moiety of sphingolipids is important for the remaining Prm1-independent fusion pathway. Taking these results into account, the suppressed fusion arrest of Δ*prm1*Δ*sur1* and Δ*prm1*Δ*ipt1* mating pairs manifests chiefly by alterations in the sphingolipid headgroup and not through alterations in sphingolipid hydroxylation.

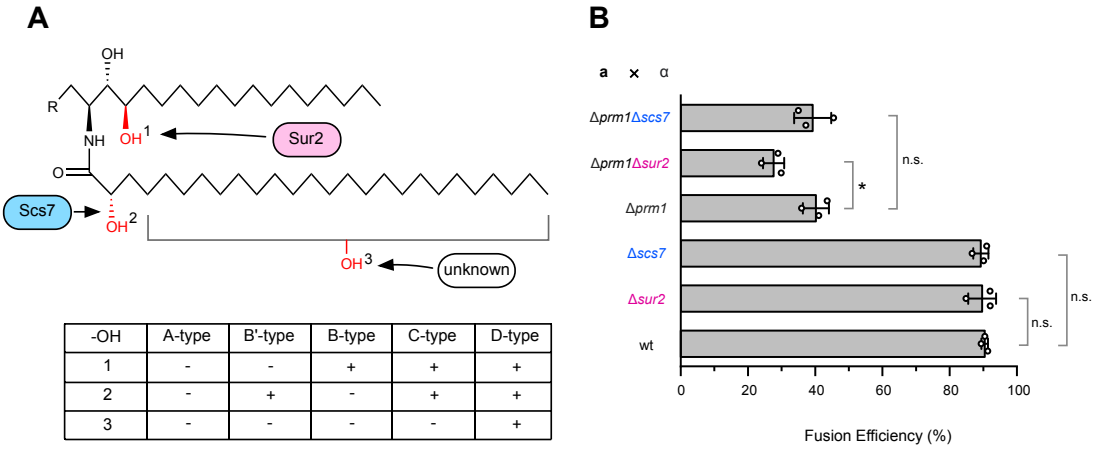

-OH	A-type	B'-type	B-type	C-type	D-type
1	-	-	+	+	+
2	-	+	-	+	+
3	-	-	-	-	+

Figure 33. Sphingolipid hydroxylation changes fail to suppress Δ*prm1* fusion defects. A. Yeast sphingolipid hydroxylation schematic. Table denotes the available types of hydroxylated sphingolipid species present, depending on the extent of hydroxylation. R group denotes IP, MIP, or M(IP)$_2$. **B.** Δ*scs7* and Δ*sur2* do not suppress Δ*prm1* × Δ*prm1* fusion defects. Fusion efficiency was determined by the BiFC assay. Error bars denote SD from 3 independent experiments. P-values are two tailed unpaired Student's t-test. *** indicates p<0.001, ** indicates p<0.01 and * represents p<0.05. p>0.05 was considered not significant (n.s.).

3.1.11 Δ*sur1* affects Δ*prm1* fusion additively

Next, the cell type requirements of the Δ*sur1* mutation for suppression of Δ*prm1* fusion defects was determined. Δ*prm1 MAT***a** was crossed to Δ*prm1*Δ*sur1 MAT*α in addition to the reciprocal cross and compared to fusion efficiencies of the Δ*prm1*Δ*sur1* × Δ*prm1*Δ*sur1* case **(Figure 34A)**. When only one cell partner of the Δ*prm1* mating pair contained a *SUR1* knockout allele, fusion arrest was suppressed to levels intermediate to that of when both

partners were Δ*sur1* (i.e. the case of Δ*prm1*Δ*sur1* × Δ*prm1*Δ*sur1*). This is in contrast to Prm1, which is required to be present in only one cell of the mating pair to support fusion (Heiman and Walter, 2000). Overall, these observations indicate a unilateral mode of action of Δ*sur1*, which is weaker than *PRM1*.

The intermediate levels of suppression observed by Δ*sur1* in one cell partner suggests that changes to sphingolipid profiles in the cell membranes of both partners is required to fully suppress Δ*prm1* fusion arrest. Upon these findings, it was expected that the hampered Δ*prm1* fusion output upon *SUR1* overexpression would also display unilateral and additive characteristics **(Figure 34B)**. Indeed, overexpression of *SUR1* in both Δ*prm1* mating partners elicited a stronger fusion arrest in comparison to only one partner overexpressing *SUR1*.

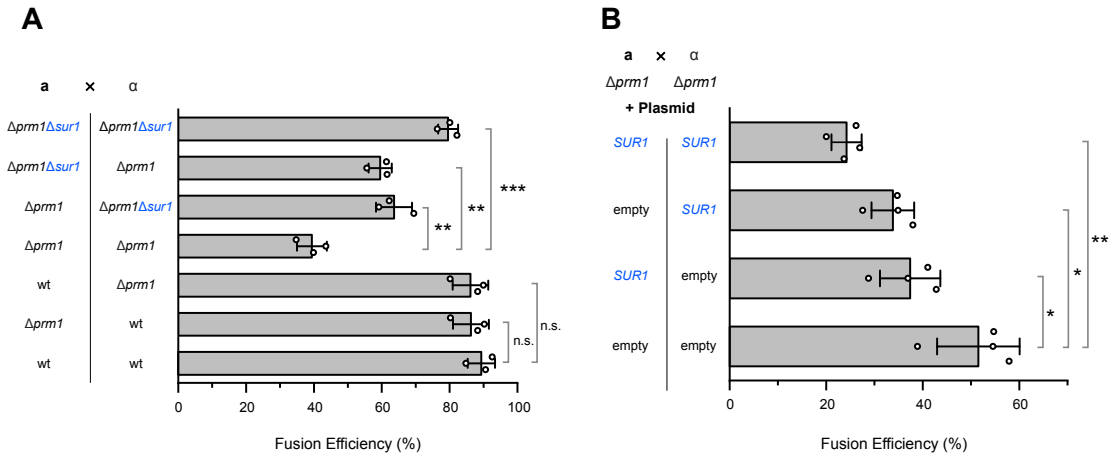

Figure 34. Additive behaviour of *SUR1* for Δ*prm1* fusion. A. *SUR1* knockout in both partners is required for full suppression of Δ*prm1* fusion arrest. Δ*prm1*Δ*sur1* was crossed to either Δ*prm1* or Δ*prm1*Δ*sur1* haploids of the other mating type. In both (A) and (B), fusion efficiency was determined by the 12-manifold BiFC assay. Error bars denote SD of 3 independent experiments each containing 3 biological replicates. **B.** An additive *SUR1*-mediated fusion arrest requirement. *SUR1* overexpression also displays unilateral additive behaviour. Error bars represent SD of 4 independent experiments. In (A) and (B), P-values are two tailed unpaired Student's t-test where *** represents p<0.001, ** represents p<0.01 and * represents p<0.05. p>0.05 was considered not significant (n.s.).

3.1.12 Δ*sur1* can restore fusion of Δ*prm1* pairs in a Ca^{2+} independent manner

In Δ*prm1* × Δ*prm1* matings, the remaining fusion activity is sensitive to extracellular levels of Ca^{2+} (Aguilar et al., 2007). Ca^{2+} influences Δ*prm1* fusion specifically at the cell-membrane fusion step, similarly to Prm1. Depleting extracellular Ca^{2+} such as through supplementation of EGTA to the mating media almost eliminates residual Δ*prm1* cell fusion (Aguilar et al., 2007). Conversely, high levels of Ca^{2+}, around 10 mM, can suppress Δ*prm1* fusion defects approaching close to the efficiency of wild type matings (Aguilar et al., 2007).

Could Δ*sur1* suppress the sensitivity of Δ*prm1* fusion to Ca^{2+}? In the presence of 10 mM EGTA, Δ*prm1*Δ*sur1* mating pairs fused less efficiently than in the presence of Ca^{2+}; over 2-fold in magnitude **(Figure 35A)**. Therefore, the deletion of *SUR1* did not suppress the sensitivity of Δ*prm1* fusion to extracellular Ca^{2+}. However, Δ*prm1*Δ*sur1* pairs exhibited reduced dependency for external Ca^{2+} than Δ*prm1* pairs for fusion. ~30% of Δ*prm1*Δ*sur1* mating pairs fused in Ca^{2+} depleted conditions, whereas only ~4% of Δ*prm1* pairs fused. This result revealed that the deletion of *SUR1* imparted a Ca^{2+} independent effect on fusion in a Δ*prm1* background. Moreover, this effect was significant; the ~30% fusion efficiency achieved in Δ*prm1*Δ*sur1* pairs under EGTA was comparable to efficiencies of Δ*prm1* × Δ*prm1* pairs in the presence of Ca^{2+} (~40%). Therefore, Δ*sur1* can partly suppress the need for external Ca^{2+} for Δ*prm1* cells to fuse (which is estimated to be ~900 μM in standard YPD agar media (Bacto™).

I next quantified the outcomes of Δ*prm1*Δ*sur1* × Δ*prm1*Δ*sur1* matings under 10 mM EGTA **(Figure 35B)**. Under Ca^{2+} depleted conditions, lysis of Δ*prm1* mating pairs became the predominant fusion arrest outcome **(compare Figure 35B to Figure 23B)**, which was consistent with previous observations (Aguilar et al., 2007). In Δ*prm1*Δ*sur1* mating pairs, both the lysed states and cytoplasmic bubble states were partly suppressed, accompanied by an increased occurrence of pairs that fused. The frequencies of each state was akin to Δ*prm1* × Δ*prm1* pairs in the presence of Ca^{2+} **(compare Figure 35B to Figure 23B)**, thereby reaffirming the ability of Δ*prm1*Δ*sur1* cells to phenocopy the fusion outcomes of the Δ*prm1* mutant, but without requiring Ca^{2+}. The reported effects of Ca^{2+} to promote membrane fusion such as charge neutralization of phospholipid headgroups may suggest a direct role of Δ*sur1* on the merging of membranes.

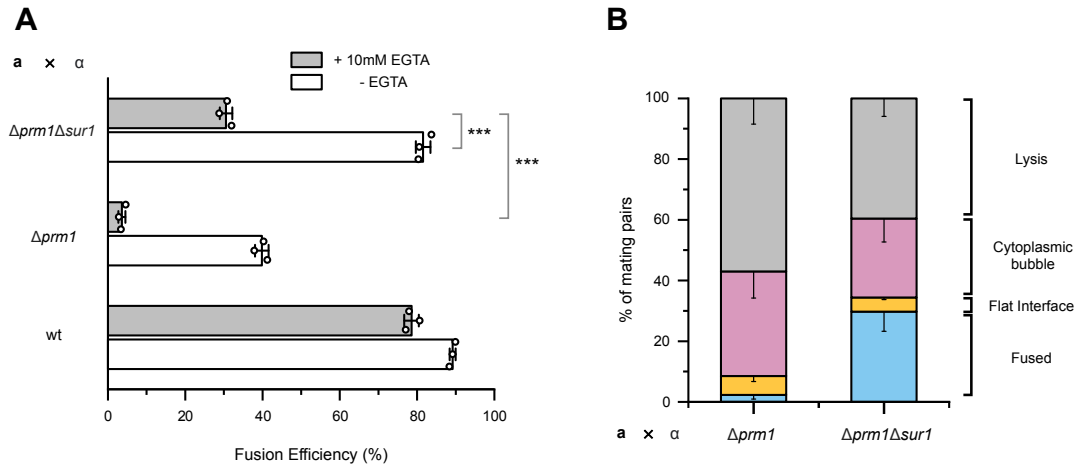

Figure 35. Mating fates of Δ*prm1*Δ*sur1* in Ca^{2+} depleted conditions. A. Partial calcium sensitivity of Δ*prm1*Δ*sur1* matings. On 10 mM EGTA, Δ*prm1* fusion arrest is partially suppressed by Δ*sur1*. Fusion efficiency was determined by the BiFC assay. Error bars represent SD of three independent experiments each containing three biological replicates. Statistical variance was calculated using two-tailed unpaired Student's t-test. *** signifies p<0.001 and ** represents p<0.01. **B.** Suppression of lysis and cytoplasmic bubble outcomes during fusion of Δ*prm1*Δ*sur1* mating pairs. Mating was conducted on YPD plates supplemented with 10 mM EGTA. Error bars represent SD from five independent experiments. In (B), >150 mating pairs were counted in each experiment.

3.1.13 Δ*prm1* fusion arrest cannot be suppressed by increasing ionic strength

The data indicates alterations in the sphingolipid head group influence the outcome of Δ*prm1* fusion. More specifically, absence of $M(IP)_2C$ sphingolipids allows Δ*prm1* fusion to proceed close to wt efficiency. I considered whether the more anionic (-2) charge of $M(IP)_2C$ compared to MIPC (-1), owing to the additional inositol phosphate head group may be relevant here. For instance, the decreased surface charge of MIPC and IPC prevalent plasma membranes in the case of Δ*sur1* and Δ*ipt1* might reduce the electrostatic repulsion of approaching membranes and thus facilitate fusion.

I therefore investigated whether increasing the ionic strength of the external environment could suppress the fusion arrest of Δ*prm1* pairs. Fusion efficiencies of Δ*prm1* mating pairs with increasing amounts of KCl in the surrounding media were determined by the BiFC assay. Mating reactions were performed on both solid agar and liquid media **(Figure 36A and B, respectively)**. The fusion arrest of Δ*prm1* could not be suppressed by

increasing the ionic strength of the media, suggesting the head group charge was not a critical factor for suppression of Δ*prm1* fusion arrest.

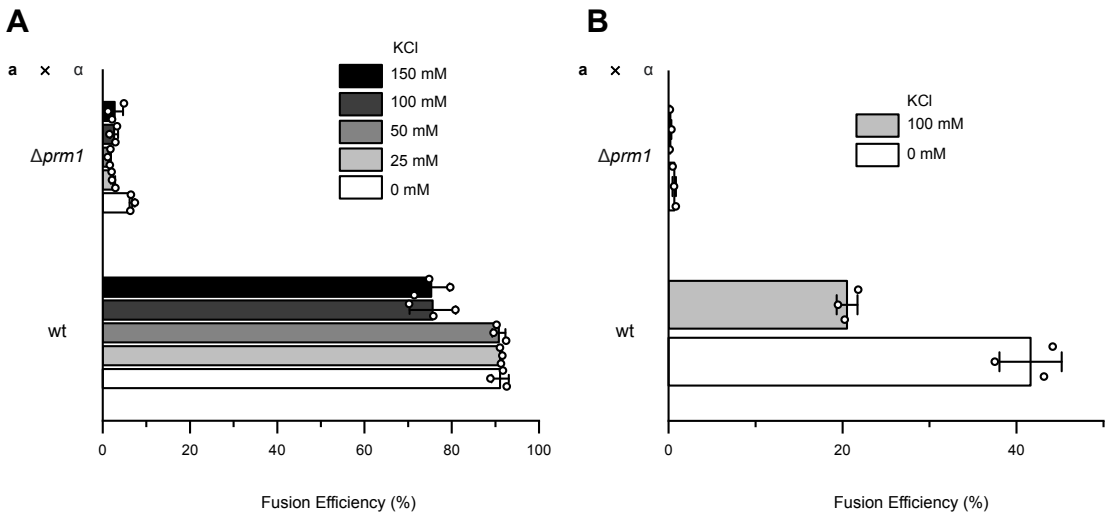

Figure 36. Inability to suppress Δ*prm1* fusion arrest by increasing ionic strength. A. Mating was conducted on 0.2 × concentrated YPD agar plates to minimise conductivity. Mixtures were mated for 3 h at 30 °C and fusion efficiency was determined by the BiFC assay. The plates were also supplemented with 10 mM EGTA. To maintain osmolarity between the different salt concentrations, sorbitol was added so that the total supplemented osmolarity of all the plates was 300 mM. **B.** Fusion BiFC assay under liquid conditions. For this, after cell wall dye staining, 2×10^6 haploid cells were mixed in liquid YPD (0.2 × concentrated) containing 10 mM EGTA. Mating mixtures without supplemented KCl contained 200 mM sorbitol. Because mating in liquid is less efficient than on solid agar surface, mating mixtures were incubated at 30 °C for 4.5 h. Error bars denote SD from three biological replicates.

3.2 Characterisation of Prm1 ectoplasmic domain

Secondary mutations of a gene which suppress phenotypes associated with the mutation of the primary gene are strong indicators that the two genes govern the same function. Since Δ*sur1*, Δ*ipt1* and Δ*csg2* could compensate specifically for the lack of *PRM1*, it suggested they enact similar functions to facilitate the plasma membrane fusion reaction. However, the mechanisms behind this function was unclear. Two potential avenues were considered for further investigations. One would be to centre on the Δ*prm1*Δ*sur1* mutant and investigate for potential changes at the fusion site with respect to Δ*prm1*. The second, which comprised my subsequent investigations, was to focus on Prm1 itself and identify

features of the protein which were important for its activity. For this, I gave particular attention to the ectodomain. Prm1 acts unilaterally, and in proteins with known roles in membrane fusion, such a mechanism is predominantly conferred by a region in the ectodomain. Therefore, I hypothesised that Prm1 might be interacting with the opposing cell-membrane.

3.2.1 Prm1 contains a hydrophobic domain and an amphipathic domain

Prm1 contains four transmembrane domains (TMD) with two ectoplasmic segments, two short cytosolic N- and C- termini and one intracellular loop (Heiman and Walter, 2000; Olmo and Grote, 2010a). The two ectoplasmic domains are ~260 residues and ~180 residues, respectively. The intracellular loop between TMD 2 and TMD 3 is ~100 residues and contains an endocytosis signal (Olmo and Grote, 2010a). Prm1 forms covalent homodimers through disulfide linkages present between ectodomains, and assembly of the covalent dimer is crucial for Prm1 to promote fusion (Engel et al., 2010; Olmo and Grote, 2010b).

Two regions of interest were discussed in earlier studies of Prm1 **(Figure 37A)**. The first was a hydrophobic domain; initially thought to be a TMD, was revealed to be part of ectodomain 1 (Olmo and Grote, 2010b). A second region in ectodomain 1 shortly after the hydrophobic domain was noted to contain amphipathic properties (Engel et al., 2010; Olmo and Grote, 2010b). The amphipathic nature of the domain is conserved amongst Prm1 homologs **(Figure 37B)**. When the domain is conceived as a helix, it displays a non-polar face and a polar face, the defining feature of amphipathic helices **(Figure 37C)** (Gautier et al., 2008). Given the reported membrane interaction functions of amphipathic helices, it has been suggested that the ectoplasmic amphipathic domain might be used by Prm1 in a similar fashion.

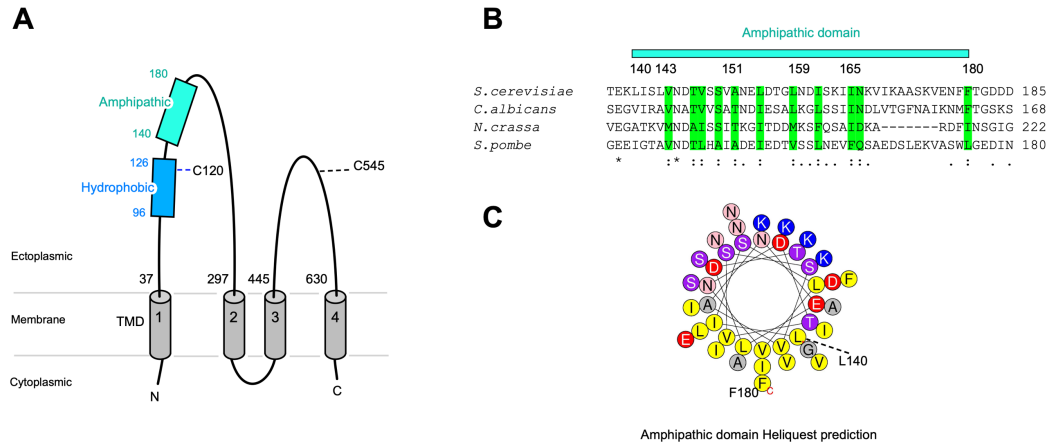

Figure 37. Prm1 topology and predicted amphipathic domain. A. Prm1 topology. Two cysteines located in the ectodomains, C120S and C545, are critical for covalent dimerisation. The amphipathic domain was denoted as between L140 and F180 in this study. **B.** MSA of the amphipathic domain in Prm1 homologs. ':' symbol denotes residues in which the properties are conserved (also highlighted in green). Residues with weakly conserved properties are denoted '.' Residues which are identical between homologs are indicated '*'. MSA was generated with Clustal Omega. **C.** Heliquest prediction of L140-F180 as an amphipathic helix (Gautier et al., 2008).

3.2.2 Prm1 AlphaFold2 model

As an initial means to explore potential structural features of Prm1 and especially the hydrophobic domain and the amphipathic domain, the structure of Prm1 was predicted by the *ab initio* multimer prediction pipeline of AlphaFold2 (Evans et al., 2022; Jumper et al., 2021) **(Figure 38)**. Both ectodomains were predicted to be predominantly α-helical. Based on the pLDDT and pAE, the two confidence metrics given by AlphaFold2, the TMDs were the most confidently scored residues, followed by the midcore of the ectodomains **(Figure 38B and 38C)**. In contrast, the AlphaFold2 model could not predict with confidence the arrangement of the ectoplasmic amphipathic domain. In the model, the domain did not contribute to make up the ectoplasmic core, which was predicted as four bundles of α-helices **(Figure 38D)**. The consequence of this structural organisation is that the amphipathic domain would be accessory (i.e not buried). The functional consequence of this amphipathic domain was investigated further in section **3.2.3**.

The approximate positions of C120 and C545 are annotated in the schematic of the Prm1 homodimer AlphaFold2 model **(Figure 38D)**. Both C120 and C545 are required for

Prm1 covalent dimers to form, and both cysteines are highly conserved in Prm1 homologs (Engel et al., 2010; Olmo and Grote, 2010b). In the AlphaFold2 model, C120 is predicted to form a *trans* disulfide bond with C545 of the other Prm1 molecule, thus linking two Prm1 molecules together. The hydrophobic domain preceding C120S was largely buried, interacting with the C545 containing α-helix of ectodomain 2 (α4). The hydrophobic domain was further investigated in section **3.2.4.**

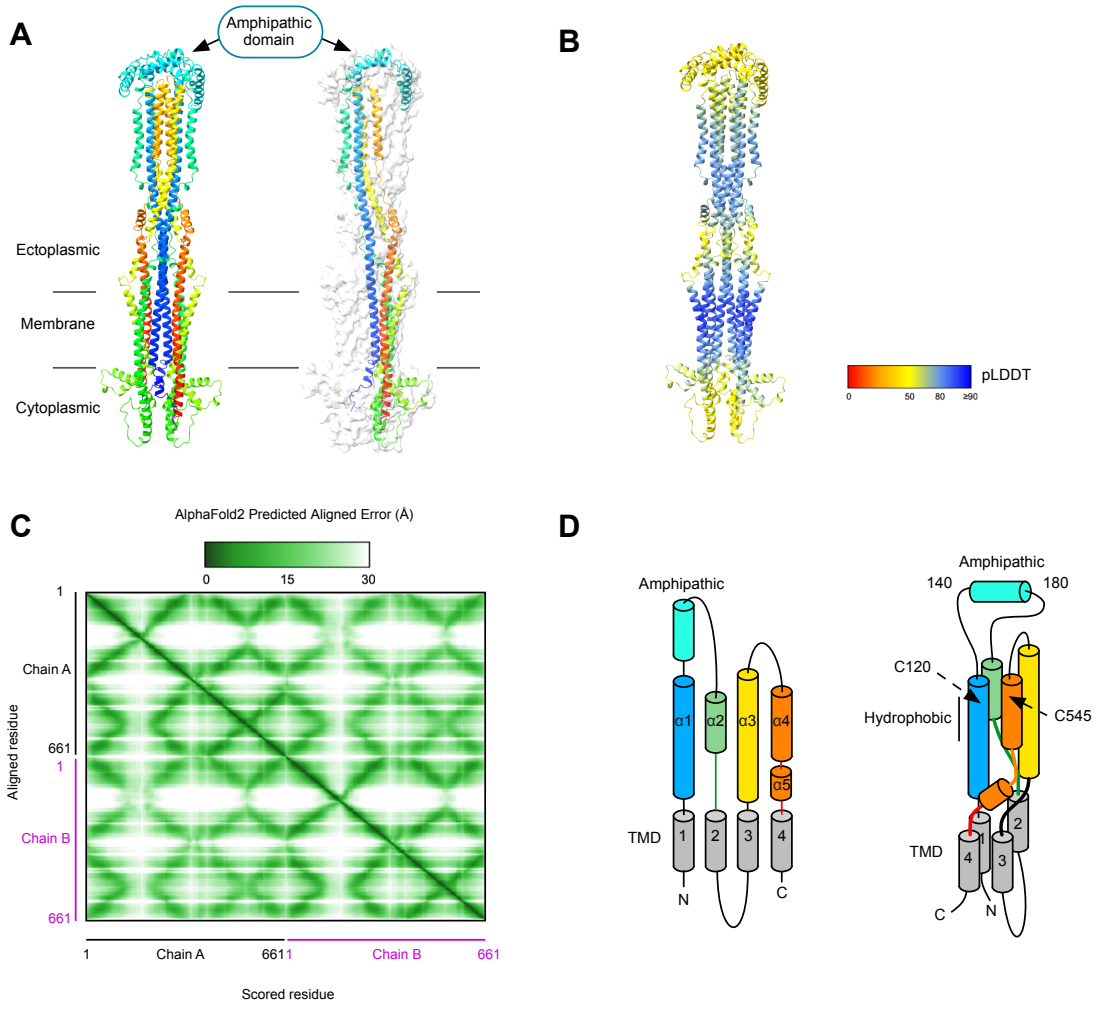

Figure 38. AlphaFold2 prediction models of Prm1 homodimer. A. AlphaFold2 model of Prm1 homodimer. AlphaFold2 multimer pipeline was ran using *S. cerevisiae* full length Prm1 sequence. Image of homodimer model was prepared using ChimeraX (Pettersen et al., 2021). **B.** pLDDT score of Prm1 homodimer. The pLDDT is a per residue confidence metric; a higher pLDDT score denotes higher confidence. **C.** Predicted alignment error (pAE) of the Prm1 homodimer. The pAE gives a confidence measure of the relative placement of domains respective to one another. Good confidence is given for the transmembrane domains. Poor confidence is given for the placement of

the amphipathic domain (residues 140-180). **D.** Prm1 schematic based on the AlphaFold2 prediction model (only one Prm1 molecule of the homodimer is depicted). Cylinders depict α-helices. In the AlphaFold2 model, ectodomain 2 α-helix 4 forms an interface with ectodomain α-helix 1 of the other monomer. The amphipathic domain is arranged as a mixture of α-helices and random coils. Given the low pLDDT of this region, it was denoted on the schematic as simply one discrete domain.

3.2.3 Amphipathic domain characterisation

3.2.3.1 Basic residues within the amphipathic domain are not required for Prm1 activity

For amphipathic helices, both the non-polar and polar residues can contribute to the membrane interactions (Giménez-Andrés et al., 2018). The C-terminal end of the amphipathic domain contains four lysines, all of which are predicted to lie on the polar face of the helix **(Figure 39A)**. In certain instances, positive charges of amphipathic helices have been reported to stabilise helix interaction with membranes. To test the relevance of the basic residues, a Prm1 construct in which the lysines were mutated to alanine was generated (Δ4K-Prm1). *CEN* plasmids encoding for Prm1 or Δ4K-Prm1 were introduced into Δ*prm1 MAT*α cells. The resultant fusion efficiency of these *MAT*α Prm1 variant cells when mixed with empty plasmid Δ*prm1 MAT***a** cells was then determined. Mating was conducted on YPD plates supplemented with 10 mM EGTA to isolate fusion promoting effects of extracellular Ca^{2+}. Because mating was conducted in EGTA+ conditions, successful fusion of Δ*prm1* mating pairs becomes almost entirely reliant upon the intrinsic activity of the complemented Prm1, allowing assessment of the functional consequence of the mutations. Δ4K-Prm1 restored Δ*prm1* fusion to similar efficiencies to that of wt-Prm1 **(Figure 39B)**. The basic residues of the amphipathic domain are therefore dispensable for Prm1 activity.

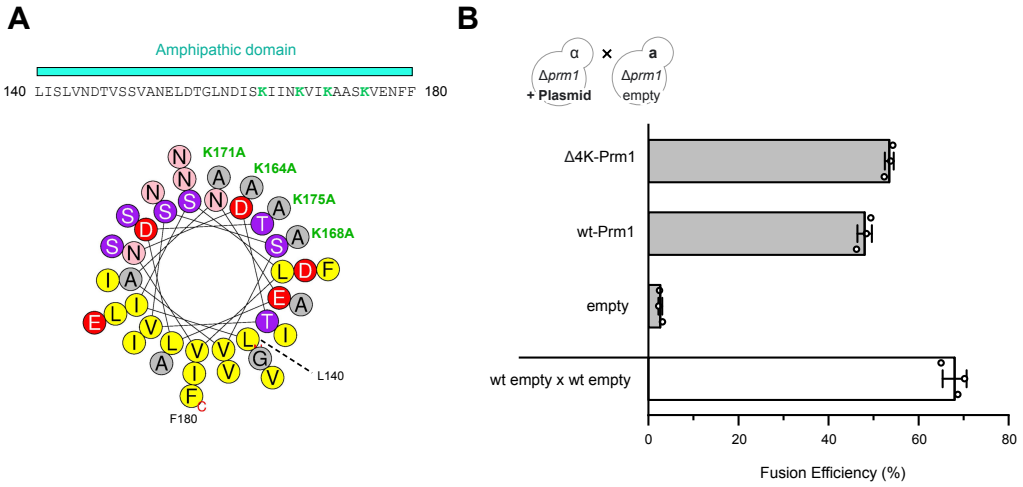

Figure 39. Positively charged residues of the amphipathic domain are not required for Prm1 activity. **A.** K164, K168, K171 and K175 were all mutated to alanine (Δ4K-Prm1). Heliquest prediction of the mutant ectoplasmic amphipathic domain is shown. **B.** The Δ4K-Prm1 mutant suppresses fusion defects of Δ*prm1* mutants as efficiently as wt-Prm1. Mating was conducted on YPD plates containing 10 mM EGTA. Fusion efficiency was determined by the BiFC assay. Error bars denote SD of three biological replicates.

3.2.3.2 Hydrophobic residues within the amphipathic domain are required for Prm1 activity

Next, I investigated the functional requirements of the hydrophobic residues within the amphipathic domain **(Figure 40A)**. For this, I assessed the effect of mutating up to two tandemly-arranged hydrophobic residues to alanine **(Figure 40B)**. Reducing the hydrophobicity by substitution of the hydrophobic residues to alanine in these variants did not affect Prm1 activity **(Figure 40B)**. I therefore asked whether more extensive mutations along the amphipathic region might be necessary. A Prm1 variant was constructed in which eight hydrophobic residues within the amphipathic region were mutated to alanine, which was designated the 8-alanine variant **(Figure 40C)**. The 8-alanine variant could only complement Δ*prm1* fusion partially, approximately 50% compared to wt-Prm1 **(Figure 40C)**. This suggested that multiple hydrophobic residues along the amphipathic domain cooperated to exert Prm1 fusion-promoting activity.

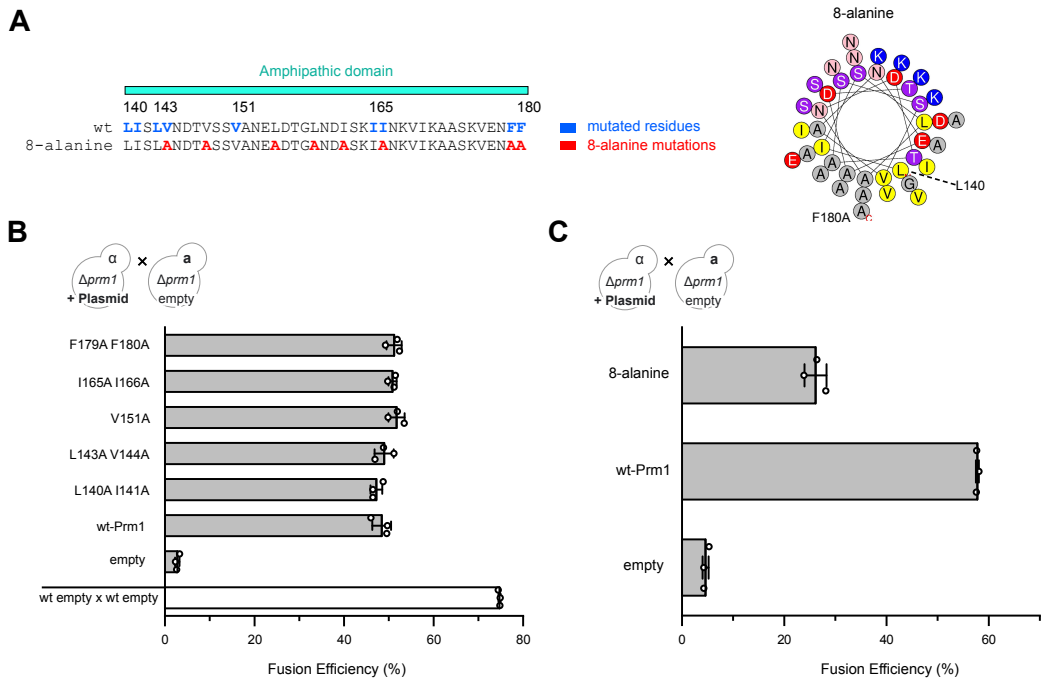

Figure 40. Cooperativity of hydrophobic residues along the amphipathic domain for efficient Prm1 activity. A. Hydrophobic residues chosen to mutate to alanine are coloured blue in the wt-Prm1 sequence. Hydrophobic residues substituted to alanine to construct the 8-alanine mutant are coloured red. Right depicts a HeliQuest prediction (Gautier et al., 2008) of the 8-alanine variant amphipathic domain. **B.** Isolated alanine mutations in the amphipathic domain do not affect Prm1 activity. Expression of each Prm1 variant is regulated under the native *PRM1* promoter in a *CEN* plasmid. **C.** 8-alanine mutation attenuates Prm1 activity. Fusion efficiency was determined by the BiFC assay. Error bars denote SD of 3 biological replicates.

3.2.3.3 Internal deletions of Prm1 ectodomain impair fusion promoting activity

In a secondary approach to probe the relevance of amphipathic region within extracellular domain 1, I generated a series of internally deleted ectodomain mutants. A Prm1 mutant was constructed in which the region comprising the predicted amphipathic region (Δ140-180) was deleted. Additionally, I constructed Prm1 variants in which the designated span of deleted residues was extended (Δ140-200 and Δ140-220). The Δ140-220 therefore comprises the most severe ectoplasmically cropped mutant. In AlphaFold2 prediction models of the dimeric variants, the overall core of the ectodomains of the homodimer remained intact (Figure 41A). Fusion of Δ*prm1* pairs with the Prm1 variants

expressed only in the *MAT*α cell under 10 mM EGTA was generally attenuated by approximately 50% in comparison to wt-Prm1 (Figure 41B).

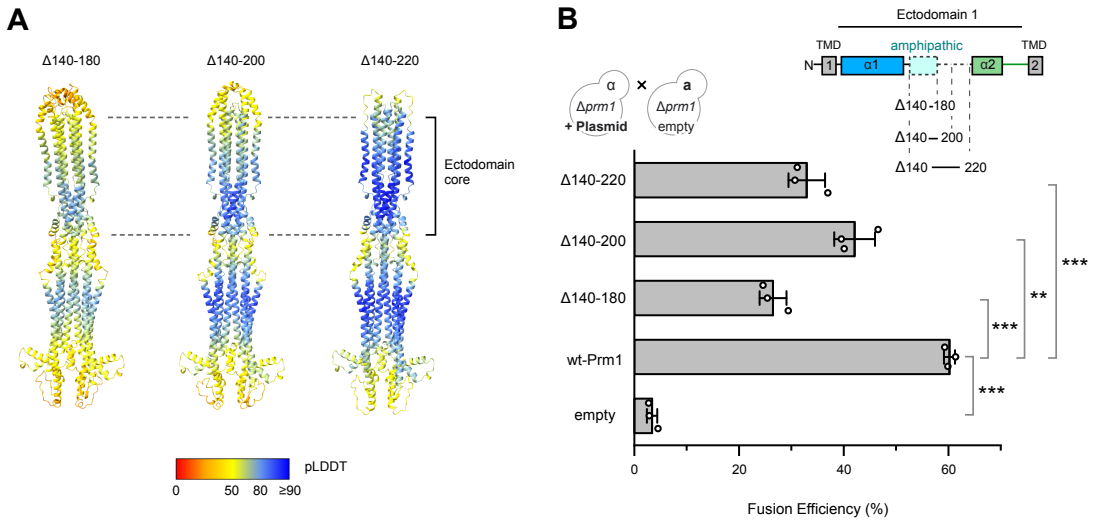

Figure 41. Removal of the amphipathic domain leads to an approximate 50% reduction in Prm1 activity. A. AlphaFold2 models of the Prm1 ectodomain variants predict a retained ectodomain core. **B.** Deletion of the amphipathic domain partially hampers fusion supporting activity of Prm1 variants. Error bars denote SD of 3 independent experiments each containing three biological replicates. Two-tailed unpaired Student's t-test was used to calculate statistical variance. *** signifies p<0.001 and ** signifies p<0.01.

3.2.3.4 Prm1 ectodomain variants form covalent dimers

The reduced activity of the Prm1 variants may have been due to an inability for the variants to form covalent dimers (Engel et al., 2010; Olmo and Grote, 2010b). To address whether the Prm1 variants still formed covalent dimers, I performed Western blot analysis of lysates derived from pheromone treated cells which expressed the various Prm1 variants. Δ*prm1 MAT***a** cells carrying Prm1-V5 *CEN* plasmids under the native *PRM1* promoter were induced to express after pheromone treatment with α-factor. Complete dimer assembly and maturation of the Prm1 mutants was retained as indicated by the >180 kDa species, suggesting that maturation of these Prm1 mutants from the monomer to the glycosylated dimer was unaltered (Figure 42). The abundance of the Prm1 mutant dimers was lower in comparison to wild type Prm1, suggesting that expression of the mutants was slightly weaker. Additionally, for the 8-alanine variant, a band ~70 kDa was observed, which likely represents the unglycosylated monomer (predicted MW of Prm1 is 73 kDa). This suggested

that covalent dimerisation or glycosylation of the 8-alanine variant in the ER may be slightly impaired. This may have contributed to the observed lower abundance of the glycosylated dimer in comparison to the rest of the variants. Nevertheless, it is unlikely that the lowered expression of the mutant dimers sufficiently explains the lower fusion efficiency observed, because it is known that low amounts of Prm1 are required at the contact sites to promote fusion (Olmo and Grote, 2010a).

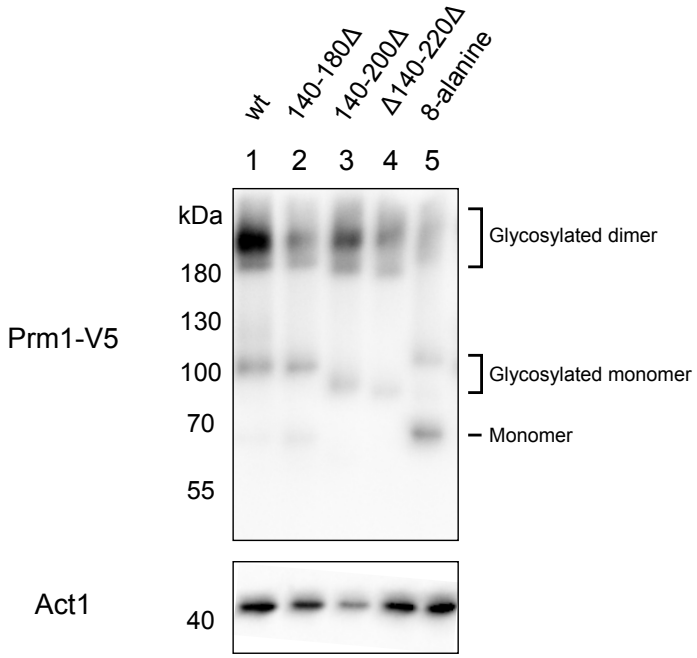

Figure 42. Prm1 ectodomain variants form glycosylated covalent dimers. Retained dimer assembly of the 8-alanine and truncated Prm1-V5 variants in pheromone treated Δ*prm1 MAT***a** cells. Actin (Act1) was used as a loading control. To preserve disulfide bonds, cell lysis and SDS-PAGE was performed without addition of reducing agents.

3.2.3.5 Prm1 ectodomain variants are targeted to cell-cell contacts of mating pairs

Next, I determined whether the Prm1 variants were localised to the site of cell fusion. To visualise localisation of the Prm1 variants during mating, pheromone regulated Prm1 variant-mNG was expressed episomally via *CEN* plasmids in Δ*prm1 MAT***a** cells. The *MAT*α cells were then mixed with Δ*fus1*Δ*fus2 MAT*α partners. Since the Δ*fus1*Δ*fus2* mutant

is defective in cell wall degradation (Gammie et al., 1998), cell fusion in Δ*fus1*Δ*fus2 MAT*α × Δ*prm1 MAT***a** mating pairs is delayed (Smith et al., 2017) because remodeling the intervening cell wall becomes entirely dependent upon the *MAT*α partner. When stained with FM4-64, the Δ*fus1*Δ*fus2* × Δ*prm1* mating pairs display flat interfaces, indicating that the plasma membranes at the cell-cell contact site were indeed separated by an undigested cell wall.

The flat interface acted as a marker to determine if Prm1 was targeted to the site of cell fusion. Fusion related membrane proteins will localise to the flat interface between contacted cells, where plasma membrane fusion will occur **(Figure 43)**. Similarly to wt-Prm1-mNG, each of the amphipathic domain Prm1-mNG variants were present at the flat interface of mating pairs, shown by the colocalisation of Prm1-mNG signal and FM4-64 signals. Therefore, the Prm1 variants were correctly targeted to the plasma membrane at the site of cell fusion. Combined with the fact that the Prm1 variants form glycosylated dimers, the loss of activity of the Prm1 variants can be attributed to the perturbation of the amphipathic domain.

Overall, the impaired fusion-promoting activity presented by the Δ140-180 mutant suggests that loss of the amphipathic region is responsible for the lost fusion activity. Removal of additional residues (Δ140-200 and Δ140-220) did not further reduce the activity, suggesting the amphipathic region was sufficient for the lost activity. Since similar levels of activity are conferred by both the 8-alanine Prm1 mutant and the Δ140-180 mutant, extensive reduction of the hydrophobicity within the amphipathic region may be sufficient to halve the activity. Furthermore, since partial fusion activity was observed in even in the most severely deleted mutant (Δ140-220), Prm1 must contain additional regions which promotes cell fusion independent of the domains deleted here.

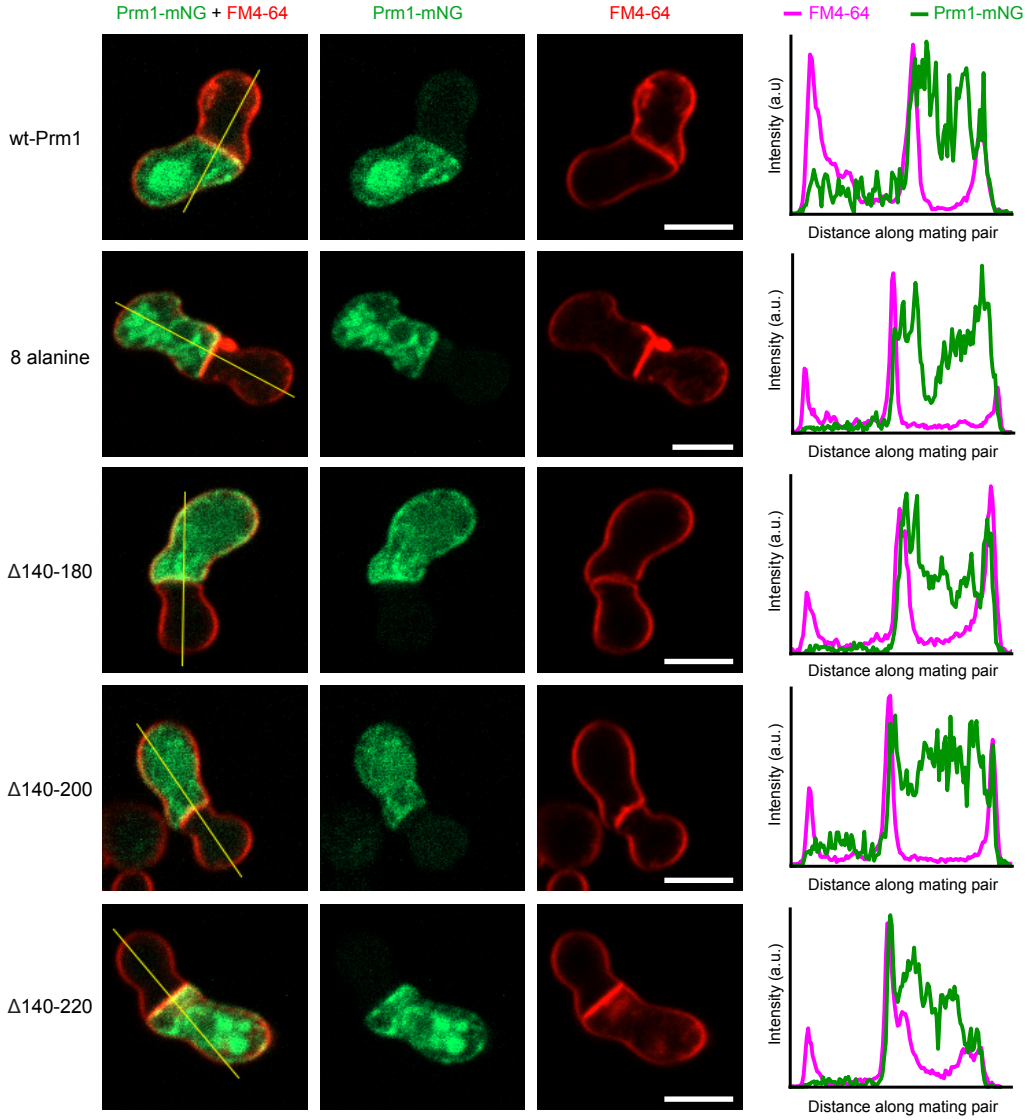

Figure 43. Targeting of the amphipathic domain Prm1 variants to cell-cell contact sites of mating pairs. Representative examples of Δ*prm1* × Δ*fus1*Δ*fus2* mating pairs, in which only the Δ*prm1 MAT***a** cell expresses Prm1 variants tagged with mNG from *CEN* plasmids. Colocalisation of Prm1 variant-mNG with FM4-64 stained plasma membranes at cell-cell contacts can be observed. Line plot along the mating pair is displayed to the right, which also indicates the colocalization of FM4-64 and Prm1-mNG signal at cell-cell contacts. Line plots were conducted in the direction starting from the Δ*fus1*Δ*fus2* partner towards the Δ*prm1* partner. Mating was conducted in the same way as the BiFC assay (excluding the staining step of cell walls). Then, mating was stopped with TAF buffer, cells were stained with FM4-64 and then imaged by confocal microscopy. Scale bar denotes 5 μm.

3.2.3.6 Absence of Sur1 does not suppress the 8-alanine Prm1 activity defect

Next, I investigated the potential mechanisms of the 8-alanine Prm1 mutant. Could Prm1 operate a *trans*-like mechanism through the putative amphipathic domain? A *trans*-interaction of the Prm1 amphipathic domain towards the opposing plasma membrane would offer an explanation to why Prm1 is only needed in one of the cells during fusion. Furthermore, as we have seen, changes in the plasma membrane through Δ*sur1* alters the fusion requirements to become more favourable. On this line, the question arose as to whether Δ*sur1* could compensate for the mutations of the amphipathic domain in Prm1 and allow fusion to recover to the wt Prm1 levels **(Figure 44)**. 8-alanine Prm1 was expressed from a *CEN* plasmid in Δ*prm1 MAT***a** cells and mated to Δ*prm1*Δ*sur1 MAT*α cells carrying an empty vector and fusion efficiencies were determined under EGTA+ mating conditions. As expected, Δ*prm1* × Δ*prm1* fusion efficiencies could be slightly restored when one of the mating partners was additionally absent for *SUR1*.

However, when the 8-alanine Prm1 variant was expressed, no additional recovery in fusion efficiencies were observed when one of the cell partners also possessed the Δ*sur1* mutation. In fact, when both cell partners were Δ*sur1*, the additional expression of 8-alanine Prm1 was redundant. In summary, the loss of Prm1 fusion activity associated with the reduced hydrophobicity within the amphipathic domain cannot be restored by sphingolipid changes to the membranes, further substantiating the amphipathic domain as a separated and specialised feature of Prm1. Conversely, the non-amphipathic domain regions of Prm1 promotes fusion in a manner that can be interchanged with sphingolipid pertubations to plasma membranes. Prm1 is more efficient at conferring this role, as Prm1 on one cell alone suffices to promote fusion, whereas sphingolipid alterations are needed on both membranes to achieve similar fusion efficiencies.

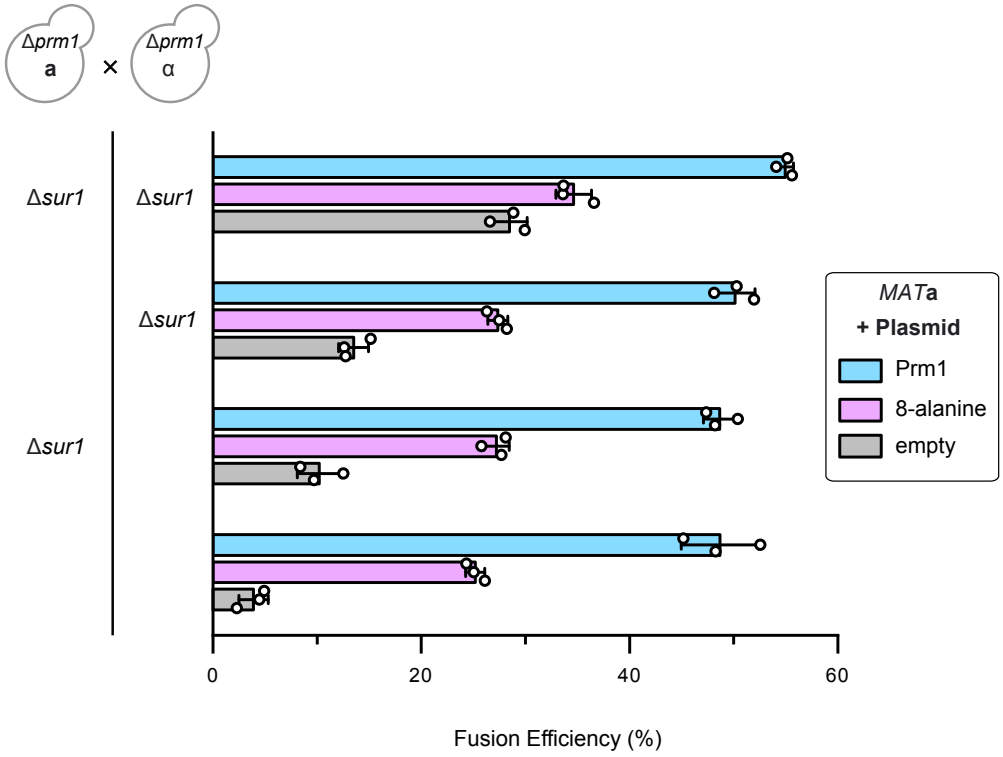

Figure 44. Δ*sur1* is unable to compensate for loss of hydrophobicity in the amphipathic domain of Prm1. Mating was conducted on YPD plates supplemented with 10 mM EGTA. Δ*prm1 MAT*α haploids containing empty plasmids were mated with Δ*prm1 MAT***a** cells carrying plasmids which expressed Prm1 (blue), the 8-alanine variant (magenta) or an empty vector (grey). Fusion efficiency was then determined by the BiFC assay. Error bars denote SD from three biological replicates. Δ*sur1* denotes Δ*prm1* cell partner that additionally possessed the Δ*sur1* mutation.

3.2.4 Prm1 hydrophobic domain characterisation

3.2.4.1 Substituting charged residues into the hydrophobic domain impairs Prm1 activity and covalent dimer assembly

Prm1 contains a stretch of residues N-terminal to C120 which are predominantly hydrophobic. Two rare acidic residues E104 and D112 within this region were previously shown to be required for covalent dimer assembly (Engel et al., 2010). From these observations and given the close proximity of the hydrophobic domain to C120, which is also required for covalent dimerisation, I hypothesized that the hydrophobic domain might

be required for dimer formation. I therefore investigated the relevance of the hydrophobic residues residing within this region for dimer formation and cell fusion.

Amongst the Prm1 homologs in *S. cerevisiae*, *C. albicans*, *N. crassa* and *S. pombe*, residues L106 and L113 show strong conservation, whereas residues F109 and I111 are absolutely conserved **(Figure 45A)**. To test if the hydrophobicity of these residues were important for Prm1 activity, the residues were substituted to alanines. The C120S mutant was included, which is defective in supporting fusion due to deficient formation of covalent dimers (Engel et al., 2010; Olmo and Grote, 2010b). Fusion efficiency of Δ*prm1* mating pairs under 10 mM EGTA and in which the Prm1 mutant was solely expressed episomally from the α partner was subsequently determined.

No deleterious effect on Prm1 activity during mating was observed when the chosen hydrophobic residues were individually substituted to alanine **(Figure 45B)**. Next, the more severe substitution of the same residues to negatively charged aspartate was tested. The aspartate mutations reduced the fusion promoting activity of Prm1, to variable degrees **(Figure 45C)**. Mutation of L106 to aspartate negatively impacted Prm1 activity the most; fusion efficiency of Δ*prm1* mating pairs expressing the L106 Prm1 mutant was almost the same as Δ*prm1* mating pairs containing empty vector controls. Therefore, although maintaining the overall hydrophobic nature of the domain retains Prm1 activity, introduction of charged residues to the domain impairs it.

Because activity was lowered with the aspartate mutations, Western blots were performed to assess if covalent dimers were formed after pheromone treatment. As a control, the C120S mutant was included, which is dimerisation deficient (Engel et al., 2010; Olmo and Grote, 2010b). The mutants were able to form glycosylated covalent dimers; however, their abundance was much lower in comparison to wt-Prm1 and were more comparable to the known dimerisation deficient C120S mutant **(Figure 45D)**. The monomeric species was slightly more abundant in the mutant samples in comparison to wt Prm1, which would be expected from a failure to dimerise. The similar abundances of the glycosylated dimers formed by the aspartate mutants and the C120S mutant, suggested that the aspartate mutants were dimerisation deficient.

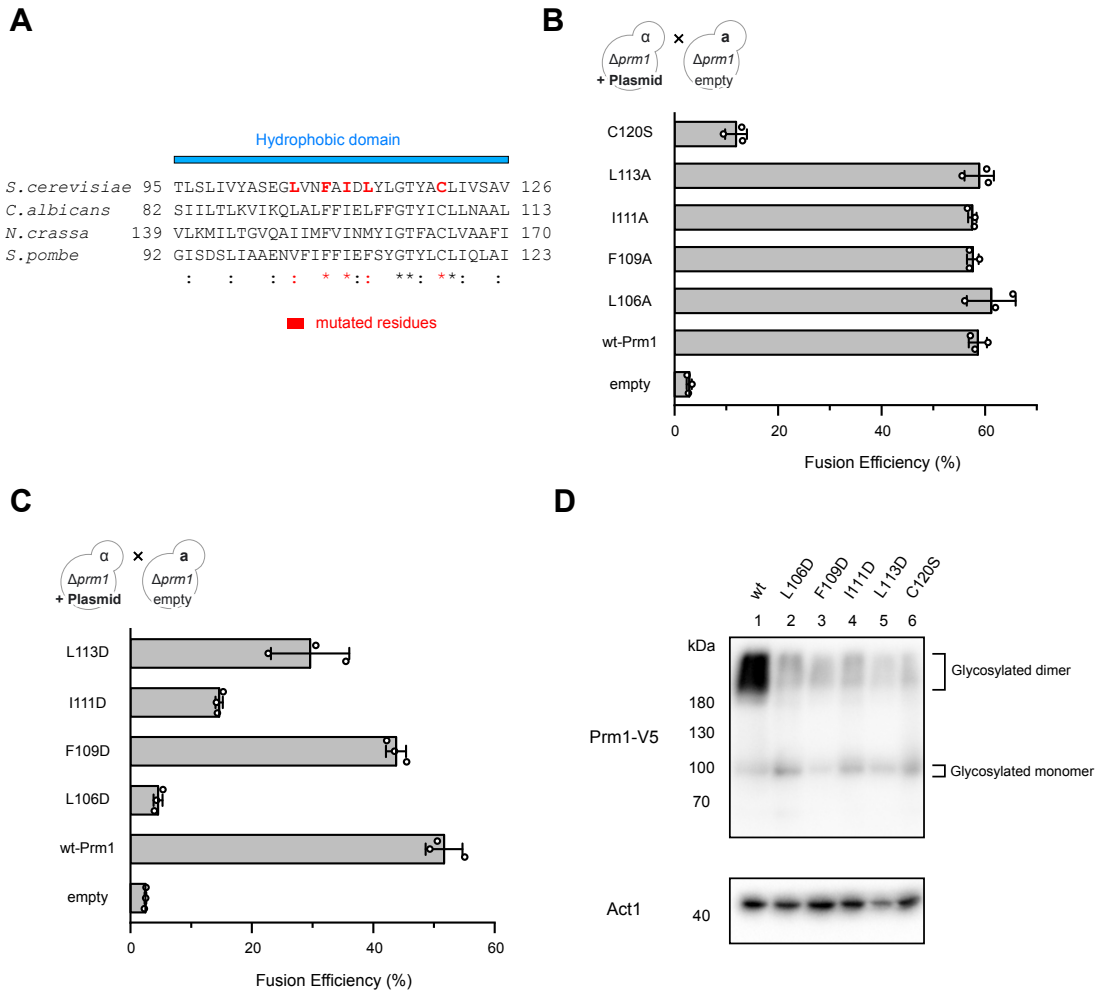

Figure 45. Hydrophobic to acidic residue substitutions in the ectoplasmic hydrophobic domain impair Prm1 fusion supporting activity. A. Residues mutated are highlighted in red. MSA was generated with Clustal Omega. Conserved substitutions are denoted ':', whereas semi-conserved substituted residues are denoted by '.'. Identical residues are denoted by *. **B.** Single mutations of hydrophobic residues to alanine. Fusion efficiency in (B) and (C) was measured with the BiFC assay. Error bars in (B) and (C) denote SD from three biological replicates. **C.** Aspartate mutants show partial loss of Prm1 activity. **D.** In the aspartate mutants, glycosylated dimer formation is weakened but not eliminated. Prm1 aspartate mutants under the *PRM1* promoter were expressed from *CEN* plasmids in Δ*prm1 MAT***a** cells by 90 min pheromone treatment.

3.2.4.2 Aspartate mutants are localised to cell-cell contacts

Although each of the aspartate mutants formed similar amounts of glycosylated covalent dimers, their resultant activities were highly variable. Some Prm1 mutants are predominantly found in the ER (Engel et al., 2010; Olmo and Grote, 2010b). Therefore, it

was determined if the aspartate mutants were still targeted to contact sites of mating pairs. Only the L106D mutant and the F109D mutant were tested since they exhibited opposite levels of activity. mNG tagged versions of these aspartate mutants were expressed via *CEN* plasmids in Δ*prm1 MAT***a** cells. The Δ*prm1* cells were then mated to Δ*fus1*Δ*fus2 MAT*α cells. As a control, the C120S mutant was also included, which is properly localized to contact sites. Both the L106D mutants and F109D mutants were observed at cell-cell contact sites **(Figure 46)**. The low fusion-promoting activity of Prm1-L106D mutant therefore cannot be explained by a lack of the mutant protein at the site of cell fusion.

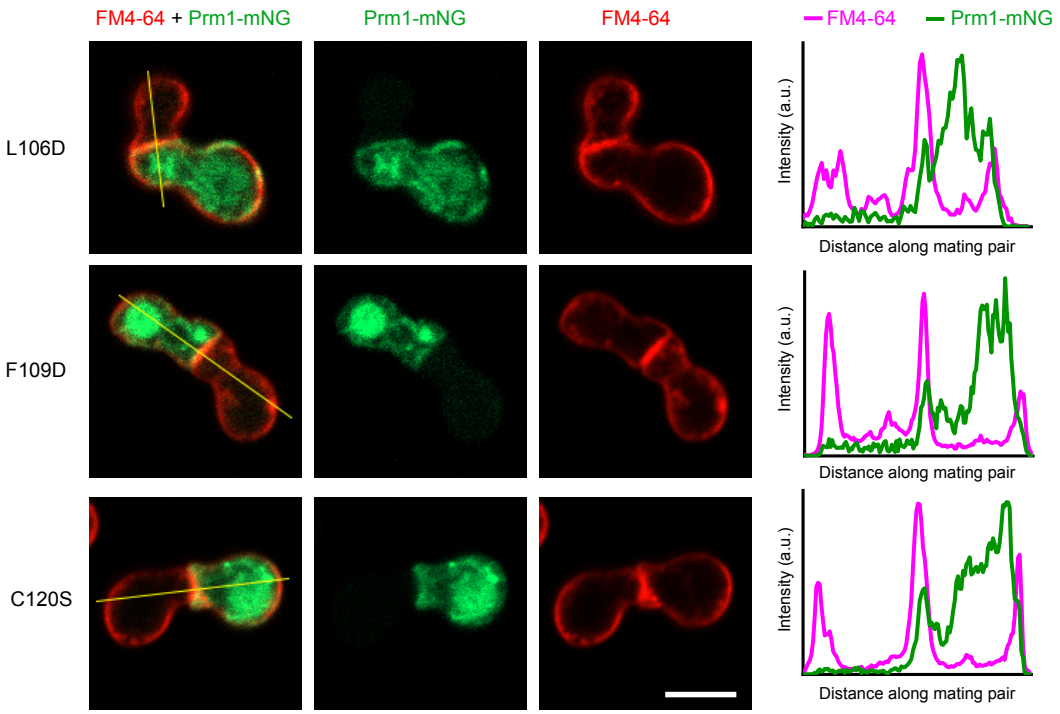

Figure 46. Localisation of L106D and F109D Prm1 mutants at cell-cell contact sites. Δ*prm1 MAT***a** cells carrying *CEN* plasmids encoding for Prm1 variants tagged with mNG under the *PRM1* promoter were mated to Δ*fus1*Δ*fus2 MAT*α cells for 3 h. Mating was stopped by addition of TAF buffer and subsequently cells were stained with FM4-64 and imaged by confocal microscopy. Line plots along the mating pair are shown on the right. Line plots were generated from the Δ*fus1*Δ*fus2* partner towards the Δ*prm1* partner. Scale bar denotes 5 µm.

3.3 Prm1 *in vitro* characterisation

I decided to investigate the effect of Prm1 *in vitro*. One of the benefits of the *in vitro* approach is that additional components can always be added to the experimental setup at

the behest of the researcher. The difficulty in reconstitution-based studies relies mainly in purification of sufficient quantities of the desired protein. The reconstitution of membrane proteins presents an additional challenge because they have to be inserted into a membrane bound vesicle.

3.3.1 Construct design and genome integration

For purification, the StrepII tag was elected which allows for affinity purification under physiological conditions. In addition, a C-terminal eGFP tag was chosen which acts as a useful marker during the purification workflow. For this, a plasmid construct encoding for Prm1-eGFP-StrepII was generated. A HRV 3C protease cleavage site was designed to lie in between Prm1 and the eGFP tag to allow for cleavage of eGFP with Precission protease. For inducible expression, the Prm1-eGFP-StrepII CDS was placed under the *GAL1* promoter.

Initial experiments consisted of Prm1-eGFP-StrepII through overexpression on 2μ plasmids, given the successful overexpression of yeast membrane proteins using this approach (Newstead et al., 2007). Contrary to expectations however, test expressions with Prm1 2μ-based constructs were negative, because many cells did not express Prm1-yeGFP-StrepII upon galactose induction **(Figure 47A)**. Reducing the time of galactose induction before imaging (4 h and 12 h) did not enhance the proportion of cells expressing Prm1-eGFP-StrepII (data not shown). The high copy number of 2μ plasmids combined with the strong *GAL1* promoter might be counter-productive in this case and lead to very low expression such as through stresses on the translation machinery or accumulation of misfolded proteins in the ER. When the construct was constitutively expressed under the *TEF1* promoter, a higher fraction of cells expressed Prm1-eGFP-StrepII compared to *GAL1*. However, it was apparent even here, a substantial proportion of cells did not express any Prm1-eGFP-StrepII **(Figure 47B)**, a behavior that may be related to the inherent instability of the 2μ plasmid.

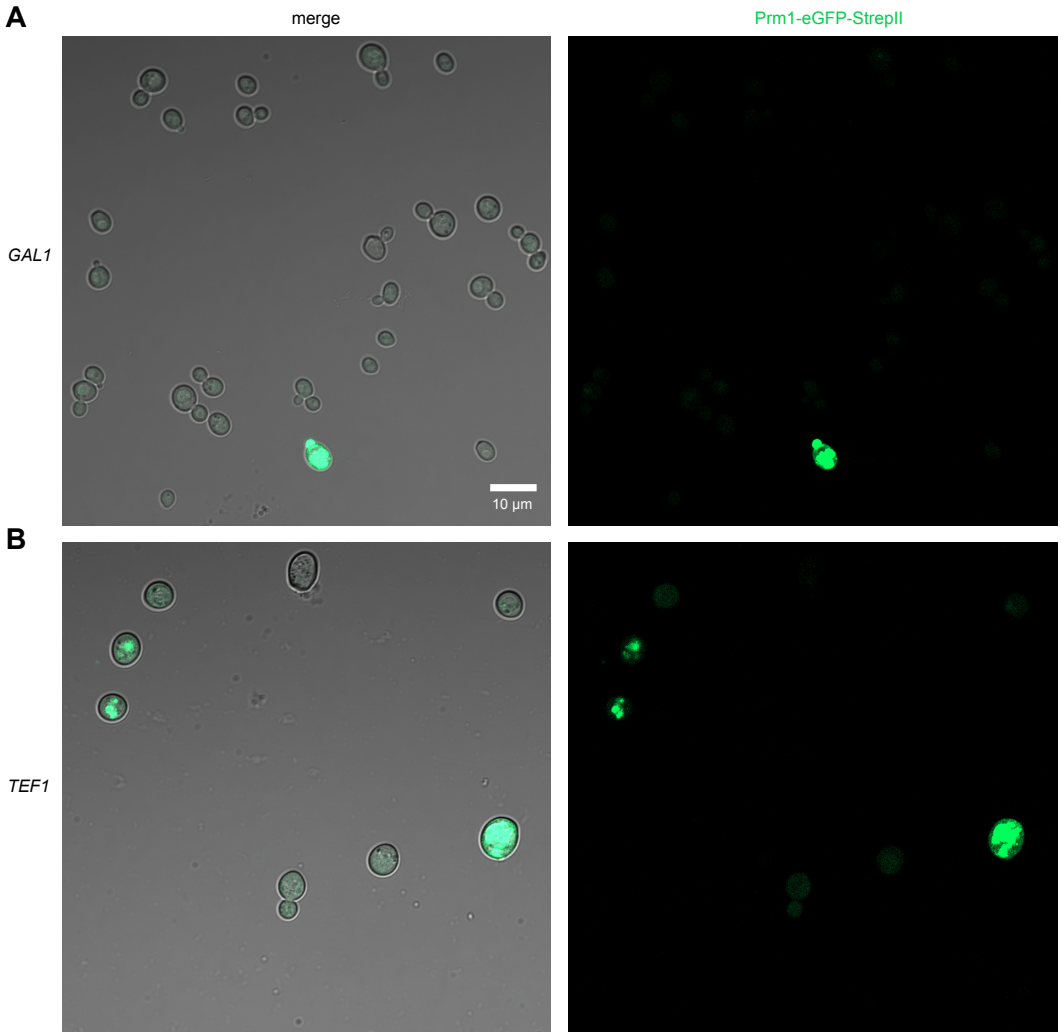

Figure 47. Expression of Prm1-eGFP-StrepII under the *GAL1* promoter and *TEF1* promoter. **A.** Expression of Prm1-eGFP-StrepII under *GAL1* promoter. Most cells fail to express Prm1-eGFP-StrepII indicated by absence of GFP signal. **B.** Constitutive expression via *TEF1* promoter. Cells were imaged after 16 h growth in SD-URA subsequent to galactose induction at OD_{600} = 0.6 (A) or grown for 16 h in SD-Ura media upon reaching OD_{600} = 0.6.

To improve expression levels, subsequent efforts switched towards incorporation of the Prm1-eGFP-StrepII coding sequence into the genome, as upon integration, every cell of a clonal population should express the target gene. Furthermore, expression of the gene can be further boosted if more than one copy is integrated into the genome. With this in mind, rDNA mediated integration was chosen. rDNA, which encode for ribosomal RNA, are found as tandem repeats on chromosome XII at between 100-200 copies per yeast cell (Kobayashi, 2011; Petes, 1979; Schweizer et al., 1969). The repetitive rDNA units are thereby ideal

targets for multiple copy integration through homologous recombination. It should be noted that the typical number of gene copies achieved via multicopy integration at rDNA sites (around 2-10 copies) (Zheng et al., 2022) is significantly lower when compared with 2μ plasmids (around 20-50 copies). Therefore, potential expression issues related to saturation of the ER from 2μ overexpression is expected to be limited. The construct was designed as shown in **Figure 48A**. To further optimise expression, the eGFP sequence was replaced with yeast codon optimised eGFP (yeGFP). When the construct is linearised through restriction site digestion, the ends of the DNA contain homologous regions towards rDNA sites. Homologous recombination of the 35S rDNA sequences then leads to integration of the plasmid derived DNA into the genome **(Figure 48B)**. Integrants were identified based on colony growth on ClonNAT plates.

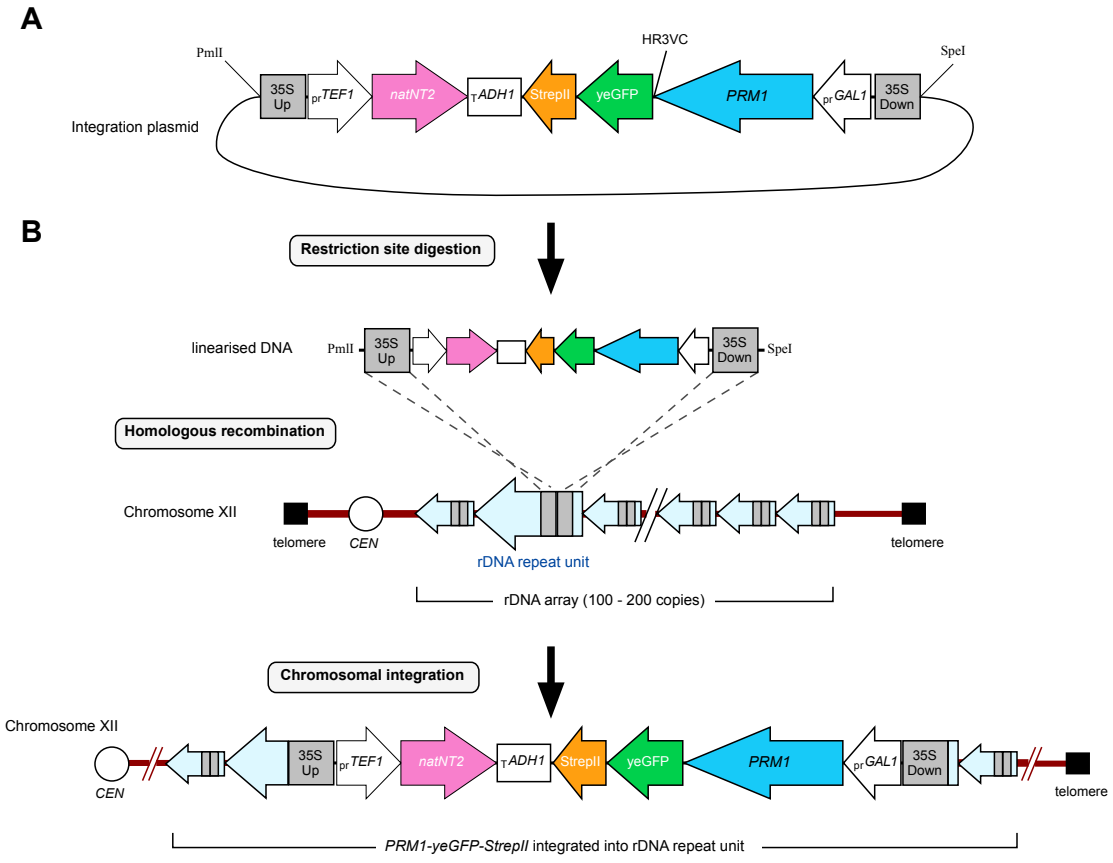

Figure 48. Integrative plasmid construct and genome integration at rDNA sites. A. Plasmid construct design. The integrative plasmid contains the Prm1-yeGFP-StrepII encoding sequence under the *GAL1* promoter. HRV3C denotes a HRV3C cleavage site. The construct also contains a natNT2 cassette for clonNAT selection of clones. The natNT2 marker and Prm1 construct sequence are flanked by 35S rDNA sequences. **B.** Integration of plasmid DNA. The plasmid is linearised using

restriction enzymes PmlI and SpeI and introduced into the cell via lithium acetate-based transformation. Homologous Recombination (dashed lines) of the 35S sequences leads to chromosomal integration of the plasmid derived DNA.

To assess whether Prm1-yeGFP-StrepII could be expressed, cells were imaged via confocal microscopy after galactose induction **(Figure 49A)**. The majority of cells expressed the protein, as expected from an integrated construct. Prm1-yeGFP-StrepII was observed on the cell surface, aswell as in intracellular compartments. This localisation is consistent with a previous study which found that a significant fraction of Prm1 is not located on the plasma membrane but transported to endosomes and the vacuole (Olmo and Grote, 2010a). The Prm1-yeGFP-StrepII expression levels of 5 randomly selected integration clones was assessed using SDS-PAGE and in-gel fluorescence **(Figure 49B)**. Both the Prm1-yeGFP-StrepII covalent homodimer (>180 kDa species) and the monomer (~125 kDa species) were detected. Based on eGFP intensity of the Prm1-yeGFP-StrepII species, all 5 clones displayed clearly higher levels of Prm1 expression than the *TEF1* promoter 2μ-based vector **(Figure 49B)**. Signal corresponding to Prm1-yeGFP-StrepII expressed from the 2μ plasmid sample was only observed after substantially increasing the contrast. Clone 2 displayed the highest GFP signal and on this basis was chosen for subsequent purifications of Prm1.

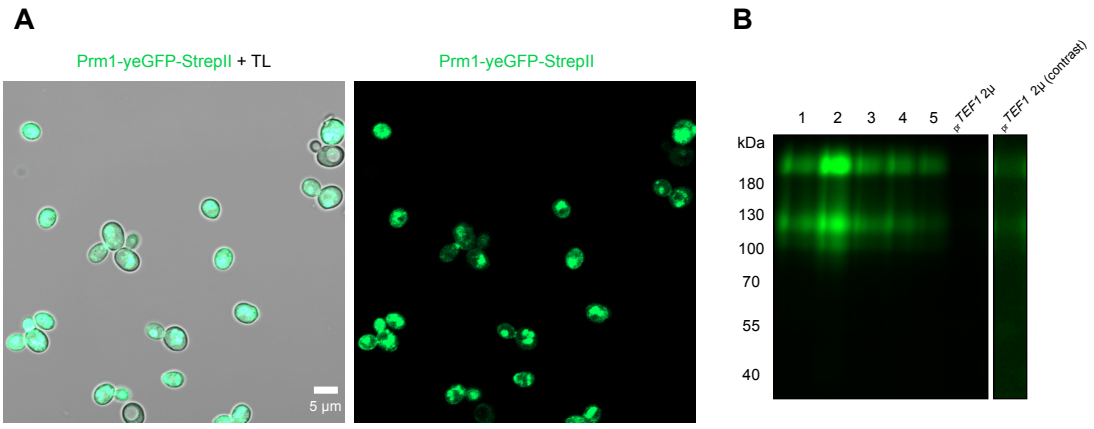

Figure 49. Efficient expression of genome integrated Prm1-yeGFP-StrepII after galactose induction. A. Expression of Prm1-yeGFP-StrepII upon galactose induction**.** After resuspension of logarithmic phase growing cells in YPGal, cells were grown for 16 h at 30 °C and imaged using confocal microscopy. **B.** In-gel fluorescence of cell lysates. Cell lysates derived from glass bead lysis were centrifuged at 20,000 × *g* for 1 h at 4 °C to crudely pellet membranes. The membranes were resuspended in SDS-PAGE sample buffer. Samples were then analysed for Prm1-yeGFP-StrepII expression by in-gel fluorescence after SDS-PAGE on a Tris-glycine 8% gel.

3.3.2 Prm1 detergent screen

For the study of membrane proteins *in vitro*, it is necessary to extract them from the native membrane environment. The most widely used agents for extraction of membrane proteins are detergents (Stetsenko and Guskov, 2017). Due to the amphipathic nature of detergents, their hydrophobic tails can insert into membranes. At high concentrations of detergent (over the critical micellar concentration (CMC)), membrane proteins are extracted as protein-detergent complexes. As the name suggests, at the CMC, detergent molecules are found as micelles. Suitable detergents have to be found for extracting membrane proteins and ideally, the detergent should keep the protein in a folded and functional state. Often times, a trial and error process has to be performed for each membrane protein to find the optimal detergent.

To assess the effectiveness of various detergents for solubilisation of Prm1, a detergent screen was performed using fluorescence-detection size-exclusion chromatography (FSEC). The method utilises size-exclusion chromatography (SEC) which separates analytes based on size. By coupling SEC to a fluorometer, the technique can be used to examine the degree of monodispersity aswell as the expression of fluorescently tagged proteins of interest. In this case, FSEC can be used to screen the effect of detergents solubilised membrane proteins directly from crude lysates without the need to purify the protein of interest (Kawate and Gouaux, 2006). A detergent treated cell lysate was ultracentrifuged at 100,000 × *g* to separate insoluble material. The supernatant, containing the detergent solubilised membrane proteins was then analysed by FSEC. In this trace, a large peak corresponding to an eGFP cleavage product was observed **(Figure 50A)**. The degradation product likely arose because insufficient amounts of protease inhibitors were added during the experiment. A substantial eGFP cleavage product signal was also observed in the no detergent control (black). Because this control was also ultracentrifuged before injection (and therefore will be depleted in membrane material); the high signal suggests the majority of the eGFP molecules are not appended to the upstream Prm1-TMD.

Nevertheless, despite the predominance of the eGFP cleavage product, it was still possible to detect the dimeric form of Prm1-eGFP-StrepII **(Figure 50B)**, which was assigned based upon the run of protein standards. Under certain detergents, a peak eluting subsequent to the dimer peak which corresponds to the monomer was observed. The Prm1-

eGFP dimer was solubilised to similar extents with all the detergents tested with the exception of CHAPS **(Figure 50B)**. LDAO and Fos-Chol13 most efficiently extracted Prm1-eGFP dimers, however they also extracted the monomer and other smaller molecular weight degradation products. Fos-Choline detergents are known to be efficient in solubilisation, although there is also evidence that proteins solubilised by this detergent are less stable (Garcia-Alai et al., 2019). OG, DDM, GDN, LMNG-CHS and Digitonin were suitable detergents for solubilisation of Prm1 as the peak corresponding to the Prm1-eGFP dimer was predominant and mostly monodisperse. Because of the high CMC of OG, which allows it to be more easily removed during dialysis, OG was chosen as the detergent for subsequent purification and reconstitution.

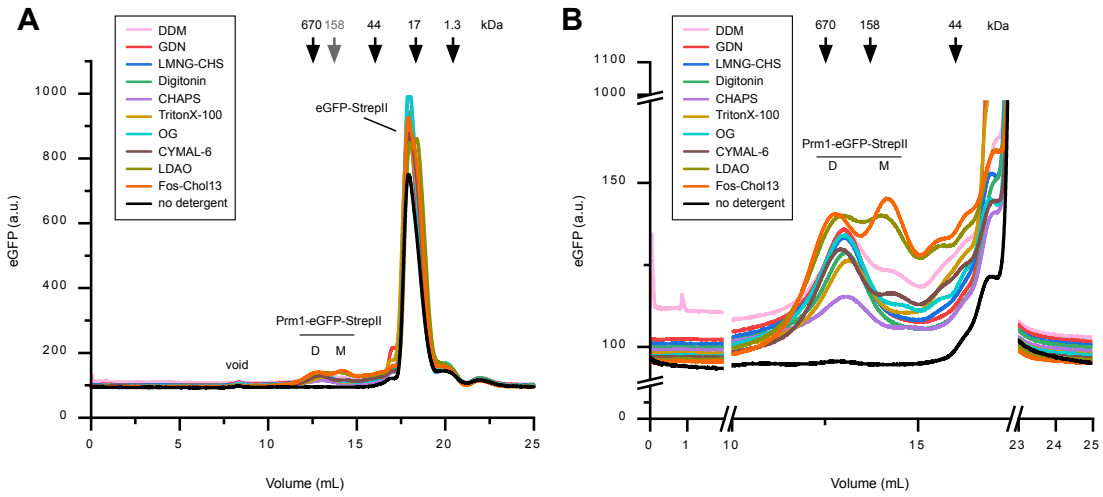

Figure 50. Prm1-eGFP-StrepII detergent screen. A. Overview of FSEC trace. D indicates the dimeric Prm1-eGFP-StrepII species. M indicates the monomeric Prm1-eGFP-StrepII species. **B.** Same data as in (A) but the display axes were adjusted to resolve the dimeric and monomeric Prm1-eGFP traces. kDa of gel filtration standards (Bio-Rad) are annotated.

3.3.3 Prm1-eGFP proteoliposomes display two subpopulations

For reconstitution of Prm1 into small liposomes, the co-micellar method was chosen. Here the detergent solubilised membrane protein is mixed with an excess of lipid, and the detergent is gently removed by dialysis. Removal of detergent from a lipid-protein-detergent micellar solution leads to the progressive formation of liposomes with membrane proteins incorporated into the bilayer. The lipid mixture contained Atto655-DOPE in order to label the resultant liposomes to facilitate their detection during flow cytometry

After overnight dialysis (16 h), Prm1-eGFP proteoliposomes were analysed by flow cytometry. As a control, empty liposomes were also prepared. On the basis of Atto655 fluorescence, two subpopulations were observed for the Prm1-eGFP proteoliposomes, which was in contrast to the empty liposomes **(Figure 51A).** The subpopulation which displayed higher Atto655 fluorescence could represent Prm1-eGFP proteoliposomes which are docked to one another. The docked subpopulation arises shortly after formation of the proteoliposomes during dialysis, because the liposome mixture was injected into the flow cytometer immediately after retrieval from the dialysis cassette. The ratios of the subpopulations observed after Prm1 proteoliposomes were incubated for 1 h at 30 °C were very similar **(Figure 51B)**, suggesting that docking between the Prm1 proteoliposomes had reached an end state.

If liposomes were docked due to Prm1, proteolytic cleavage of Prm1 may lead to undocking of liposomes. To test this, proteinase K was added to the liposomes (final concentration 0.33 mg/mL) and the liposomes were incubated at 25 °C for 2 h. Addition of proteinase K reduced the frequency of the highly Atto655 fluorescent population (39.3% compared to 56.9%) **(Figure 51C).** The fraction of the weaker Atto655 signal population concomitantly increased, suggesting some of the docked Prm1 proteoliposomes had become undocked. As expected, the empty liposome population remained as a single undocked population after proteinase K treatment.

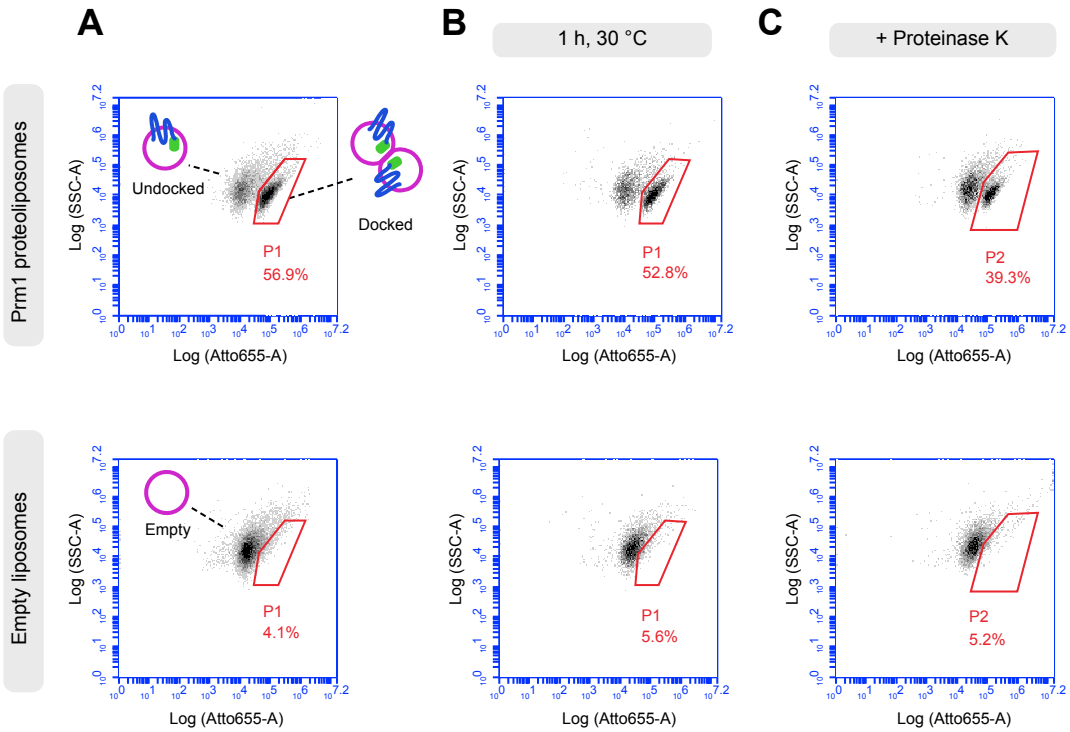

Figure 51. Identification of a docked Prm1 proteoliposome subpopulation by flow cytometry. **A.** Prm1-eGFP proteoliposome mixtures display a secondary docked subpopulation. P1 region defines the more Atto655 fluorescent subpopulation which correspond to docked Prm1-eGFP proteoliposomes. Liposome mixtures were directly measured after removal from the dialysis cassette. 10,000 events are displayed in each plot. **B.** Liposome populations after 1 h incubation at 30 °C under gentle agitation (300 rpm). 3,700 events are displayed. **C.** Docking of Prm1 proteoliposomes is partially reversible by proteinase K treatment. Samples were treated for 2 h at 25 °C. 4,700 events are displayed.

It should be clarified that new regions had to be defined to distinguish the docked subpopulations when proteinase K was added (denoted region P2 in **Figure 51**). This was done because for unknown reasons, the entire population (i.e. both the docked and undocked subpopulations) of the proteinase K treated liposomes were more Atto655 fluorescent than the respective non-treated samples. This effect, termed hereafter as 'proteinase K-mediated Atto shift', occurred irrespective of whether Prm1 was reconstituted into liposomes or not and can be more clearly seen in overlaid histograms of the proteinase K and non-proteinase K treated samples **(Figure 52A)**. No further shift was seen upon extended proteinase K incubation to 4 h **(Figure 52B)**. To account for the proteinase K-mediated Atto shift, the region P2 in the proteinase K treated samples was accordingly

shifted with respect to region P1 used in the proteinase K absent samples. Overall, the reversible nature of the highly fluorescent Atto655 subpopulation supported the idea that this subpopulation consisted of docked Prm1 proteoliposomes and that a subset of these could become undocked following proteolytic cleavage of Prm1.

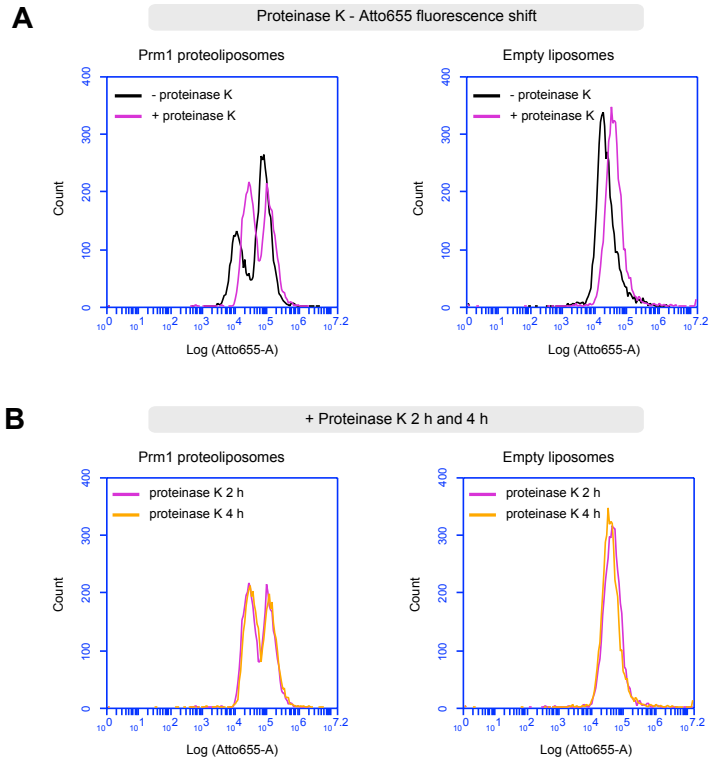

Figure 52. Proteinase K-mediated shift of Atto665 fluorescence. A. Overlay histograms show the enhanced Atto655 fluorescence of both the empty liposome and Prm1 proteoliposome populations upon 2 h addition of proteinase K (magenta) compared to without (black). **B.** Proteinase K treated liposomes after 2 h (magenta) and 4 h (orange). 4,700 events are displayed in all the plots.

3.3.4 Reconstituted Prm1 does not further dock to large liposomes

I performed a second experiment to determine whether Prm1 proteoliposomes could undergo an additional round of docking. For this, Prm1-eGFP proteoliposomes containing Atto655-DOPE were mixed with large liposomes (400 nm) which were labelled with Rhodamine-PE. Because of the different fluorescent lipid probes, docking of Prm1-eGFP proteoliposomes to the large liposomes would result in the presence of a Rhodamine+ and Atto655+ subpopulation.

When empty Atto655-DOPE labelled liposomes were mixed with the large Rhodamine-PE labelled liposomes, the Rhodamine-labelled liposomes displayed higher Atto655 fluorescence, which was attributed to background from spurious association of Atto655-DOPE labelled liposomes with the Rhodamine-PE labelled liposomes **(Figure 53)**. The reciprocal trend was observed for the empty Atto655-DOPE labelled liposome subpopulation; they tended to display higher Rhodamine fluorescence in comparison to the single empty Atto655-DOPE liposome control. However, no enrichment of Rhodamine+Atto655+ entities were detected when Prm1 proteoliposomes were mixed with the Rhodamine-PE labelled liposomes. This indicated that the Prm1-eGFP proteoliposomes could not further dock to other liposomes **(Figure 53)**.

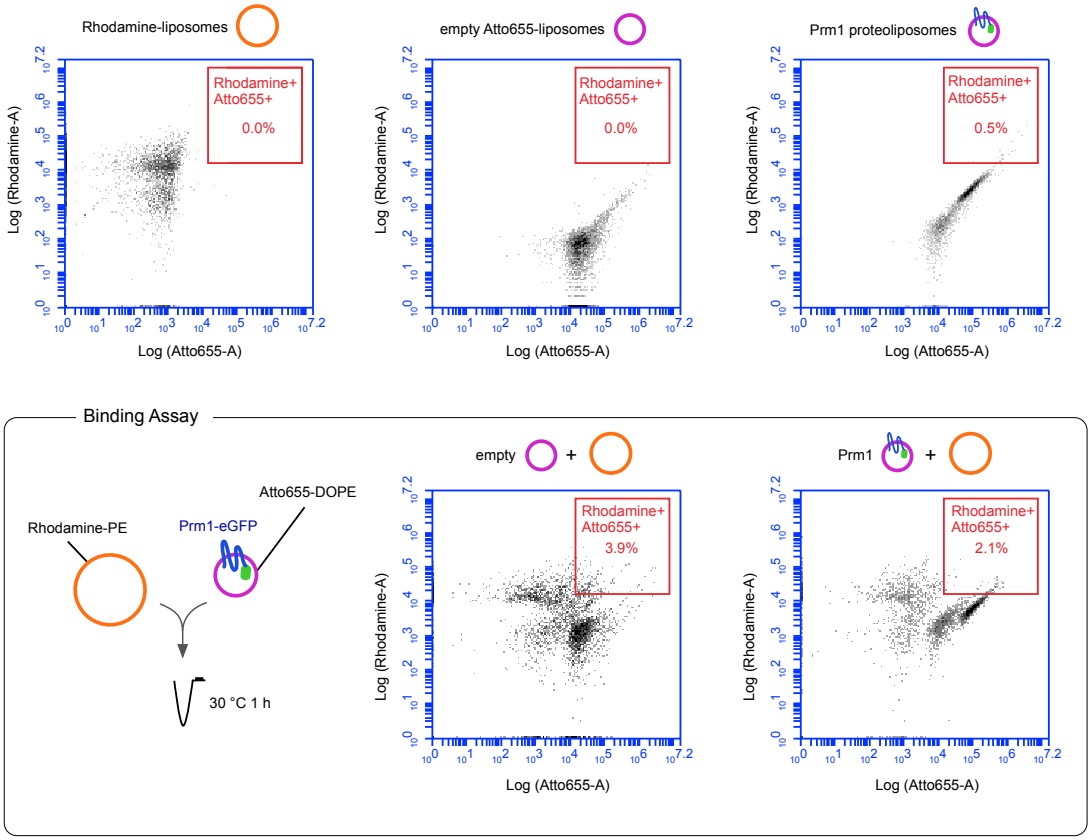

Figure 53. No docking of Prm1-eGFP proteoliposomes to 400 nm Rhodamine labelled liposomes. 400 nm liposomes labelled with Rhodamine-PE were mixed with either empty liposomes or Prm1 proteoliposomes labelled with Atto655-DOPE at 30 °C for 1 h at 300 rpm. When Prm1-eGFP present Atto655 labelled liposomes were mixed with Rhodamine labelled liposomes, no enrichment of a subpopulation which was Rhodamine+ and Atto655+ was observed. 3,900 events are displayed in each density plot.

3.3.5 eGFP-eGFP interactions are not responsible for the high Atto655 subpopulation

eGFP is known to form weak dimers (Phillips, 1997). During reconstitution into liposomes, membrane proteins can integrate in either the outside-out or inside-out orientations. Therefore, the docked liposome population may have arisen from *trans* eGFP-eGFP interactions between inside out Prm1-eGFP molecules anchored on different liposomes.

To cleave eGFP, Precission protease (gifted by Nathalie Bleimling, MPI Dortmund) was added to an aliquot of Prm1-eGFP-StrepII, which contains a precission protease/Human Rhinovirus (HRV 3C) cleavage site in between the C-terminus of Prm1 and eGFP. Successful cleavage of eGFP from Prm1 was monitored by SDS-PAGE and in-gel fluorescence of eGFP. Release of eGFP from Prm1 could be observed by the GFP fluorescent band between 25 kDa and 35 kDa (eGFP-StrepII is 30 kDa) and weak GFP signal associated to the full length Prm1-eGFP-StrepII species, for both the monomeric and dimeric forms. In addition, stain-free imaging showed that the bands corresponding to the dimeric and monomeric species of Prm1-eGFP-StrepII under Precission treatment were shifted in comparison to the untreated control, consistent with loss of eGFP. However, Prm1-eGFP cleavage was incomplete, because low GFP fluorescence indicative of the Prm1-eGFP dimer was still evident **(Figure 54)**.

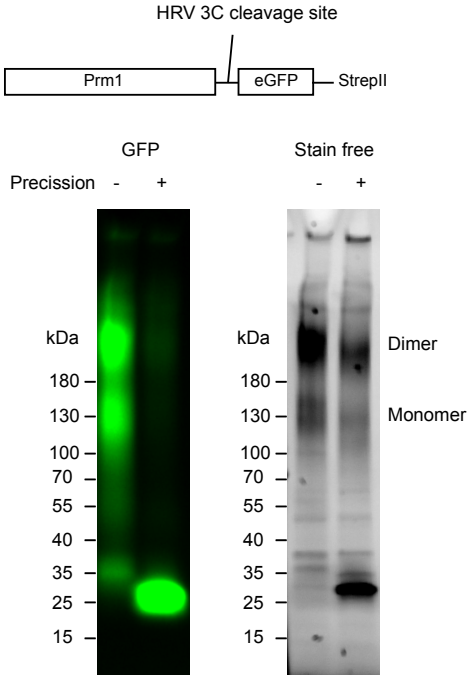

Figure 54. In-gel fluorescence of eGFP-cleaved Prm1-eGFP-StrepII via Precission protease. Precission protease recognises and cleaves the HRV 3C cleavage sequence. Aliquots of Prm1-eGFP-StrepII were prepared in SDS sample buffer without reducing agent and without heating to preserve eGFP fluorescence. SDS-PAGE was conducted on a 4-15% stain free gel. Left: GFP channel image. The ~30 kDa eGFP band indicates release of the eGFP-StrepII tag due to Precission cleavage. Faint high MW associated eGFP signal corresponding to uncleaved Prm1-eGFP-StrepII can be observed in the Precission treated sample. Right: Stain-free image. Image was contrast adjusted.

The aliquot of Precission protease-treated Prm1-eGFP-StrepII was used to prepare proteoliposomes by dialysis (referred as eGFP-cleaved Prm1 proteoliposomes). When compared to the Prm1-eGFP derived proteoliposomes, the eGFP-cleaved Prm1 proteoliposome population contained lower GFP signal, as expected **(Figure 55)**. In contrast, Atto655 intensities of the liposome populations were consistent, suggesting similar concentrations of Atto655-DOPE were incorporated into the liposomes between the experiments.

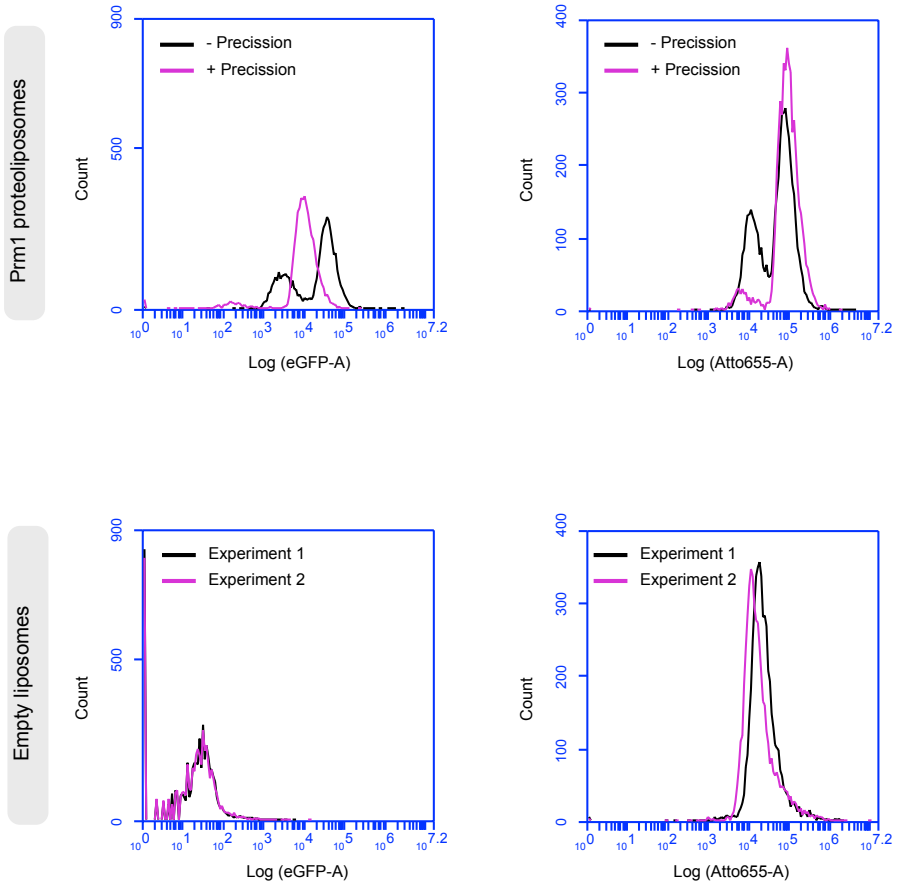

Figure 55. Comparison of eGFP fluorescence between eGFP-cleaved and non-cleaved Prm1-eGFP proteoliposomes. Overlaid histogram plots of Prm1-eGFP-StrepII proteoliposomes which prior to dialysis were treated with Precission in order to cleave eGFP. Lower GFP fluorescence intensity of the Prm1 proteoliposomes show that eGFP had been cleaved by Precission (although not completely). Atto655-DOPE histogram plots of the Prm1 proteoliposomes remained comparable to Prm1-eGFP proteoliposomes, with two bimodal distributions at ~10^4 and 10^5, respectively. In empty liposome control preparations, one unimodal distribution was observed at ~10^4, which was observed across 2 independent experiments. For these histograms, the experiment 1 empty liposomes and the non-Precission-treated proteoliposome data are from the same samples as those shown in Figure 51 and Figure 52. 5,000 events per sample are displayed.

Furthermore, the eGFP-cleaved Prm1 proteoliposomes retained the bimodal Atto655 distribution **(Figure 55)**, strongly suggesting that eGFP-eGFP interactions were not responsible for the formation of the docked subpopulation. Plotting the data as SSC versus Atto655 fluorescence plots allowed the quantitation of the docked subpopulation,

which constituted nearly the entire population (~90% of the total liposomes) **(Figure 56B)**.

Upon proteinase K addition, after 2 h the frequency of the docked eGFP-cleaved Prm1 proteoliposome subpopulation decreased (90.3% to 77.0%), with an accompanied increase of the frequency of the undocked Prm1 proteoliposome subpopulation (9.7% to 23.0%) **(Figure 56B)**. This increase represents an approximate 2-fold enhancement of the initial number of undocked proteoliposomes. Prolonged proteinase K incubation to 4 h did not further affect the distribution. As found in previous experiments, the addition of proteinase K again led to a proteinase K-mediated Atto655 shift in the populations (data not shown) and therefore the regions to quantify the high intensity Atto655 docked entities in these plots were slightly shifted compared to the non-proteinase K treated plots.

In this experiment, I also investigated if covalent dimers of Prm1 were needed for docking **(Figure 56A and 51B)**. To reduce disulfide bonds, DTT was added to the Prm1/OG mixture before reconstitution and also to the dialysis buffer during reconstitution. Docking did not require Prm1 covalent dimers, because the ratio of undocked to docked Prm1 proteoliposomes was practically identical to non-reduced Prm1 proteoliposomes **(Figure 56B)**. However, the presence of DTT influenced the extent of undocking upon proteinase K treatment. In a reduced environment, 35% of Prm1 proteoliposomes were undocked after 2 h proteinase K treatment, whilst 23% of Prm1 proteoliposomes were undocked in the same period without DTT treatment. After 4 h, the frequency of the undocked subpopulation slightly increased when DTT was present (35% to 40%), whereas no further undocking occurred in the DTT absent Prm1 proteoliposomes **(Figure 56B and 56C)**. 4 h was the endpoint of the undocking reaction, because no further undocking was observed after 6 h of proteinase K treatment for both the DTT and non-DTT treated samples **(Figure 56D)**.

To summarise, Prm1-mediated docking did not require Prm1 to be covalently dimerised. However, the status of covalent dimerisation influenced both the rate and the extent of protease induced liposome release; from initially being docked to becoming undocked. Reconstituted Prm1 which was covalently dimerised provided a higher resistance to the undocking reaction. In contrast, if the covalent dimers were reduced, their anchored liposomes were more susceptible to undocking. Finally, in both cases, there was always a

residual, docked subpopulation of proteoliposomes which persisted after protease addition, even after extended incubations (6 h).

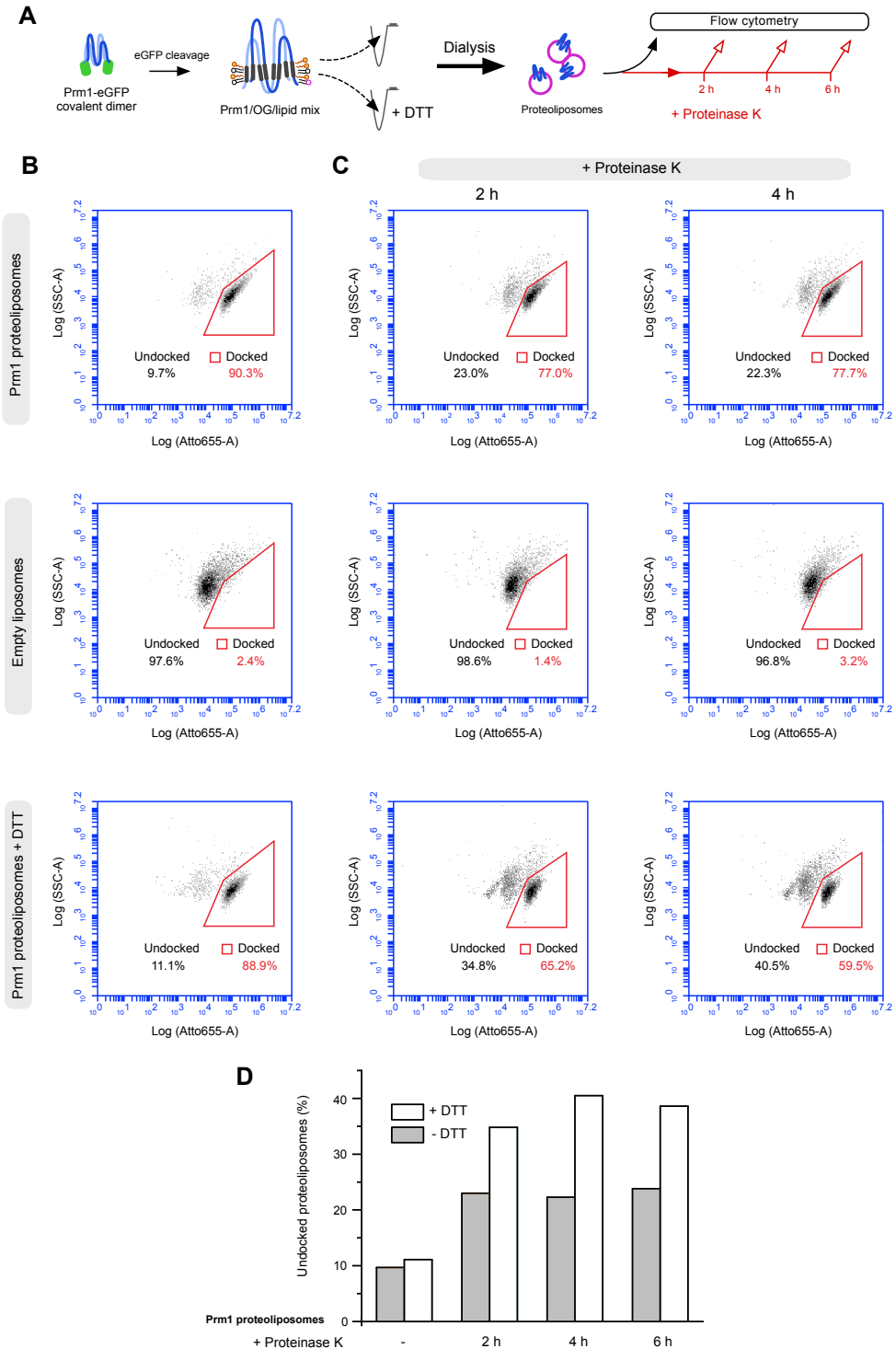

Figure 56. Proteinase K-mediated undocking of eGFP-cleaved Prm1 proteoliposomes is enhanced when Prm1 is reduced. A. Workflow of experiment. eGFP was released from Prm1-eGFP/OG mixtures by addition of Precission protease. For simplicity, OG micelles are not illustrated. The resultant Prm1/OG mixture was mixed with lipid mix containing Atto655-DOPE and

subsequently Prm1 proteoliposomes were prepared by dialysis. To reduce disulfide bonds, 10 mM DTT was added to the Prm1/OG/lipid mixture and to the dialysis buffer. The Prm1 proteoliposomes were measured by flow cytometry immediately after retrieval from the dialysis cassette (black arrow), or proteinase K was added (red arrow) and aliquots were analysed by flow cytometry at 2 h intervals (red unfilled arrows). **B.** eGFP cleaved Prm1 proteoliposomes still form docked subpopulations. Covalent dimerisation of Prm1 is not required for proteoliposome docking. **C.** Prm1 proteoliposomes after 2 h and 4 h proteinase K treatment. Because not all plots recorded the same number of events, plots were normalized so that the first 4,200 events are displayed in each plot for B and C panels. Percentages were calculated from all events recorded. **D.** Undocked liposome quantitation from the flow cytometry plots shown in panel (B) and (C). Data for the 6 h proteinase K incubation timepoint was included. Minus (-) indicates no proteinase K addition.

3.3.6 Reconstituted Prm1 is efficiently cleaved by proteinase K

The remainder of eGFP-cleaved Prm1 proteoliposomes which stayed docked after proteinase K treatment may have been due to incompletely digested Prm1. Furthermore, reduced Prm1 proteoliposomes may be degraded more efficiently by proteinase K, which would explain the greater extent of undocking. To investigate this idea, aliquots of proteinase K treated eGFP-cleaved Prm1 proteoliposomes ± DTT at 4 h (when no more undocking occurred) were assessed by SDS-PAGE, providing a snapshot of the proteolysis reaction.

In control eGFP-cleaved Prm1 proteoliposomes without addition of proteinase K (lane 1), the >180 kDa species representative of the covalent dimer could be observed, both in the eGFP channel and the stain-free channel (which stains proteins based on tryptophan residues) **(Figure 57)**. In this lane, the weak eGFP intensity of the glycosylated dimer band represented Prm1-eGFP covalent dimers where eGFP was not cleaved by Precission.

In DTT+ conditions without proteinase K (lane 2), the dimer species was depleted, and accordingly there was an enrichment of a 100 kDa MW band, the expected size of the glycosylated Prm1 monomer **(Figure 57)**. The species running approximately 130 kDa likely corresponded to the monomeric, glycosylated Prm1-eGFP-StrepII species. This result confirmed that the addition of DTT to eGFP-cleaved Prm1 successfully reduced the disulfide bonds which linked two Prm1 monomers together. In both eGFP-cleaved Prm1 proteoliposome samples without proteinase K (lanes 1 and 2), free GFP from Precission mediated cleavage was detected because GFP was too large to diffuse out of the dialysis membrane used during reconstitution (2K MWCO).

In the proteinase K treated proteoliposomes (lanes 3 and 4), the full length Prm1 molecules were efficiently cleaved, evidenced by the absence of the >180 kDa dimer and 100-130kDa monomer bands **(Figure 57A and 57B)**. Note that the faint bands which ran slightly higher than 130 kDa (labelled unknown) are not Prm1 because the band appears in empty liposome controls (lane 5). In addition, proteinase K treatment led to the appearance of degradation products of various sizes. Of note, was a fluorescent band at ~55 kDa **(Figure 57C and 57D)**. This likely represents a degradation product of Prm1-eGFP-StrepII, which arose as a consequence of proteinase K cleavage. The eGFP moiety was not degraded, because it is likely within the liposome lumen and therefore protected from protease cleavage. Two possible representative products are inferred from the size of the fragment **(Figure 57E)**. The first (i) is a TMD 4-eGFP-StrepII (~35 kDa) fragment of Prm1 which is dimerised (~70 kDa). The second (ii) is a monomeric remnant of Prm1 ectodomain 2 linked to TMD 4-eGFP-StrepII (~55 kDa). The implications of the degradation product (ii) are speculated in the discussion.

In conclusion, the proteolytic degradation of reconstituted Prm1 by proteinase K was efficient, resulting in the loss of full length Prm1 molecules. The remaining highly Atto655 fluorescent subpopulation of liposomes are not releasable by proteinase K treatment, thus calling into question whether these remaining liposomes actually represent docked liposomes. Therefore, an alternative explanation is that this subpopulation may correspond to fused liposomes.

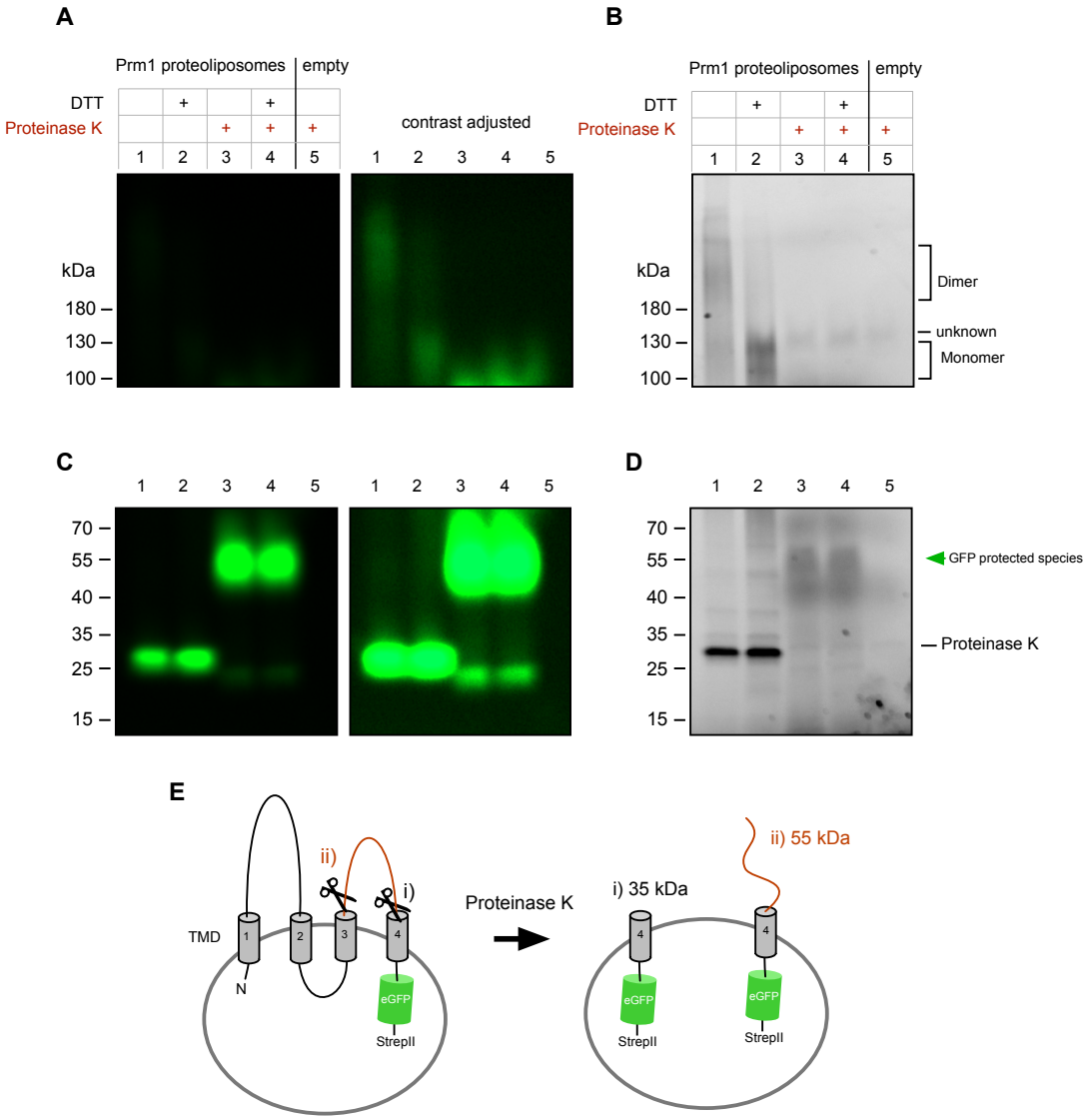

Figure 57. Efficient proteolysis of eGFP-cleaved Prm1 proteoliposomes after proteinase K treatment. **A.** In-gel GFP fluorescence of eGFP-cleaved Prm1 proteoliposomes treated with proteinase K. Precission treated Prm1-eGFP-StrepII was reconstituted into liposomes. Aliquots of the proteinase K-treated Prm1 proteoliposomes after 4 h (same as those used in Figure 56) were loaded to assess Prm1 degradation. **B.** The same gel imaged using stain-free imaging, which was contrast adjusted to better detect the Prm1 species. **C.** Lower part of the gel in eGFP channel. Green arrowheads denote the Prm1 fragments which coincide with GFP fluorescence. Proteinase K band was assigned based on the band presence in the empty liposome sample (lane 5) and consistent with the protein MW (29 kDa). **D.** Lower part of the gel in stain-free channel. **E.** Possible identity of the GFP protected species. i) An eGFP fragment tethered only to TMD4 (35 kDa) which for unknown reasons ran as a dimer (~70 kDa). ii) Proteinase K cleavage at the beginning of ectodomain 2, which would result in an ~55 kDa fragment (excluding post translational modifications).

3.3.7 DLS measurements of Prm1 proteoliposomes

As a complementary method to analyse the proteoliposomes, the sizes of the liposomes were investigated with dynamic light scattering (DLS). The method measures fluctuations in the intensity of scattered light based on the Brownian motion of particles, which in turn is related to the size of the particles. DLS of empty liposomes indicated they were approximately 120 nm diameter in size **(Figure 58).** In contrast, for Prm1-eGFP-StrepII proteoliposomes, a shoulder peak ranging from ~75 nm to 500 nm was observed, indicating the proteoliposomes were on average larger in size. When proteinase K was added, the shoulder peak disappeared, and Prm1 proteoliposomes displayed a peak equivalent to empty liposomes. As expected, addition of proteinase K had no effect on intensity profile of the liposomes. These results support the idea that Prm1 proteoliposomes are docked, and that proteolytic degradation of Prm1 leads to undocking.

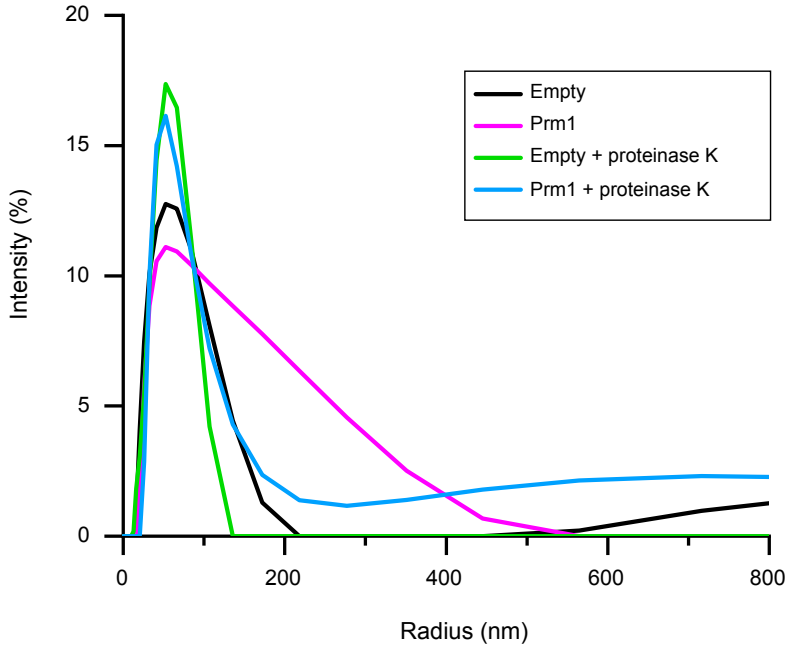

Figure 58. Prm1-eGFP-StrepII proteoliposomes are larger than empty liposomes measured via DLS. Upon Proteinase K addition, the size of the Prm1 proteoliposomes were reduced. The low intensities at high radius in empty liposomes (after 450 nm) and Prm1 proteoliposomes treated with proteinase K (after ~300 nm) may correspond to dirt contaminants.

Chapter 4. Discussion

4.1 M(IP)$_2$C levels strongly influence the outcome of the Δ*prm1* membrane fusion reaction

Here I show for the first time a group of genetic suppressors of Δ*prm1*, a mutant sensitised for fusion at the stage of membrane merger. Until now, with the exception of external Ca^{2+}, no other suppressor of the Δ*prm1* cell fusion phenotype had been found in budding yeast, which has impeded progress towards understanding the function of Prm1 during cell fusion. In *N. crassa*, the single-pass transmembrane protein LFD1 was found to behave redundantly to Prm1 since a percentage of *lfd-1* mutants also display unfused membranes and lysis during mating (Palma-Guerrero et al., 2014). Interestingly, overexpression of LFD1 can suppress *N. crassa* Δ*prm1* fusion arrest. *S. cerevisiae* does not contain a LFD1 homolog and the lack of domain characterisation for LFD1 makes it unclear how exactly fusion is being restored.

I show that suppression of Δ*prm1* fusion arrest is mediated by the reduction of mannosylated sphingolipid levels. More specifically, from the data I was able to isolate one specific sphingolipid species to be responsible, namely the M(IP)$_2$C species. Without Prm1, the head group identity of the sphingolipids within the plasma membranes becomes a significant determinant of cell-cell membrane fusion reaction. Further evidence which supports that M(IP)$_2$C levels have a strong impact on Δ*prm1* fusion is that raising the levels of M(IP)$_2$C by overexpression of either *SUR1* or *IPT1* further arrests fusion of Δ*prm1* × Δ*prm1* crosses. The overexpression of *IPT1* inhibited the fusion of Δ*prm1* mating pairs to lesser extents than *SUR1*; a simple explanation for this is that Sur1 levels are rate-limiting for M(IP)$_2$C production. In this scenario, overproduction of Sur1 would conceivably increase M(IP)$_2$C levels to greater extents than by overproducing Ipt1. The updated fusion landscape from the results in this study are summarised here **(Figure 59)**. One interesting detail found was that the influence of M(IP)$_2$C levels on fusion of the plasma membranes is only important in the context of a Δ*prm1* null background **(Figure 59)**. In other words, Prm1

overrides the fusion arresting effects of $M(IP)_2C$. This observation offers clues as to how Prm1 supports fusion.

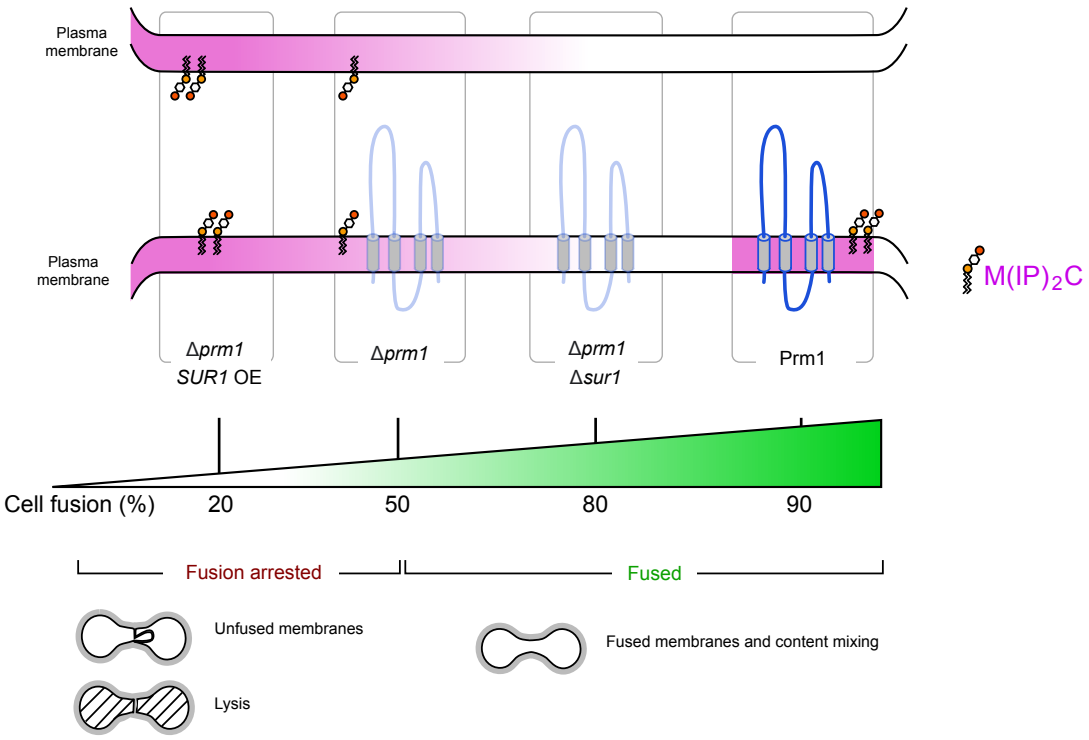

Figure 59. Summary of cell-cell fusion outcomes with $M(IP)_2C$ and Prm1. Absence of Prm1 leads to ~50% of cells failing to fuse, leading to dead-end fusion outcomes. However, this can be suppressed if $M(IP)_2C$ levels are reduced in both of the fusing membranes (magenta). Fusion of Δ*prm1* membranes can be further inhibited by increasing $M(IP)_2C$, resulting in mating pairs predominantly displaying fusion arrested outcomes. Finally, Prm1-containing cells fuse efficiently, independent of $M(IP)_2C$ levels. OE, overexpression.

4.1.1 Pertubation of $M(IP)_2C$ is not related to cell fusion defects due to lipid raft biogenesis

One of the principal functions of sphingolipids are for the assembly of lipid rafts. Bagnat and Simons showed that biogenesis of lipid rafts were important for yeast cell fusion at early stages of the mating process (Bagnat and Simons, 2002a, 2002b). Here, depletion of lipid rafts leads to cell-cell pairing defects due to impaired pheromone signalling. Furthermore, cell wall remodelling is impaired, resulting in mating pairs with undigested

cell walls. Because my investigations with *SUR1* when overexpressed or deleted did not give rise to these phenotypes and instead affected later stages of fusion i.e. cytoplasmic bubbles and lysis, we can conclude that lipid raft biogenesis is not disrupted.

4.2 Δ*sur1* acts similarly to Ca^{2+} to suppress fusion arrest

Because $M(IP)_2C$ is more anionic than the precursor sphingolipids, the deletion of *SUR1* leads to a less negative surface charge on the plasma membrane. From this, a hypothesis was proposed in which the reduced surface charge was relevant for the suppressed fusion arrest in Δ*prm1*Δ*sur1* × Δ*prm1*Δ*sur1* crosses. This was because less negative surface charges would lower the electrostatic repulsion of two approaching lipid bilayers. To test this hypothesis, I investigated if raising the ionic strength, which should screen electrostatic interactions could suppress Δ*prm1* fusion arrest. No suppression was found and therefore the electrostatic model cannot explain the restored fusion in Δ*prm1*Δ*sur1* pairs.

A clue to understanding the mechanism of Δ*sur1* on fusion emerged from investigations of Δ*prm1*Δ*sur1* × Δ*prm1*Δ*sur1* crosses in the presence of EGTA. A fraction of Δ*prm1*Δ*sur1* mating pairs fused without the presence of Ca^{2+}, such that their fusion levels mimicked that of Δ*prm1* mutants when supported by external Ca^{2+}. Moreover, the deletion of *SUR1* or the presence of external Ca^{2+} imparted similar effects on the mating outcomes of Δ*prm1* mutants, as both lysis and cytoplasmic bubbles were suppressed. This revealed ability of Δ*sur1* to replace external Ca^{2+} suggests they might elicit a common mechanism to promote plasma membrane fusion.

How might Ca^{2+} promote the membrane fusion of Δ*prm1* mutants? Studies have indicated Ca^{2+} has affinity for membranes containing certain anionic lipids (such as PS) which promote membrane docking and fusion (Papahadjopoulos et al., 1988; Witkowska et al., 2021). In the case of PS containing membranes, Ca^{2+} is stronger at promoting fusion than other divalent cations such as Mg^{2+}, which is likely tied to the observation that Ca^{2+} can dehydrate PS head groups whilst Mg^{2+} cannot (Sundler, 1984). Therefore, it is proposed that Ca^{2+} promotes fusion by forming anhydrous complexes with PS containing membranes in *trans* (Papahadjopoulos et al., 1988). Interestingly, suppression of Δ*prm1* fusion defects specific only to Ca^{2+} and could not be suppressed by other divalent cations (Aguilar et al.,

2007). This opens the question to whether external Ca^{2+} interacts with PS or other anionic lipids with affinity to Ca^{2+} which are present on the plasma membranes and promote fusion in the absence of Prm1.

The dehydration of phospholipids lowers the energy barrier required for two contacting membranes to form stalks, which is considered the on-pathway intermediate of membrane fusion (Chernomordik and Kozlov, 2008). Notably, other properties, such as the spontaneous curvature of lipids can also influence this energy barrier. The spontaneous curvature of lipids depends on the relative size of the head group to the acyl chains. Lipids that possess spontaneous negative curvature i.e. small head groups relative to acyl chains favour the formation of stalks (Chernomordik and Kozlov, 2008). With this notion in mind, changes in the plasma membranes by Δ*sur1*-mediated sphingolipid alterations may lower the energy barrier for fusion by promoting the presence of lipids with spontaneous negative curvature. Interestingly, the simplest sphingolipid precursor ceramide, contains spontaneous negative curvature owing to its small head group and could possibly be elevated in Δ*sur1* plasma membranes. Furthermore, the enrichment of such lipids in both membranes would be expected to lower the energy barrier more than if they were enriched in only one membrane; a feature that is consistent with the observed additive nature of Δ*prm1*Δ*sur1* membranes on fusion.

Another possible mode of action for Ca^{2+} to promote plasma membrane fusion is by interaction with Ca^{2+} binding proteins. One implicated Ca^{2+} regulated fusion effector is the yeast synaptotagmin homolog Tcb3. Tcb3 partly suppresses lysis of Δ*prm1* × Δ*prm1* pairs, possibly via its C2 domain which binds Ca^{2+} (Aguilar et al., 2007). Tcb3 is likely not the only Ca^{2+} regulated effector involved, because fusion efficiencies of Δ*prm1*Δ*tcb3* × Δ*prm1*Δ*tcb3* pairs do not mimic Δ*prm1* pairs without Ca^{2+}. In other systems, Ca^{2+} effectors promote fusion by organising fusion-related proteins at fusion sites. For instance, extracellular annexins, which are Ca^{2+}dependent phospholipid binding proteins, cooperate with the fusogen Syncytin to promote fusion of osteoclasts (Verma et al., 2018). Here, the presence of annexin (Anx5) also recruited a binding partner S100A4 to regulate osteoclast fusion, thereby highlighting the significant multi-protein organisation ability of Ca^{2+}. One idea could be that in the case of Δ*sur1*, the sphingolipid alterations can organise membrane proteins in a similar manner to Ca^{2+}which promotes fusion.

4.3 The Prm1 amphipathic domain is responsible for 50% of fusion promoting activity

Disrupting the conserved amphipathic domain of Prm1 by i) reducing the hydrophobicity across the domain or ii) deleting regions encompassing the domain impaired its fusion-promoting activity by 50%. Thus, here I have established one of the major functional domains for Prm1 activity. Amphipathic domains folded as amphipathic α-helices are suited for interaction with membranes; the hydrophobic side of the helix inserts between the acyl chains of the bilayer, whilst the hydrophilic side interacts with the phospholipid head groups (Drin and Antonny, 2010). It is not surprising therefore that many proteins involved in membrane remodelling processes utilise amphipathic helices. For instance, some amphipathic helices are adapted for sensing curved membranes, known as Amphipathic Lipid Packing Sensor (ALPS) motifs. GTPase Activating Protein for Arf1 (ArfGAP1), which promotes the disassembly of COPI coated vesicles during Golgi transport, possesses an ALPS motif thought to facilitate its targeting to Golgi sized-vesicles. Indeed, Arf1GAP has a preference to bind to small 30 nm radius liposomes (with high curvature) rather than larger ones *in vitro* (Mesmin et al., 2007). Conversely, other amphipathic helices can deform membranes by imposing membrane curvature, such as the N-BAR domain proteins (Simunovic et al., 2015). Epsins, which are involved in clathrin-mediated endocytosis, possess an N-terminal amphipathic helix which generates membrane curvature; this is exemplified by its ability to tubulate liposomes (Ford et al., 2002).

It is therefore tempting to conceive that the putative Prm1 amphipathic helix operates similarly and can deform membranes. This deformation may help to initiate the lipidic rearrangements that occur during membrane fusion. For instance, the GTPase atlastin was suggested to utilise its amphipathic helix to interact with and deform ER membranes to promote ER fusion; however, the exact mechanism is still unclear (Faust et al., 2015). As the Prm1 amphipathic domain is situated in the ectodomain, it is well placed to possibly deform the opposing plasma membrane of the other cell. Such a mechanism in *trans* would offer an explanation to the long-standing question of why Prm1 is only needed in one cell partner. Therefore, future biochemical studies should address whether the Prm1 amphipathic domain can actually interact and deform membranes or recognise curvature.

Finally, it is important to reiterate that there remains 50% of Prm1 fusion-promoting activity which is independent of the amphipathic domain. This activity, provided by the remaining regions of Prm1 is conferred by currently unknown mechanisms.

4.4 The hydrophobic domain of Prm1 has a role additional to dimerisation

4.4.1 Few covalent dimers are needed for Prm1 activity

Here the influence of the hydrophobic domain in the first ectodomain of Prm1 was investigated. The prevailing hypothesis was that this domain contributed to forming interactions with other Prm1 molecules during assembly of covalent homodimers. The data here suggests this to be the case. Switching conserved hydrophobic residues to charged residues, which would predictably interfere with hydrophobic mediated interactions, affected the amounts of covalent dimers formed. The aspartate mutants were generally impaired in promoting fusion, initially suggesting that impaired dimerisation was responsible, akin to the C120S mutant. The F109D mutant however was an interesting exception, because its fusion promoting activity was comparable to wild type Prm1, even though covalent dimerisation was affected. Therefore, although the abundance of covalent F109D mutant dimers are reduced, these dimers were sufficient to support fusion. The C277S mutant reported by Grote (Olmo and Grote, 2010b) behaved similarly. This reaffirms the idea that low amounts of Prm1 are needed at contact sites to support fusion (Olmo and Grote, 2010a).

4.4.2 Role of the Prm1 hydrophobic domain

In contrast to F109D, the L106D, I111D and L113D Prm1 mutants were impaired for supporting fusion, even though they each formed similar levels of covalent dimers. This suggests the hydrophobic domain serves another role important for Prm1 activity *in addition* to formation of covalent dimers. Since the L106D and I111 mutants are more defective than L113D and F109D, certain residues such as L106 and I111 within the hydrophobic domain are more critical for mediating this function.

What could this role be? The role might be intrinsically related to the question why Prm1 requires to be disulfide linked. Prm1 cysteine mutants which cannot form any covalent dimers fail to support fusion of Δ*prm1* mating pairs; however, can still self-associate into complexes (Engel et al., 2010). Thus, one interpretation is that a highly stable Prm1 complex is required for its function as a fusion-promoting protein. The hydrophobic domain, in tandem with disulfide bond formation, is likely needed to ensure a sufficiently stable and active Prm1 homodimer. An alternative idea is that similar to the Prm1 amphipathic domain characterised in this study, the hydrophobic residues such as L106 be required by Prm1 downstream to dimer assembly, such as insertion into the plasma membrane of the opposing mating partner, which was speculated previously (Engel et al., 2010; Olmo and Grote, 2010b). As described in those reports, for such a mechanism to occur, it has to be addressed how the hydrophobic domain would be free to interact with the membrane, given the nearby C120-C545 disulfide bond. Whether the hydrophobic domain can interact with membranes remains therefore an open question.

4.5 Prm1 can dock membranes by itself *in vitro*

4.5.1 A docking function of Prm1 which does not require covalent dimerisation

Through studying reconstituted Prm1 in artificial vesicles, I uncovered a capacity of Prm1 to dock membranes due to the presence of a high intensity Atto655 subpopulation. Prm1-mediated liposome docking occurred quickly, shortly after or concurrently with the formation of proteoliposomes during dialysis. Once docking occurred, no further rounds of docking could follow, suggesting that no additional Prm1 was available. Furthermore, Prm1 mediated docking is stable, given that the ratio of docked to undocked Prm1 proteoliposomes remained the same after 1 h. Because the stable high intensity Atto655 subpopulation already arose at the onset of flow cytometry analysis, I could not induce docking from initially undocked liposomes, which would have provided additional support for a docking reaction. However, the strongest evidence which corroborated that liposomes were indeed docked by Prm1 was that the intense Atto655 subpopulation could be reversed by protease. Importantly, I also found that Prm1-mediated docking did not rely on covalent

dimerisation. This is in stark contrast to the established Prm1 fusion-supporting activity in cells, which is severely dependent on covalent dimerisation. Together, these two observations support the idea that in cells, Prm1 covalent dimerisation is intrinsic to its fusion-promoting activity and possibly orchestrates a step in fusion subsequent to docking of plasma membranes.

4.5.2 The remaining docked subpopulation after protease addition may constitute fused liposomes

Protease induced undocking of Prm1 proteoliposomes was partial, even though SDS-PAGE analysis indicated that the full length Prm1 which was anchored on the liposomes was cleaved. Two interpretations are possible. The first is that the remaining docked population after protease treatment are fused liposomes. The setup of the experiments performed here unfortunately cannot distinguish between docked liposomes and fused liposomes and therefore this question remains to be addressed in future studies. Work on viral fusogens and SNAREs have found that at low temperatures, docking occurs readily, whilst membrane fusion is more favourable at higher temperatures (Tsurudome et al., 1992; Weber et al., 1998). If Prm1 has the capacity to fuse membranes, pore formation would be predicted to follow this trend and occur quickly upon temperature rise, especially if liposomes are pre-docked at low temperatures and ‘ready’ to fuse.

The existence of fused liposomes might reconcile the different rates and extents of protease induced undocking observed when Prm1 was disulfide bonded or not. If covalent dimers are required for fusing membranes, a greater proportion of the ‘docked’ subpopulation would in fact be fused when Prm1 is covalently dimerised. Consequently, there would be few truly docked liposomes that are available for release by protease. Conversely, when Prm1 is not covalently dimerised, few proteoliposomes are fused and therefore more proteoliposomes would be in the docked state and available to become undocked.

4.5.2.1 The 55 kDa degradation product may contain residual docking capacity

A second interpretation utilises the ~55 kDa GFP protected degradation product of Prm1 observed upon protease addition. If this product is not simply a dimer of a Prm1 TMD 4-eGFP-StrepII, the next most likely candidate would be a truncated part of ectodomain 2 linked to TMD 4-eGFP-StrepII. Because a residual ectodomain is present, it could be possible that a region of this domain still has the capacity to dock to membranes, thereby explaining why a docked subpopulation remains. However, the question would remain why non-covalently dimerised Prm1 proteoliposomes were more readily undocked after protease addition, even though the SDS-PAGE profiles of the degradation products between the DTT- and DTT+ samples were similar.

4.6 A model of Prm1, Δ*sur1* and Ca^{2+} action

The dissection of Prm1 activity found in this study is summarised in **Figure 60A**. The uncovered putative amphipathic helix required by Prm1 opens the question that Prm1 might act to shape membranes during membrane fusion. Although the capacity of the putative amphipathic helix to interact with membranes remains to be experimentally determined, such an interaction would be consistent with the unilateral mechanism of Prm1. Further extension of this notion suggests that this domain might also contribute for the observed ability of Prm1 to dock membranes *in vitro*. Disulfide linkages are also critical for Prm1 activity *in vivo* and from *in vitro* experiments, are not involved in Prm1 docking. How this covalent dimerisation exactly confers Prm1 activity remains to be addressed.

It is becoming evident from different cell fusion systems that spatial organisation of fusion proteins is critical for efficient fusion (Deneke and Pauli, 2021; Verma et al., 2018). For *S. cerevisiae*, it is still unclear as to how the fine structure of the plasma membrane might be organised for fusion. Under this idea, I speculate that the remaining regions of Prm1 may provide such a function for yeast cell fusion and that the effects of Ca^{2+} and Δ*sur1* function similarly. Here, Prm1 would act as an accessory protein and mediate the organisation of currently unknown fusion factors which then facilitate membrane merger and pore formation; a role that was similarly hypothesised by Engel and Walter (Engel and

Walter, 2008) **(Figure 60B, i)**. Unidentified fusion factors such as a cell fusogen(s) are likely to exist, because Δ*prm1* × Δ*prm1* crosses are never completely blocked for fusion. Because I found that Prm1 overrides $M(IP)_2C$ effects, in this model, Prm1 would be able to organise fusion factors despite the presence of $M(IP)_2C$, allowing fusion to be promoted even under regimes of high $M(IP)_2C$ levels from Sur1 overproduction. In addition to proteins, it is mutually conceivable that Prm1-mediated organisation extends to lipids to establish a membrane fine structure that is favourable for fusion **(Figure 60B, ii)**. Certain lipids have been found to be more fusogenic than others in both model membranes and cellular contexts, such as the aforementioned negative spontaneous curvature inducing lipids. Prm1 might enrich these fusogenic lipids. Furthermore, Prm1 overrides the inhibitory fusion effects of $M(IP)_2C$ during fusion. In the lipid organisation model, Prm1 may do so by excluding $M(IP)_2C$ from eventual fusion sites. A piece of evidence which suggests that Prm1 can organise the membrane environment comes from an observation in *S. pombe* (Curto et al., 2014). By using a genetically encoded PS probe, the authors found that the PS distribution at the cell-cell contact site was perturbed in Δ*prm1* × Δ*prm1* mating pairs, however it is unclear as to what consequences altered PS distribution may have on fusion in yeast.

In this model, when Prm1 is absent, fusion factors and/or fusogenic lipids are disorganised **(Figure 60C)**, which results in fusion arrested outcomes; lysis and cytoplasmic bubbles. Under this framework, $M(IP)_2C$ sphingolipids organise the fusion factors less efficiently, whereas MIPC and IPC prevalent sphingolipids in the Δ*sur1* and Δ*ipt1* mutants organise more efficiently, thus partially compensating for Prm1 absence. Additionally, Δ*sur1*-restored organisation in membranes of both cell partners would be predicted to cooperate and promote fusion additively, and is thus consistent with the data. Finally, a manner in which Ca^{2+} could promote organisation is through unknown Ca^{2+} sensitive effectors, analogous to annexins in osteoclast fusion (Verma et al., 2018) **(Figure 60D)**. Here, both Δ*sur1* and Ca^{2+} would help organise the same fusion factors, which would perhaps explain how they can substitute for one another. However, it is important to reaffirm that when Prm1 is present, both Ca^{2+} and Δ*sur1* are dispensable, suggesting they constitute secondary backup mechanisms for fusion. How this might be achieved is unclear; it could be that when Prm1 is present, the degree of organisation achieved may be great

enough so that organisation in only one of the plasma membranes is enough and consequently obviates the organisation provided by Ca^{2+} and Δ*sur1*.

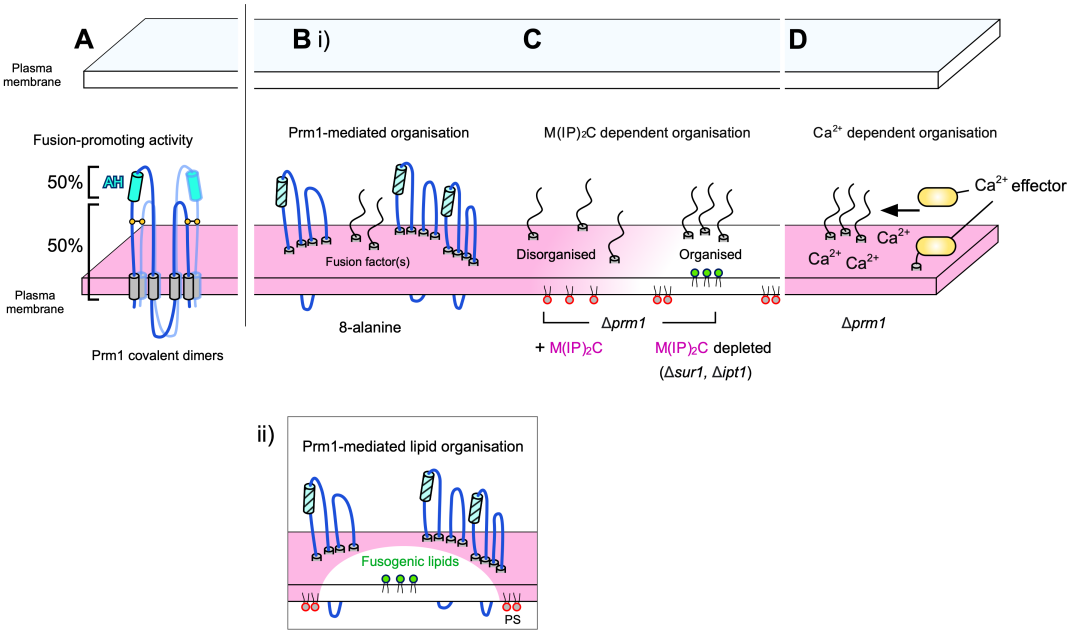

Figure 60. Dissection of Prm1 regions for function and hypothetical models. **A.** Summary of dissected Prm1 domains. The putative amphipathic helix (AH) located in the ectodomain accounts for ~50% of fusion-promoting activity of Prm1. For this activity, the AH might be involved in deforming the membrane of the other cell. The remaining 50% activity of Prm1 is conferred by the remaining regions of the protein. For Prm1 activity, it is critical that Prm1 is covalently dimerised (disulfide linkages are represented by orange links). **B(i).** Hypothetical model of how Prm1 promotes fusion which does not require the amphipathic domain. Hatched cylinder represents the inactive amphipathic domain, such as the 8-alanine mutation. The unknown fusion factors are represented as single-pass TMD proteins. Prm1 may organise fusion factors so that fusion is more favourable. For simplicity, dimers are not illustrated. **B(ii).** Alternatively, Prm1 may organise the local lipid environment to promote fusion. Prm1 may be able to restrict the fusion inhibiting $M(IP)_2C$ (pink) away from fusion sites. Enrichment of fusogenic lipids (green) such as negative spontaneous curvature lipids may also contribute to efficient fusion. Prm1 is implicated to organise PS in *S. pombe*, and this may be necessary for membrane fusion for currently unknown reasons. **C.** Overlapping functions of 8-alanine Prm1 mutant and Δ*sur1*. In the absence of Prm1 and the presence of $M(IP)_2C$, fusion factors are poorly organised, and thus fusion is inefficient. Reduction of $M(IP)_2C$ in the plasma membrane can partially organise fusion factors and compensate for the 8-alanine mutant. **D.** Ca^{2+} mediated organisation of fusion factors by Ca^{2+} effectors (orange), which here are depicted as extracellular proteins or membrane proteins.

Chapter 5. Concluding remarks and future perspectives

5.1 Concluding remarks

Since the discovery of Prm1 two decades ago, the exact function of this protein in the plasma membrane fusion step has puzzled researchers. My investigations begin to shed light on its molecular mechanism. Prm1 is able to dock membranes of different vesicles together. This reveals for the first time a fungal multi-pass membrane protein involved in cell fusion with capacity to directly interact with membranes, without the need for a protein cofactor. The ectoplasmically located amphipathic domain is central for 50% of Prm1 fusion promoting activity *in vivo* and might be used to deform membranes. Ca^{2+} and Δ*sur1* act redundantly to Prm1, indicating they perform similar mechanisms for cell fusion. The spatial organisation role for Prm1 speculated here provides a framework for how Ca^{2+} and Δ*sur1* orchestrate fusion and offers new hypotheses to test, such as whether lipid organisation is altered in Δ*sur1* mutants. The speculated ability of Prm1 to not only deform membranes but organise the membrane fine structure of the fusion site, all point Prm1 to the core of the membrane fusion reaction in yeast.

5.2 Future perspectives

In vitro experiments using the 8-alanine mutant will clarify if docking is facilitated solely by the amphipathic domain, or if Prm1 contains other regions which can mediate docking. This could be complemented with liposome binding assays using synthetic peptides of the amphipathic domain. The newly designated regions of Prm1 responsible for activity should serve as useful references for future investigations. In particular, the Δ140-220 mutant which is significantly trimmed, will be a suitable variant to further pinpoint the exact regions which are important for mediate the organisation mechanism proposed here. Furthermore, the Δ*prm1*Δ*sur1* mutant will provide a useful background to investigate not only the remaining determinants of fusion, but whether phospholipid distribution is altered,

which would provide further support for Δ*sur1* as a lipid organiser. Development of sphingolipid probes which allow visualisation of sphingolipids would present a major tool to study the membrane organisation at the cell-cell contact site during membrane fusion. Finally, in addition to docking membranes, Prm1 may in itself be a fusogen. *In vitro* fusion assays which can detect for occurrence of lipid mixing would be able to address this question in future investigations.

6. References

Aguilar PS, Baylies MK, Fleissner A, Helming L, Inoue N, Podbilewicz B, Wang H, Wong M. 2013. Genetic basis of cell – cell fusion mechanisms. *Trends in Genetics* **29**:427–437. doi:10.1016/j.tig.2013.01.011

Aguilar PS, Engel A, Walter P. 2007. The Plasma Membrane Proteins Prm1 and Fig1 Ascertain Fidelity of Membrane Fusion during Yeast Mating. *Mol Biol Cell* **18**:547–556. doi:10.1091/mbc.e06-09-0776

Akimov SA, Molotkovsky RJ, Kuzmin PI, Galimzyanov TR, Batishchev O V. 2020. Continuum models of membrane fusion: Evolution of the theory. *Int J Mol Sci*. doi:10.3390/ijms21113875

Alkaabi KM, Yafea A, Ashraf SS. 2005. Effect of pH on Thermal-and Chemical-Induced Denaturation of GFP, Applied Biochemistry and Biotechnology.

Avinoam O, Fridman K, Valansi C, Abutbul I, Zeev-Ben-Mordehai T, Maurer UE, Sapir A, Danino D, Grünewald K, White JM, Podbilewicz B. 2011. Conserved eukaryotic fusogens can fuse viral envelopes to cells. *Science (1979)* **332**:589–592. doi:10.1126/science.1202333

Aydin H, Sultana A, Li S, Thavalingam A, Lee JE. 2016. Molecular architecture of the human sperm IZUMO1 and egg JUNO fertilization complex. *Nature* **534**:562–565. doi:10.1038/nature18595

Bagnat M, Simons K. 2002a. Cell surface polarization during yeast mating. *Proceedings of the National Academy of Sciences* **99**:14183–14188. doi:10.1073/pnas.172517799

Bagnat M, Simons K. 2002b. Lipid rafts in protein sorting and cell polarity in budding yeast Saccharomyces cerevisiae. *Biol Chem* **383**:1475–1480. doi:10.1515/BC.2002.169

Bardwell L. 2004. A walk-through of the yeast mating pheromone response pathway. *Peptides (NY)* **25**:1465–1476. doi:10.1016/j.peptides.2003.10.022

Beeler TJ, Fu D, Rivera J, Monaghan E, Gable K, Dunn TM. 1997. SUR1 (CSG1/BCL21), a gene necessary for growth of Saccharomyces cerevisiae in the presence of high Ca2+

concentrations at 37°C, is required for mannosylation of inositolphosphorylceramide. *Molecular and General Genetics* **255**:570–579. doi:10.1007/s004380050530

Bender A, Sprague GF. 1989. Pheromones and pheromone receptors are the primary determinants of mating specificity in the yeast Saccharomyces cerevisiae. *Genetics* **121**:463–476.

Bender A, Sprague GF. 1986. Yeast peptide pheromones, a-factor and α-factor, activate a common response mechanism in their target cells. *Cell* **47**:929–937. doi:10.1016/0092-8674(86)90808-1

Benton DJ, Gamblin SJ, Rosenthal PB, Skehel JJ. 2020. Structural transitions in influenza haemagglutinin at membrane fusion pH. *Nature* **583**:150–153. doi:10.1038/s41586-020-2333-6

Bianchi E, Doe B, Goulding D, Wright GJ. 2014. Juno is the egg Izumo receptor and is essential for mammalian fertilization. *Nature* **508**:483–487. doi:10.1038/nature13203

Blount BA, Driessen MRM, Ellis T. 2016. GC preps: Fast and easy extraction of stable yeast genomic DNA. *Sci Rep* **6**:1–4. doi:10.1038/srep26863

Brizzio V, Gammie AE, Rose MD. 1998. Rvs161p interacts with Fus2p to promote cell fusion in Saccharomyces cerevisiae. *Journal of Cell Biology* **141**:567–584. doi:10.1083/jcb.141.3.567

Brukman NG, Nakajima KP, Valansi C, Flyak K, Li X, Higashiyama T, Podbilewicz B. 2023. A novel function for the sperm adhesion protein IZUMO1 in cell–cell fusion. *Journal of Cell Biology* **222**. doi:10.1083/jcb.202207147

Cappellaro C, Mrsa V, Tanner W. 1998. New Potential Cell Wall Glucanases of Saccharomyces cerevisiae and Their Involvement in Mating, JOURNAL OF BACTERIOLOGY.

Chalbi M, Barraud-Lange V, Ravaux B, Howan K, Rodriguez N, Soule P, Ndzoudi A, Boucheix C, Rubinstein E, Wolf JP, Ziyyat A, Perez E, Pincet F, Gourier C. 2014. Binding of sperm protein Izumo1 and its egg receptor juno drives cd9 accumulation in the intercellular contact area prior to fusion during mammalian fertilization. *Development (Cambridge)* **141**:3732–3739. doi:10.1242/dev.111534

Chang F, Herskowitz I. 1990. Identification of a Gene Necessary for Cell Cycle Arrest by a Negative Growth Factor of Yeast: FAR1 Is an Inhibitor of a Gl Cyclin, CLN2, Cell.

Chernomordik L V, Frolov VA, Leikina E, Bronk P, Zimmerberg J. 1998. The Pathway of Membrane Fusion Catalyzed by Influenza Hemagglutinin: Restriction of Lipids, Hemifusion, and Lipidic Fusion Pore Formation, The Journal of Cell Biology.

Chernomordik L V., Kozlov MM. 2008. Mechanics of membrane fusion. *Nat Struct Mol Biol* **15**:675–683. doi:10.1038/nsmb.1455

Christianson TW, Sikorski RS, Dante M, Shero JH, Hieter P. 1992. Multifunctional yeast high-copy-number shuttle vectors. *Gene* **110**:119–122. doi:10.1016/0378-1119(92)90454-W

Clark T. 2018. HAP2/GCS1: Mounting evidence of our true biological EVE? *PLoS Biol* **16**. doi:10.1371/journal.pbio.3000007

Clarke NG, Dawson RM. 1981. Alkaline O leads to N-transacylation. A new method for the quantitative deacylation of phospholipids. *Biochem J* **195**:301–306. doi:10.1042/bj1950301

Clemente-Ramos JÁ, Martín-García R, Sharifmoghadam MR, Konorni M, Osumi M, Valdivieso MH. 2009. The tetraspan protein Dni1p is required for correct membrane organization and cell wall remodelling during mating in Schizosaccharomyces pombe. *Mol Microbiol* **73**:695–709. doi:10.1111/j.1365-2958.2009.06800.x

Curto MÁ, Sharifmoghadam MR, Calpena E, De León N, Hoya M, Doncel C, Leatherwood J, Valdivieso MH. 2014. Membrane organization and cell fusion during mating in fission yeast requires multipass membrane protein Prm1. *Genetics* **196**:1059–1076. doi:10.1534/genetics.113.159558

Dean N, Zhang YB, Poster JB. 1997. The VRG4 gene is required for GDP-mannose transport into the lumen of the Golgi in the yeast, Saccharomyces cerevisiae. *Journal of Biological Chemistry* **272**:31908–31914. doi:10.1074/jbc.272.50.31908

Deneke VE, Pauli A. 2021. The Fertilization Enigma: How Sperm and Egg Fuse. *Annu Rev Cell Dev Biol 2021* **37**:391–414. doi:10.1146/annurev-cellbio-120219

Drin G, Antonny B. 2010. Amphipathic helices and membrane curvature. *FEBS Lett*. doi:10.1016/j.febslet.2009.10.022

Duncan R. 2019. Fusogenic Reoviruses and Their Fusion-Associated Small Transmembrane (FAST) Proteins. *Annu Rev Virol* **6**:341–363. doi:10.1146/annurev-virology-092818-015523

Eggeling C, Ringemann C, Medda R, Schwarzmann G, Sandhoff K, Polyakova S, Belov VN, Hein B, von Middendorff C, Schönle A, Hell SW. 2009. Direct observation of the nanoscale dynamics of membrane lipids in a living cell. *Nature* **457**:1159–1162. doi:10.1038/nature07596

Ejsing CS, Sampaio JL, Surendranath V, Duchoslav E, Ekroos K, Klemm RW, Simons K, Shevchenko A. 2009. Global analysis of the yeast lipidome by quantitative shotgun mass spectrometry. *Proc Natl Acad Sci U S A* **106**:2136–2141. doi:10.1073/pnas.0811700106

Engel A, Aguilar PS, Walter P. 2010. The yeast cell fusion protein Prm1p requires covalent dimerization to promote membrane fusion. *PLoS One* **5**:1–8. doi:10.1371/journal.pone.0010593

Engel A, Walter P. 2008. Membrane lysis during biological membrane fusion: Collateral damage by misregulated fusion machines. *Journal of Cell Biology* **183**:181–186. doi:10.1083/jcb.200805182

Erdman S, Lin L, Malczynski M, Snyder M. 1998. Pheromone-regulated genes required for yeast mating differentiation. *Journal of Cell Biology* **140**:461–483. doi:10.1083/jcb.140.3.461

Evans R, O'Neill M, Pritzel A, Antropova N, Senior A, Green T, Žídek A, Bates R, Blackwell S, Yim J, Ronneberger O, Bodenstein S, Zielinski M, Bridgland A, Potapenko A, Cowie A, Tunyasuvunakool K, Jain R, Clancy E, Kohli P, Jumper J, Hassabis D. 2022. Protein complex prediction with AlphaFold-Multimer. *bioRxiv* 2021.10.04.463034. doi:10.1101/2021.10.04.463034

Fasshauer D, Sutton RB, Brunger AT, Jahn R. 1998. Conserved structural features of the synaptic fusion complex: SNARE proteins reclassified as Q- and R-SNAREs. *Proceedings of the National Academy of Sciences* **95**:15781–15786. doi:10.1073/pnas.95.26.15781

Faust JE, Desai T, Verma A, Ulengin I, Sun TL, Moss TJ, Betancourt-Solis MA, Huang HW, Lee T, McNew JA. 2015. The atlastin C-terminal tail is an amphipathic helix that perturbs the bilayer structure during endoplasmic reticulum homotypic fusion. *Journal of Biological Chemistry* **290**:4772–4783. doi:10.1074/jbc.M114.601823

Fédry J, Liu Y, Péhau-Arnaudet G, Pei J, Li W, Tortorici MA, Traincard F, Meola A, Bricogne G, Grishin N V., Snell WJ, Rey FA, Krey T. 2017. The Ancient Gamete Fusogen HAP2 Is a Eukaryotic Class II Fusion Protein. *Cell* **168**:904-915.e10. doi:10.1016/j.cell.2017.01.024

Feng J, Dong X, Pinello J, Zhang J, Lu C, Iacob RE, Engen JR, Snell WJ, Springer TA. 2018. Fusion surface structure, function, and dynamics of gamete fusogen HAP2. *Elife* **7**:1–25. doi:10.7554/eLife.39772

Fleißner A, Diamond S, Glass NL. 2009. The Saccharomyces cerevisiae PRM1 homolog in Neurospora crassa is involved in vegetative and sexual cell fusion events but also has postfertilization functions. *Genetics* **181**:497–510. doi:10.1534/genetics.108.096149

Ford MGJ, Mills IG, Peter BJ, Vallis Y, Praefcke GJK, Evans PR, Mcmahon HT. 2002. Curvature of clathrin-coated pits driven by epsin.

Fu C, Heitman J. 2017. PRM1 and KAR5 function in cell-cell fusion and karyogamy to drive distinct bisexual and unisexual cycles in the Cryptococcus pathogenic species complex, PLoS Genetics. doi:10.1371/journal.pgen.1007113

Fujihara Y, Lu Y, Noda T, Oji A, Larasati T, Kojima-kita K. 2020. Spermatozoa lacking Fertilization Influencing Membrane Protein (FIMP) fail to fuse with oocytes in mice 1–8. doi:10.1073/pnas.1917060117

Gamage DG, Leikina E, Quinn ME, Ratinov A, Chernomordik L V., Millay DP. 2017. Insights into the localization and function of myomaker during myoblast fusion. *Journal of Biological Chemistry* **292**:17272–17289. doi:10.1074/jbc.M117.811372

Gammie AE, Brizzio V, Rose MD. 1998. Distinct Morphological Phenotypes of Cell Fusion Mutants. *Mol Biol Cell* **9**:1395–1410. doi:10.1091/mbc.9.6.1395

Gautier R, Douguet D, Antonny B, Drin G. 2008. HELIQUEST: A web server to screen sequences with specific α-helical properties. *Bioinformatics* **24**:2101–2102. doi:10.1093/bioinformatics/btn392

Gietz RD, Schiestl RH. 2007. Microtiter plate transformation using the LiAc/SS carrier DNA/PEG method. *Nat Protoc* **2**:5–8. doi:10.1038/nprot.2007.16

Giménez-Andrés M, Čopič A, Antonny B. 2018. The many faces of amphipathic helices. *Biomolecules* **8**:1–14. doi:10.3390/biom8030045

Grote E. 2010. Secretion is required for late events in the cell-fusion pathway of mating yeast. *J Cell Sci* **123**:1902–1912. doi:10.1242/jcs.066662

Grote E. 2008. Cell Fusion Assays for Yeast Mating Pairs In: Chen EH, editor. Cell Fusion: Overviews and Methods. Totowa, NJ: Humana Press. pp. 165–196. doi:10.1007/978-1-59745-250-2_10

Haber JE. 2012. Mating-type genes and MAT switching in Saccharomyces cerevisiae. *Genetics* **191**:33–64. doi:10.1534/genetics.111.134577

Hagen DC, McCaffrey G, Sprague GF. 1986. Evidence the yeast STE3 gene encodes a receptor for the peptide pheromone a factor: Gene sequence and implications for the structure of the presumed receptor. *Proc Natl Acad Sci U S A* **83**:1418–1422. doi:10.1073/pnas.83.5.1418

Hanson BA, Lester RL. 1980. The extraction of inositol-containing phospholipids and phosphatidylcholine from Saccharomyces cerevisiae and Neurospora crassa. *J Lipid Res* **21**:309–315. doi:10.1016/s0022-2275(20)39810-2

Hashida-Okado T, Ogawa A, Endo M, Yasumoto R, Takesako K, Kato I. 1996. AUR1, a novel gene conferring aureobasidin resistance on Saccharomyces cersvisiae: A study of defective morphologies in Aur1p-depleted cells. *Molecular and General Genetics* **251**:236–244. doi:10.1007/BF02172923

Hechtberger P, Zinser E, Saf R, Hummel K, Paltauf F, Daum G. 1994. Characterization, quantification and subcellular localization of inositol-containing sphingolipids of the yeast, Saccharomyces cerevisiae. *Eur J Biochem* **225**:641–649. doi:10.1111/j.1432-1033.1994.00641.x

Heiman MG, Walter P. 2000. Prm1p, a Pheromone-Regulated Multispanning Membrane Protein, Facilitates Plasma Membrane Fusion during Yeast Mating. *J Cell Biol* **151**:719–730. doi:10.1083/jcb.151.3.719

Inoue H, Nojima H, Okayama H. 1990. High efficiency transformation of Escherichia coli with plasmids. *Gene* **96**:23–28. doi:10.1016/0378-1119(90)90336-P

Inoue N, Hagihara Y, Wada I. 2021. Evolutionarily conserved sperm factors, DCST1 and DCST2, are required for gamete fusion. *Elife* **10**:1–12. doi:10.7554/eLife.66313

Ivanovic T, Choi JL, Whelan SP, van Oijen AM, Harrison SC. 2013. Influenza-virus membrane fusion by cooperative fold-back of stochastically induced hemagglutinin intermediates. *Elife* **2013**. doi:10.7554/eLife.00333

Jenness DD, Burkholder AC, Hartwell LH. 1983. Binding of α-factor pheromone to yeast a cells: Chemical and genetic evidence for an α-factor receptor. *Cell* **35**:521–529. doi:10.1016/0092-8674(83)90186-1

Jin H, Carlile C, Nolan S, Grote E. 2004. Prm1 Prevents Contact-Dependent Lysis of Yeast Mating Pairs. *Eukaryot Cell* **3**:1664–1673. doi:10.1128/ec.3.6.1664-1673.2004

Jin H, McCaffery JM, Grote E. 2008. Ergosterol promotes pheromone signaling and plasma membrane fusion in mating yeast. *Journal of Cell Biology* **180**:813–826. doi:10.1083/jcb.200705076

Jones GM, Stalker J, Humphray S, West A, Cox T, Rogers J, Dunham I, Prelich G. 2008. A systematic library for comprehensive overexpression screens in Saccharomyces cerevisiae. *Nat Methods* **5**:239–241. doi:10.1038/nmeth.1181

Jumper J, Evans R, Pritzel A, Green T, Figurnov M, Ronneberger O, Tunyasuvunakool K, Bates R, Žídek A, Potapenko A, Bridgland A, Meyer C, Kohl SAA, Ballard AJ, Cowie A, Romera-Paredes B, Nikolov S, Jain R, Adler J, Back T, Petersen S, Reiman D, Clancy E, Zielinski M, Steinegger M, Pacholska M, Berghammer T, Bodenstein S, Silver D, Vinyals O, Senior AW, Kavukcuoglu K, Kohli P, Hassabis D. 2021. Highly accurate protein structure prediction with AlphaFold. *Nature* **596**:583–589. doi:10.1038/s41586-021-03819-2

Kawate T, Gouaux E. 2006. Fluorescence-Detection Size-Exclusion Chromatography for Precrystallization Screening of Integral Membrane Proteins. *Structure* **14**:673–681. doi:10.1016/j.str.2006.01.013

Kemble GW, Danieli T, Whitet JM. 1994. Lipid-Anchored Influenza Hemagglutinin Promotes Hemifusion, Not Complete Fusion **76**.

Kitajima T, Chiba Y, Jigami Y. 2006. Saccharomyces cerevisiae α1,6-mannosyltransferase has a catalytic potential to transfer a second mannose molecule. *FEBS Journal* **273**:5074–5085. doi:10.1111/j.1742-4658.2006.05505.x

Klose C, Surma MA, Gerl MJ, Meyenhofer F, Shevchenko A, Simons K. 2012. Flexibility of a eukaryotic lipidome - insights from yeast lipidomics. *PLoS One* **7**. doi:10.1371/journal.pone.0035063

Knop M, Siegers K, Pereira G, Zachariae W, Winsor B, Nasmyth K, Schiebel E. 1999. Epitope tagging of yeast genes using a PCR-based strategy: More tags and improved practical routines. *Yeast* **15**:963–972. doi:10.1002/(SICI)1097-0061(199907)15:10B<963::AID-YEA399>3.0.CO;2-W

Kobayashi T. 2011. Regulation of ribosomal RNA gene copy number and its role in modulating genome integrity and evolutionary adaptability in yeast. *Cellular and Molecular Life Sciences*. doi:10.1007/s00018-010-0613-2

Koga A, Takayama C, Ishibashi Y, Kono Y, Matsuzaki M, Tani M. 2022. Loss of tolerance to multiple environmental stresses due to limitation of structural diversity of complex sphingolipids. *Mol Biol Cell* **33**:ar105. doi:10.1091/mbc.E22-04-0117

Lamas-Toranzo I, Hamze JG, Bianchi E, Fernández-Fuertes B, Pérez-Cerezales S, Laguna-Barraza R, Fernández-González R, Lonergan P, Gutiérrez-Adán A, Wright GJ, Jiménez-Movilla M, Bermejo-álvarez P. 2020. TMEM95 is a sperm membrane protein essential for mammalian fertilization. *Elife* **9**:1–18. doi:10.7554/eLife.53913

Leikina E, Crowe M, Chernomordik L V., Diao J, Goykhberg J, Gamage DG, Prasad V, Millay DP, Kozlov MM. 2018. Myomaker and Myomerger Work Independently to Control Distinct Steps of Membrane Remodeling during Myoblast Fusion. *Dev Cell* **46**:767-780.e7. doi:10.1016/j.devcel.2018.08.006

Levine TP, Wiggins CAR, Munro S. 2000. Inositol phosphorylceramide synthase is located in the Golgi apparatus of Saccharomyces cerevisiae. *Mol Biol Cell* **11**:2267–2281. doi:10.1091/mbc.11.7.2267

Lisman Q, Pomorski T, Vogelzangs C, Urli-Stam D, van Delwijnen WDC, Holthuis JCM. 2004. Protein Sorting in the Late Golgi of Saccharomyces cerevisiae Does Not Require

Mannosylated Sphingolipids. *Journal of Biological Chemistry* **279**:1020–1029. doi:10.1074/jbc.M306119200

Magliery TJ, Wilson CGM, Pan W, Mishler D, Ghosh I, Hamilton AD, Regan L. 2005. Detecting protein-protein interactions with a green fluorescent protein fragment reassembly trap: Scope and mechanism. *J Am Chem Soc* **127**:146–157. doi:10.1021/ja046699g

Markin VS, Kozlov MM, Borovjagin VL. 1984. On the Theory of Membrane Fusion. The Stalk Mechanism, Gen. Physiol. Biophys.

Matheos D, Metodiev M, Muller E, Stone D, Rose MD. 2004. Pheromone-induced polarization is dependent on the Fus3p MAPK acting through the formin Bni1p. *Journal of Cell Biology* **165**:99–109. doi:10.1083/jcb.200309089

Mesmin B, Drin G, Levi S, Rawet M, Cassel D, Bigay J, Antonny B. 2007. Two lipid-packing sensor motifs contribute to the sensitivity of ArfGAP1 to membrane curvature. *Biochemistry* **46**:1779–1790. doi:10.1021/bi062288w

Millay DP, Gamage DG, Quinn ME, Min YL, Mitani Y, Bassel-Duby R, Olson EN. 2016. Structure-function analysis of myomaker domains required for myoblast fusion. *Proc Natl Acad Sci U S A* **113**:2116–2121. doi:10.1073/pnas.1600101113

Millay DP, O'Rourke JR, Sutherland LB, Bezprozvannaya S, Shelton JM, Bassel-Duby R, Olson EN. 2013. Myomaker is a membrane activator of myoblast fusion and muscle formation. *Nature* **499**:301–305. doi:10.1038/nature12343

Misamore MJ, Gupta S, Snell WJ. 2003. The Chlamydomonas Fus1 protein is present on the mating type plus fusion organelle and required for a critical membrane adhesion event during fusion with minus gametes. *Mol Biol Cell* **14**:2530–2542. doi:10.1091/mbc.E02-12-0790

Miyado K, Yamada G, Yamada S, Hasuwa H, Nakamura Y, Ryu F, Suzuki K, Kosai K, Inoue K, Ogura A, Okabe M, Mekada E. 2000. Requirement of CD9 on the Egg Plasma Membrane for Fertilization. *Science (1979)* **287**:321–324. doi:10.1126/science.287.5451.321

Moi D, Nishio S, Li X, Valansi C, Langleib M, Brukman NG, Flyak K, Dessimoz C, de Sanctis D, Tunyasuvunakool K, Jumper J, Graña M, Romero H, Aguilar PS, Jovine L,

Podbilewicz B. 2022. Discovery of archaeal fusexins homologous to eukaryotic HAP2/GCS1 gamete fusion proteins. *Nat Commun* **13**. doi:10.1038/s41467-022-31564-1

Moo WK, Eun JK, Kim JY, Park JS, Oh DB, Shimma YI, Chiba Y, Jigami Y, Sang KR, Hyun AK. 2006. Functional characterization of the Hansenula polymorpha HOC1, OCH1, and OCR1 genes as members of the yeast OCH1 mannosyltransferase family involved in protein glycosylation. *Journal of Biological Chemistry* **281**:6261–6272. doi:10.1074/jbc.M508507200

Mori T, Kuroiwa H, Higashiyama T, Kuroiwa T. 2006. GENERATIVE CELL SPECIFIC 1 is essential for angiosperm fertilization. *Nat Cell Biol* **8**:64–71. doi:10.1038/ncb1345

Morimoto Y, Tani M. 2015. Synthesis of mannosylinositol phosphorylceramides is involved in maintenance of cell integrity of yeast Saccharomyces cerevisiae. *Mol Microbiol* **95**:706–722. doi:10.1111/mmi.12896

Mortimer RK, Johnston JR. 1986. Genealogy of principal strains of the yeast genetic stock center. *Genetics* **113**:35–43. doi:10.1093/genetics/113.1.35

Nelson B, Parsons AB, Evangelista M, Schaefer K, Kennedy K, Ritchie S, Petryshen TL, Boone C. 2004. Fus1p Interacts with Components of the Hog1p Mitogen-Activated Protein Kinase and Cdc42p Morphogenesis Signaling Pathways to Control Cell Fusion during Yeast Mating. *Genetics* **166**:67–77. doi:10.1534/genetics.166.1.67

Newstead S, Kim H, von Heijne G, Iwata S, Drew D. 2007. High-throughput fluorescent-based optimization of eukaryotic membrane protein overexpression and purification in Saccharomyces cerevisiae. *Proc Natl Acad Sci U S A* **104**:13936–13941. doi:10.1073/pnas.0704546104

Noda T, Blaha A, Fujihara Y, Gert KR, Emori C, Deneke VE, Oura S, Panser K, Lu Y, Berent S, Kodani M, Cabrera-Quio LE, Pauli A, Ikawa M. 2022. Sperm membrane proteins DCST1 and DCST2 are required for sperm-egg interaction in mice and fish. *Commun Biol* **5**:1–6. doi:10.1038/s42003-022-03289-w

Noda T, Lu Y, Fujihara Y, Oura S, Koyano T, Kobayashi S, Matzuk MM, Ikawa M. 2020. Sperm proteins SOF1, TMEM95, and SPACA6 are required for sperm−oocyte fusion

in mice. *Proceedings of the National Academy of Sciences* 201922650. doi:10.1073/pnas.1922650117

Ohto U, Ishida H, Krayukhina E, Uchiyama S, Inoue N, Shimizu T. 2016. Structure of IZUMO1-JUNO reveals sperm-oocyte recognition during mammalian fertilization. *Nature* **534**:566–569. doi:10.1038/nature18596

Olmo VN, Grote E. 2010a. Prm1 targeting to contact sites enhances fusion during mating in Saccharomyces cerevisiae. *Eukaryot Cell* **9**:1538–1548. doi:10.1128/EC.00116-10

Olmo VN, Grote E. 2010b. Prm1 functions as a disulfide-linked complex in yeast mating. *Journal of Biological Chemistry* **285**:2274–2283. doi:10.1074/jbc.M109.068874

Palma-Guerrero J, Leeder AC, Welch J, Glass NL. 2014. Identification and characterization of LFD1, a novel protein involved in membrane merger during cell fusion in Neurospora crassa. *Mol Microbiol* **92**:164–182. doi:10.1111/mmi.12545

Papahadjopoulos D, Meers PR, Hong K, Ernst JD, Goldstein IM, Düzgünes N. 1988. Calcium-Induced Membrane Fusion: From Liposomes to Cellular MembranesMolecular Mechanisms of Membrane Fusion. Boston, MA: Springer US. pp. 1–16. doi:10.1007/978-1-4613-1659-6_1

Pérez-Vargas J, Krey T, Valansi C, Avinoam O, Haouz A, Jamin M, Raveh-Barak H, Podbilewicz B, Rey FA. 2014. Structural basis of eukaryotic cell-cell fusion. *Cell* **157**:407–419. doi:10.1016/j.cell.2014.02.020

Petes TD. 1979. Yeast ribosomal DNA genes are located on chromosome XII (aneuploid mapping/mitotic recombination), Genetics.

Pettersen EF, Goddard TD, Huang CC, Meng EC, Couch GS, Croll TI, Morris JH, Ferrin TE. 2021. UCSF ChimeraX: Structure visualization for researchers, educators, and developers. *Protein Science* **30**:70–82. doi:10.1002/pro.3943

Phillips GN. 1997. Structure and dynamics of green fluorescent protein. *Curr Opin Struct Biol* **7**:821–827. doi:10.1016/S0959-440X(97)80153-4

Pinello JF, Clark TG. 2022. HAP2-Mediated Gamete Fusion: Lessons From the World of Unicellular Eukaryotes. *Front Cell Dev Biol*. doi:10.3389/fcell.2021.807313

Pinello JF, Liu Y, Snell WJ. 2021. MAR1 links membrane adhesion to membrane merger during cell-cell fusion in Chlamydomonas. *Dev Cell* **56**:3380-3392.e9. doi:10.1016/j.devcel.2021.10.023

Podbilewicz B. 2014. Virus and Cell Fusion Mechanisms. *Annu Rev Cell Dev Biol* **30**:111–139. doi:10.1146/annurev-cellbio-101512-122422

Podbilewicz B, Leikina E, Sapir A, Valansi C, Suissa M, Shemer G, Chernomordik L v. 2006. The C. elegans Developmental Fusogen EFF-1 Mediates Homotypic Fusion in Heterologous Cells and In Vivo. *Dev Cell* **11**:471–481. doi:10.1016/j.devcel.2006.09.004

Podbilewicz B, White JG. 1994. Cell Fusions in the Developing Epithelia of C. elegans. *Dev Biol* **161**:408–424. doi:10.1006/dbio.1994.1041

Quinn ME, Goh Q, Kurosaka M, Gamage DG, Petrany MJ, Prasad V, Millay DP. 2017. Myomerger induces fusion of non-fusogenic cells and is required for skeletal muscle development. *Nat Commun* **8**:1–9. doi:10.1038/ncomms15665

Rand R. 1989. Hydration forces between phospholipid bilayers. *Biochimica et Biophysica Acta (BBA) - Reviews on Biomembranes* **988**:351–376. doi:10.1016/0304-4157(89)90010-5

Runge KE, Evans JE, He ZY, Gupta S, McDonald KL, Stahlberg H, Primakoff P, Myles DG. 2007. Oocyte CD9 is enriched on the microvillar membrane and required for normal microvillar shape and distribution. *Dev Biol* **304**:317–325. doi:10.1016/j.ydbio.2006.12.041

Saeed IA, Ashraf SS. 2009. Denaturation studies reveal significant differences between GFP and blue fluorescent protein. *Int J Biol Macromol* **45**:236–241. doi:10.1016/j.ijbiomac.2009.05.010

Salim D, Bradford WD, Freeland A, Cady G, Wang J, Pruitt SC, Gerton JL. 2017. DNA replication stress restricts ribosomal DNA copy number. *PLoS Genet* **13**. doi:10.1371/journal.pgen.1007006

Salzman V, Porro V, Bollati-Fogolín M, Aguilar PS. 2015. Quantitation of yeast cell-cell fusion using multicolor flow cytometry. *Cytometry Part A* **87**:843–854. doi:10.1002/cyto.a.22701

Sapir A, Choi J, Leikina E, Avinoam O, Valansi C, Chernomordik L v., Newman AP, Podbilewicz B. 2007. AFF-1, a FOS-1-Regulated Fusogen, Mediates Fusion of the Anchor Cell in C. elegans. *Dev Cell* **12**:683–698. doi:10.1016/j.devcel.2007.03.003

Schmidt TGM, Batz L, Bonet L, Carl U, Holzapfel G, Kiem K, Matulewicz K, Niermeier D, Schuchardt I, Stanar K. 2013. Development of the Twin-Strep-tag® and its application for purification of recombinant proteins from cell culture supernatants. *Protein Expr Purif*. doi:10.1016/j.pep.2013.08.021

Schweizer E, Mackechnie C, Halvorson H 0. 1969. The Redundancy of Ribosomal and Transfer RNA Genes in Saccharomyces cerevisiae, J. Mol. Biol.

Shelton JM, Li H, Ramirez-Martinez A, Bassel-Duby R, Bi P, Cannavino J, Sánchez-Ortiz E, McAnally JR, Olson EN. 2017. Control of muscle formation by the fusogenic micropeptide myomixer. *Science (1979)* **356**:323–327. doi:10.1126/science.aam9361

Shemer G, Suissa M, Kolotuev I, Nguyen KCQ, Hall DH, Podbilewicz B. 2004. EFF-1 Is Sufficient to Initiate and Execute Tissue-Specific Cell Fusion in C. elegans. *Current Biology* **14**:1587–1591. doi:10.1016/j.cub.2004.07.059

Sheu Y-J, Santos B, Fortin N, Costigan C, Snyder M. 1998. Spa2p Interacts with Cell Polarity Proteins and Signaling Components Involved in Yeast Cell Morphogenesis. *Mol Cell Biol* **18**:4053–4069. doi:10.1128/mcb.18.7.4053

Shi C, Kaminskyj S, Caldwell S, Loewen MC. 2007. A role for a complex between activated G protein-coupled receptors in yeast cellular mating. *Proc Natl Acad Sci U S A* **104**:5395–5400. doi:10.1073/pnas.0608219104

Sievers F, Wilm A, Dineen D, Gibson TJ, Karplus K, Li W, Lopez R, McWilliam H, Remmert M, Söding J, Thompson JD, Higgins DG. 2011. Fast, scalable generation of high-quality protein multiple sequence alignments using Clustal Omega. *Mol Syst Biol* **7**. doi:10.1038/msb.2011.75

Sikorski RS, Hieter P. 1989. A system of shuttle vectors and yeast host strains designed for efficient manipulation of DNA in Saccharomyces cerevisiae. *Genetics* **122**:19–27. doi:0378111995000377 [pii]

Simons K, Ikonen E. 1997. Functional rafts in cell membranes. *Nature* **387**:569–572. doi:10.1038/42408

Simunovic M, Voth GA, Callan-Jones A, Bassereau P. 2015. When Physics Takes Over: BAR Proteins and Membrane Curvature. *Trends Cell Biol*. doi:10.1016/j.tcb.2015.09.005

Smith JA, Hall AE, Rose MD. 2017. Membrane curvature directs the localization of Cdc42p to novel foci required for cell-cell fusion. *Journal of Cell Biology* **216**:3971–3980. doi:10.1083/jcb.201703169

Steele RE, Dana CE. 2009. Evolutionary history of the HAP2/GCS1 gene and sexual reproduction in metazoans. *PLoS One* **4**. doi:10.1371/journal.pone.0007680

Stein A, Weber G, Wahl MC, Jahn R. 2009. Helical extension of the neuronal SNARE complex into the membrane. *Nature* **460**:525–528. doi:10.1038/nature08156

Stein RA, Smith JA, Rose MD. 2016. An amphiphysin-Like domain in Fus2p is required for Rvs161p interaction and cortical localization. *G3: Genes, Genomes, Genetics* **6**:337–349. doi:10.1534/g3.115.023960

Stetsenko A, Guskov A. 2017. An overview of the top ten detergents used for membrane protein crystallization. *Crystals (Basel)* **7**. doi:10.3390/cryst7070197

Striebeck A, Robinson DA, Schüttelkopf AW, van Aalten DMF. 2013. Yeast Mnn9 is both a priming glycosyltransferase and an allosteric activator of mannan biosynthesis. *Open Biol* **3**. doi:10.1098/rsob.130022

Sundler R. 1984. Role of Phospholipid Head Group Structure and Polarity in the Control of Membrane Fusion In: Kates M, Manson LA, editors. Membrane Fluidity. Boston, MA: Springer US. pp. 563–583. doi:10.1007/978-1-4684-4667-8_19

Surma MA, Klose C, Klemm RW, Ejsing CS, Simons K. 2011. Generic Sorting of Raft Lipids into Secretory Vesicles in Yeast. *Traffic* **12**:1139–1147. doi:10.1111/j.1600-0854.2011.01221.x

Sutton RB, Fasshauer D, Jahn R, Brunger AT. 1998. Crystal structure of a SNARE complex involved in synaptic exocytosis at 2.4 Å resolution. *Nature* **395**:347–353. doi:10.1038/26412

Tang S, Lu Y, Skinner WM, Sanyal M, Lishko P v, Ikawa M, Kim PS. 2022. Human sperm TMEM95 binds eggs and facilitates membrane fusion. *bioRxiv*. doi:doi.org/10.1101/2022.06.10.495573

Tedford K, Kim S, Sa D, Stevens K, Tyers M. 1997. Regulation of the mating pheromone and invasive growth responses in yeast by two MAP kinase substrates. *Current Biology* **7**:228–238. doi:10.1016/S0960-9822(06)00118-7

Terrance K, Lipke PN. 1987. Pheromone induction of agglutination in Saccharomyces cerevisiae a cells. *J Bacteriol* **169**:4811–4815. doi:10.1083/jcb.130.6.1333

Trueheart J, Boeke JD, Fink GR. 1987. Two genes required for cell fusion during yeast conjugation: evidence for a pheromone-induced surface protein. *Mol Cell Biol* **7**:2316–28. doi:10.1128/MCB.7.7.2316.Updated

Tsurudome M, Glück R, Graf R, Falchetto R, Schaller U, Brunner J. 1992. Lipid interactions of the hemagglutinin HA2 NH2-terminal segment during influenza virus-induced membrane fusion. *Journal of Biological Chemistry* **267**:20225–20232. doi:10.1016/S0021-9258(19)88690-8

Uemura S, Kihara A, Inokuchi JI, Igarashi Y. 2003. Csg1p and Newly Identified Csh1p Function in Mannosylinositol Phosphorylceramide Synthesis by Interacting with Csg2p. *Journal of Biological Chemistry* **278**:45049–45055. doi:10.1074/jbc.M305498200

Uemura S, Kihara A, Iwaki S, Inokuchi JI, Igarashi Y. 2007. Regulation of the transport and protein levels of the inositol phosphorylceramide mannosyltransferases Csg1 and Csh1 by the Ca 2+-binding protein Csg2. *Journal of Biological Chemistry* **282**:8613–8621. doi:10.1074/jbc.M606649200

van den Ent F, Löwe J. 2006. RF cloning: A restriction-free method for inserting target genes into plasmids. *J Biochem Biophys Methods* **67**:67–74. doi:10.1016/j.jbbm.2005.12.008

Vance TDR, Yip P, Jiménez E, Li S, Gawol D, Byrnes J, Usón I, Ziyyat A, Lee JE. 2022. SPACA6 ectodomain structure reveals a conserved superfamily of gamete fusion-associated proteins. *Commun Biol* **5**. doi:10.1038/s42003-022-03883-y

Verma SK, Leikina E, Melikov K, Gebert C, Kram V, Young MF, Uygur B, Chernomordik L V. 2018. Cell-surface phosphatidylserine regulates osteoclast precursor fusion. *Journal of Biological Chemistry* **293**:254–270. doi:10.1074/jbc.M117.809681

Villasmil ML, Francisco J, Gallo-Ebert C, Donigan M, Liu HY, Brower M, Nickels JT. 2016. Ceramide signals for initiation of yeast mating-specific cell cycle arrest. *Cell Cycle* **15**:441–454. doi:10.1080/15384101.2015.1127475

von Besser K, Frank AC, Johnson MA, Preuss D. 2006. Arabidopsis HAP2 (GCS1) is a sperm-specific gene required for pollen tube guidance and fertilization. *Development* **133**:4761–4769. doi:10.1242/dev.02683

Waszczak N, DeFlorio R, Ismael A, Cheng N, Stone DE, Metodiev M V. 2019. Quantitative proteomics reveals a Gα/MAPK signaling hub that controls pheromone-induced cellular polarization in yeast. *J Proteomics* **207**. doi:10.1016/j.jprot.2019.103467

Weber T, Zemelman B V, McNew JA, Westermann B, Gmachl M, Parlati F, Söllner TH, Rothman JE. 1998. SNAREpins: Minimal Machinery for Membrane Fusion. *Cell* **92**:759–772. doi:10.1016/S0092-8674(00)81404-X

Weichert M, Herzog S, Robson SA, Brandt R, Priegnitz BE, Brandt U, Schulz S, Fleißner A. 2020. Plasma membrane fusion is specifically impacted by the molecular structure of membrane sterols during vegetative development of neurospora crassa. *Genetics* **216**:1103–1116. doi:10.1534/genetics.120.303623

Wiggins CAR, Munro S. 1998. Activity of the yeast MNN1 α-1,3-mannosyltransferase requires a motif conserved in many other families of glycosyltransferases. *Proc Natl Acad Sci U S A* **95**:7945–7950. doi:10.1073/pnas.95.14.7945

Witkowska A, Heinz LP, Grubmüller H, Jahn R. 2021. Tight docking of membranes before fusion represents a metastable state with unique properties. *Nat Commun* **12**:3606. doi:10.1038/s41467-021-23722-8

Wong JL, Johnson MA. 2010. Is HAP2-GCS1 an ancestral gamete fusogen? *Trends Cell Biol* **20**:134–141. doi:10.1016/j.tcb.2009.12.007

Xie Y, Miao Y. 2021. Polarisome assembly mediates actin remodeling during polarized yeast and fungal growth. *J Cell Sci*. doi:10.1242/jcs.247916

Ydenberg CA, Stein RA, Rose MD. 2012. Cdc42p and Fus2p act together late in yeast cell fusion. *Mol Biol Cell* **23**:1208–1218. doi:10.1091/mbc.E11-08-0723

Yofe I, Schuldiner M. 2014. Primers-4-Yeast: A comprehensive web tool for planning primers for Saccharomyces cerevisiae. *Yeast* **31**:77–80. doi:10.1002/yea.2998

Zhang J, Pinello JF, Fernández I, Baquero E, Fedry J, Rey FA, Snell WJ. 2021. Species-specific gamete recognition initiates fusion-driving trimer formation by conserved fusogen HAP2. *Nat Commun* **12**:4380. doi:10.1038/s41467-021-24613-8

Zhang N-N, Dudgeon DD, Paliwal S, Levchenko A, Grote E, Cunningham KW. 2006. Multiple Signaling Pathways Regulate Yeast Cell Death during the Response to Mating Pheromones. *Mol Biol Cell* **17**:3409–3422. doi:10.1091/mbc.E06

Zhang Q, Vashisht AA, O'Rourke J, Corbel SY, Moran R, Romero A, Miraglia L, Zhang J, Durrant E, Schmedt C, Sampath Srinath C., Sampath Srihari C. 2017. The microprotein Minion controls cell fusion and muscle formation. *Nat Commun* **8**. doi:10.1038/ncomms15664

Zhao H, Shen Z, Kahn PC, Peter N, Zhao HUI. 2001. Saccharomyces cerevisiae Sexual Cell Adhesion Molecules Sexual Cell Adhesion Molecules. *J Bacteriol* **183**:2874. doi:10.1128/JB.183.9.2874

Zheng H, Wang K, Xu X, Pan J, Sun X, Hou J, Liu W, Shen Y. 2022. Highly efficient rDNA-mediated multicopy integration based on the dynamic balance of rDNA in Saccharomyces cerevisiae. *Microb Biotechnol* **15**:1511–1524. doi:10.1111/1751-7915.14010

7. Publications and conferences

7.1 Publications

Shek A. and Hernandez J.M., Membrane protein Prm1 and $M(IP)_2C$ regulate cell-cell fusion in *S. cerevisiae* during mating. **Manuscript in preparation.**

7.2 Conferences

2022: Cell-Cell Fusion Gordon Research Conference

Easton, MA, USA.
Conference: Oral Presentation and Poster
Presentation: Mechanism of Action of Sphingolipids and Membrane Protein Prm1 in Cell Fusion During Yeast Mating.

2021: Virtual IMPRS Student's Symposium

Max Planck Institute of Molecular Physiology, Dortmund.
Symposium: Virtual poster
Prize for 2nd best poster
Poster: Genetic overexpression screen reveals novel genes involved in cell-cell fusion of *S. cerevisiae*.

2019: Ruhr symposium

Max Planck Institute of Molecular Physiology, Dortmund.
Symposium: Oral presentation
Talk: Searching for novel proteins involved in yeast mating using Gain-of-fusion and suppression.

2019: 29th Conference of Yeast Genetics and Molecular Biology

Gothenburg, Sweden.
Conference: Poster
Poster: Identifying Novel Fusion Proteins in *S. cerevisiae* Mating Using Suppression and Sufficiency Criteria.